Development and validation of a 3D vibrating contact probe for micro-CMMs

JAMES DAVID CLAVERLEY, BSc.

Thesis submitted to the University of Nottingham
for the degree of Doctor of Philosophy

JULY 2014

Abstract

The state-of-the-art in dimensional metrology in terms of accuracy and 3D measurement is the micro-co-ordinate measuring machine, or micro-CMM. Current manufacturing trends are inclined towards miniaturisation, and all developments in this area are dependent on the capabilities of dimensional metrologists. Currently, the main limiting factor in the advancement of co-ordinate metrology at the micrometre scale is the design, manufacture and resulting accuracy of contacting micro-CMM probes. With this in mind, this thesis describes the development of a novel 3D vibrating micro-CMM probe. The main contributions of this thesis are as follows.

Firstly, the current state of contact probing at the micrometre scale is reviewed and a clear set of knowledge gaps are identified for developments in this area.

Secondly, the concept of a novel 3D vibrating micro-CMM probe is introduced as the background knowledge for this thesis. The mechanical and electrical properties of this vibrating micro-probe are modelled, as well as its intended operation. The operational model of the vibrating micro-probe focusses on the surface interaction forces that are prevalent when probing at the micrometre scale.

Thirdly, the operation of the vibrating micro-probe is validated experimentally. Initially, the ability of the vibrating micro-probe to counteract the surface interaction forces is investigated. Other areas of validation are in the determination of the probing point repeatability, the linearity error, and isotropy of the probe.

Finally, the intended operation of the probe is compared to current national and international specification standards and guidelines for the operation of CMM probes. This work is directly aimed at ensuring that the developed vibrating micro-probe is capable of operating in an industrial or commercial metrology environment. A detailed set of operating strategies are also developed for efficient use of the vibrating micro-probe.

It is concluded that the developed vibrating micro-probe will be able to address the current needs of the micro-CMM community. It is also concluded that the vibrating micro-probe has the ability to operate in a non-contact mode, further increasing its usefulness.

List of publications by the author

This is a list of publications that were written by the author during the period of registration and relate to the development of the vibrating micro-probe.

First author

1. Claverley, J.D. & Leach, R.K. A vibrating micro-scale CMM probe for measuring high aspect ratio structures. *Microsystem Technologies* **16**, 1507-1512 (2009).

2. Claverley, J.D., Georgi, A. & Leach, R.K. Modelling the Interaction Forces between an Ideal Measurement Surface and the Stylus Tip of a Novel Vibrating Micro-scale CMM Probe. *Precision Assembly Technologies and Systems IPAS 2010*, 131-138 (2010).

3. Claverley, J.D. & Leach, R.K. A novel three-axis vibrating micro-CMM probe with isotropic probing forces. *Proceedings of the 11th euspen,* **1**, 59-62 (2010).

4. Claverley, J.D. & Leach, R.K. Verifying the capability of a three axis vibrating micro-scale CMM probe to operate in a non-contact mode. *Proc. 26th ASPE Annual Meeting,* Session IV (2011).

5. Claverley, J.D., Sheu, D.-Y. & Burisch, A. Assembly of a novel MEMS-based 3D vibrating micro-scale co-ordinate measuring machine probe using desktop factory automation. *IEEE International Symposium on Assembly and Manufacturing (ISAM),* 1-5 (2011).

6. Claverley, J.D., Burisch, A., Leach, R.K. & Raatz, A. Semi-automated assembly of a MEMS-based micro-scale CMM probe and future optimization of the process chain with a view to desktop factory automation. *Precision Assembly Technologies and Systems IPAS 2012*, 9-16 (2012).

7. Claverley, J.D. & Leach, R.K. Development of a three-dimensional vibrating tactile probe for miniature CMMs. *Precision Engineering* **37**, 491-499 (2013).

8. Claverley, J.D. & Leach, R.K. Three-dimensional characterisation of a novel vibrating tactile probe for miniature CMMs. *Proc LAMBDAMAP 2013.* 257-266 (2013).

Co-author

1. Smale, D., Ratchev, S., Segal, J., Leach, R.K. & Claverley, J.D. Assembly of the stem and tip of an innovative micro-CMM probe. *Euspen 9th International Laser Metrology and Machine Performance Conference,* 442-451 (2009).

2. Rajaguru P, Stoyanov S, Tang Y K, Bailey C, Claverley J D, Leach R K & Topham D. Numerical modelling methodology for design of miniaturised integrated products - an application to 3D CMM micro-probe development. *11th International Thermal, Mechanical & Multi-Physics Simulation, and Experiments in Microelectronics and Microsystems (EuroSimE),* 1-8 (2010).

3. Smale, D., Haley, S., Segal, J., Ronaldo, R., Ratchev, S., Leach, R.K. & Claverley, J.D. Utilisation of FIB/SEM Technology in the Assembly of an Innovative Micro-CMM Probe. *Precision Assembly Technologies and Systems IPAS 2010*, 105-112 (2010).

4. Stoyanov, S., Rajaguru, P., Tang, Y.K., Bailey, C., Claverley, J.D. & Leach, R.K. Reduced order modelling for risk mitigation in design of miniaturised/integrated products. *33rd International Spring Seminar on Electronics Technology (ISSE),* 402-407 (2010).

5. Leach, R.K., Claverley, J.D., Giusca, C., Jones, C.W., Nimishakavi, L., Sun, W., Tedaldi, M. and Yacoot, A. Advances in engineering nanometrology at the National Physical Laboratory. *Measurement Science and Technology* **23**, 74002 (2012).

Acknowledgements

Firstly, I would like to thank Mr. Frank Murphy, who recognised my talent for science and encouraged me towards physics and engineering. I only hope this thesis lives up to your expectations, Sir.

The technical work is this thesis was completed under the supervision of Richard Leach, from NPL. I would like to thank Richard for his guidance and support, and for turning my 'extremely's into 'very's, my 'drastic's into 'large's, and for deleting my 'extensive's, 'severe's and 'also's.

I could not have navigated the academic requirements of a PhD without the guidance of my supervisors at the University of Nottingham. I would like to thank Prof. Svetan Ratchev, and Dr Joel Segal for their patience, especially given the number of times they had to explain the difference between 'aim', 'objective', 'question', 'scope'. *&c.* I hope that I have finally got this sorted out!

My colleagues at NPL have been instrumental in helping develop my skills as a metrologist. Although there are too many to mention, some deserve a tip-of-the-hat: Chris Jones, Claudiu Giusca, Lakshmi Nimishakavi and Andrew Lewis. Thanks Chaps.

Throughout the project, there have been many people whose paths I have crossed. These helpers and visitors and collaborators made a lasting impression on the project, and on me personally. Special mention should go to (in no particular order), Dong-Yea Sheu, Arne Burisch, Florine Hiersemenzel, Alex Georgi, Anne-Laure Sudres and Dr. Chris Shaw.

This work was funded by the UK National Measurement Office Engineering and Flow Metrology Programme 2008 to 2011 and 2011 to 2014, by the EPSRC Grand Challenge project 3D Mintegration (EP/C5342212/1), and by the European Commission under the MIDEMMA Project, an FP7 project with contract number FoF-NMP-2011-5-28561.

My biggest thanks go to my family. To Mummy and Daddy, who taught me the importance of kindness, of calmness and of gin. To my sister Megan, whose confidence and intelligence inspires me.

And to Ian, whom I love; you truly are my better half. I would be lost without you.

This thesis is dedicated to my Grampa, who never saw it completed. I miss you.

Contents

List of Figures

List of Tables

Declaration

A majority of this thesis, submitted to the University of Nottingham for the degree of Doctor of Philosophy, is the work of the author alone. The specific contributions of others, which are properly referenced throughout the text, are noted here.

The work presented in this thesis relies heavily on the concept of a 3D vibrating micro-CMM probe, that was developed by Richard Leach, Ben Hughes and Alan Wilson at the National Physical Laboratory, UK. The concept was further developed as part of the EPSRC Grand Challenge project, 3D Mintegration. Some amount of modelling work was completed before the beginning of this PhD towards the proof-of-concept operation of the vibrating micro-probe, primarily by Stoyan Stoyanov at the University of Greenwich.

During the completion of this PhD, several colleagues at NPL, external collaborators and MSc students contributed work. Christopher Jones (NPL) assisted greatly in the development of the control and sensing software (section 5.3.1.4). Florine Hiersemenzel (formerly of King's College London) and Anne-Laure Sudres (formerly of Arts et Métiers, ParisTech) contributed considerable time to the completion of the experimental validation (specifically section 5.5.1 and section 5.5.4). Alex Georgi (formerly of the University of North Carolina, Charlotte, USA) assisted in the design of the Version 1 probe interface (as shown in figure 6.3), and was involved in the development of the concept of the surface interaction forces model (section 4.4.2).

The triskelion-flexure MEMS devices were fabricated at Cranfield University by Chris Shaw and Rob Dorey.

Some artwork was produced with the assistance of Julian Game from the NPL Graphics team, to the author's specifications.

Abbreviations

ASME	American Society of Mechanical Engineers
CAD	Computer aided design
CMM	Co-ordinate measuring machine
CNC	Computer numerical control
DRIE	Deep reactive-ion etching
EDM	Electro-discharge machining
FEA	Finite element analysis, often referred to as 'FE analysis'
FPGA	Field programmable gate array
HAR	High aspect ratio
HIPE	High internal phase emulsion
IC	Integrated circuit
ISO	International Organisation for Standardisation
LDV	Laser Doppler vibrometer
LIGA	'Lithographie, Galvanoformung, Abformung', or 'Lithography, Electroplating, and Molding'
MEMS	Micro-electro-mechanical system
METAS	Das Eidgenössische Institut für Metrologie, the NMI for Switzerland
MNT	Micro- and nanotechnology
NIST	National Institute of Standards and Technology, the NMI for the United States of America
NMI	National Measurement Institute
NMS	National Measurement System of the United Kingdom
NPL	National Physical Laboratory, UK
OPED	One pulse electro-discharge machining
PCB	Printed circuit board
PTB	Physikalisch-Technische Bundesanstalt, the NMI for Germany
PZT	Lead zirconate titanate, a common piezoelectric material
VCS	Virtual contacting sphere tip of the vibrating micro-probe
VDI	Verein Deutscher Ingenieure (Association of German Engineers)
VNCS	Virtual non-contacting sphere tip of the vibrating micro-probe
VSL	NMi van Swinden Laboratorium, the NMI for The Netherlands (now called NMi)
WEDG	Wire electro-discharge grinding

Chapter 1

Introduction

1.1 Motivation and aim

Current trends in manufacturing are inclined towards miniaturisation [1]. The ability of the manufacturing community to continue developments in millimetre and sub-millimetre scale production is directly dependant on the capability of the dimensional metrology community to carry out traceable measurements at these scales.

Developments in dimensional metrology often take their lead from the current state-of-the-art in manufacturing. Also, it is often the case that new avenues of research in dimensional metrology are first addressed at National Metrology Institutes (NMIs).

Currently, the state-of-the-art in dimensional metrology in terms of accuracy and 3D measurement is the micro-co-ordinate measuring machine, or micro-CMM. This thesis describes the work completed towards the development of a high precision contacting probing system for micro-CMMs. Specifically this work has the following **Thesis Aim**:

"to develop and operate a contacting probe such that it enables existing micro-CMMs to reliably measure sub-100 μm features in three dimensions to an uncertainty below 100 nm".

It is proposed that a micro-scale electro-mechanical system (MEMS) based vibrating micro-CMM probe can address this **Thesis Aim**. This thesis describes the development, modelling and initial validation of the **NPL vibrating micro-probe**.

1.2 Thesis objectives

There are several specific **Thesis Objectives** associated with the **Thesis Aim**. These **Thesis Objectives** will be further refined in the following chapters, including the definition of several specific **Research Questions**.

- **Thesis Objective 1** - To develop and validate methods to operate the vibrating micro-probe such that it can counteract surface interaction forces in 3D.
- **Thesis Objective 2** - To develop and validate a new concept of isotropy that can be applied to the vibrating micro-probe.
- **Thesis Objective 3** - To ensure the developed vibrating micro-probe can be used in an industrial metrology environment and can adhere to existing specification standards.

1.3 Approach and thesis structure

Chapter 1 has described the main motive behind this work, including defining an overall **Thesis Aim** and **Thesis Objectives**.

Chapter 2 introduces some amount of background information to give context to this work. As part of this background information, a set of requirements are defined that all micro-CMM probes should adhere to. Also, a review of the current state-of-the-art in terms of micro-CMM probing technology is presented. A wide range of existing technologies are discussed, with specific reference to the requirements. From this, the **Thesis Objectives** for the work can be refined.

In Chapter 3 the concept, design and manufacture of the vibrating micro-probe will be presented. This represents the background knowledge to the thesis, on which the foreground knowledge, developed during this PhD, relies. The research approach that will be used to address the **Thesis Aim** is described. This overview will describe the basic tools that will be used to demonstrate the operation of the vibrating micro-probe. Also, a clear set of metrics for success will be defined in the form of specific **Research Questions**, which can be referred to at all stages of the thesis.

Chapter 4 is the first technical chapter of the thesis. The theoretical and modelling work completed, with respect to the development of the vibrating micro-probe, is described in detail. An operational model is developed to define the operation of the micro-probe, especially with respect to the surface interaction forces, as defined in **Thesis Objective 1**. A mechanical model of the micro-probe is also developed to define isotropic operation, as required for **Thesis Objective 2**. These models will be used to define the theoretical capability of the probe and to define several initial operating conditions, that may be used to define the requirements of the experimental validation.

In Chapter 5 the experimental work completed towards validating the capability of the probe is presented. As required by **Thesis Objective 1**, the operation of the micro-probe will be validated, especially with respect to the surface interaction forces. The isotropic operation of the probe will also be validated experimentally, as required by **Thesis Objective 2**. The experimental apparatus and procedures will be described in detail. A dedicated design of experiment section will clearly define the tests to be completed, and the results of these tests will be presented and discussed. Also, a preliminary uncertainty analysis will be completed.

The requirements of **Thesis Objective 3** are directly addressed in Chapter 6. Several concept operational strategies for the vibrating micro-probe are introduced, along with a detailed description of its adherence to existing specification standards. The rules and strategies for operating the vibrating micro-probe in a real measurement environment, as well as suggested operational parameters, will be defined, with justification and comparison to existing systems.

The work will be concluded in Chapter 7, which will especially address the successful attainment of the **Thesis Objectives**. The specific **Research Questions**, which act as metrics for the

success of the research, will also be answered. Finally, future work will be suggested that will help continue development of the probe towards the requirements of the **Thesis Aim** and beyond.

The thesis is appended by several sections which contain information pertinent to the completed work.

Chapter 2

Context and literature review

2.1 Introduction to context and literature review

In order to fully justify the **Thesis Objectives**, and define specific **Research Questions**, context is required with regards to co-ordinate metrology, micro-CMMs and micro-CMM probes. This chapter will give some background information into the area of micro-CMMs.

Following the definition of this background information, a review of existing micro-CMM probes will be completed. Several main groupings of micro-CMM probes will be identified based on the major technology used to operate them. Any validation tests performed on these micro-CMM probes will be discussed.

From the literature review, the current capabilities of micro-CMM probes can be identified, as well as their limitations. The identified capabilities will allow for the definition of a set of requirements for micro-CMM probes. The identified limitations will allow a clear definition of the gaps in existing knowledge and the lack of capabilities of existing micro-CMMs to be defined. These knowledge gaps will, in turn, help to define the requirements for the operation of the vibrating micro-probe.

2.2 Background and context

A short introduction to pertinent background information will now be given. This information, related to the areas of dimensional metrology, co-ordinate metrology and micro-co-ordinate metrology, will provide context for the rest of this work.

2.2.1 Dimensional metrology

Any introduction to dimensional metrology can fill (several) text books [2, 3, 4, 5, 6]. However, in the interest of brevity, several definitions can be presented that will be useful in the context of this thesis.

- The metre is defined as

  "the length of the path travelled by light in vacuum during a time interval of $\frac{1}{299\,792\,458}$ *of a second"* [7].

- Calibration is an operation that establishes a relation between quantity values with measurement uncertainties provided by measurement standards and corresponding indications with associated measurement uncertainties. The act of calibration then uses this information to establish a relation for obtaining a measurement result from an indication [8].

- Traceability in measurement is the concept of establishing a valid calibration of a measuring instrument or measurement standard, by a step-by-step comparison with better standards up to an accepted or specified standard. In general, the concept of traceability implies eventual reference to an appropriate national or international standard [9].

- Precision engineering is a discipline concerned with the production, manufacture and assembly of parts with low tolerances. The processes tend to be highly accurate, highly repeatable and highly stable over time [10].

Following these four brief definitions, the area of co-ordinate metrology can now be introduced, which is one of the main manifestations of dimensional metrology in manufacturing engineering.

2.2.2 Co-ordinate metrology

Following the manufacturing revolution, pioneered by the development of the assembly line and automotive production, the need for accurate dimensional engineering metrology became instantly apparent. These assembly lines were involved in mass production of complex machinery and relied on the standardisation and interchangeability of parts to ensure that all the output products were of identical high quality [2].

The development of the co-ordinate measuring machine (CMM) in the mid-20th Century allowed for the automation of the ever more complex measurements required by the production industry. A CMM is formally defined as any measuring device with the means to move a probing system and the capability to determine spatial co-ordinates on a workpiece surface [11]. Until the development of the CMM, dimensional metrology was usually performed by a dedicated core of technicians, making use of a suite of metrological instruments and rigs specifically designed for

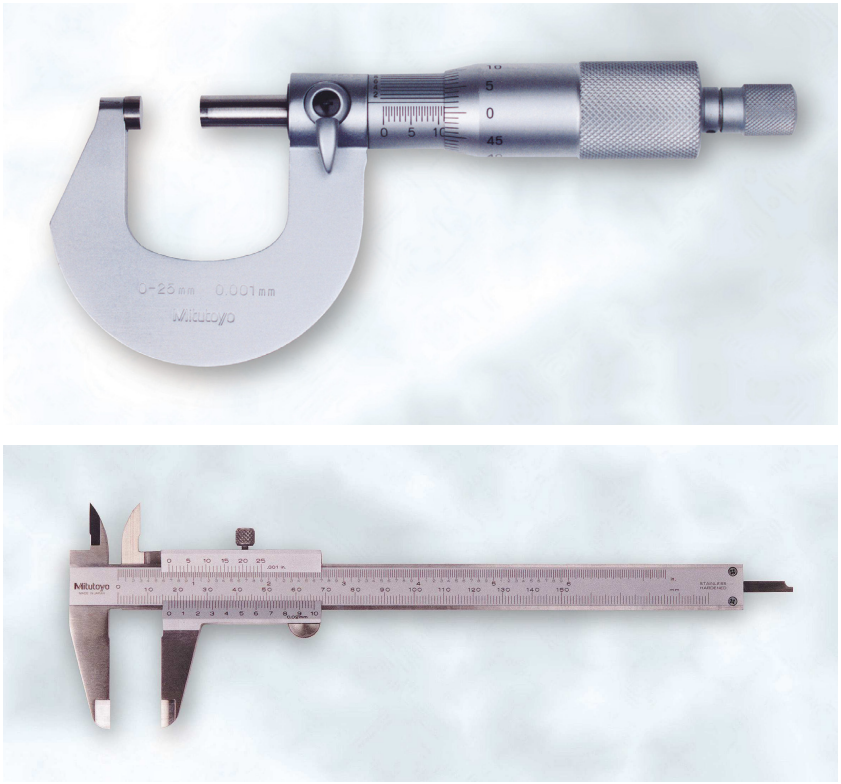

Figure 2.1: Instruments used for dimensional metrology: a micrometer (top) and a pair of vernier callipers (bottom). Image courtesy of Mitutoyo

each measurement task. A selection of classical length metrology tools is shown in figure 2.1. To ensure traceable measurement, each instrument had to be calibrated. Also, measurements often relied on the skill and knowledge of the operator to take the measurement accurately and efficiently, wasting as little time as possible.

The arrival of the CMM did not necessarily increase the accuracy of the measurements taken; but instead it allowed for automation, easily facilitating multiple measurements on multiple samples. It consolidated many of the previously mentioned metrological tools into one instrument, and relied much less on the skill and knowledge of the operator [6].

Early CMMs were manually driven, relying on probing systems that were triggered with physical contact switches. Modern CMMs are now usually operated using computer numerical control (CNC) software, and accurate strain gauge based probing systems. Although both early CMMs and modern CMMs rely on the thermal and mechanical stability of granite metrology blocks, recent developments have resulted in high accuracy CMMs instrumented with precision glass or ceramic scales, and even, for traceability, linear interferometers. This enables the most modern CMMs to boast less than 10 nm resolution on their measurement scales. An image of a typical CMM is shown in figure 2.2.

The accuracy of any CMM can be traced back to the squareness of the machine's axes, as well as the linearity, straightness and rotational effects on those axes [6, 12]. The accuracy of the CMM

Figure 2.2: A typical bridge type CMM

is determined at a predefined temperature, atmospheric pressure and relative humidity, and also free from any external vibrations and electric and magnetic interference.

CMMs are a common sight in many precision manufacturing facilities. CMMs have been invaluable in increasing the speed of measurements taken in a production environment. As such, CMMs have been the subject of extensive investigations in research environments. The use of CMMs in research environments has helped develop a better understanding of measurement uncertainties in manufacturing, as well as help identify areas for improvement in manufacturing processes and precision engineering.

The prevalence and extensive use of CMMs in industry, however, has meant that developments in the area of co-ordinate metrology have been led almost exclusively by the requirements of precision manufacturing engineers.

2.2.3 Micro-CMMs

An essential requirement of CMMs is that they should stay in step with developments in precision manufacturing. The current state of micro-machining and production requires many instruments to be used to measure the dimensions of micro- and nano-technology (MNT) parts. Increased complexity, high aspect ratios and structures that may be constructed from materials that are

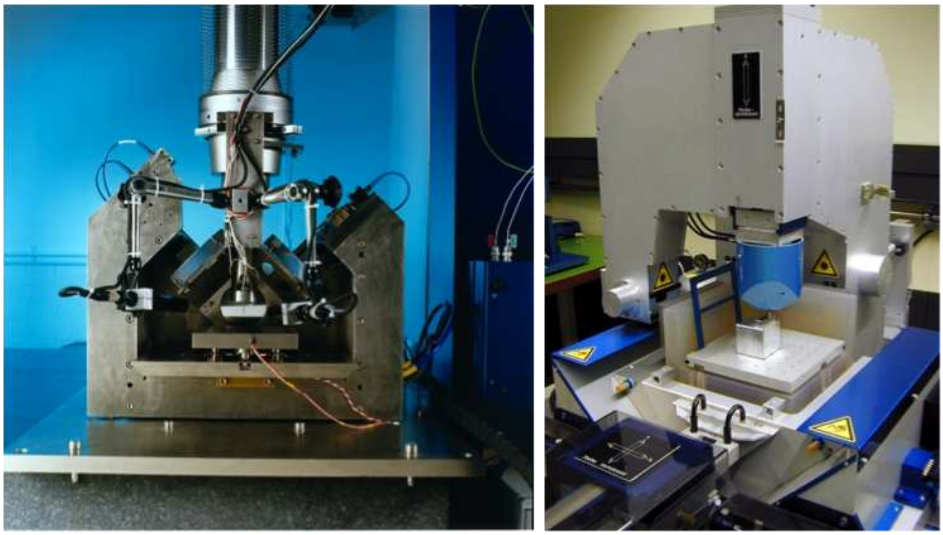

Figure 2.3: the NPL Small CMM developed in 1999 (left) and the METAS Ultraprecision CMM developed in 2001 (right – courtesy of METAS, CH)

difficult to contact with a mechanical probe (for example, polymers or bio-materials [13]) are additional problems beyond the small dimensions and tolerances [3].

An early solution to the lag in metrological capability was to custom-build a CMM capable of micro-scale measurements. Indeed, many National Measurement Institutes (NMIs) and private laboratories built their own micro-scale CMMs to meet this demand. The first recognisable and operational micro-CMM was developed at the National Physical Laboratory (NPL) in 1999 [14, 15]. The NPL Small CMM (SCMM) was retrofitted to a classical CMM and was capable of measuring to a volumetric uncertainty of 200 nm within a measurement volume of 50 mm by 50 mm by 50 mm [16]. The SCMM was fully traceable, by virtue of its three orthogonal interferometers. A concurrent project at the Technical University of Eindhoven (TUE, Eindhoven, NL) designed and built a micro-CMM that would act as the prototype for a commercial machine [17]. Several other micro-CMMs were developed by NMIs and other research institutions over the following years [18, 19, 20, 21, 22, 23]. Two custom-built micro-CMMs, also known as µCMMs or miniature CMMs, are shown in figure 2.3.

In this thesis, micro-CMMs will be defined, according to guideline VDI/VDE 2617 Part 12.1 - *Accuracy of co-ordinate measuring machines - Characteristics and their checking - Acceptance and reverification tests for contacting CMMs measuring micro-geometries* [24], as

> "*a contacting CMM (of various types and makes) which is used to measure geometries whose dimensions range between a few micrometres and approximately 1 mm*".

This guideline, published by the Verein Deutscher Ingenieure (Association of German Engineers), is used to define the micro-CMM in this thesis as it is the only standardisation organisation to have done so.

Figure 2.4: The Zeiss F25 micro-CMM (left) and the IBSPE Isara 400 Ultra Precision CMM (right – courtesy of IBSPE).

Recent years have seen some commercial groups develop micro-CMMs, typically with tens of millimetres range and tens of nanometres accuracy in the x, y and z directions.

The Zeiss F25 micro-CMM [25] was developed by Carl Zeiss AG (Oberkochen, DE) in collaboration with TUE [17, 26]. The F25 was developed in direct response to the need for quality assurance through the measurement of size, form and position of small manufactured parts. The measurement volume is one cubic decimetre (100 mm by 100 mm by 100 mm), the resolution on the glass-ceramic scales on all measurement axes is 7.8 nm and the quoted MPE_E (the maximum permissible error of indication for size (or length) measurements, now called $E_{L,MPE}$) is 250 nm [27].

The Isara 400 Ultra Precision CMM by IBS Precision Engineering (IBSPE, Eindhoven, NL) was developed to address the problem of off-Abbé measurement by aligning three linear interferometers to orthogonally intersect at the centre of the spherical probe tip [28]. The Abbé principle states that if errors in parallax are to be avoided, the measuring system must be placed coaxially with the axis along which the displacement is to be measured on the work piece [29, 30]. The measurement volume is (400 mm by 400 mm by 100 mm), the resolution on the laser interferometer scales on all measurement axes is 1.6 nm and the quoted 3D measurement uncertainty is 109 nm [31, 32]. Two commercially available micro-CMMs are shown in figure 2.4.

Several other micro-CMM platforms exist (*e.g.* [33, 34]) or are being developed (*e.g.* [35]). However, a full review of the current micro-CMM landscape is not required for this introduction and is outside of the scope of this thesis, which is focused on micro-CMM probes. Several reviews of existing micro-CMMs can be found elsewhere [3, 36].

Micro-CMMs are becoming more common in manufacturing and research environments, and have many commercial applications in precision manufacturing; especially medical, optical and

consumer parts. Their importance to current developments in precision manufacturing is evident from the current number of UK national and EU Framework 7 projects that are involved in the enhancement of micro-CMM technology, *e.g.* the funding sources for this PhD being the UK National Measurement Office, the EPSRC and the European Commission.

2.2.4 CMM Probes

Extensive research has been carried out in the area of CMM probing, ever since the inception of the field in 1973, when Sir David McMurtry invented the first "touch trigger" CMM probing system [37]. Since then, further refinement of these probing systems has resulted in high precision contacting probing systems which, when coupled with modern CMMs, can result in dimensional measurement on 3D parts with an uncertainty of 1 µm or better [38]. However, probe development has lagged behind for some years, with most CMM manufacturers content with simply shrinking their current probe technology to fit the ever more accurate machines. Recent developments in high accuracy probing tend to rely on piezo-resistive strain gauges or optical detection mechanisms to increase the repeatability of triggering for more accurate surface detection.

It quickly became essential that new probing systems were designed to complement the high precision motion platforms that are a constituent part of micro-CMMs. New designs for contacting probing systems suitable for micro-CMMs, also known as micro-CMM probes, are an essential part of development in this area, because a major contribution to the uncertainty of micro-scale co-ordinate measurement can be attributed to the contacting probing system [39].

Early probing systems were physical contact switches. During operation, the probes would report contact with the surface of a workpiece by activating a pilot light, or any such other indicator. At such a time as indicated by the probe, the operator could record positional information from the scales of the CMM and build up dimensions of the workpiece. Subsequent developments to CMM probes enabled them to perform length measurements over a small distance, therefore, further reducing errors due to stylus deformation (which are minimised initially due to the stiffness of the styli). Also, to enable the early, manual, CMMs to operate under CNC, the probes became more than pure analogue indicators, instead being instrumented with strain gauges and mechanical flexures.

Research in the area of CMM probing has focused on designing more versatile probe heads that still maintain the measurement accuracy demanded by modern manufacturing standards. A major breakthrough in CMM probe research was the development of the scanning head; able to maintain contact with the measurement surface while scanning a path taking thousands of data points [39]. Developments have also included the use of reflexing heads that incorporate precision angle measurement into the probe system, enabling it to index to certain angles during measure-

ment. These, and other, developments enable CMMs to become more versatile, measuring truly three-dimensional objects without the need for moving the artefact for access.

Certain requirements of micro-co-ordinate metrology cannot be realised by simply using classical CMM probing systems with suitably small stylus tips. Instead, significant redesign of both the probing system and micro-manipulation platform are required. However, following recent developments in micro-manipulation, it has been suggested that micro-CMMs are now hindered mostly by the inaccuracy, reduced sensitivity and reduced versatility of existing probing systems [39, 40]. The main sources of error of existing micro-CMM probes will now be reviewed.

2.3 Review of existing micro-CMM probes

In this section, the wide range of technologies developed to enhance micro-CMM probes beyond that of classical CMM probing systems will be discussed. These technologies were usually developed with certain capabilities in mind, such that specific requirements are addressed. For each major grouping of technologies, the technical specifications of several constituent micro-CMM probes will be reported and discussed, focussing on the main unique capability of each system. Following this, the main limitations of the grouping will be discussed.

The main groupings considered as viable technologies for micro-CMM probe development are: mechanical probes, silicon-based probes, optomechanical probes and vibrating probes. Within these groupings a wide range of technologies are employed to realise the final working micro-CMM probes. Also, several diverse testing procedures are used to validate the capability of the probes, both off- and on-machine. It should be noted that these groupings do not exactly correlate with that defined within VDI/VDE Guideline 2617 Part12.1 [24]. However, the four groupings were chosen to better correlate with both technology and operating principles.

Several other reviews of micro-CMM probes exist elsewhere, including Bos *et. al.* [36], Weckenmann *et. al.* [39] and Leach [3]. However, there have been several advances since these reviews were published.

Finally, it should be noted that, due to the recent development of micro-CMMs and, therefore, the recent need to develop new micro-CMM probes, a great deal of the research discussed here occurred simultaneously. To some minor extent, the four main groupings described here indicate a chronological description of the developments in this area, but there is considerable overlap.

2.3.1 Mechanical micro-CMM probes

At the onset of the development of micro-CMM platforms, the obvious technology suitable for micro-CMM probes was that which is used for classical CMM probes. These highly refined mechanical probes were based on the same concepts as many classical CMM probes, but were

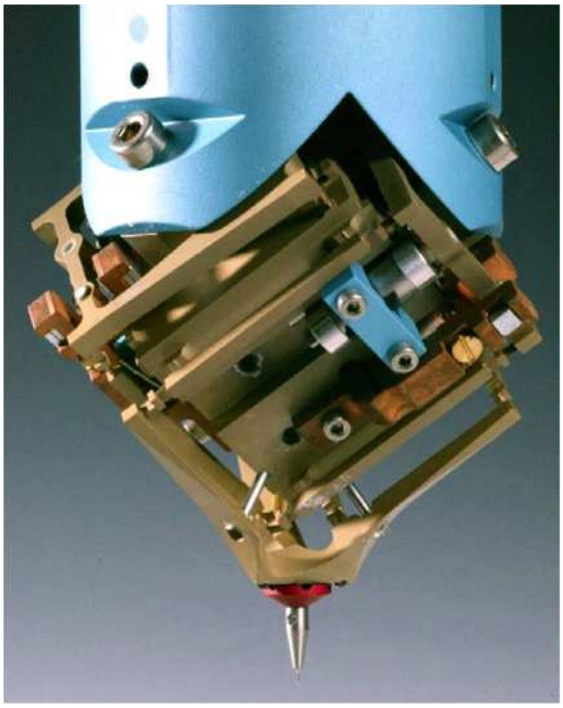

Figure 2.5: Image of the METAS TouchProbe (courtesy of METAS, CH)

optimised for sensitive detection and low force probing. Similar optimisation exercises have taken place for classical CMM probes with specific applications in mind [41]. Also, some consideration was taken to reduce the volume of the mechanism within the measurement volume of the micro-CMM and to reduce mass.

2.3.1.1 METAS TouchProbe

The METAS TouchProbe is a mechanical CMM probe head refined to obtain a probing error of approximately ±10 nm [42, 18]. The operation of the probe relies on precision flexural hinges and inductive sensors. The mechanical section of the probe is manufactured from a single block of aluminium using electro-discharge machining (EDM), which negates the need for assembly. An image of the probe is shown in figure 2.5.

The mechanics of the METAS TouchProbe are designed such that the stylus tip of the probe has only three degrees of freedom, and that all the axes of the probe have the same orientation with respect to gravity, resulting in isotropic stiffness. The mechanical flexures of the METAS TouchProbe are 60 µm thick, resulting in a stiffness at the probe tip of 20 $\mathrm{N\,m^{-1}}$ (isotropic). As the resulting moving mass of the probe is 7 g, the deformation of the flexures due to gravity would be high, so a set of permanent magnets are used to compensate. The moving mass of the probe (7 g) is too high to not result in dynamic contact forces capable of damaging the measurement surface during probing, so a further mechanism was developed to compensate. Research has been conducted into the damage caused to the measurement surface and the CMM probe tip while point probing [43] and scanning [44], which is closely linked to the various effects on elastic

compression of surfaces due to applied pressure fields [45]. These effects are especially important considering the range of probe tip diameters, from 100 µm to 1 mm. The resulting probing speed used to reduce surface damage is 1 mm s^{-1}. The stylus assembly is kinematically mounted to the probe head and is magnetically secured. This system allows for easy replacement, making the use of this probing system relatively simple.

Various testing methods have been employed to validate the capability of this probe. Initially, the probe was installed onto a linear measuring machine, and was used to measure the length of a calibrated gauge block. The repeatability of these measurements was 5 nm, and the linearity error of the probe when deflecting 150 µm was 20 nm [42]. More complete tests, including full 3D characterisation of the probe errors, were completed once the probe was installed on a micro-CMM [18]. This probing system was designed to be installed only on the METAS precision micro-CMM. The METAS TouchProbe is commercially available [46].

2.3.1.2 NPL Small CMM probe

A similar research based probe was developed for the NPL SCMM. The basis of the design was that, during the development of the NPL SCMM [14, 16, 40, 47], no suitable probe could be found that would operate both isotropically, and with a low enough probing force to ensure no plastic deformation of the workpiece during measurements [43]. The probing force calculations by Pril [48] and van Vliet [43] suggest that a 1 mm diameter spherical probe tip would damage an aluminium measurement surface if operated at an approach speed higher than 1 mm s^{-1} and with a probing force higher than 10 mN. To attain these requirements, a new mechanical, flexure based probe with capacitance sensors was designed. Peggs [14] states that the design of the probe was modified from Pril [48, 49, 50] and Yang [51].

The NPL SCMM probe had a triskelion (three-legged) design and consisted of three beryllium-copper (Be-Cu) flexures connecting three tungsten carbide tubes to a central island, which supported the stylus and a 300 µm diameter sphere. The flexures were fitted with capacitance sensors. The design of the NPL SCMM probe is shown in figure 2.6.

The probe was determined to have near isotropic stiffness, of approximately 10 N m^{-1}. The working range of the probe is 20 µm, and the resolution of the capacitance sensors allows for 3 nm resolution on stylus tip motion. An image of the final realised SCMM probe is shown in figure 2.7.

The CMM probe was mounted onto a host CMM that was fitted with three orthogonal mirrors, the positions and rotations of which were measured using three dual-beam interferometers. Once installed onto the NPL SCMM, the resulting expanded uncertainty of the system ($k = 2$) is 38 nm. The SCMM probe contributes approximately 14 nm to this overall 3D volumetric uncertainty. No published work reports any of the tests completed on this probe before installation on the

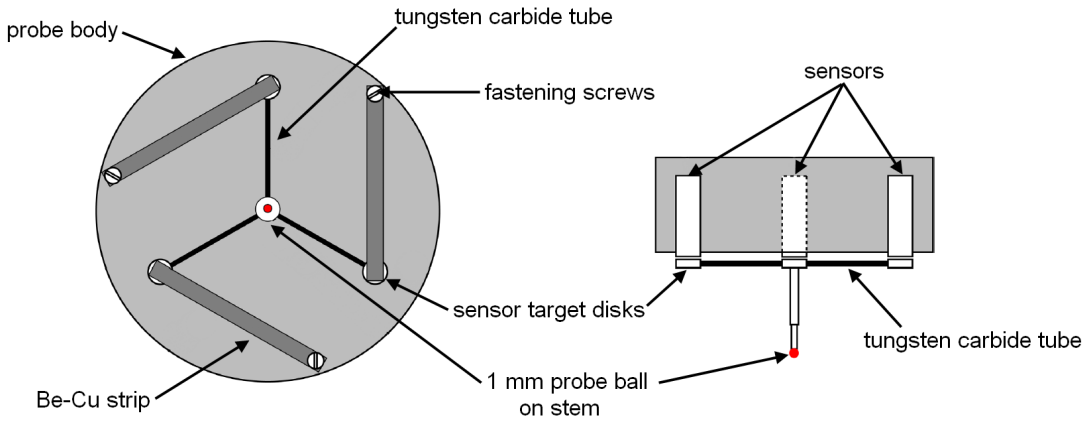

Figure 2.6: Schematic of the NPL Small-CMM probe from below (left) and from the side (right)

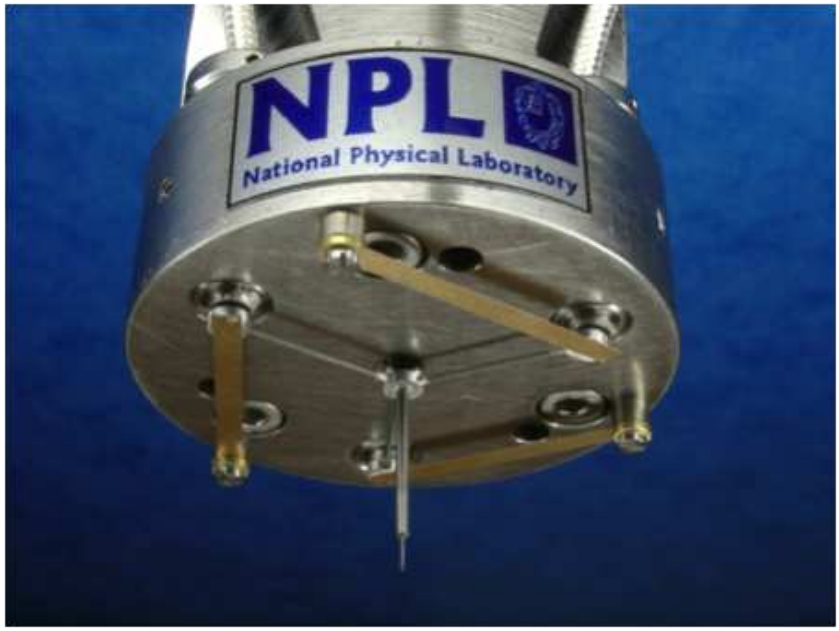

Figure 2.7: Image of the NPL Small-CMM probe

NPL SCMM. However, this probe was made available to purchase commercially, and has been involved in several research projects [52].

2.3.1.3 IBSPE Triskelion probe

During the development of a new ultra-precision micro-CMM, the Isara series from IBS Precision Engineering (IBSPE, Eindhoven, NL) [32, 31], a probe based on the NPL SCMM probe was designed and built. This probe refined many of the aspects of the NPL SCMM probe, including the manufacture of a monolithic flexure body.

The first generation of the IBSPE ultra-precision touch probe was implemented on the Isara 100, which was based on an original design by Ruijl [53, 54]. As with the NPL SCMM probe, the IBSPE touch probe consisted of a triskelion flexure system, with capacitance sensors. The monolithic manufacture of the flexure body, which included the capacitance sensor targets, allowed for greater control over the geometry and function of the flexures, and also reduced the errors associated with assembly. As with the NPL SCMM probe, the main body (apart from the flexures, stylus and stylus tip) was manufactured from Invar to ensure low thermal expansion.

Several tests were completed on the IBSPE Triskelion probe to validate its performance. These included determination of the sensitivity of the probe, through controlled displacement of the stylus tip. This displacement was measured using a laser interferometer. When the stylus tip is displaced by 5 µm in 3D, the probe exhibits error of less than 15 nm.

Following the development of the Isara 100 and the ultra-precision touch probe, IBSPE began production of the Isara 400 [55] and also a line of commercial Triskelion probes [56]. At the time of writing, three variants of the Triskelion probe are available, each with unique properties designed for different applications. The specifications of the three Triskelion probe variants are summarised in table 2.1.

Table 2.1: Specifications of the three commercially available Triskelion probes from IBSPE [56]

	Triskelion A-250 standard probe	**Triskelion B-35 micro-tip probe**	**Triskelion C-500 HAR probe**
Probe tip radius / µm	250	35	500
Suspended mass / mg	160	75	300
Probe stiffness (at tip) / N m^{-1}	70	x and y: 13 z: 20	x and y: 35 z: 113
Resolution (RMS) / nm	2	2	2
3D measurement uncertainty of tip deflection / nm	<15	<20	<20

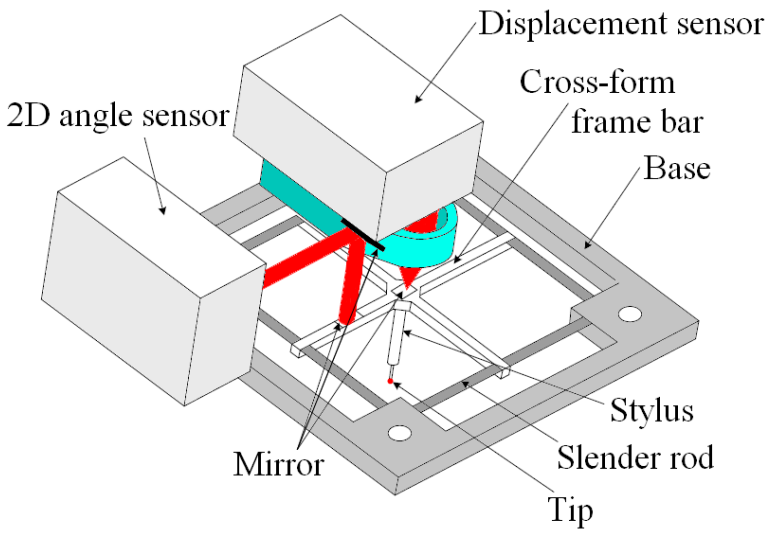

Figure 2.8: Schematic of the DVD-pickup head micro-CMM probe from STUT, TW

2.3.1.4 DVD-pickup head probes

A 3D mechanical probe design has been developed in the Southern Taiwan University of Technology (STUT), Taiwan, which uses DVD-pickup heads as the sensing element [57]. The DVD-pickup heads are intended to be significantly cheaper than any capacitance sensor-based detection system, but still maintain a similar level of accuracy. The probe uses a set of slender tungsten rods as flexing elements. A sphere-tipped stylus is attached to the centre of a cross-form frame, which is in turn suspended from the slender rods. The crossed elements are instrumented with micro-mirrors that form the reflecting part of the optical detection system [58]. A schematic of the probe is shown in figure 2.8.

During testing, the 2 mm long stylus was tipped with a 0.3 mm diameter ruby sphere. Several other parameters were determined during testing. The most important of these is the probing error, which is close to 100 nm in 3D, or 50 nm in one axis. The triggering force is near isotropic at 0.08 mN, and it can be estimated that the actual contact force will be near to 0.1 mN. During the testing of the probe, the thermal drift of the probing point was determined to be about 10 nm per hour. It was suggested that this is mostly due to the focus drift on the DVD-pickup heads, rather than the deformation of the suspension structure and the stylus.

The main virtue of the probe is the price, estimated at around 100 USD, which is significantly cheaper than most other micro-CMM probes available at this time. However, little further work seems to have been completed with regards to commercialisation.

A similar probe, based on the use of DVD pickup heads as sensing elements, has been developed at Hefei University of Technology [59] [60]. This system comprises a floating plate, suspended by four micro-wires which act as flexures. The movement of the floating plate is detected by

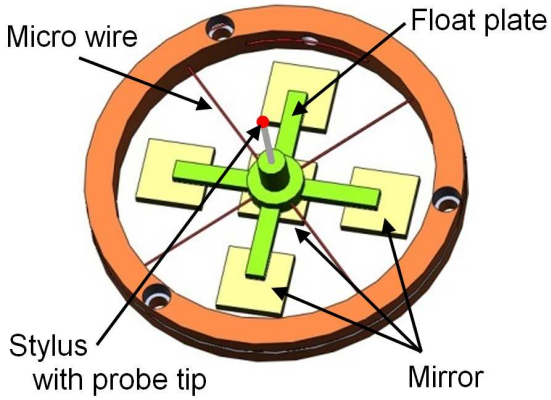

Figure 2.9: Schematic of the DVD-pickup head probe from Hefei, CN

four DVD-pickup heads which are used as focus sensors. A schematic of the probe is shown in figure 2.9.

During testing, the probe was shown to be near-isotropic in the xy-plane, with a contact force of about 109 µN. Although no formal determination of the probing error is determined, the standard deviation of the determination of the contact point was estimated at 10 nm. This value was determined through the use of a simple electrical detection circuit. A recent enhancement to this system was the inclusion of a laser interferometer onto the centre of the floating island to detect z contact to a high accuracy [61].

2.3.1.5 Summary of existing mechanical micro-CMM probes

In order to initiate the field of micro-co-ordinate metrology, a set of suitable contacting probes had to be developed to operate with the previously-developed high accuracy manipulation stages. Existing CMM probes were no longer suitable because of high probing forces when used with small diameter stylus tips (below 1 mm).

Several other probes exist that fit into the mechanical category. These have not been included because they were either initially developed and no further work has been completed on them [62, 63], little or no literature can be found that tests the probing error of the system [64], they are in the very early stages of development [65], or some aspect of their design does not qualify them as a micro-CMM probe [66, 67].

One major area of development in micro-scale probes is the need to reduce the probing force. At the micro-scale, where these probes will be operating, errors due to high probing forces are in the same order of magnitude as the desired probing accuracy. The pressure field generated at the surface when a miniature tip comes into contact may be sufficient to cause plastic deformation [43]. Reducing the contact force during measurement will greatly reduce the possible damage caused and increase the accuracy of the measurement.

Reduced stylus diameter results in a more compliant system that requires more sensitive detection methods than are used on conventional, mechanical probe heads. To address the need for low force probing, with high detection sensitivity, a class of probes was developed that rely on the precision manufacture of silicon (Si) flexures. This grouping of micro-CMM probes is therefore called "silicon-based probes".

2.3.2 Silicon-based micro-CMM probes

One solution to reduce the probing forces imparted on a measurement surface calls for the use of silicon flexures, membranes or meshes to suspend the stylus [50].

The design and production of silicon-based micro-probes takes advantage of the well-developed manufacturing techniques of the integrated circuit (IC) industry. Etching and deposition can be used to produce highly complex designs, consisting of many functional materials and mechanical features (flexures, hinges, membranes, *etc.*).

Using silicon to suspend the microprobe reduces the overall contact force exerted on the measurement surface and also serves to make surface contact detection more sensitive. Increased probe sensitivity becomes ever more essential as the stylus diameter is reduced to allow better access to small and high aspect ratio features and micro-structures. The actual detection mechanism can take various forms, either optical or electrical.

Several varied detection mechanisms were theorised by Haitjema *et. al.* [50]. Optical detection techniques were suggested where the deflection of the stylus alters the orientation of a mirror or prism that, in turn, alters the position of a reflected laser, similar to the previously mentioned DVD-pickup head probes. Alternatively, interferometric measurements could be taken from the top of the stylus. The displacement of the stylus could also be detected by using a capacitor sensor.

However, one of the most common detection methods for silicon-based micro-probes is the use of piezoresistive sensors. Several commercial probes are available that use this detection technique.

It should be noted that silicon-based micro-CMM probes, by virtue of their use of mechanical flexures, are a unique subset of the group of mechanical probes. As such, a useful property of silicon as a mechanical material is that, due to its brittle nature, it will fail (*i.e.* snap or break) rather than over strain. This will result in an unambiguous definition of a damaged probe.

2.3.2.1 Xpress Gannen probe

The Gannen probe was developed at TUE [49] and commercialised by the company Xpress Precision Engineering (Xpress PE, Eindhoven, NL) [68]. The initial prototype has the flexures manufactured from silicon, but an aluminium suspension body was then glued in place to allow

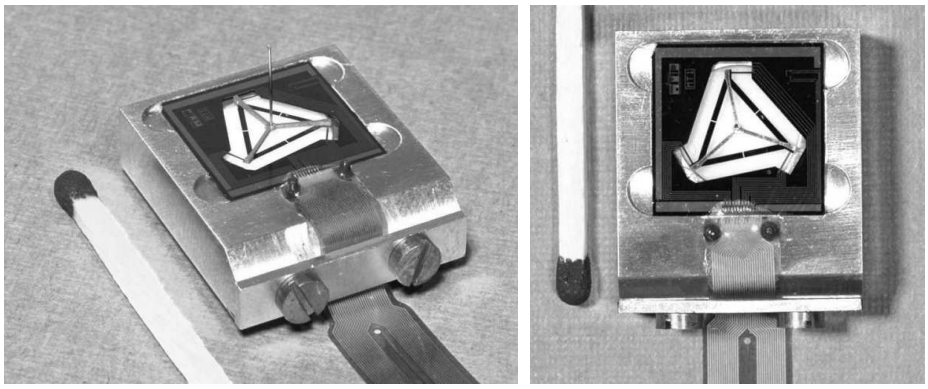

Figure 2.10: Images of the TUE silicon microprobe prototype: isometric view (left) and top view (right) [49]

the assembly of a sphere-tipped stylus. The sensors for the probing system are poly-silicon strain gauges. It is usual, in more classical mechanical micro-CMM probes, for the strain gauges to be assembled onto the flexure elements manually, using adhesive. However, this assembly can cause large hysteresis to occur during use. Therefore, taking advantage of the MEMS manufacturing techniques available for silicon-based micro-probes, the strain gauges and suspension elements were manufactured through vapour deposition directly onto a silicon substrate. Subsequently, the strain gauges and the suspension elements were etched in one step. This manufacturing process eliminated all hysteresis due to strain gauge assembly [50]. An image of the prototype Gannen probe is shown in figure 2.10.

During testing, the probe system exhibited less than 30 nm linearity error over deflections of several micrometres.

The development of this probe was continued by Bos [69], whereby the entire probe (apart from the stylus) was manufactured using silicon processing. Therefore, no assembly of an aluminium suspension body was required. The final probe, the Gannen XP [68] has a moving mass of 25 mg and isotropic stiffness of 480 $\mathrm{N\,m^{-1}}$. An image of the Gannen XP probe is shown in figure 2.11.

During testing, the Gannen XP probe exhibits a 10 nm linearity error over deflections of approximately 5 µm. A thorough description of the development and initial testing of the Gannen probe can be found in [69].

As with the commercial probing system developed by IBSPE, the Gannen probe by Xpress has several configurations depending on measurement requirements [68]. These configurations include various stylus tip diameters, down to 50 µm. The technical specifications of these various probes are shown in table 2.2.

2.3.2.2 PTB Boss-probe

Research at the Physikalisch-Technische Bundesanstalt (PTB, Braunschweig, DE) has resulted in the development of a silicon based micro-CMM probe that can also be used as a miniature

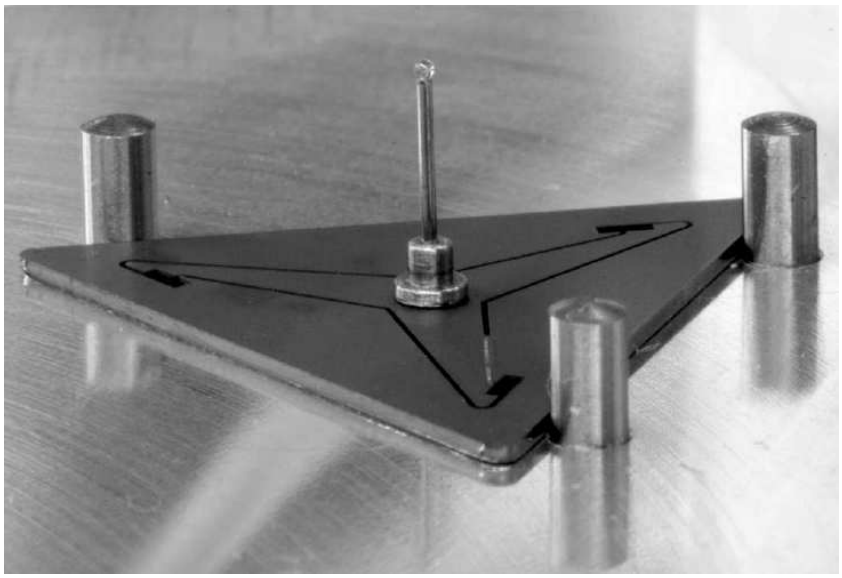

Figure 2.11: Image of the fully realised Gannen probe [69]

Table 2.2: Various specifications of micro-CMM probe available from Xpress PE [68]. A dash (-) indicates that no information was available at the time of writing.

	Gannen XP	**Gannen XM**	**Heimen series**
Available tip diameters / μm	120, 300, 500	50, 120, 300, 500	various
Repeatability / nm	2	4	-
Combined 3D uncertainty / nm	45 ($k=2$)	156 ($k=2$)	270 ($k=2$)
Mass / mg	50	50	25
Stiffness at probe tip / N m^{-1}	400 (isotropic)	x and y: 10 z: 50	-
Contact force (typical) / mN	0.4	0.01	-

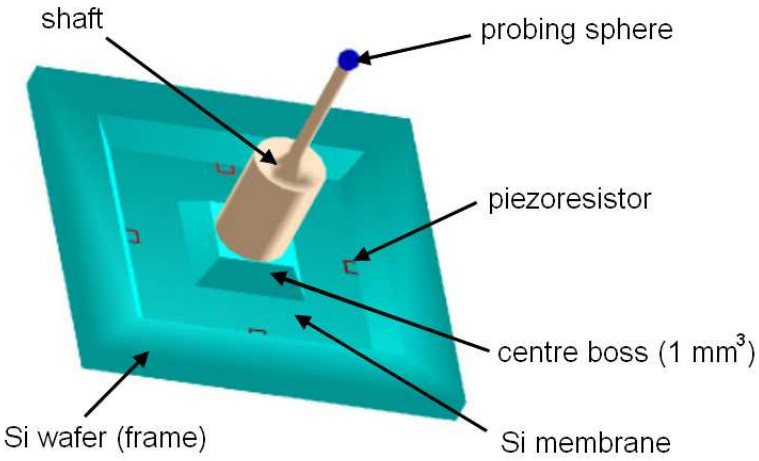

Figure 2.12: Schematic of the Boss-probe developed at PTB

force sensor [70]. This probe is constructed from a silicon membrane with a central locating 'boss' structure. A micro-stylus is suspended from the boss structure. The silicon membrane has had piezoresistive strain sensors etched onto it. These sensors detect deformation of the membrane that results from probe contact with a measurement surface [71]. A schematic of a prototype Boss-probe is shown in figure 2.12.

Initial probing experiments with this prototype design showed that the Boss-probe exhibited significant anisotropy *i.e.* it had significantly different stiffness properties in the lateral and vertical directions [72]. The properties of the Boss-probe prototype are shown in table 2.3. This anisotropy results in a force measuring range of up to 10 mN in lateral probing directions and up to 1.5 N in the vertical direction [73]. The stiffness in the vertical direction was also determined using a micro-force sensor by Dai *et. al.* to be about 3.6 kN m^{-1} [74].

To further develop the Boss-probe concept, several concept probes were designed and modelled [75]. The aim was to directly address the anisotropy of the system. The modelled systems included the prototype single membrane Boss-probe (the original prototype design), two dual membrane systems (one parallel design, where the two membranes were positioned in the same orientation, and another inverse design, where one membrane was positioned upside down compared to the other), and two flexure systems (one four beam and one eight beam system. The

Table 2.3: The properties of the Boss-probe in the lateral and vertical probing directions [73]

	Lateral probing	**Vertical probing**
Resolution / nm	3	5
Repeatability / nm	<10	<20
Stiffness / mN µm^{-1}	0.1	55
Measuring range / µm	700	50

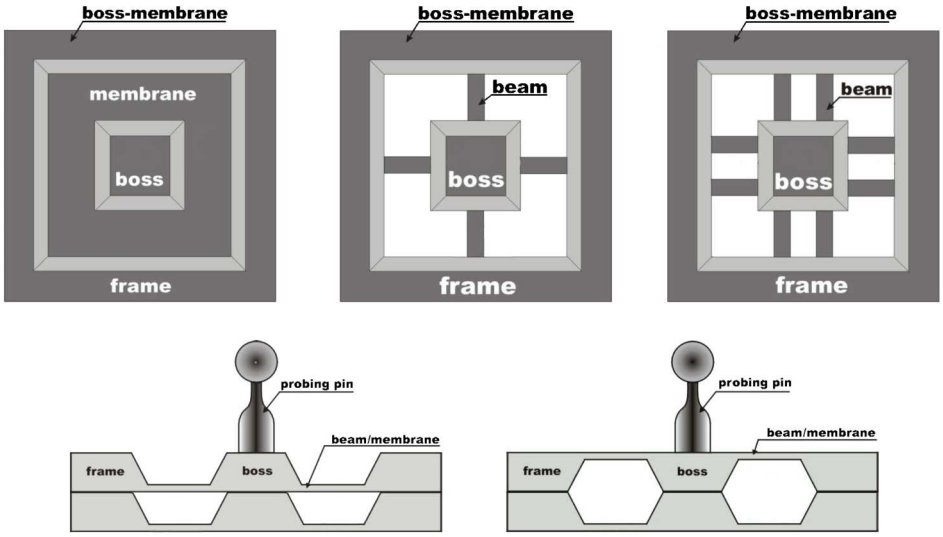

Figure 2.13: Designs for several boss-probes [75]. Single membrane (original design) - top left, four bar - top middle, eight bar - top right, parallel dual membrane - bottom left, and inverse dual membrane - bottom right

basic designs of these probes are shown schematically in figure 2.13, and a photograph of some realised designs is shown in figure 2.14.

Initially, the parallel dual membrane system was modelled. The parallel dual membrane Boss-probe exhibited a stiffness ratio of 0.75 (where the vertical stiffness was 0.75 times the stiffness of that in the lateral direction). For the single membrane design, this ratio is usually between 20 and 30 (depending on the geometry) and could be as high as 35.

Extensive work has been completed on the development of this probe, and the infrastructure surrounding it. This includes work on the development of suitable packaging concepts [76]. However, the suitability of the dual membrane system relies heavily on the ability of the manufacturing process to produce matched pairs of probes, and on a reliable assembly process.

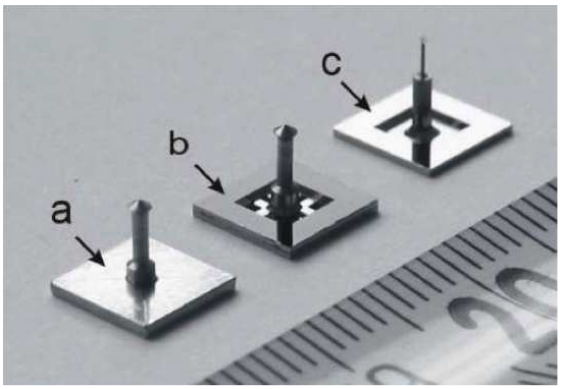

Figure 2.14: Image of three realised PTB Boss-probes a) dual membrane (inverse), b) eight beam and c) single piezoresistor instrumented silicon membrane (original design) [75]

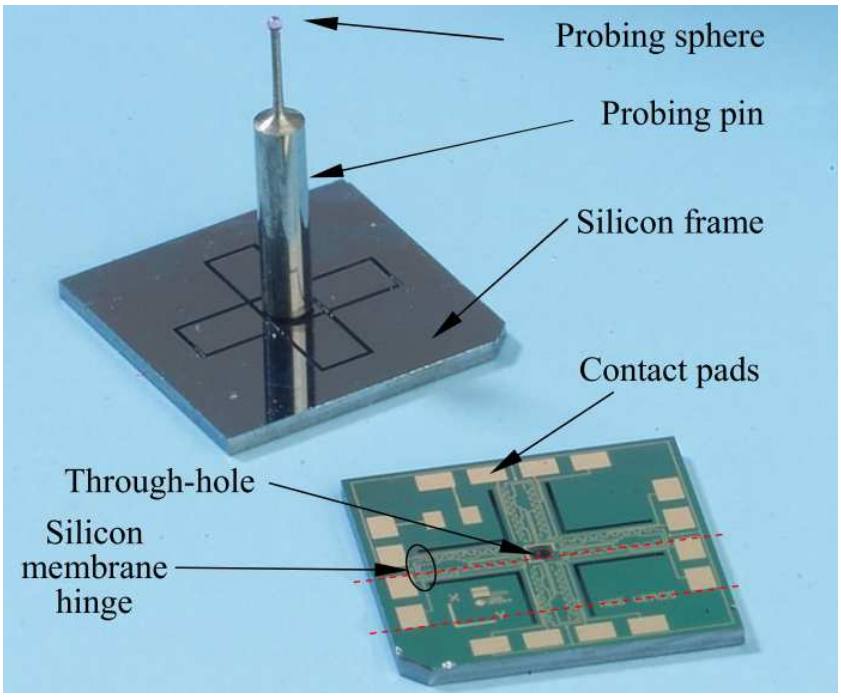

Figure 2.15: Image of the Zeiss SSP probe [77]

2.3.2.3 Zeiss SSP probe

A commercial collaboration between IMTEK (University of Friburg, DE) and Carl Zeiss AG (Oberkochen, DE) has resulted in a novel three-axis silicon-based micro-CMM probe based on piezoresistive transducers [77]. The probe consists of a flexible cross structure, fabricated through a deep reactive ion etching technique (DRIE).

Initially, the probe was realised as a three-axis force sensor; however its applications in dimensional metrology became apparent during testing. These tests involved: the assembly of a contacting stylus element with a tip diameter of 0.3 mm, the determination of the anisotropy to be close to 4 (stiffness ratio) with the vertical probing force being close to 1 mN. The resolution of measurements taken in the lateral direction is about 10 nm. An image of the probe is shown in figure 2.15.

The probe is now sold commercially as the SSP Probe, and is available from Carl Zeiss AG for use on the F25 micro-CMM [78]. As such, it is thought to be one of the most widely used micro-CMM probes in the world. However, because it relies on being installed on an F25 to properly operate; little further research has been completed on it. Some initial exploratory work was conducted by NPL in 2008 into micro-sphere tipped stylus fabrication and use. The fabricated micro-stylus was implemented on the Zeiss SSP probe [79].

2.3.2.4 Summary of silicon-based micro-CMM probes

Silicon-based micro-CMM probes take advantage of well-established fabrication techniques from the IC and MEMS industry. The fabricated probes are very sensitive, allowing low force triggering on surface contact. However, many of these probe exhibit considerable anisotropy. Therefore, the design of these probes requires careful consideration of geometry and kinematics. Again, some probes have been omitted for various reasons, even though they can be used to take some form of dimensional measurement at the micro-scale [80, 81].

A second problem can occur when the flexures of these probes are reduced in thickness to operate at lower contact probing forces. The "thinness" of the silicon suspension could have the adverse effect of giving false readings due to inertia [82]. This means that the probe must often be moved at very slow speeds, which slows the measurement process. The effect of false triggering due to inertia is not limited to silicon-based micro-CMM probes [83], but is more commonly observed when using thin silicon flexures. When low force probing is employed, the effect of surface interaction forces, such as electrostatic interactions or capillary forces, may also become apparent. These surface interaction forces will be discussed and investigated in detail in chapter 4.

To further address the need for low force probing, a class of probes was developed to rely on optical measurements of the stylus tip being used for contact detection. These "optomechanical probes" were developed almost simultaneously to the silicon-based probes.

2.3.3 Optomechanical micro-CMM probes

The mechanical and silicon-based probes described in the previous section are limited due to the need to detect flex in the suspension elements of the probe (usually mechanical flexures). The inclusion of these flexures could limit the capability of the micro-CMM probe. The flexures on most mechanical and silicon-based micro-CMM probes result in probing forces in the millinewton range, which can still result in plastic deformation of measurement surfaces.

Therefore, with the aim to significantly reduce the contact force of probing systems, while still maintaining a similar sensitivity, a new concept was developed that relies on optical detection of the stylus tip, negating the need for flexure elements. Instead, the stylus tip is suspended by other means.

2.3.3.1 PTB fibre probe

A micro-CMM probing system was designed at PTB [84, 71], where the stylus is an optical fibre and the stylus tip is a sphere, formed through laser melting of the stylus [85]. The fibre probe tip is illuminated via a fibre-coupled source and its position is then mapped using a measuring

microscope. The microscope is attached to the fibre probe so that the stylus tip is always kept within the field of view. A 10× objective lens is used to identify sensitive movement in the x- and y-axes. Through the use of sub-pixel imaging, a resolution of 50 nm can be achieved [86]. A diagram of the fibre probe is shown in figure 2.16. It can be seen that any contact in the z-axis will only result in the probe tip becoming unfocused and, therefore, this probe is considered to be 2D only.

A 3D version of the fibre probe was subsequently developed [73], which deploys a second measuring microscope with an angled mirror to view the fibre horizontally above the contacting tip. At this position, a second sphere was assembled. This second sphere is used to measure movement in the z-axes [19]. A diagram of the 3D fibre probe from PTB is shown in figure 2.17.

The sphere tip of the 3D fibre probe has a diameter below 100 µm, and can be as low as 25 µm, allowing it to measure sub-millimetre features with few access problems. However, at this scale, the probe tip is very likely to stick to the measurement surfaces, due to the interaction of the probe tip with the surface interaction forces. This effect is not helped by the low probing forces exhibited by the 3D fibre probe, which have been measured as being in the order of 10 µN [71]. Also, the 3D fibre probe does not exhibit isotropic probing forces.

Measurements taken with the 3D fibre probe can have uncertainties of between 0.2 µm and 0.5 µm and it has been successfully used to perform measurements on high aspect ratio structures fabricated by the X-ray LIGA process [87, 88]. Finally, because the 3D fibre probe relies on optical detection of the illuminated probe tip, there are several limitations on the geometries that the probe can measure. Although the probe is able to access high aspect ratio (HAR) structures, such as cylindrical holes 200 µm in diameter and over 1 mm in depth, the ability of the optical system to detect the sphere is severely limited below several hundred micrometres depth. This limitation is due to certain optical and aperture limitations of the optical measurement system.

This probing concept is commercially available from Werth Messtecnik as a 2D probe [89]. A 3D version of the Werth fibre probe is also available; however no technical details of this probe were available at the time of writing [90].

A similar optomechanical probe has been developed at the Harbin Institute of Technology (Harbin, CN) that addressed the issue of HAR measurement [91]. This probe utilises a second 'effluent' fibre to ensure the position of the probe tip can be determined while the probe tip is inside a HAR structure. The basic concept of the Harbin spherical coupling probe is shown in figure 2.18, however it will not be further investigated as the operating principle is nearly identical to the PTB fibre probe.

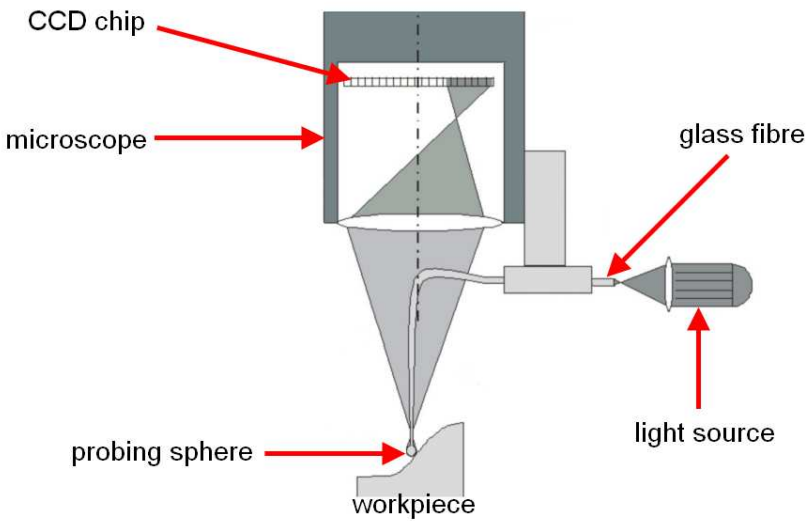

Figure 2.16: Schematic of the 2D fibre probe from PTB [71].

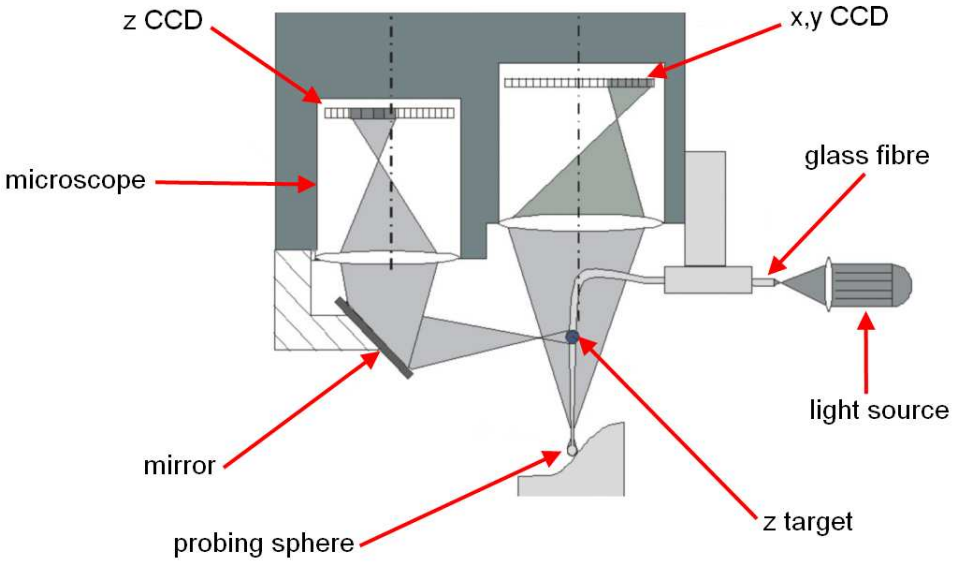

Figure 2.17: Schematic of the 3D PTB fibre probe. The position of the two micro-spheres are measured to give accurate data on the of position of the sphere tip in x, y and z [73].

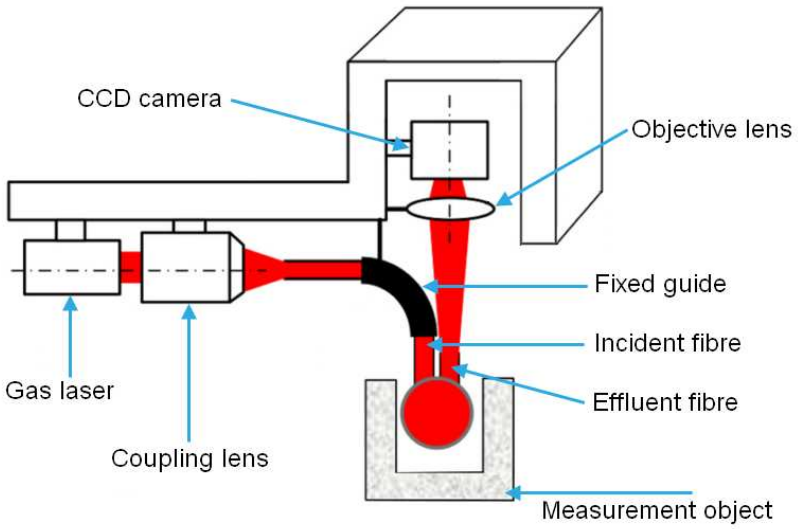

Figure 2.18: Schematic of the Harbin spherical coupling probe [91]

2.3.3.2 NIST fibre deflection probe

A probe has been developed at the National Institute for Standards and Technology (NIST), USA, which aims to negate the issue with detecting the illuminated sphere tip when inside a high aspect ratio hole. To achieve this, the optical detection system is focused on the stem of the fibre probe rather than its tip [92]. The operating principle of the system is shown in figure 2.19.

During the development of this probe, tests conducted suggest that the probe exhibits linearity errors of 30 nm. When used on a precision CMM, diameter measurements taken using the fibre deflection probe have an uncertainty of 110 nm ($k = 2$) [94, 95]. Also, the contact force of the fibre defection probe is estimated at less than 2 µN (depending on stylus length and stylus tip diameter) [96] and could be as low as 0.2 µN. The use of the detection system to measure the deflection of the shaft rather than the position of the stylus-tip has resulted in measurements being taken in holes 100 µm in diameter to a depth of 5 mm [93]. The probing system described in figure 2.19 is, however, only a 2D system. Like the PTB fibre probe, the fibre deflection probe concept was developed as a 2D probe and then extended into 3D.

To extend the capabilities of the fibre detection probe into 3D, a concept of 'buckling' measurement was developed [97]. This allows the optical system to detect z-axis contact with a measurement surface. The concept of 'buckling' measurement is shown graphically in figure 2.20.

The addition of the 'buckling' detection, which theoretically extends the capability of the fibre detection probe into 3D, allows for comparison to the PTB fibre probe. The PTB fibre probe is limited in the detection of the position of the probe tip during high aspect ratio probing, whereas the fibre deflection probe is not limited when using this buckling technique (although it is expected that the buckling measurement will result in relatively low accuracy measurements). Both probes have stylus tips whose diameter is in the order of 100 µm and lower, and both are,

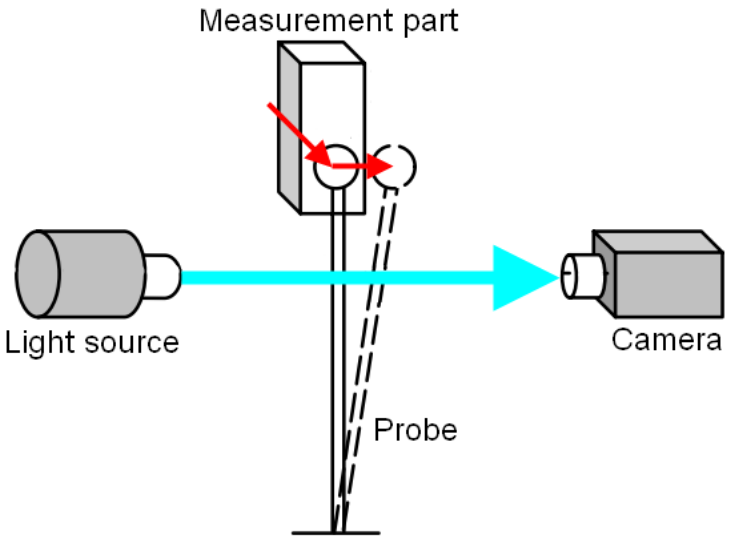

Figure 2.19: Schematic of the operating principle of the NIST fibre deflection probe [93].

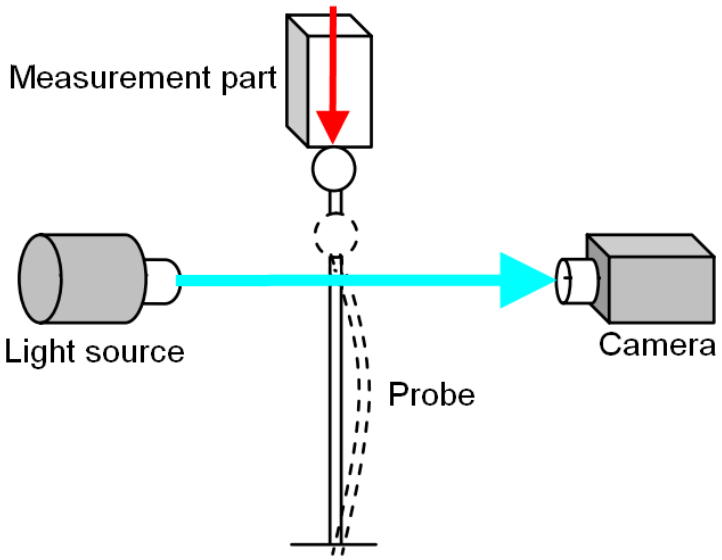

Figure 2.20: Concept of using 'buckling' measurement to increase the capability of the NIST fibre deflection probe into 3D [97].

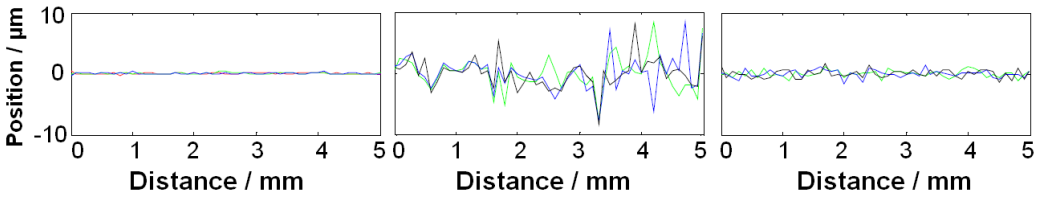

Figure 2.21: An indication of measurement noise due to adhesion when measuring the surface of a gauge block in single point mode (left), in scanning mode (no piezoelectric buzzer) (centre) and in pseudo-scanning mode (using the piezoelectric buzzer) (right) [97].

therefore, affected by surface interaction forces. This effect is directly addressed by the fibre deflection probe by the addition of a piezoelectric buzzer, which results in the capability to perform pseudo-scanning through acoustic excitation of the fibre. The inclusion of the piezoelectric buzzer has a marked effect on this system when performing scanning measurements by reducing surface stiction. This effect is shown in figure 2.21.

A similar probe has been developed at the University of South Australia (UniSA, Mawson Lakes, AU). The UniSA fibre Bragg probe operates in a similar manner to the NIST fibre deflection probe in that optical measurements are taken from the shaft of a micro-CMM probe. The optical signals that are collected during operation are from a fibre Bragg grating (FBG) integrated into the stylus shaft of the probe, which is illuminate axially. This FBG allows precise measurements of the deflection of the stem to be collected, resulting in a probe with a measured resolution of 60 nm and an estimated accuracy of 100 nm [98]. The UniSA fibre Bragg probe will not be described further as it is still in the early stages of development.

2.3.3.3 Summary of existing optomechanical micro-CMM probes

Optomechanical CMM probes rely on taking an optical measurement from the stylus tip, or stylus shaft rather than any instruments or flexures attached to the top of the stylus. The main design reasoning behind these probes is to reduce the contact probing force by employing flexible optical fibres as the stylus element. Also, by removing all other moving parts, such as mechanical flexure systems, the contact force is further reduced. The probes described in this section exhibit contact probing forces of less than 10 µN.

However, all measurements taken using contact methods are influenced by surface interaction forces. When taking measurements at such small dimensions with probes capable of reduced probing forces of a few micronewtons, these surface interaction forces become problematic. Surface interaction forces become influential enough to pull the probe tip towards the measurement surface (snap-in) [82, 69], possibly causing damage at the point of contact and giving a false reading of surface contact. Surface interaction forces could also tend to hold the probe at the contact area while the CMM is retracting, causing unnecessary strain to the probe. A graphical description of this snap-in and snap-back effect can be seen in figure 2.22.

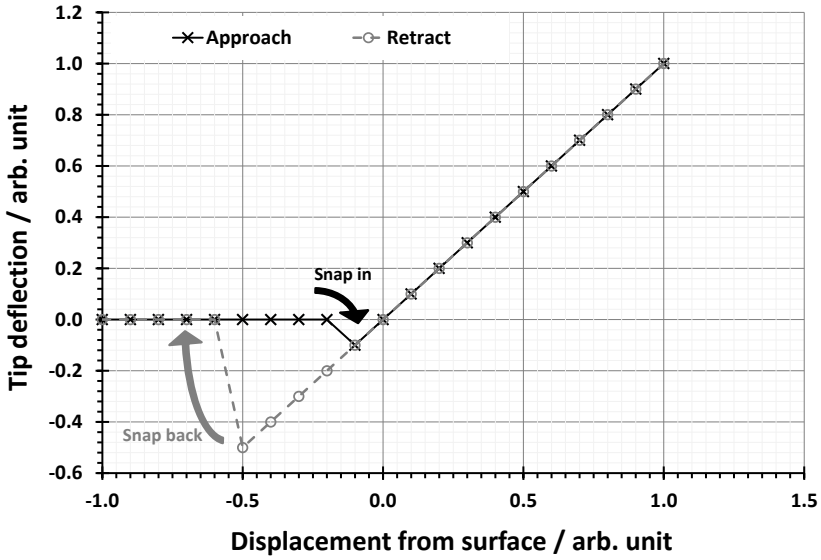

Figure 2.22: Graph showing the snap in and snap back effect – data for indication only

When probing with optomechanical probes, the sticking effect becomes problematic as the probe tips stick easily to most measurement surfaces. The compliance of these probes means that the force required to break the hold is high; either the feature being measured does not afford the probe sufficient clearance or the stiffness of the micro-stylus would result in permanent damage to the probing system. This effect is somewhat counteracted by the piezoelectric buzzer described by Muralikrishnan *et. al.* [97], and a similar system is available for the commercial fibre probe from Werth [89].

Regardless, the overall capability of these probes is similar. Both fibre-based probes can boast measurement uncertainties less than 100 nm on high aspect ratio features (inkjet nozzles, optical ferrules, etc.) [88, 99, 100, 101, 102]. Several probes have again been omitted from this review for similar reasons to those omitted from the previous sections [103, 104].

The simultaneous developments of silicon based micro-CMM probes and optomechanical systems to address the need for low force contact probing is an indication of the importance of this requirement. However, during their developments, it became apparent that both technologies suffer from problems that require further study. The lack of 3D measurement was addressed in both the PTB and the NIST fibre probes, and the anisotropy of some silicon-based probes was addressed by PTB. However, the issue of dealing with the surface interaction forces has only been addressed by NIST in the fibre deflection probe, with the addition of a piezoelectric buzzer. This breakthrough has prompted the most recent set of developments in micro-CMM probe research to focus on surface-force counteraction through the use of forced vibration.

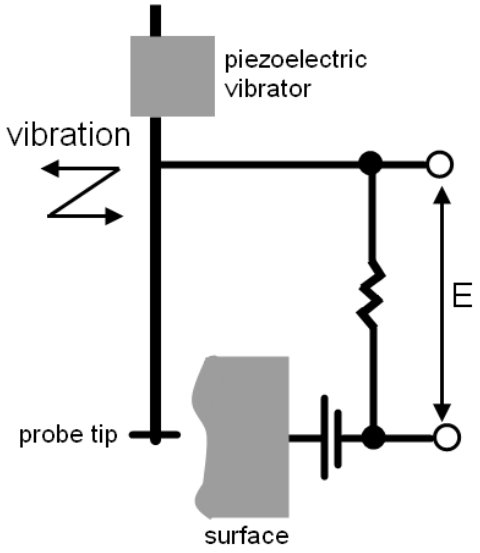

Figure 2.23: Schematic of the operating principle of the vibroscanning probe

2.3.4 Vibrating micro-CMM probes

It is a known problem that reduction of probing force increases the susceptibility of the micro-CMM probe to surface interaction forces [69, 105]. Therefore, research has been conducted into counteraction this effect by using vibrating probe-tips. The main aim of a vibrating micro-CMM probe is to force the probe tip to vibrate at a frequency and amplitude such that is it unaffected by surface interaction forces. Once this is achieved, the probes will experience neither snap-in or sticking (and therefore snap-back).

An early use of vibration to counteract the surface interaction forces was deployed in the NIST fibre deflection probe, which used a piezoelectric buzzer to acoustically activate the probe shaft. The use of piezoelectric actuators to vibrate probe systems will now be considered, along with other oscillation techniques.

2.3.4.1 Vibroscanning probe for micro-holes

An early contacting probe, which was developed for the measurement of micro-holes, was the vibroscanning probe [106]. This utilised electric detection of contact between metallic surfaces with a precision stylus manufactured by electro discharge grinding. The stylus is assembled onto a piezoelectric vibrator, which is positioned by the precision 3D axes of an electro-discharge machining (EDM) system. After the EDM process has machined a micro-hole, the vibroscanner can be placed in the hole and take dimensional measurements. A schematic of the vibroscanning concept is shown in figure 2.23.

From figure 2.23 it can be seen that, when the probe contacts the measurement surface, the output circuit will record a signal. As the probe is vibrating, the intermittent signal will indicate

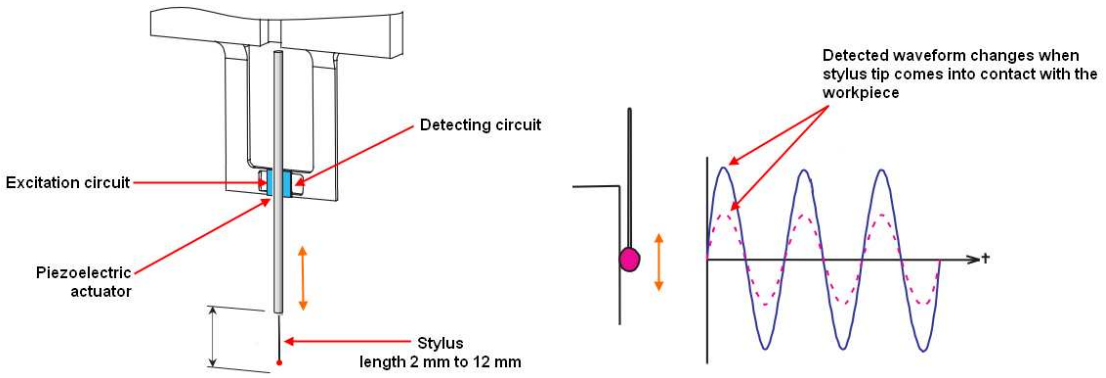

Figure 2.24: Schematic of the operating principle of the Mitutoyo UMAP probe [111].

the time for which the probe is in contact with the surface, from which an appreciation of the current position of the probe can be calculated.

The probe concept was developed further to include dual heads [107, 108].

2.3.4.2 Mitutoyo UMAP probe

One of the first commercially available vibrating micro-CMM probes was the UMAP system from Mitutoyo Corporation [109, 110]. This probe, also known as the Ultrasonic Probe, was designed for micro-hole measurement, such as fuel injector nozzles, optical ferrules or micro-machined holes. To achieve this, the UMAP probe has a 30 µm diameter stylus tip. During operation, a piezoelectric excitation circuit vibrates the stylus vertically at several kilohertz. When the stylus tip contacts a workpiece surface the detected wave-form changes from that which was generated [111]. The estimated contact force is 1 µN. The operation principle of the UMAP probe is shown in figure 2.24.

When in operation, the UMAP probe relies on an optical system to initially detect the position of features [39]. This means the UMAP probing system and CMM is a multi-sensor system. The measurement uncertainty of the UMAP probe, when installed on a suitable precision CMM, is quite high in comparison to other micro-CMM probes. With an estimated repeatability of about 100 nm, the system is not capable of the high accuracy measurement common with most micro-CMM probing systems. Also, the probe is only able to vibrate in 1D (vertical direction), but is able to detect in 2D. An indexing head must be employed to realise 3D measurement [112].

2.3.4.3 UNCC Virtual probe

A probe has been developed at the University of North Carolina (UNCC, Charlotte, USA), in collaboration with Insitutec Inc., which consists of a high aspect ratio probe shank (1:700) attached at one end to a quartz oscillator [113]. When in use, the oscillator causes the free end, or probing end, to vibrate at an amplitude greater than the probe shank diameter, and

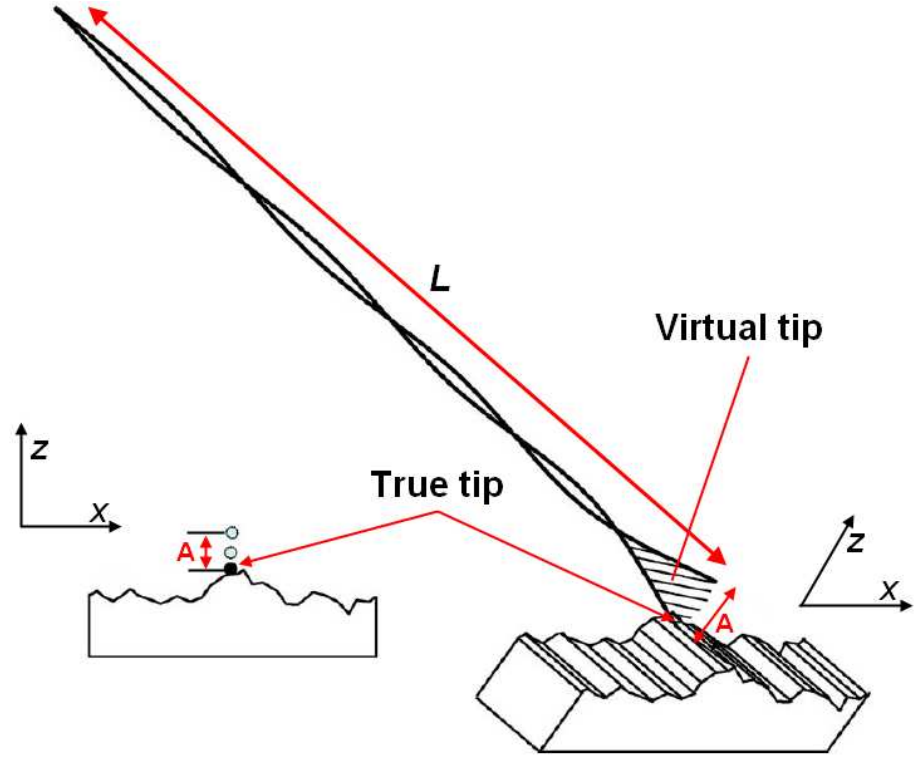

Figure 2.25: Schematic of the operating principle of the UNCC Virtual probe. The probe has a length, L, and a virtual tip diameter equal to the amplitude, A, of the vibration of the free end [113].

a "virtual tip" is formed. These oscillations have a frequency of several tens of kilohertz (the quartz oscillators used are used for timekeeping and have a resonant frequency of approximately 32 kHz). The virtual tip is defined as the surface region on the shank which the interaction with the specimen surface alters the vibration response. The virtual tip diameter, equivalent to the vibration amplitude at the free end of the shank, is about 30 µm. A diagram of the operating principle of the Virtual probe is shown in figure 2.25. The Virtual probe is also sometimes referred to as the Standing Wave probe.

When using this probe, a probing force of up to 100 µN is imparted onto the measurement surface [114]. Also, the probe can repeatably resolve surface features of 5 nm. However, due to its design, it is only capable of oscillation and detection in 1D.

Despite being only a 1D probe, the standing wave probe has been successfully used to measure fuel injection nozzles and glass ferrules [115]. This was achieved through the use of several stacked coarse and fine position motion stages, and a rotation stage. This stacked system has also successfully completed dimensional measurements on low density foams, such as high inertial phase emulsion (HIPE) or aerogel [116, 117], which is a clear indication of the ability of the probing system to operate at very low forces.

The development of this probe included analysis of surface interaction forces, to ensure that the probe was capable of counteracting the snap-in and stiction effects common when probing at the

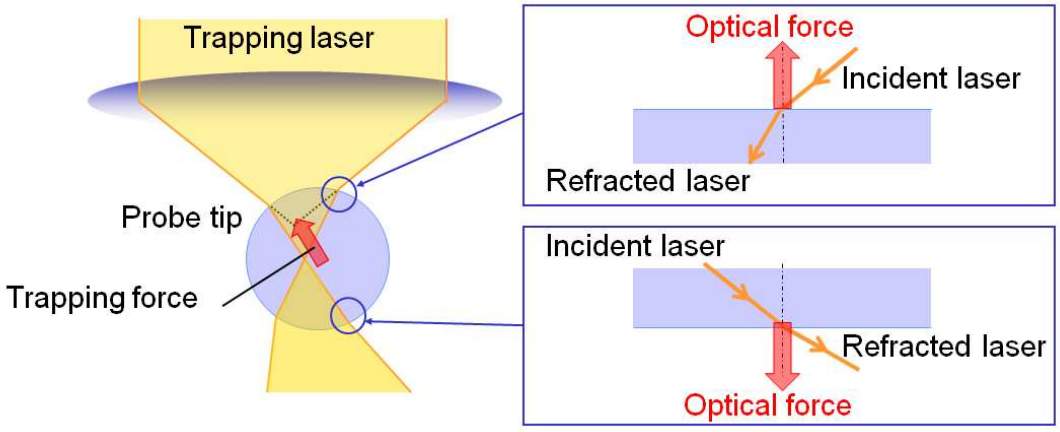

Figure 2.26: Schematic of the operating principle of the laser trapped vibrating probe (courtesy of Dr. M. Michihata)

micrometre scale. Further developments have included investigations into viability of shrinking this probe to obtain tip diameters of only a few micrometres [114]. The scaling investigation concluded that, by reducing the shank diameter and vibration amplitude, a virtual tip with diameter only a few micrometres would still be able to counteract the surface interaction forces.

2.3.4.4 Laser trapped vibrating probe

Methods used to vibrate the probe tip vary greatly. In an attempt to reduce the contact probing force further, a novel micro-CMM probe has been developed at Osaka University, Japan. This micro-CMM probe operates by laser trapping an 8 µm to 10 µm diameter silica sphere and optically recording its interactions with the measurement surface [118]. By ensuring that there is no mechanical contact between the micro-sphere and the micro-CMM, the contact probing force of this probe has been reduced to several nanonewtons. A graphical description of laser trapping is shown in figure 2.26.

The trapping force, as shown in figure 2.26, will compensate for any deviations of the sphere from the equilibrium position. An optical measurement system is employed, using the same optical path as the trapping laser, that detects the current position of the probe and all deflections. The optical measurement system works in a similar way to that used with the PTB fibre probe.

Further development of the concept of laser-trapping has allowed this probe to operate in an oscillating mode [119, 120]. The probe is forced to vibrate in the z-axes at frequencies up to 50 MHz. The point of contact is then categorised as a change in the amplitude of the vibration of the probe. This probe has also been optimised for operation with fibre delivered laser light, rather than that delivered through a microscope objective [121, 122].

Currently, this probe is unable to measure in the x- or y-axes; however, the addition of off-axis circular motion into the trapping beam has been theorised to allow sloped surfaces to be

measured (limited to the aperture of the laser delivery system) [123, 124]. Also, little information is available on the tip's interaction with any liquid layers or surface interaction forces on the measurement surface.

A recently theorised addition to this technology is the use of interference of light between the probe tip and the measurement surface to enhance the determination of z position [125].

2.3.4.5 Summary of vibrating micro-probes

The continuing development of micro-CMM probing systems towards truly micro-scale probing has led to the need for low force systems that can counteract the effect of the surface interaction forces. To facilitate this requirement, probing systems have been developed that vibrate. When this vibration is perpendicular to the measurement surface (or parallel to the surface normal), the motion of the stylus tip should be such that the attractive force due to the surface interaction forces is not sufficient to adhere the stylus tip to the measurement surface.

One major limitation of the vibrating probes is that the technologies currently used to produce the vibration usually result in only 1 dimensional oscillation. In the case of the UMAP system and the laser-trapped probe this is vertical oscillation, for the Virtual probe this is lateral oscillation. Therefore, any attempt to use these probing systems on 3D micro-CMMs would rely on rotation axes on the micro-CMM or articulating probe heads to property orient the probe. New developments in the use of the virtual probe have included the implementation of precision manipulation and rotation stages and active indexing heads to allow 3D probing [117]. A PhD project at TUE is also considering the applications of vibrating micro-CMM probes in 3D [126].

2.4 Capabilities of existing micro-CMM probes

Several universally agreed requirements exist for any micro-CMM probe [42, 69]. These requirements can act as a score card for the probe, and can also be used to make comparisons between systems. These requirements of micro-CMM probing systems can be identified directly from the completed review of existing micro-CMM probes.

- **Stylus dimensions** – This refers to the shape, length and diameter of the stylus shaft, and also the shape, size and form of the stylus tip (and therefore, the aspect ratio of the stylus; the value of its length divided by its diameter [83]). The micro-CMM probe should have a stylus tip (usually spherical) that has a diameter smaller than the size of the features to be measured. The stylus tip should also have good spherical form [39].
- **Probe error** – This refers to any errors in the dimensional measuring capability of the probe. These should be clearly defined, especially when the probe is used to take traceable dimensional measurements. These errors may be reported in terms of repeatability of

surface point detection, uncertainty in the determination of the tip deflection, linearity error of length measurement or even an indication of resolution of the probe detection [39].

- **Isotropy** – If a micro-CMM probe is isotropic, this refers to its ability to act (usually in terms of probing force) equally in all probing directions [83]. This is often reported as the ratio between the lateral and vertical stiffnesses, any ratio other than unity indicates a degree of anisotropy.
- **Probing force** – One of the main problems created by the reduced dimension of the measurement is the damage that can be caused by the probe itself. Even with forces as low as a few millinewtons, a stylus tip that is only a few micrometres in size could potentially cause damage to the sample, effectively ruining the measurement [44].
- **Ease of use** – An obvious requirement that is often overlooked; any probe that is easy to use often becomes commercially viable. This requirement also relates to the applicability of the probe to the current specification standards and, therefore, the ability to make direct comparisons to other micro-CMMs and micro-CMM probing systems.

These five requirements are applicable to all probing systems, to a certain degree. The importance of each requirement depends on the final application of the probe. A summary of all the reviewed micro-CMM probes is shown in table 2.4, using the identified requirements as metrics for comparison.

2.5 Limitations of existing micro-CMM probes

When developing probes for use on micro-CMMs, there are several requirements to adhere to. These requirements are: stylus dimensions, probe error, isotropy of the probing system, probing force and ease of use. While completing measurements at the micrometre scale, certain limitations of any probe used to take the measurement become apparent [127]. These limitations are linked directly to the requirements for micro-CMM probes. The limitations of the reported micro-CMM probes will now be discussed.

2.5.1 Stylus dimensions

One major limit for micro-CMM probes are the dimensions of the stylus. The relevant dimensions of a stylus can be seen in ISO 10360-1:2001 *Geometrical Product Specifications (GPS) — Acceptance and reverification tests for coordinate measuring machines (CMM) — Part 1: Vocabulary* [11], and are shown schematically in figure 2.27, along with the general nomenclature of the probing system.

It is obvious that the stylus shaft must have a diameter less than that of the spherical stylus tip. Also, the stylus tip must be reduced to the order of size of the features to be measured [39, 69].

Table 2.4: Summary of the capabilities of the reviewed micro-CMM probes, as defined by the micro-CMM probe requirements. Probe errors reported in [square brackets] are the associated error of a CMM using that probe. Stiffness values reported as a single number indicate isotropic operation, whereas a range of values indicates anisotropy. In the case of anisotropic operation, the stiffness ratio (lateral/vertical) is indicated in {brackets}. Capabilities reported with a dash (-) are either not available, or not applicable. The stiffnesses of the vibrating micro-CMM probes are not reported in the literature, and are therefore indicates as (?).

		Stylus length / mm	**Tip diameter / µm**	**Probe error (3D) / nm**	**Stiffness at tip / N m^{-1}**	**Probing force / mN**	**Reference**
mechanical	**METAS TouchProbe**	< 5	100 to 1 000	10	20	< 0.5	[18, 44]
	NPL SCMM Probe	> 5	300	< 40	10	0.1	[14, 16, 15]
	IBSPE Triskelion A	6 to 13	250	< 15	70	0.07	[56]
	IBSPE Triskelion B and C	6 to 13	35 to 500	< 20	13 to 113 {0.65 and 0.31}	0.01 to 0.12	[56]
	DVD-pickup head probes	2	300	10 to 100	-	0.1	[57, 59]
silicon-based	**Xpress Gannen XP**	~ 6	50 to < 500	45	400	0.4	[68]
	Xpress Gannen XM	~ 6	50 to < 500	156	10 to 50 {0.2}	0.01	[68]
	PTB Boss-probe 2002	~ 5	300	~ 30	100 to (55×10^3) {0.002}	10 to (1.5×10^3)	[19, 74]
	PTB Boss-probe 2005	5	200	-	(5.5 to 7.4) $\times 10^3$ {0.75}	< 300	[75]
	Zeiss SSP probe	< 5	125 to 300	[< 250]	-	1	[27, 77]
opt.mech.	**PTB 3D fibre probe**	> 5	25 to < 100	[200 to 500]	-	0.01	[19, 71, 73]
	NIST 2D fibre deflection probe	> 5	< 100	30, [110]	-	(2 to 0.2) $\times 10^{-3}$	[92, 94, 95, 96]
vibrating	**Vibroscanning probe 1993**	-	-	-	?	-	[106]
	Mitutoyo UMAP probe	2 to 12	30	[500 to 1 000]	?	1×10^{-3}	[111]
	UNCC virtual probe	> 10	30	< 50	?	~ 0.1	[113, 114]
	Laser trapped probe	< 0.05	8 to 10	-	?	$\ll 0.01$	[118, 119]

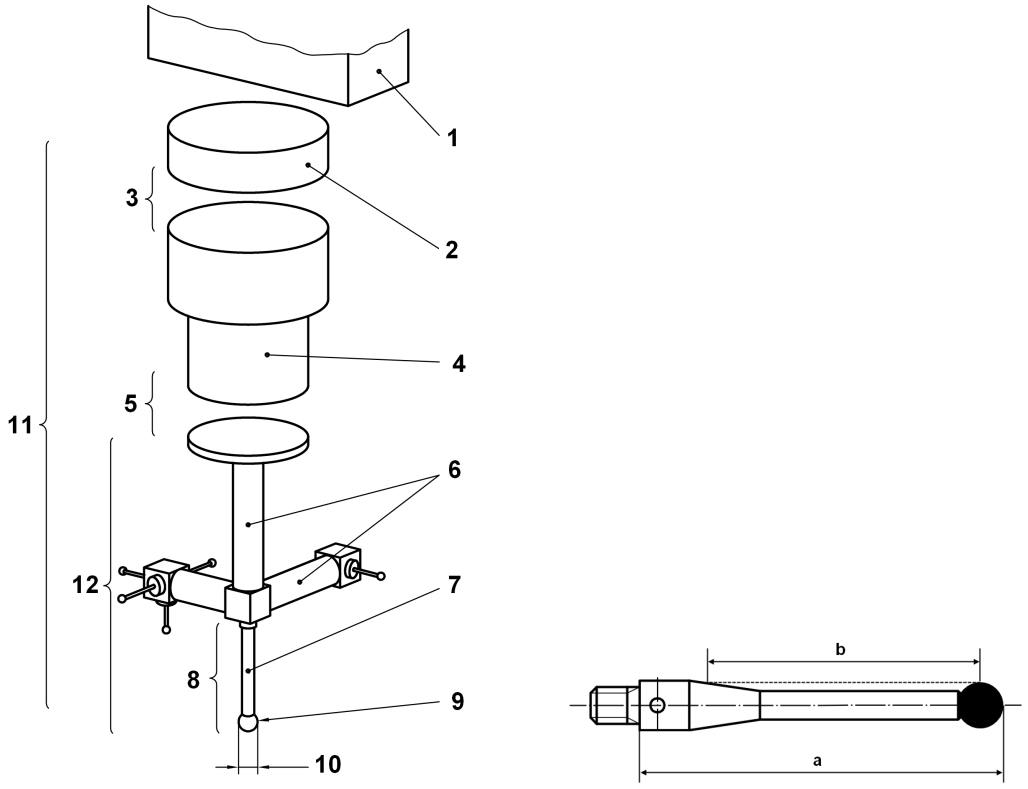

1 Ram
2 Probe extension
3 Probe changing system
4 Probe
5 Stylus changing system
6 Stylus extension
7 Stylus shaft
8 Stylus
9 Stylus tip
10 Tip diameter
11 Probing system
12 Stylus system (composed of stylus system components)
a Stylus length
b Effective working length [83]

Figure 2.27: Probe and stylus nomenclature according to ISO 10360-1:2001 [11]

The stylus shaft must also be long enough to allow the probe to penetrate some of the high aspect ratio features common in modern micro-structures, while remaining rigid enough to not bend significantly and exhibit high probing errors. Probing errors due to stylus bend arise from the anisotropic stiffness of the shaft itself (*i.e.* the relationship between the near infinite stiffness of the stylus in the direction of the shaft, compared to the finite lateral stiffness). Therefore, it is usual for the stylus shaft on a micro-CMM probe to have a stylus length of several millimetres, with the upper section (close to the probe) being of a large diameter (several times that of the stylus tip diameter). The lower section of the stylus is then of a suitable diameter to attach to the stylus tip, but is of a shorter, effective working, length.

Of the probes reviewed in this chapter, most of the recently developed systems have stylus tip diameters below 100 µm. Those with stylus tip diameters above 100 µm are the NPL SCMM probe, the DVD-pickup probe, the PTB Boss probe, several configurations of the Xpress Gannen probe and the IBSPE Triskelion probe, and the Zeiss SSP probe. The lower bound of the stylus tip diameters is 8 µm to 10 µm, as used in the laser trapped vibrating probe. The other probes have stylus tips that range from 30 µm to 70 µm in diameter.

Similarly, the effective stylus length of any micro-CMM probe is of importance. The effective stylus length, coupled with the stylus tip diameter, defines the aspect ratio of the probing system. The aspect ratio can be seen as an indication of the depth of the smallest diameter hole that can be measured. Of the probes reviewed in this chapter, the probes with the highest aspect ratios were optomechanical (the PTB fibre probe and the NIST fibre deflection probe), the virtual, or standing wave, probe and the UMAP probe (which in one configuration can achieve an effective stylus aspect ratio of 100 [109]). These are unique from all the other probes reviewed because their styli are formed from optical fibres rather than tungsten or other metallic or cemented carbide shafts.

However, it should be noted that, although the aspect ratio of the PTB fibre probe is high (often over 20), the requirement for an optical system to be able to image the stylus tip can cause problems. These problems usually occur when structures on the measurement part, such as side walls, obstruct the vision system. A similar problem affects the laser trapped vibrating probe, which often cannot measure features with an aspect ratio above unity.

2.5.2 Probe error

Several measures of the capability of the probe to complete measurements are often quoted, including probing repeatability of triggering, probe resolution, and length measuring error over a specific deflection length. All of these measures have the virtue of indicating some ability of the probe, however, none of these truly indicate the capability of the probe to complete accurate co-ordinate measurements. The ability of the probe to complete accurate co-ordinate measurements can only be obtained by installing the probe onto a micro-CMM and testing it. This is difficult

to achieve when developing a probe and, therefore, several alternative measures are considered. For the purpose of this review, either the repeatability of the triggering point, or the uncertainty in the tip deflection, will be considered as an indication of probe error.

Of all the reviewed probes, the most usual value for repeatability of triggering is below 50 nm, with the DVD-pickup head quoted as having a repeatability of 50 nm, and the virtual probe quoted as having the ability to repeatably resolve features of 5 nm. Similarly, a typical uncertainty on the measurement of the stylus tip deflection of 20 nm to 50 nm ($k = 2$). As an indication, the IBSPE Triskelion probe has a configuration that exhibits a 3D measurement uncertainty on tip deflection of 15 nm, and the Gannen probe from Xpress has a configuration that exhibits a 3D measurement uncertainty on tip deflection of 45 nm.

For probes with sub 100 µm diameter stylus tips, in order to keep to probe error at this low level, the stiffness at the probe tip is usually increased. This is because the effects of the surface interaction forces become increasingly detrimental to probes with stylus tips below 100 µm in diameter.

Surface interaction forces, such as the capillary force or the electrostatic force, are usually not significant on the macro-scale, being overpowered by gravity or by the probing forces of classical CMMs. This is not the case for micro-scale co-ordinate metrology, which, if it aims to accurately measure high aspect ratio micro-structures, will be performing contacting probing with micro-styli whose tip diameters will be below 100 µm. In fact, surface interaction forces can become increasingly disruptive when using a micro-stylus with a tip diameter reduced below 200 µm [69]. Surface interaction forces also become more disruptive when the distance between the stylus tip and the measurement surface is reduced below 1 µm. The strength of the interaction forces will increase as the stylus tip approaches the measurement surface, and may cause false triggering and damage to both the probe and the measurement surface. This effect of false triggering can occur when the stylus tip snaps in to the measurement surface before true contact is made. This 'snap-in' is due to the attractive effect of the surface interaction forces and the compliance of the probe not being suitable to counteract the effect of such forces. A graphical description of snap-in and snap-back is shown previously in figure 2.22. Adhesion to the measurement surface while retracting could also cause damage to the probe. Counteraction of these surface forces is essential if any micro-CMM probe is to be accurate while probing at the micro-scale to nanometre accuracy [128]. It can be seen in figure 2.28 that, at the micrometre level, the effect of the van der Waals interaction could be over one hundred times more influential on the surface interaction force of the CMM probe than the gravitational force, and that the effect of surface tension due to any liquid contamination on the measurement surface could be highly significant.

By stiffening the CMM probe trigger system in an attempt to solve the problem of snap-in and adhesion to the measurement surface (leading to snap-back), the contact probing force will increase, possibly leading to damage to the measurement surface. It is, therefore, far more useful

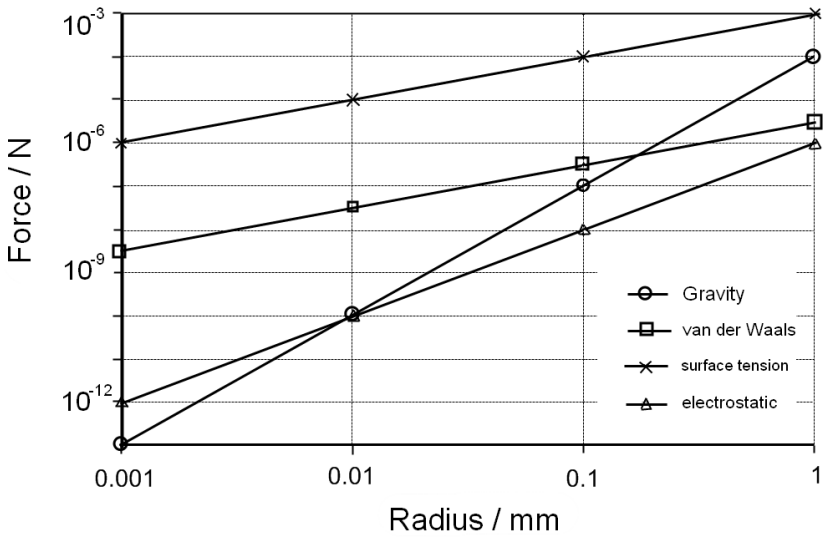

Figure 2.28: Graph showing the adhesion forces (van der Waals, surface tension and electrostatic) between spherical objects and grippers compared to the gravitational force [105].

to counteract or use the effects of the surface interaction forces in a controlled fashion. This can be achieved by vibrating the stylus tip.

Of the probes reviewed in this chapter, several employ vibration to increase accuracy. These are the UMAP probe, the virtual probe, the laser trapped vibrating probe and also the most up-to-date fibre deflection probe, which uses a piezoelectric buzzer to reduce surface adhesion. These probes all exhibit low probe error, either being highly repeatable or exhibiting a lower uncertainty in determination of the deflection of the stylus tip, despite having stylus tips significantly below 100 µm in diameter.

2.5.3 Isotropy

When referring to any CMM probe, isotropy describes the ability of the probe to act equally in all probing directions, and usually refers to the probing force. Therefore, any probe that acts with a greater force laterally than vertically (or *vice versa*) can be said to be anisotropic. The ratio between the two stiffnesses is a measure of the anisotropy.

Of the probes reviewed in this chapter, several exhibit isotropy. These isotropic probes tend to have been designed specifically to be isotropic. The isotropic probes include; the METAS touch probe ($20\,\mathrm{N\,m^{-1}}$), the NPL SCMM probe ($10\,\mathrm{N\,m^{-1}}$), one configuration of the IBSPE Triskelion probe ($70\,\mathrm{N\,m^{-1}}$) and one configuration of the Gannen probe from Xpress ($400\,\mathrm{N\,m^{-1}}$). However, several other probes exhibit severe anisotropy ranging from a stiffness ratio of four (the Zeiss SSP probe) to fifty-five (one early configuration of the Boss-probe). All of the optomechanical probes and the vibrating probes are entirely anisotropic. This is because these probes only act in 1D or 2D.

The need for isotropy is twofold. Firstly, the ability to act isotropically impacts directly on the probing error. In an isotropic probing system, the uncertainty associated with the full 3D determination of the deflection of the stylus tip is usually lower. This is because the combination of the lateral and vertical probing errors is reduced when the individual probing errors are reduced and similar. Secondly, it is easier to implement surface scanning with a micro-CMM probe that is isotropic. This is because the scanning control algorithm does not have to compensate for changing probe reactions as well as the changes in the measurement surface normal.

2.5.4 Probing force

Combining all of the previous requirements of stylus dimensions (especially the stylus tip diameter), counteraction of surface forces, stiffness and isotropy, results in an understanding of the force on the measurement surface during probing. When probing with stiff and anisotropic probes, that have stylus tip diameters below 100 µm and may also experience snap-in or surface adhesion, it is highly likely that significant surface damage may be caused during probing. Therefore, once the previous requirements have been considered, the possibility of surface damage due to the use of the probe must be addressed. This effect has been investigated with regards to the METAS touch probe, with research continuing in this area [44, 129].

Of the probes reviewed in this chapter, all report probing forces below 0.1 mN, except for the PTB Boss-probes. Several probes have reported probing forces in the micronewton range, however, the lowest probing forces is usually attained by the vibrating probes. The probing force of a vibrating probe is difficult to measure using conventional means, such as a force sensor, and is therefore usually estimated.

2.5.5 Ease of use

Finally, the ease of use of the probe is a serious consideration. Several of the probes reviewed in this chapter are presented as purely research-based probes. These are difficult to use, with often time-consuming start-up routines. For example, the laser trapped vibrating micro-probe operates with a 10 µm silica sphere. This sphere is not physically attached to the probing system and, therefore, must be installed at the beginning of each probing operation. The sphere tip is also lost any time the probing operation over-travels such that the sphere moves out of the path of the focused laser. Likewise, the METAS touch probe was designed for use on the METAS precision CMM, and, although the probe is commercially available, is difficult to use without access to that specialised CMM. Several probes reviewed in this chapter are commercially available, such as the Triskelion probes from IBSPE, the Gannen probes from Xpress, the SSP probes from Zeiss and the UMAP probe from Mitutoyo. These probes are, undoubtedly, easier to use and come with clear operation instructions.

2.5.6 Summary of current micro-CMM probe limitations

The current limitations of existing micro-CMM probes have been reviewed. These limitations were reviewed with respect to the five identified probing requirements.

As both the capabilities and the limitations of these existing systems have been presented and discussed, the existing knowledge gaps can now be clearly defined.

2.6 Key knowledge gaps

The current state of micro- and nano-scale metrology can be depicted graphically, as shown in figure 2.29. Precision engineering is becoming prevalent in the blank space in the area of 3D metrology on the micrometre scale. The **aim** of this thesis is to extend the ability of CMMs in the direction of the arrow. Engineering structures are being produced in the area depicted with a question mark; however, there are few known solutions for traceable metrology at these specifications.

All of the reviewed micro-CMM probes have attempted to address one or more of the obstacles faced when completing measurements at the micro-scale.

All current research is carried out with probe dimensions in the order of the size of the features that are being measured. While all of these methods effectively reduce the probing force to an acceptable level, where very little damage is done to the measurement surface, only the methods that address the problem of surface interaction forces will produce an accurate result. This problem is best addressed by probes that vibrate. This is somewhat addressed by the Virtual probe, however, this probe only vibrates in one dimension. Vibrating micro-probes also have the added effect of reducing the probing force. Contact with the measurement surface is registered as a change in the amplitude of the vibration (during intermittent contact with the measurement surface), rather than a direct contact signal.

Therefore, three key knowledge gaps can be identified that are hindering the continued development in the area of micro-CMM probing.

Firstly, there is a need to counteract surface interaction forces in 3D. This need stems from several of the previously mentioned probing requirements, including stylus dimensions and probe error. In order to continue reducing the diameter of the stylus tip, while maintaining low probing error, it is essential to address the effect of the surface interaction forces. This is being addressed, to some extent, in several existing vibrating micro-CMM probes, but not in full 3D. As micro-parts become more complex, the need for true 3D measurement will increase, and this knowledge gap will have to be addressed. In this context, 'true 3D' is referring to the ability of the probing system to act in 3D, without the need for external manipulation systems.

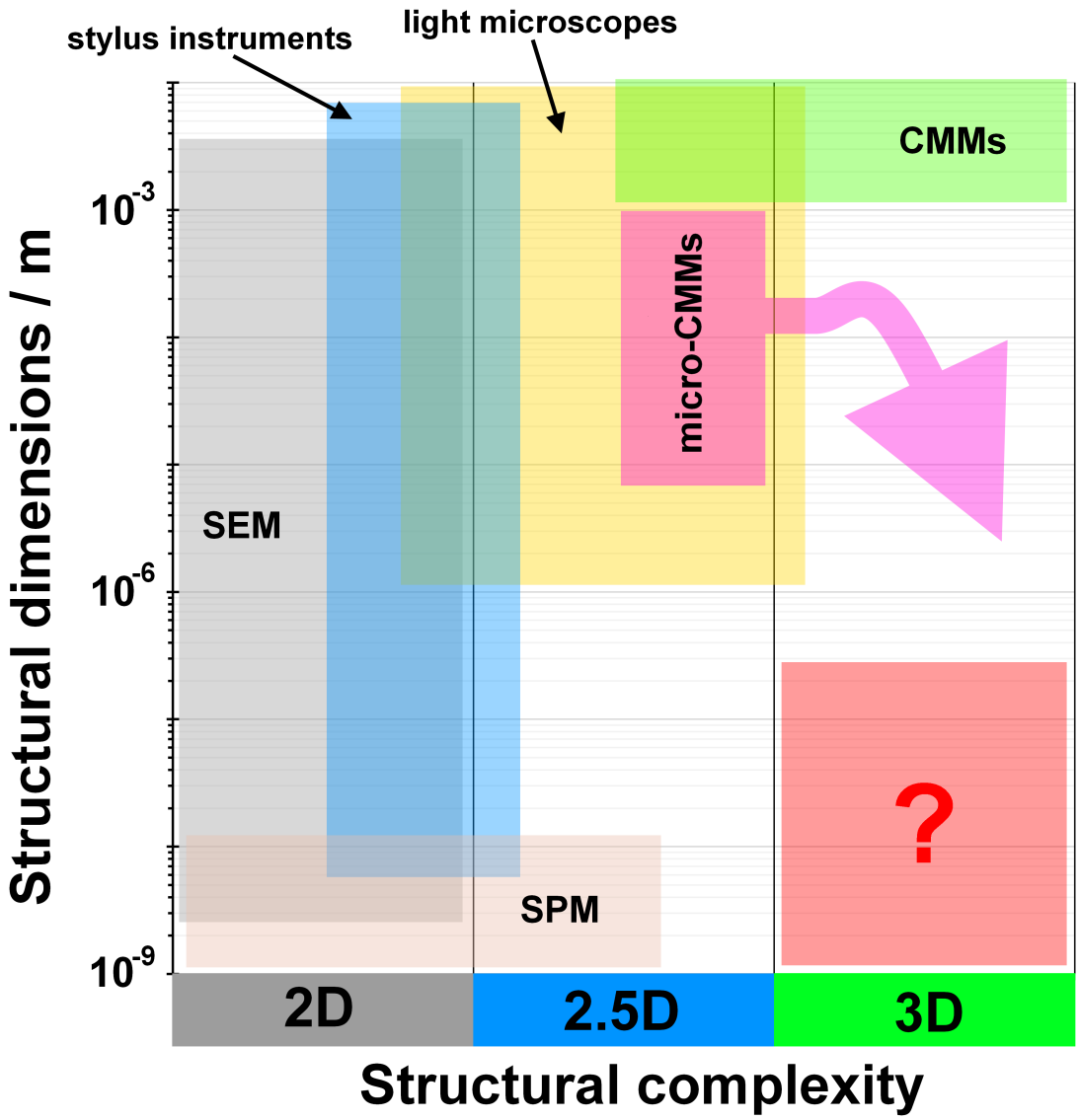

Figure 2.29: Diagram to illustrate the lack of 3D dimensional metrology on the micro- and nano-scale [130]

Secondly, any newly developed micro-CMM probe should act isotropically. This is essential to help result in the lowest overall probing error, and to ensure that the possibility to implement surface scanning with that probe is increased.

Finally, all new probes should operate easily in an industrial metrology environment with a clear set of operational strategies. This will make the probe commercially viable. Also, the probe should operate within the framework of existing specification standards, so that it is easy to test, easier to implement within existing industrial environments and easier to compare to existing technologies.

These three identified knowledge gaps correlate exactly with the **Thesis Objectives**.

Therefore, to address these three knowledge gaps, a vibrating micro-CMM probe was designed at NPL. This probe forms the subject of this thesis; however some work was completed before the start of this PhD. This background knowledge, and some minor work involving the manufacture and assembly of the probe, will be reported in Chapter 3.

2.7 Conclusions on the review of existing micro-CMM probes

Following this review of existing micro-CMM probes, which includes a review of their capabilities with respect to a set of standard, universally agreed, requirements, it can be concluded that there are several gaps in the current body of knowledge which must be addressed. These gaps will directly impact on the ability of the project results to address the **Thesis Aim**:

> *"to develop and operate a contacting probe such that it enables existing micro-CMMs to reliably measure sub-100 μm features in three dimensions to an uncertainty below 100 nm"*

To address this **Thesis Aim**, a novel vibrating contacting probe for micro-CMMs has been designed at NPL. A set of **Thesis Objectives** can be developed, based on the identified knowledge gaps, to investigate the capability of the NPL vibrating micro-probe to address the **Thesis Aim**. The **Thesis Objectives** will directly address the three main features that the NPL vibrating micro-probe should exhibit to be more advanced than its predecessors. The **Thesis Objectives** are:

- **Thesis Objective 1** - To develop and validate methods to operate the vibrating micro-probe such that it can counteract surface interaction forces in 3D.
- **Thesis Objective 2** - To develop and validate a new concept of isotropy that can be applied to the vibrating micro-probe.

- **Thesis Objective 3** - To ensure the developed vibrating micro-probe can be used in an industrial metrology environment and can adhere to existing specification standards.

From the three **Thesis Objectives**, several **Research Questions** can be defined. These **Research Questions** are more detailed than the **Thesis Objectives**, and can be directly addressed and firmly concluded on at the end of the thesis as metrics for success. The **Research Questions** will be presented in Chapter 3.

The background knowledge of the concept of the NPL vibrating micro-probe will be presented in Chapter 3, and a research approach will be developed.

Chapter 3

Background and research approach

3.1 Introduction to background and research approach

In this chapter, the concept, design and manufacture of the NPL vibrating micro-probe will be presented. This represents the background knowledge to the thesis.

The **Thesis Objectives**, identified from the literature review in Chapter 2, will be discussed further, with respect to the development of a new probe. Following this, the requirements specific to the NPL vibrating micro-probe will quantified as a set of **Research Questions**. These **Research Questions** will contain clear metrics for success. The research approach will then be presented, defining the theoretical and experimental work needed to address the **Research Questions**.

3.2 The NPL vibrating micro-probe - background knowledge

To address the need for 3D counteraction of surface interaction forces, and the need for isotropic operation, a micro-CMM probe was conceived at NPL that was designed to operate in a vibrating mode [131]. This probe is referred to as the NPL vibrating micro-probe, or the vibrating micro-probe. The design of the vibrating micro-probe is based on a silicon-based micro-probe, also designed at NPL [132, 133].

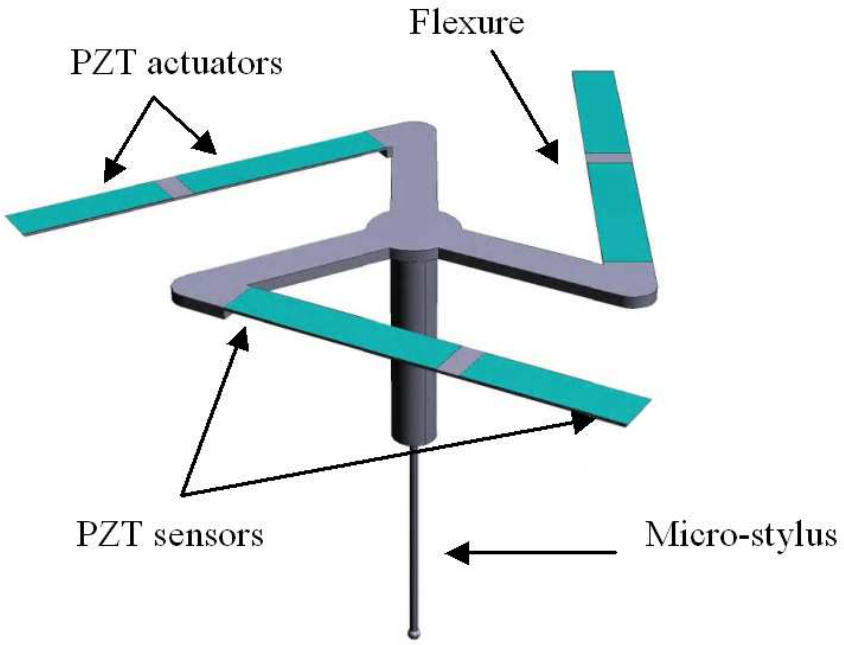

Figure 3.1: Schematic of the NPL vibrating micro-probe

3.2.1 The concept and design of the vibrating micro-probe

The vibrating micro-probe consists of a triskelion flexure array, housed in a MEMS device, assembled with a sphere tipped micro-stylus [133]. The system was designed to vibrate by using six piezoelectric actuators (two on each flexure). It was suggested that the vibration of the probe could be controlled such that the stylus tip is always vibrating normal to the measurement surface [131]. The vibration of the probe could also be controlled so that the acceleration of the stylus tip is sufficient to counteract the surface interaction forces between the micro-stylus tip and the measurement surface during contact measurement.

Interaction with the measurement surface produces a change in vibration characteristics and is determined by two PZT sensors on either end of each flexure. The basic design of the vibrating micro-probe is shown in figure 3.1.

The mechanical design of the flexures was completed to mimic the capabilities of the NPL SCMM probe [16], as well as emulate several of the design features of the probe by Pril *et. al.* [49, 50].

Computational mechanics and finite element (FE) analysis was used to model and simulate the performance of the conceptual design of the vibrating micro-probe. Simulations were used to compare several design options for the layout of the piezoelectric sensors for their output sensitivity [131]. The four modelled cases are shown figure 3.2, with the manufactured case being D.

Several further FE analyses were completed using the vibrating micro-probe as a test case [134, 135]; however, these did not result in any changes to the design.

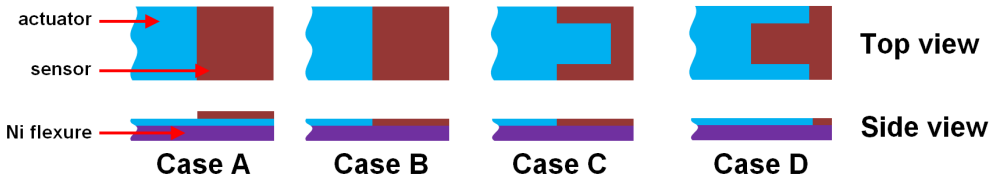

Figure 3.2: Diagram of the four investigated design options for the layout of the piezoelectric elements [131].

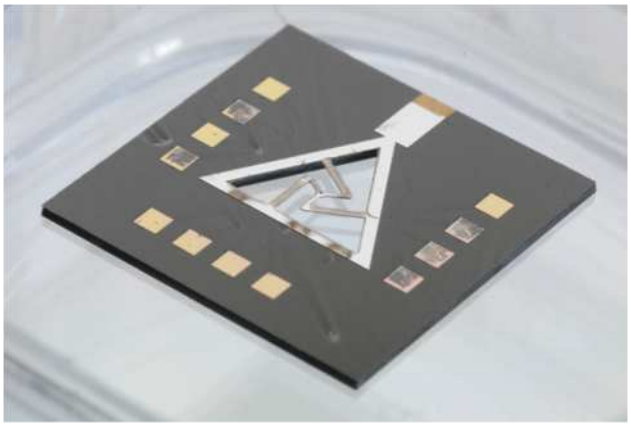

Figure 3.3: Image of the triskelion chip. When assembled with a micro-stylus this will form a vibrating micro-probe.

3.2.2 Manufacture of the triskelion chip

To fully realise the probe, MEMS production methods were used. This enabled very small and thin flexures to be made via deposition and chemical etching. The realised triskelion-flexure MEMS device is shown in figure 3.3. To best control the sensitivity of the sensors, a sol-gel spinning technique enabled the PZT elements to be deposited onto the flexures to a well-controlled thickness. It is essential that the thickness of the PZTs be controlled during production because the thickness of the PZT sensors is responsible for 83 % of the sensitivity of the device output [136].

The drive and sensing capabilities of the vibrating micro-probe were designed to be achieved through the integration of PZT and the triskelion flexures to create a unimorphic structure [131]. The composite sol gel deposition process was also used to compensate for the incompatibility between sintered PZT (processed at 1200 °C) and the mechanical and electrical materials (nickel, platinum and silicon), which are processed at 700 °C. To provide the active and sensing elements on the flexures of the probe, PZT thick films were deposited at these low temperatures resulting in a high quality functional ceramic integrated directly with the materials. The PZT layer was deposited on a sacrificial silicon substrate. The metallic structural support material was then deposited. After completion of the device, the sacrificial silicon layer was removed, resulting in a silicon-free device. The active structure of the device was manufactured from nickel rather than silicon in order to realise a more physically robust structure. A full account of the manufacture

of the triskelion chip can be found in [131]. A number of adjustments had to be made to the initial design dimension of the flexure width, primarily to accommodate the electrical connection tracks to the actuator and sensor areas, and to allow for the potential threat of PZT over-etch during the creation of the flexure legs.

3.2.3 Production of the micro-stylus

The sphere-tipped stylus is manufactured from tungsten by using a hybrid process of wire electro-discharge grinding (WEDG) and one-pulse electric discharge machining (OPED) [137]. A tungsten rod, approximately 50 µm in diameter, is produced using WEDG. The tip is then subjected to a single, high-energy pulse that melts the material. This rapidly solidifies into a sphere due to surface tension forces. The diameter can be controlled by varying the duration and peak electric discharge current of the pulse. Currently, this vibrating micro-probe uses a stylus tipped with a nominally 70 µm diameter sphere. The surface roughness of the spherical tips produced using this technique are significantly better that those fabricated using WEDG or micro-EDM alone [137].

An important effect of decreasing the size of the probe tip is the reduced ability to ascertain its effective radius through classical qualification. Such qualifications are essential for the operation of any CMM to ensure the radius correction is properly included in any contacting measurements taken [138]. The measurement of stylus tips is a major challenge, especially as classical techniques, such as the measurement of a precision reference sphere, are unsuitable. Initial diameter and form quality control measurements can be taken during the manufacturing process, by using the movement axes of the manufacturing platform as measurement axes [139]. Currently, novel techniques, such as multi-reversal using three spheres [140], result in an average radius and form value, and an indication of the 3D shape of the sphere; however, this and other techniques quickly become unsuitable for spheres below approximately 100 µm. Optical techniques for the calibration of the shape, form and surface texture of probe tips below 100 µm with target uncertainties below 20 nm are being developed at NPL [141]. This level of uncertainty is required because the form variation of probe tips below 100 µm is similar to the desired uncertainty of the resulting measurement, therefore, a more detailed, and indexed, map of the probe tip is required to more accurately apply probe radius corrections. As of yet, no probe tip calibration has been completed on the stylus.

3.2.4 Assembly of the vibrating micro-probe

Several assembly routes were suggested for the vibrating micro-probe [142, 143]. Assembly of the flexure MEMS device and the spherical stylus tip was finally completed using a miniaturised assembly setup comprising a dedicated miniature robot [144]. The setup is installed at Technische Universität Braunschweig (TUB, Braunschweig, DE). A micro-gripper was connected to the robot

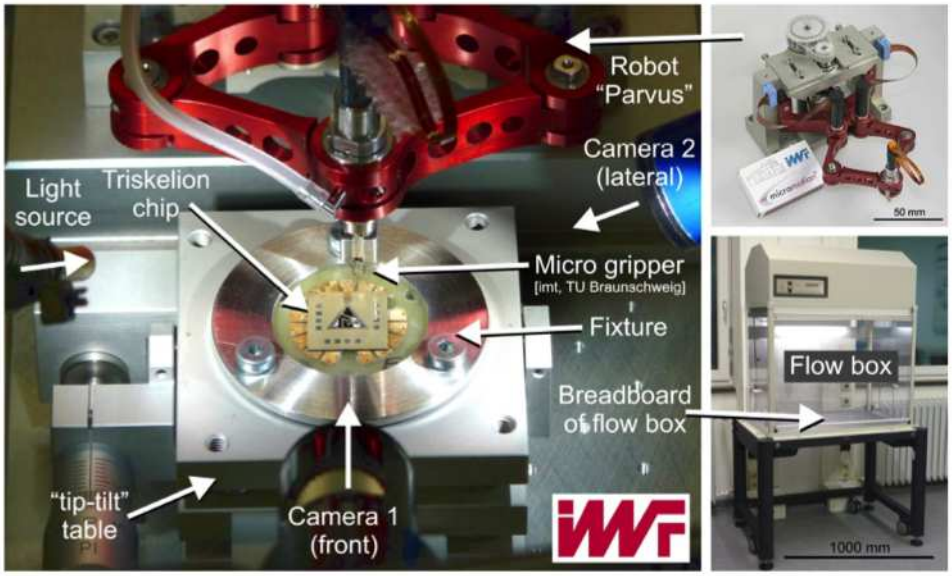

Figure 3.4: Image of the assembly system setup at TU Braunschweig. The flow box enclosure for the assembly system ensures a low noise environment for operation, free from disturbing air currents. Image courtesy of TU Braunschweig

and two microscope cameras were arranged within the workspace with front and lateral views. A fixture was designed and manufactured to hold the triskelion chip on a tip-tilt table within the robot's workspace. The capability of this setup beyond that of conventional assembly systems, including accuracy, repeatability and the scope for automation, is fully described elsewhere [145, 146]. The setup is shown in figure 3.4.

Each assembled vibrating micro-probe was visually inspected to establish the orthogonality of the stylus. This test was completed under a microscope in comparison to a miniature right-angle standard. Each completed probe was also functionally tested by applying a lateral force on the stylus to verify sound adhesion between the assembled parts. Twelve micro-CMM probes were successfully assembled using the method described in [146]. A photograph of a completed micro-CMM probe is shown in figure 3.5, and a video of the assembly process can be found at [147].

As a prototype assembly method, processing small volumes of parts, the semi-automated system described in [145] is sufficient. Automation is used to ensure repeatable volumes of adhesive are deposited on the triskelion and to ensure repeatable placing of the stylus at the triskelion. However, many operations, such as picking up and handling of the stylus, and fine adjustments of the position of the stylus before curing, are completed under manual control. Should there be a need to scale up the process for higher production volumes, more automation would have to be implemented.

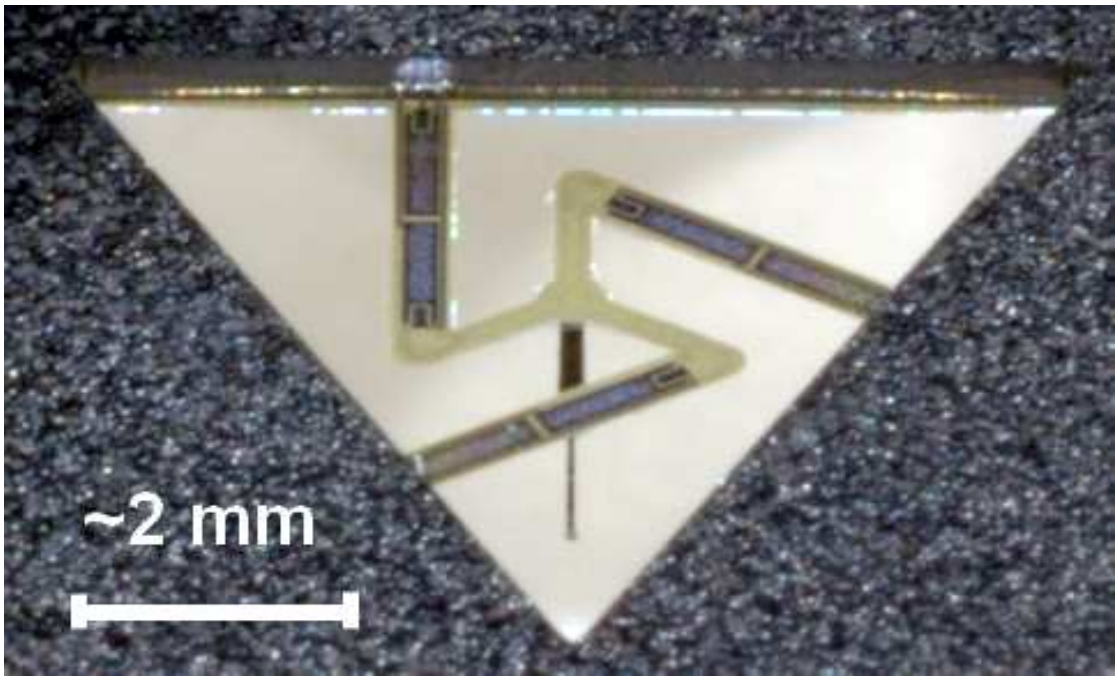

Figure 3.5: Image of an assembled vibrating micro-probe

3.2.5 Summary of the background knowledge regarding the NPL vibrating micro-probe

A vibrating micro-probe has been designed at NPL to address the limitations of existing micro-CMM probes. Some background work was completed towards this **aim** before this PhD started, however this has been clearly highlighted. A detailed scope of this thesis will be further defined in this chapter.

The design and intended operation of the NPL vibrating micro-probe is the subject of several patents [148, 149, 150].

3.3 Research approach

It is clear from Chapter 2 that all recently developed micro-CMM probes are limited in their ability to operate in micro-scale environments, i.e. below 100 µm. Highly refined mechanical micro-probes cannot act with a low enough probing force in order to avoid damaging the measurement surface. Through the development of optomechanical micro-probes, and silicon-based micro-probes, probing forces have been reduced and more accurate measurements attained. However, as these systems became more sensitive, the effect of surface interaction forces on the probes becomes highly detrimental to their operation. To address this, a method for counteracting surface interaction forces in 3D must be developed, through the use of the existing vibrating micro-probe concept. This development must include new characterisation techniques suitable

for comparing classical probes with 3D vibrating probes. New operation strategies should also be suggested and discussed to highlight the ease of use of the vibrating micro-probe.

Due to the complex nature of this research, a clear definition of the scope of this work is required, along with a good understanding of the requirements of micro-CMM probes. A complete research approach can now be set out. A clear set of metrics will be described at the end of this chapter, in the form of several **Research Questions**, to allow quantification of success.

A basic overview of the research approach, and how it is used to link all the individual chapters of this thesis, is shown in figure 3.6. The research approach consists of four main stages. Initially, an extensive literature review is completed into the existing capabilities of micro-CMM probes. This has been completed and is reported in Chapter 2. Through analysis of this literature, three main knowledge gaps have been identified that are preventing further development in this area. These three knowledge gaps are: a lack of ability to counteract surface interaction forces in three dimensions on the micro-scale; no existing definition of isotropy for vibrating micro-CMM probes; and no agreed strategies for use for any 3D isotropic vibrating micro-CMM probes. These three knowledge gaps correlate directly with the objectives of this work.

With this definition complete, the second stage, a theoretical modelling stage, can be addressed. An understanding of surface interaction forces at the micro-scale, and how the mechanical and geometrical considerations of the vibrating micro-probe can be utilised to define the theoretical capabilities of the probe will be defined. This stage of the work will be reported in Chapter 4.

The third stage is experimental validation of the vibrating micro-probe. The main experimental work will focus on confirming that the probe has the ability to counteract surface interaction forces in three dimensions at the micro-scale, and also that the vibration of the probe are analogous to isotropic behaviour in more classical micro-probes. This stage of the work will be reported in Chapter 5.

The final stage involves work to ensure the developed probing system is relatively easy to use. This will involve the development of normative strategies for use of 3D vibrating micro-CMM probes. It will also ensure that the developed micro-probe is adherent to existing specification standards and is, therefore, easily comparable to existing, more classical, micro-CMM probes. This stage of the work will be reported in Chapter 6.

Using all of the described stages, a set of informed conclusions can be drawn as to the capability of the new probe, and a clear direction for future work can be defined. This stage of the work will be reported in Chapter 7.

A detailed description of the research domain will now be completed. This will begin with a definition of the scope of the work, in the context of the **Thesis Aim**. The areas of research that are outside the scope of this thesis will also be clearly defined.

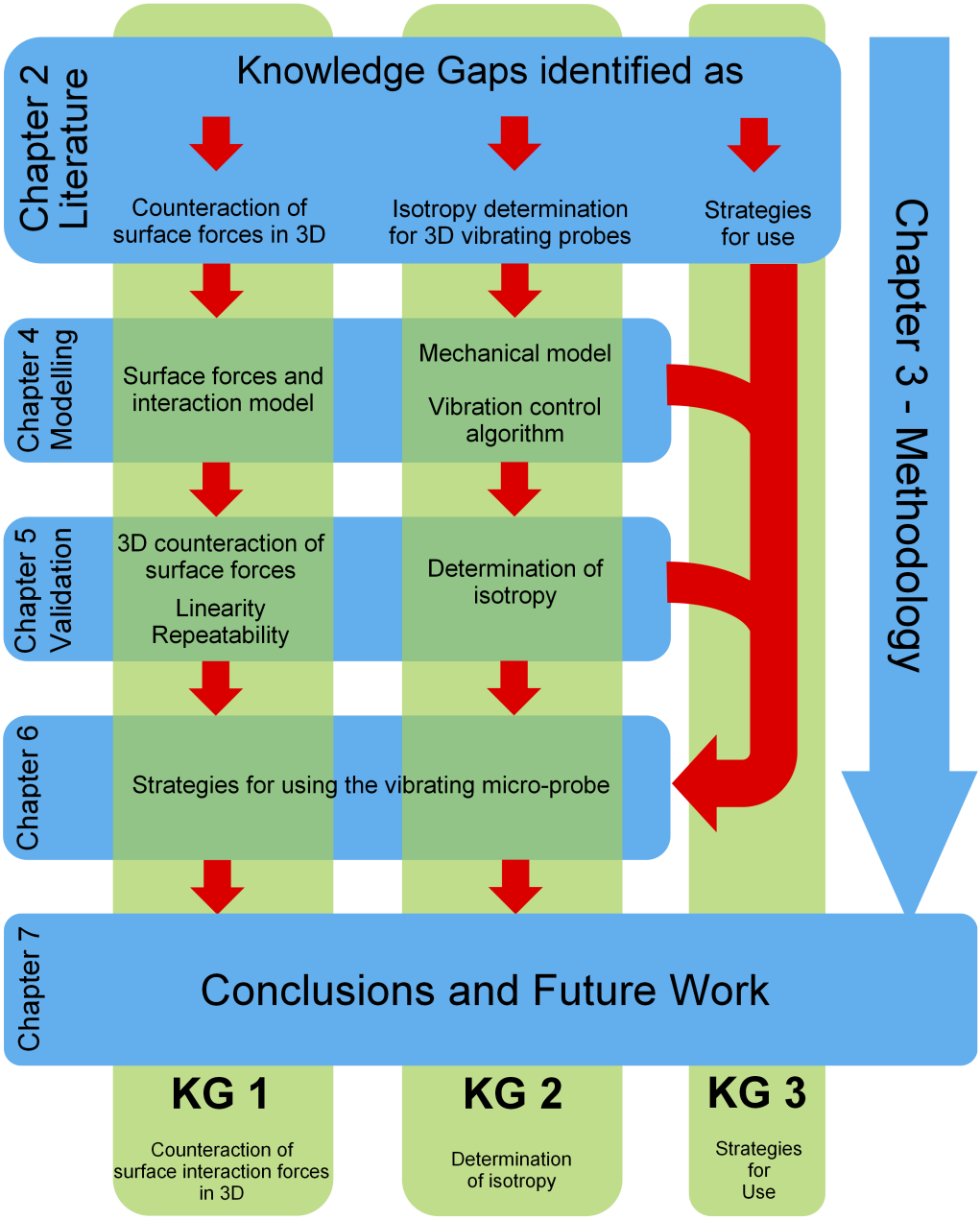

Figure 3.6: Graphical representation of the thesis structure, detailing the work included in each chapter, including the research approach that links them.

3.4 Definition of scope and research domain

This thesis is clearly defined by the **Thesis Aim**:

> *"to develop and operate a contacting probe such that it enables existing micro-CMMs to reliably measure sub-100 μm features in three dimensions to an uncertainty below 100 nm"*

To address this **Thesis Aim**, there are three main knowledge gaps that must be considered. Firstly, there currently exist no ways to counteract the surface interaction forces in three dimensions. Therefore, methods to counteract the surface interaction forces in three dimensions should be developed. Secondly, a new concept of isotropy must be developed for application to vibrating micro-CMM probes. Lastly, a set of operational procedures should be defined for the newly developed probe, whose mode of operation differs significantly from that of existing classical micro-probes. These operational procedures will help operate the probe such that it is easy to use, adheres to existing specification standards, and can be directly compared to other probes. The three main knowledge gaps define the three **Thesis Objectives**.

These three **Thesis Objectives** will now be discussed so as to clearly define the scope of the work. Following this, a clear definition of any work outside this scope, but still related to the development of a micro-CMM probe, will also be discussed.

3.4.1 Counteraction of surface forces

Even though the method of vibrating a stylus tip to negate the effect of stiction has already been documented, the developed methods are only one dimensional. Also, the existing methods cannot easily, if at all, be expanded into two or three dimensions. There are several methods that have been attempted, including: extensive alteration of the CMM probe head to allow manipulation of a one dimensional vibration through articulation and rotation [117] or the random application of agitation to simply mitigate the effect of surface interaction forces [89, 97]. Therefore, an improvement on vibration control is an area of investigation and development within this project.

3.4.2 Isotropy

Isotropy is clearly defined for static CMM probes as having equal stiffness (measured in newtons per metre) in all directions of operation. Isotropy has also been linked to the sensitivity of the detection capability of the probe [82]. The importance of isotropy during micro-CMM probing has been described previously in section 2.5.3. One way of determining the probing forces, and therefore isotropy, of classical CMM probes is to use a force sensor [72, 151]. However, this is not the case for vibrating systems because, due to the mode of intended operation, there is reduced surface contact time, meaning existing force sensors may not react fast enough to determine the

contact force. A further reason for the lack of expertise in the characterisation of the isotropy of a vibrating system is that there is a lack of 3D vibrating micro-CMM probes whose isotropy requires determination.

In terms of measures of the capability of micro-CMM probes, most definitions are equivalent, *i.e.* probing repeatability of triggering, probe resolution, length measuring error over a specific deflection length. However, it is expected that when considering isotropy, normal definitions do not apply to a vibrating micro-probe. Instead, an alternate definition of isotropy will be developed, that focuses on the vibration frequency and characteristics of the micro-probe.

3.4.3 Ease of use

It is essential that any developed probe be easy to implement in an industrial metrology environment, if it is to be commercially viable. Due to the novel mode of operation, and the unique testing procedures that will be planned, it is expected that significant changes to classical operating procedures will be needed for the vibrating micro-probe to act in a similar, or at least comparable, way to classical micro-probes. Therefore, new operational strategies will be developed from experience gained during work completed in testing and validation, and will define expected operation for the vibrating micro-probe.

Also, an important inclusion into the **Thesis Aim** is that any probe developed during this work should be immediately applicable to existing micro-CMM platforms, such that no major alterations to the operation mechanics or kinematics of the system are required. Once installed onto a suitable CMM, the probe should adhere to existing specification standards. The suitable standards will be reviewed and the adherence of the vibrating micro-probe will be discussed.

3.4.4 Limits

It is essential that a set of clear limits are placed on this work from the beginning. This is especially true when the work is a continuation of previous developments [131]. Also, given the possible size of the project, and its reliance on several experimental technologies, it is prudent to define what is outside of the scope of the project. Much of the work described by these limits is essential to the development of the vibrating micro-probe, and, when necessary, will be nominally described within the text of this thesis and will be correctly referenced.

3.4.4.1 Predefined design

The design of the vibrating micro-probe that is presented here has not been developed within the scope of this thesis. The design process occurred previous to the start of this PhD. No further major changes will be made to the design. A geometrical and mechanical study into use of the triskelion structure as a low force transfer artefact has been completed elsewhere

[152, 153], the results of which had little effect on this work. It should be noted, however, that one superficial changes was been made to the probe design, to include a polymer encapsulation layer. This change was completed in consultation with the manufacturer and resulted in no discernible mechanical change to the system. The reasoning behind this change is described in Chapter 6.

3.4.4.2 Manufacture of the triskelion-flexure MEMS devices

Following on from the initial design exercise, a clear manufacturing route for the triskelion-flexure MEMS chip, containing the active elements and the triskelion flexure array, was developed. This process, which made the first prototype chips used for the formulation of this project, was completed in an external research laboratory. The manufacturing routes taken advantage of during the work were well established at the beginning of this project. Any manufacturing runs completed during this project were commissioned and funded by the project. A description of the route can be found elsewhere [135]. No major changes were made to the manufacturing route used.

3.4.4.3 Manufacture of the micro-stylus

The styli described as part of the developed probe are monolithic tungsten micro-styli that are made through a hybrid manufacturing technique of WEDG and OPED [137, 139]. The manufacture of the micro-styli is a process that is still experimental and is far beyond the development scope of this PhD. However, the production technique was adopted and developed to manufacture a stylus that was nominally ideal for the vibrating micro-probe.

3.4.4.4 Assembly of the vibrating micro-probe

Following the manufacture of the triskelion-flexure MEMS chip and the micro-stylus, The assembly of these constituent parts must be considered. A complete vibrating micro-probe is assembled from one triskelion-flexure MEMS chip and one micro-stylus. The development of a specialised micro-scale assembly route for these probes occurred during the working period of the PhD, and was completed in collaboration with external research establishments [145, 146]. However, because the physical assembly was completed at an external establishment and using specialised equipment that was developed as part of an external project, this work will be referred to, but not described in detail.

3.4.4.5 Measurement of the stylus-tip

A physical property of the micro-stylus, that is essential for the operation of the probe, is the quality of the stylus tip. This quality is almost exclusively related to its form error, or sphericity.

This stylus tip form error is a contributor to the final probing uncertainty. For the purpose of this PhD, and especially because the manufacturing of these styli is outside the scope of the work, it is assumed that the tips are perfectly spherical. It is known that, qualitatively, the stylus tips are not truly spherical, however, because of the size of the stylus tips (less than 100 µm), it is widely acknowledged that classical probe tip verification techniques, such as probing of a high precision reference sphere [138] is not fully suitable [140]. Direct characterisation of stylus tips, through interferometry, is a technique that is being developed as part of an a Europe-wide research project [141], and may be the preferred technique for the high precision characterisation of micrometre scale stylus tips.

However, verification of the virtual stylus tip will be discussed in the fourth stage of this PhD. Most importantly, the strategies required for probe tip verification will be suggested, but the implementation of these strategies involves installing the probe on a micro-CMM. Given the complexity of this task, the installation of the probe onto an existing micro-CMM is deemed outside the scope of this project.

3.5 Definition of research questions

So far, the contents of this chapter has described the knowledge gaps that are blocking the development of a vibrating micro-probe and, therefore, the objectives of this work. These knowledge gaps were highlighted with direct reference to literature published in the area of micro-CMMs.

Also, a clear specification of requirements for any probe has been described, against which the operation of any new probes can be judged. These requirements will now be presented with direct reference to the NPL vibrating micro-probe.

3.5.1 Stylus dimensions

Although the development of the experimental technique for the manufacturing of the micro-styli is outside the scope of the project (as is the probe assembly technique), the design of the stylus is within the scope. A stylus must be designed that allows the probe to measure sub-100 µm features to high accuracy in 3D. Also, the stylus should have dimensions that are reasonable by comparison to other existing micro-CMM probes, in terms of tip diameter and length, *i.e.* aspect ratio. The dynamic response of any designed stylus should also be considered, given that the final probing system is designed to vibrate.

3.5.2 Probe error

Several measures of the capability of the probe to complete measurements are often quoted, including probing repeatability of triggering, probe resolution or length measuring error over a specific deflection length.

Any new micro-CMM probe should exhibit highly repeatable operation. The repeatability of a probing system is a major contribution to any uncertainty calculation completed after a measurement has been made, and will, therefore, have a direct effect on the accuracy of the micro-CMM. It is usual that a repeatability is quoted by the manufacturer as an indication of the reliability of the system. It is unusual for a user of a commercial micro-CMM to try and determine the repeatability of the probing system, as this will require the probe to be removed from the micro-CMM and tested. Testing procedures for the repeatability of a probe are best determined during development.

Repeatability tests on probes are usually completed though the repeated probing of ideal surfaces, using an external precision manipulation system. Through running these tests for extended periods, a clear indication of the capability of the probing system over individual probing points and drift over extended periods of time can be determined. It is usual that an ideal surface, such as a gauging surface, is used, and that the time period is several hours. A gauging surface is usually used because it is a polished, flat surface, is free from contamination (if well kept) and is a good example of a surface used during routine measurements of micro-CMMs. The extended test period of several hours is an extreme condition for testing, as it is unusual that a measurement task will take this long. However, if the probe proves to be repeatable over several hours, it can be deemed to be suitable for use over an extended time period, which is a useful trait for any CMM probing system, regardless of scale.

In order to directly address the **Thesis Aim** of reliably reducing the 3D measurement uncertainty of micro-CMMs to below 100 nm using the vibrating micro-probe, it is estimated that the repeatability of the probe should be below 10 nm. A probing error of 10 nm is comparable to the most accurate probe currently available, as described in table 2.4.

The accuracy of the probe should also be determined using an external precision manipulation system. Due to the requirements of these CMMs to measure linear distances to sub-micrometre accuracy, the probe is also required to have some form of distance measurement capability, which must be accurate, as well as repeatable. The inclusion of strain gauges into modern, commercially available, probes, both macro-scale and micro-scale, has resulted in probes that can determine distance measurement within the operation range of the strain gauge, and also within the elastic range of the flexures. Subsequently, an indication of a zero position within the probing operation can be determined. Some appreciation of the over-travel of the probe can also be gained, to the benefit of the both the measurement system, and the safety system of the CMM.

To determine the accuracy of the probe, a similar experimental setup to the repeatability tests will be required. However, a further capability of the precision manipulation system is that it be accurate in its positioning capability, so that a direct comparison can be made between the position of the stage and the signals collected from the probe. From this, a length measurement scale can be attributed to the probe. A major limitation of the determination of this length scale will be the repeatability of the probe, as from this an appreciation of the accuracy of any scale conversion from probe output to length can be obtained. However, it is estimated that it should be a requirement of the probe that it accurately determine length to 20 nm over the maximum over-travel of the probe. In the case of a vibrating probe, this over-travel distance is not a function of the elastic limit of either the strain gauges or the flexures, but instead is a distance equal to the amplitude of the vibration of the probe.

3.5.3 Isotropy

Isotropy is an essential characteristic of any CMM probe, and it describes the capability of the CMM to act equally in all probing directions. This becomes particularly useful when the probing system is being used to take measurements in scanning mode, and the action of the probe is constantly changing with the surface of the measured part. Currently, isotropy is validated on static probes through determining the spring constant in each probing direction, or at least in the vertical and lateral directions.

Due to the active nature of the vibrating micro-probe, it is difficult to use the spring constant method for determining the extent of isotropy. Therefore, a new concept of isotropy, with respect to vibrating probes, is to be developed. This will involve ensuring that the probe is able to act equally in all probing directions, by ensuring that it can vibrate at the same amplitude and frequency in all probing directions. To determine whether the probe acts isotropically, a validation experiment will be run where the probe is interacted with an array of angled faces. Initially, these experiments will be run in the lateral directions. Through these experiments, the ability of the probe to act equally in each lateral direction will be confirmed. The probe will be deemed to act isotropically if it is able to vibrate with similar amplitudes (to within a pre-defined range) in all lateral and vertical directions, while being active at one vibration frequency.

3.5.4 Probing force

The probing force of a CMM probe is often quoted as an indication of the amount of measurement surface damage that can occur during use. However, during the development of new micro-CMM probes, as reported in Chapter 2, several attempts were made to lower the probing force, usually by reducing the stiffness of any suspension elements, and increasing the sensitivity of any sensor elements. This had the adverse effect of making the probes susceptible to the surface interaction forces, which resulted in the development of vibrating probes.

As with isotropy, methods to determine the probing force for a vibrating micro-probe are not yet available. Therefore, some indication of the probing force of the vibrating micro-probe will be estimated.

3.5.5 Ease of use

As has been previously stated, the ease of use of any probe will have a marked effect on its uptake in industry. To address this, a set of operational strategies will be developed, based on lessons learnt during testing, to ensure the probe is easy to use. Also, a clear statement on the adherence of the probe to existing specification standards will be made.

3.5.6 Summary of research questions

Using the previously defined micro-CMM probing requirements, and also the **Thesis Objectives** derived from the knowledge gaps, a succinct set of **Research Questions** can be defined. These will be revisited in Chapter 7 as a definition of the success of this work. These **Research Questions** are directly linked to the three **Thesis Objectives**, and are numbered accordingly.

Research Questions related to **Thesis Objective 1** - To develop and validate methods to operate the NPL vibrating micro-probe such that it can counteract surface interaction forces in 3D:

- **1.1** Can a stylus be designed that has a stylus tip diameter below 100 µm, an aspect ratio similar to existing micro-manufactured features, and is suitable for use with a vibrating micro-probe?
- **1.2** Can a vibrating micro-probe be operated with a probe point repeatability of 10 nm?
- **1.3** Can a vibrating micro-probe be operated with a length measuring error over the maximum deflection length of 20 nm?

Research Questions related to **Thesis Objective 2** - To develop and validate a new concept of isotropy that can be applied to the vibrating micro-probe:

- **2.1** Can a new concept of isotropy be developed that relates to a vibrating micro-probe, and can this concept be used with the vibrating micro-probe?
- **2.2** Can any indication of the probing force of a vibrating micro-probe be determined?

Research Questions related to **Thesis Objective 3** - To ensure the developed probe can be used in an industrial metrology environment and can adhere to existing specification standards:

- **3.1** Can a set of operational strategies be developed for a vibrating micro-probe that prove its ease of use?
- **3.2** Can a vibrating micro-probe be adherent to existing specification standards?

The five micro-CMM probing requirement of stylus dimensions, probe error, isotropy, probing force and ease of use are inexorably linked, such that some cannot be fulfilled without others. For example, if the detection capability of the probe is very repeatable, then it is more likely that an accurate scale can be put on its operation. Likewise, for a probe to act isotropically, it should also act accurately in all directions. All of these requirements are also closely linked to the probe's ability to counteract the surface interaction forces that are prevalent at the operation scale of this probe.

Following the work contained within these first three chapters, especially the definition of the **Thesis Aim**, **Objectives** and **Research Questions**, the technical work of this thesis can now be presented.

Chapter 4

Theoretical modelling of the vibrating micro-probe

4.1 Introduction to modelling of the vibrating micro-probe

The contents of this chapter will report all of the theoretical work conducted with regards to the NPL vibrating micro-probe. A wide range of modelling work has been completed, both finite element (FE) and analytical.

The work described in this section builds on the earlier modelling exercises that were carried out during the early stages of the design process. The previous work, described by Stoyanov *et. al.* [131], was sufficient for informing the design process; however, little further work was continued to model the mechanical characteristics of the probe or its operation. In order that the operational requirements be correctly defined, and to allow for efficient design of experiments, several further models were developed.

Firstly, the mechanical aspects of the constituent parts of the micro-probe will be considered and modelled. This will include: the mechanical characteristics of the triskelion-flexure MEMS, especially its frequency response to applied masses (corresponding to assembled styli); and the design and mechanical characteristics of micro-styli suitable for use with the triskelion-flexure MEMS to form a fully working probe.

Following this, a set of models of the probe when operating in vibrating mode were developed. These models will consider both the mechanical operation of the probe and the electrical operation of the probe. The electrical model will begin to estimate the input signals required to control the vibration of the vibrating micro-probe.

The combination of the mechanical and electrical models can be used to design a set of algorithms that will control the vibration of the probe during use, ensuring that the interaction vector between the probe and the measurement surface is always optimal and therefore isotropic. This will directly address the development requirements of **Thesis Objective 2**.

Subsequently, a detailed analysis of the surface interaction forces prevalent in low force, high accuracy contact probing will be conducted. This exercise is essential for the continued development and validation of the probe, as the counteraction of these interaction forces is the main reason for the probe operating in a vibrating mode. Once the investigation into the surface interaction forces is complete, their effect on the operation of the vibrating micro-probe can be considered. This will directly address the development requirements of **Thesis Objective 1**.

At all stages in the modelling process, the limitations of the developed models are considered and discussed. This is essential, as the validation experiments will be developed based on the results of these models. Therefore, an understanding of any possible errors is key.

4.2 Mechanical modelling of the constituent parts of the micro-probe

4.2.1 Introduction to mechanical modelling

The vibrating micro-probe is a MEMS formed from the assembly of two major structural elements. These are the triskelion-flexure MEMS and a sphere-tipped micro-stylus. As can be seen from the contents of Chapter 3, the design of the triskelion-flexure MEMS has been predetermined before the start of this PhD. Therefore, as few changes can be made to the triskelion-flexure MEMS, instead work has been completed in better understanding its mechanical characteristics, both statically and during dynamic operation.

Conversely, the design of the sphere-tipped micro-stylus was undetermined during the design stage of the probe, and was identified as a research requirement in **Research Question 1.1**. Therefore, a set of model based techniques have been developed to determine the optimal geometry for the stylus, based on knowledge of the existing constraints. There are two main constraints placed on the design of the micro-stylus. A geometrical constraint is that the stylus must fulfil the requirements for use as part of a micro-probe by having a suitable aspect ratio (therefore, a suitable tip diameter and effective stylus length). A second constraint is that, when assembled with the triskelion-flexure MEMS, the stylus should not significantly interfere with the mechanical characteristics. A further limitation stems for the capability of the techniques available for the manufacture of the sphere-tipped micro-stylus.

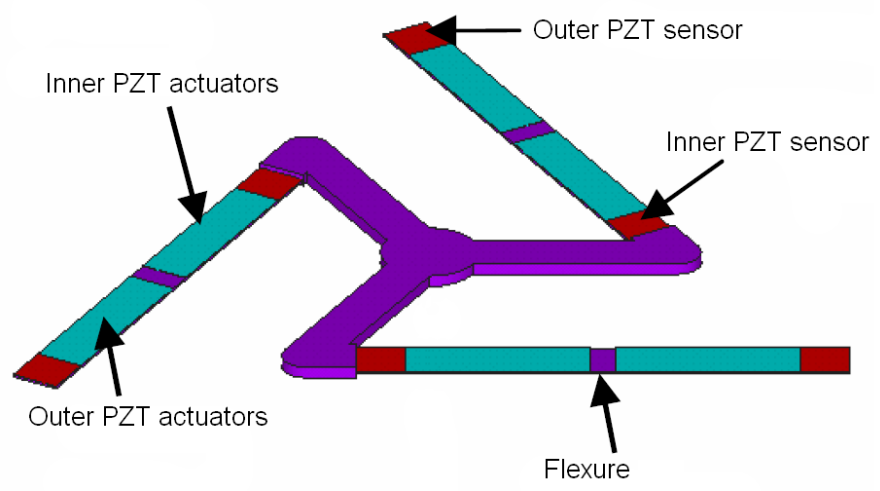

Figure 4.1: Concept design for the triskelion-flexure MEMS [131]

The work completed in the area of mechanical modelling of the triskelion-flexure MEMS and the sphere-tipped micro-stylus will be presented and discussed. To conclude, the final design of the sphere-tipped micro-stylus will be presented.

4.2.2 Modelling the triskelion flexure system

During the design process, an FE model of the triskelion-flexure MEMS was programmed to enable certain aspects of the device to be tested. This model was developed by Stoyanov *et. al.* at the University of Greenwich (London, UK) [131]. These aspects were initially limited to geometrical design and material makeup based on certain requirements, including isotropy and ease of manufacture. Following this, a further design step was implemented that investigated the sensitivity of the piezoelectric sensors with respect to size, shape and position.

The FE model of the probe was constructed in ANSYS Release 11.0 [154]. The flexures and connecting arms were programmed with standard material properties similar to that of nickel: an elastic modulus of 207 GPa, a Poisson's ratio of 0.31 and a density of 8 800 $\mathrm{kg\,m^{-3}}$ [155]. The generic boundary condition for the model is that the ends of the flexures, which would attach to the silicon chip, are constrained in all six degrees of freedom. The FE model of the triskelion-flexure array was meshed using the ANSYS default fine meshing parameters, resulting in a model consisting of approximately 40 000 elements.

The triskelion-flexure structure is oriented such that the piezoelectric elements are upwards facing, in the $+z$ direction and, therefore, gravity is made to act in the $-z$ direction. An image of the physical model is shown in figure 4.1.

Modal analysis of the triskelion-flexure MEMS was completed from 1 kHz to 30 kHz and indicated that the structure had a natural frequency of approximately 5 kHz [131]. The results of these investigations form the background for this work on the modelling of the triskelion-flexure

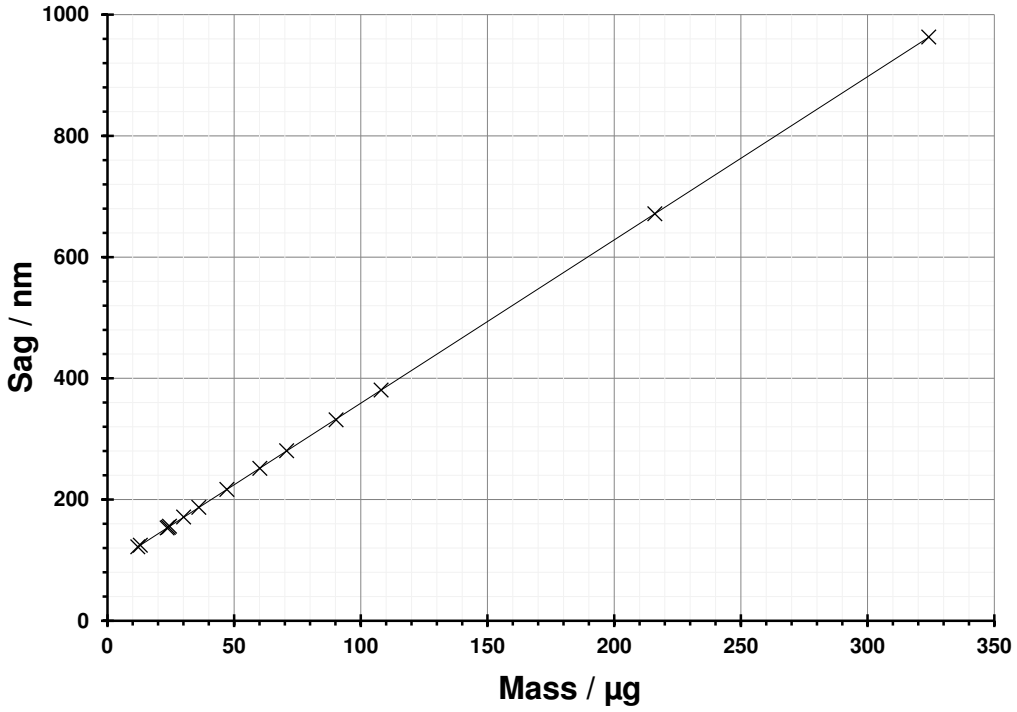

Figure 4.2: Graph of the deflection of the FE model of the triskelion plotted against applied mass

MEMS. Following the initial investigation, the FE model was transferred from the University of Greenwich to NPL for further analysis, and the following work was completed.

The first test completed on the FE model of the triskelion-flexure MEMS was an investigation into its elastic properties. This is an important property to note due to its close link to resonance, and therefore to the dynamic performance of the vibrating micro-probe.

To complete the harmonic analysis test, a range of point masses up to 250 µg were implemented in the FE model at the central island of the triskelion-flexure structure and the resulting deflection was recorded. These masses were simulating the effect of assembling a stylus onto the z motion of the central island of the triskelion-flexure MEMS, with a mass of 250 µg being an estimate for the upper limit of the mass of a sphere-tipped micro-stylus of sufficient aspect ratio for this micro-probe. This upper mass limit is estimated as the mass of a tungsten carbide test stylus, 3 mm long and 150 µm in diameter. The results of these tests are shown in figure 4.2, where resulting deflection of the triskelion-flexure MEMS is plotted against the applied mass.

The data shown in figure 4.2 is a force versus displacement plot. Therefore, the gradient of the best fit line through the data is an indication of the spring constant of the triskelion-flexure MEMS. To convert the applied mass to the applied force, an acceleration factor equal to the acceleration due to gravity is used, in this case $9.81\,\mathrm{m\,s^{-2}}$. Some uncertainty is present in the data shown in figure 4.2. Assuming that all the input parameters are correct, there is a finite error in the measured deflection equal to the resolution of the solution of the model. The resulting

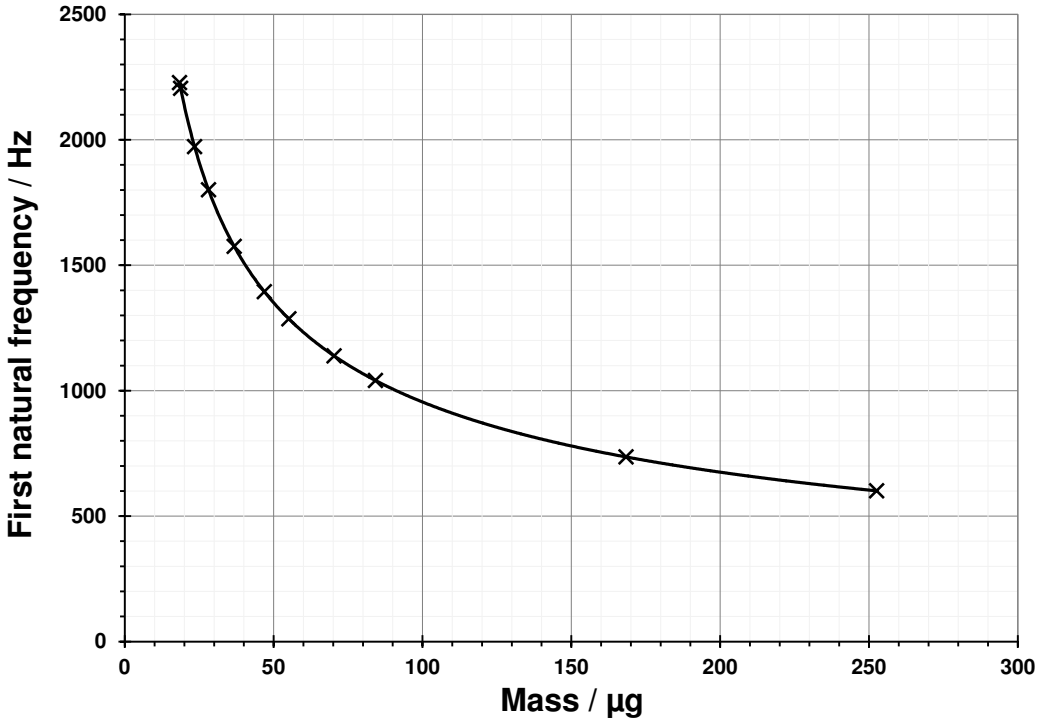

Figure 4.3: Graph of the first natural frequency of the FE model of the triskelion plotted against applied mass

spring constant estimate for the triskelion-flexure device is $3.6\,\mathrm{N\,m^{-1}} \pm 0.1\,\mathrm{N\,m^{-1}}$. As it is unlikely that a stylus will be constructed that has a mass below 10 µg, any styli with masses below 10 µg were omitted from the calculation of the spring constant. Also, it has been previously determined that, for small deflections of the triskelion-flexure system, there exists a parasitic rotation of the central island [152], further suggesting that low mass styli should not be considered.

Following this static investigation, an understanding of the dynamic response due to applied mass can also be considered. The resulting first natural frequency of the triskelion flexure MEMS can be calculated by considering the spring constant calculated using the previously noted equation. The results of this analysis are shown in figure 4.3.

Through this analysis, an appreciation of the mechanical properties of the triskelion-flexure MEMS have been obtained, especially its mechanical reaction to the assembly of a micro-stylus whose mass lies in the range 1 µg to 250 µg. From this analysis, an estimate of the spring constant of the system has been calculated, as well as an understanding of the effect any assembled micro-stylus will have on the resonance frequency of the resulting completed probe. To continue this investigation, a more complete description of the micro-stylus is required, beyond its mass.

4.2.3 Modelling the stylus

The sensitivity of any classical CMM probe is closely related to the compliance of the stylus compared to that of the probe's flexures and sensors. Ideally, an infinitely stiff stylus should be used so that the force imparted on the stylus as a result of surface contact is transmitted directly to the probe's sensors. This is, however, an impossible scenario, and the best case results when the stiffness of the stylus is several orders of magnitude higher than the flexures of the probe, or when the resulting bending of the stylus can be estimated, or even measured during the qualification of the probe. It is essential, therefore, to understand the physical properties of the stylus prior to manufacture, so that the optimal stylus can be designed and assembled with the triskelion-flexure MEMS to form a probe. This requirement is specifically addressed in **Research Question 1.1**.

Another essential requirement for the design of a stylus is ensuring that its geometry is suitable for the intended measurement task. For many mechanical CMM probes, especially those associated with classical CMMs, the probe styli are interchangeable, and in fact can be individually designed and manufactured for specific measurement tasks without much cost or effort. This is not the case for most micro-CMM probes.

Finally, classical modelling exercises are not entirely applicable when considering a vibrating micro-CMM probe. As well as the classical tests for geometry, stiffness and deflection, the effect of the micro-stylus on the vibration of the probe, especially its frequency and amplitude, must be calculated, and the effect of forced vibration on the micro-stylus itself must be considered.

Therefore, a set of trial micro-styli were designed that fulfilled the dimensional and material requirements for the micro-probe. The dimensional constraints were that the spherical stylus tip should have a diameter of less than 100 µm, a shaft diameter that tapered from a maximum of 200 µm to a minimum of 30 µm and a total length between 1 mm and 3 mm. This results in a set of probes whose aspect ratios range from 5 to 100. These constraints offer an aspect ratio able to access typical structures in MEMS and micro-manufactured products. These dimensional limits are defined according to the required tip diameter and aspect ratio, but also from the standard stylus design paradigm. It should be noted that there are sometimes two calculable aspect ratios for any given stylus; the aspect ratio (as calculated by the full length of the stylus and its maximum diameter) and the effective aspect ratio, or effective working aspect ratio (as calculated from the stylus tip diameter and the effective working length [83]. See figure 2.27 for further details). In most cases throughout this work, the effective stylus aspect ratio will be reported, as it best describes the working capability of the stylus. A list of eighteen test stylus designs is presented in table 4.1. A graphical representation of the stylus geometry is shown in figure 4.8 (on page 94) and in relation to the triskelion flexure MEMS in figure 4.6 (on page 93).

Table 4.1: Description of the eighteen modelled styli used to investigate the mechanics of the vibrating micro-probe

Name		Length / mm	Upper diameter / µm	Lower diameter / µm	Stylus aspect ratio	Effective stylus aspect ratio
No stylus		0	0	0	-	-
Composite 1	**a**	1	50	30	10	16.67
	b	2	50	30	20	33.33
	c	3	50	30	30	50
Composite 2	**a**	1	100	50	5	10
	b	2	100	50	10	20
	c	3	100	50	15	30
Composite 3	**a**	1	200	70	2.5	7.14
	b	2	200	70	5	14.29
	c	3	200	70	7.5	21.43
Stylus 1	**a**	1	30	30	33.33	33.33
	b	2	30	30	66.67	66.67
	c	3	30	30	100	100
Stylus 2	**a**	1	50	50	20	20
	b	2	50	50	40	40
	c	3	50	50	60	60
Stylus 3	**a**	1	70	70	14.29	14.29
	b	2	70	70	28.57	28.57
	c	3	70	70	42.86	42.86

Table 4.2: Material properties of tungsten, tungsten carbide and nickel [155]

	Tungsten (W)	**Tungsten carbide (WC)**	**Nickel (Ni)**
Density / kg m^{-3}	19 254	15 000 (6 % Co) 14 200 (12 % Co)	8 907
Young's modulus / GPa	411.0	534.4	199.5 (soft) 219.2 (hard)
Poisson's ratio	0.280	0.22	0.312 (soft) 0.306 (hard)

Following the definition of these eighteen test styli, a set of tests can be devised that will enable an ideal stylus be chosen from this test set, or that a new stylus be designed, based on the results of the described tests, that is more ideal.

One initial observation is that composite stylus 2a and 3a, which has an effective aspect ratio of below 10, is likely to be geometrically unsuitable for the vibrating micro-probe. Therefore, this stylus will no longer be considered in these tests (although, for completeness, the results will be reported).

The material constraints placed on the stylus require it to be manufactured from a material with low density and high Young's modulus. The former allows for a low stylus mass, resulting in a higher operational frequency. The latter of these constraints helps to ensure high stiffness of the stylus, hence ensuring maximum sensitivity to transmit amplitude changes due to contact with the measurement surface. However, these two properties are usually mutually exclusive. The requirement of the high stiffness of the material was chosen as the property to focus on when choosing suitable materials, because it relates to the mechanical properties of the material rather than just its mass.

The most suitable material that fulfils the stiffness requirement, while also exhibiting a relatively low density, is tungsten carbide. However, most physical realisations of this material are a metal matrix composite, such as cemented carbide or tungsten-carbide cobalt. Due to this, the manufacturing process intended to produce a monolithic stylus with a spherical tip will not function well, resulting in either a very rough, non-spherical tip, a tip with a heavily carbonised surface, or no recognisable spherical tip at all [137]. Therefore, given the limits placed on the design of the stylus due to the manufacturing method, tungsten will be considered as the most suitable material for the manufacture of the stylus. The physical properties of tungsten, tungsten carbide and nickel (the material used to manufacture the triskelion flexure device) are considered in table 4.2.

Given the material properties of tungsten, the respective ideal masses of the eighteen test styli can be calculated. This would be a reasonable estimate for the resulting mass of a stylus produced to these specifications. Included in the mass for each test stylus is a sphere of the same material, 70 µm in diameter. A stylus tip diameter of 70 µm was chosen to represent a size smaller than the

current state-of-the-art for micro-CMM styli. The resulting calculated masses for the eighteen test styli are shown in table 4.3.

Following these definitions, a set of calculations can be completed that estimate the effect each of these styli will have on the ideal operation of the micro-probe. Firstly, using the previously-described estimations of resonance changes due to increased mass, the resonance frequencies of probes assembled from any of the described test styli can be calculated. These results are shown in table 4.3.

Also, it is important to calculate the resonant frequencies of the micro-styli themselves. It is essential to ensure that the styli remain straight while the probe is active and, therefore, an indication of the natural frequency of the styli will demonstrate this.

Simple beam theory states that the resonance frequencies of a cantilevered, circular cross-sectional beam are

$$f_n = \frac{\beta_n^2}{2\pi}\frac{D}{L^2}\sqrt{\frac{E_b}{16\rho}}, \tag{4.1}$$

where β_n is a constant linked to the frequency mode that is wished to be calculated (in the case of calculating the first natural frequency, $\beta_n = 1.875$), D is the diameter of the beam, L is the length of the beam, ρ is the density of the beam material and E_b is the Young's modulus of that material [156]. This equation is valid for the styli described in table 4.1 that have a single diameter over their entire length. To calculate the first resonant frequency of the composite styli, however, the styli should be modelled using FE analysis.

A simple 3D CAD model of each stylus was made using SolidWorks 2008 SP5 [157]. This CAD model was then imported into ANSYS Workbench 11.0 SP1 [154]. ANSYS allows the material properties of tungsten to be associated with the model of the stylus, and subsequently a frequency analysis to be completed. The end of the stylus not attached to the spherical tip is constrained in all six degrees of freedom. The FE models of the styli were meshed using the ANSYS default fine meshing parameters, resulting in models consisting of approximately 8 000 to 15 000 elements. Once the frequency analysis is completed, any resonant frequencies detected within the range of the test are output by ANSYS. For all tests, the range from 0 Hz to 1 MHz was chosen, as this represents a highly extended maximum operational range of the probe. The first resonant frequencies of each non-composite stylus can also be determined through FE analysis. It is expected that the main contribution to the resonance of the composite styli will be the effective part, which has a smaller diameter than the main shaft. A set of estimated resonant frequencies can be analytically calculated for the composite styli taking into account only the effective stylus. The results of these various calculations and tests are shown in table 4.3.

The differences between the resonance frequencies of the non-composite styli calculated analytically and through FE analysis is due to the addition of the spherical stylus tip in the 3D CAD

Table 4.3: Results of the stylus modelling exercise. The results shown in [square brackets] are estimated only.

Name		Mass / µg	Sag / nm	Triskelion resonance / Hz	Stylus resonance / kHz (analytical)	Stylus resonance / kHz (FE)
No stylus		0	58.0	[4 370.00]	-	-
Composite 1	**a**	8.18	102.0	3 782.09	[348.99]	48.55
	b	16.36	127.0	2 674.34	[87.25]	15.32
	c	24.54	156.0	2 183.59	[38.78]	7.56
Composite 2	**a**	30.08	171.0	1 972.49	[581.66]	133.33
	b	60.16	251.2	1 394.76	[145.41]	39.08
	c	90.23	331.5	1 138.82	[64.63]	18.94
Composite 3	**a**	108.04	380.5	1 040.75	[814.32]	185.14
	b	216.08	671.5	735.92	[203.58]	59.78
	c	324.12	963.0	600.88	[90.48]	29.34
Stylus 1	**a**	4.33	80.5	5 197.98	38.78	23.05
	b	8.66	104.0	3 675.53	9.70	7.04
	c	12.09	124.5	3 001.05	4.31	3.42
Stylus 2	**a**	12.03	122.0	3 118.79	64.64	52.39
	b	24.06	154.0	2 205.32	16.16	14.45
	c	36.09	187.0	1 800.63	7.18	6.80
Stylus 3	**a**	23.58	153.0	2 227.71	90.49	67.16
	b	47.16	216.5	1 575.23	22.62	19.22
	c	70.74	280.5	1 286.17	10.05	8.99

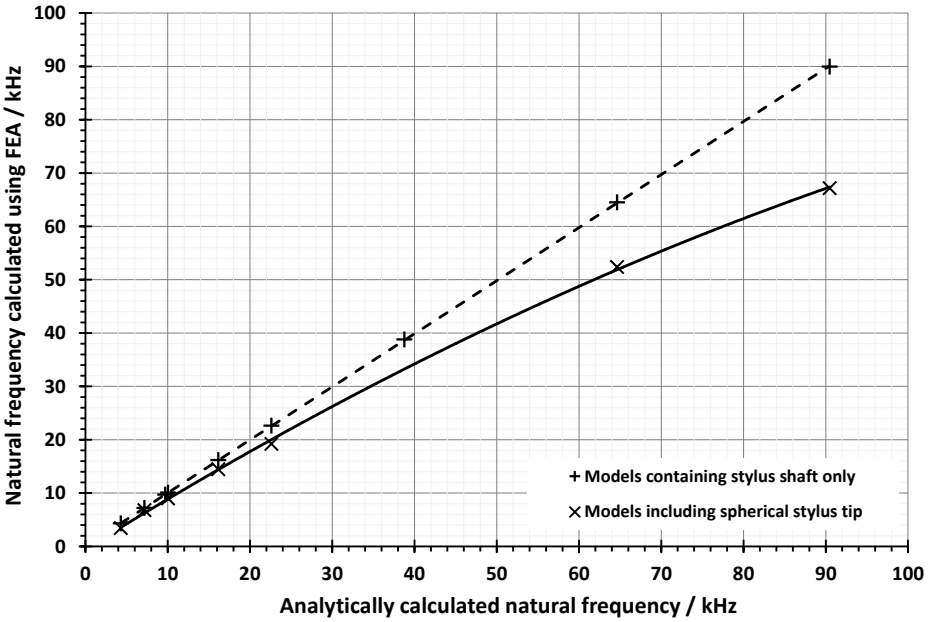

Figure 4.4: Graph showing the close correlation between resonance as calculated analytically and via FE analysis when considering the non-composite stylus shafts only. Also, the relationship between the analytical calculation and the FE models containing the spherical stylus tip are presented.

model. When analysed without a spherical stylus tip, the FE and analytical results correlated to within 0.6 %, which confirms the validity of the FE model. This correlation, and a comparison between the analytical and the FE results that include a spherical stylus tip are shown in figure 4.4.

The natural frequencies calculated from the FE analysis of the 3D models that include the spherical stylus tip also correlate well with the effective aspect ratio of the stylus. This correlation is not so clear when considering the stylus aspect ratio. These relationships are shown in figure 4.5.

The close correlation of the natural frequency determined by FE analysis to the effective aspect ratio suggests that the resonant behaviour of the stylus is closely related to the effective part of the stylus. This suggestion was previously made when analytically calculating the natural frequency of the composite styli based only on the behaviour of the effective stylus. Although the data from figure 4.5 suggests that this assumption is reasonable, the difference between the analytically calculated natural frequencies of the composite styli and those calculated through FE analysis show that the entire stylus does have an effect on the behaviour of the stylus. Therefore, when considering any composite stylus design, either a more complete analytical solution should be developed or FE analysis should be used.

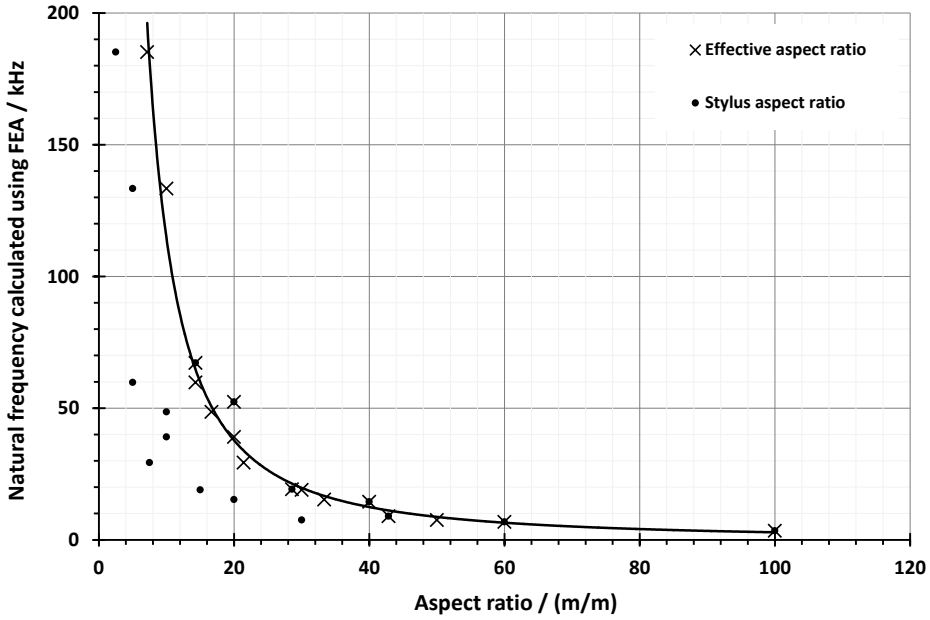

Figure 4.5: Graph showing the correlation between effective stylus aspect ratio and the resulting natural frequency, as calculated using FE analysis. The data corresponding to the stylus aspect ratio is also presented.

4.2.4 Composite modelling of the triskelion flexure system and the stylus

Following the separate investigations into the dynamics of the individual components of the probe, an investigation was completed into the assembled probe system. The 3D model of the triskelion flexure system was assembled with the various micro-styli and the tip of each stylus was then subject to displacements of 1 µm in the x-, y- and z-axes. The FE models of the assembled probes are shown in figure 4.6. These displacements formed a sphere of twenty-six points around the centre of the stylus tip. The raw static output voltage of the piezoelectric sensors was recorded and used as a measure of the sensitivity of the micro-CMM probe.

The simulated output voltage was used rather than making a calculation of the deformation of the stylus because the desired output of the vibrating micro-probe is a piezoelectric signal. Also, with the stylus dimensions being between 200 µm and 30 µm, it is highly likely that all of the styli will bend to some degree. The most suitable stylus will, therefore, be the stylus that bends the least and, therefore, also the stylus that produces maximum piezoelectric output from the sensors on the vibrating micro-probe model. For this work, both stylus 3 and composite stylus 3 were neglected because the final shaft diameter of 70 µm will result in a sphere tip that, although below 100 µm as stated in the requirements, is larger than the more refined requirement of 70 µm diameter.

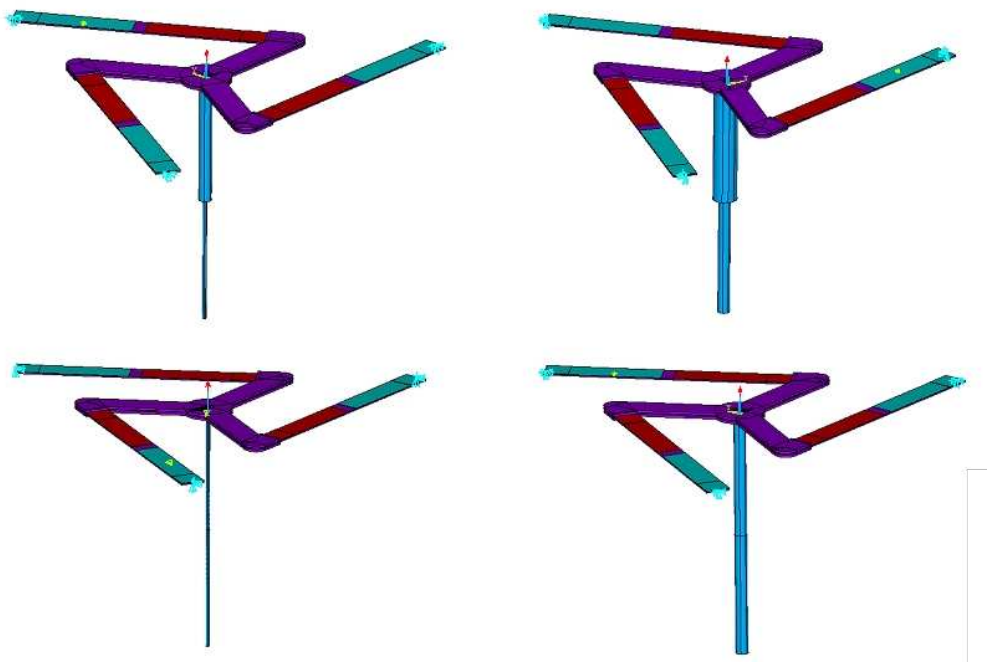

Figure 4.6: Four assembled probes used for sensitivity testing using FE analysis, clockwise from top left: composite stylus 1, composite stylus 2, stylus 2 and stylus 1. Each micro-stylus was modelled with a total length of 1 mm, 2 mm and 3 mm.

The combined sensor output of the vibrating micro-probe averaged over all twenty-six displacement points is plotted against the effective aspect ratio of the stylus [158]. This plot is shown in figure 4.7.

It can be seen that the main factor in determining the sensitivity of the vibrating micro-probe is the length of the stylus rather than its diameter, with all styli (except stylus 1) showing the similar sensor output for each specific length.

4.2.5 Summary of the mechanical modelling of the probe

A detailed analysis of the constituent parts of the vibrating micro-probe has been presented and discussed. Following this, several conclusions can be drawn.

When considering the geometric design, mass, aspect ratio (both probe and effective) and resonant frequency of the sphere-tipped stylus, and the resulting sensitivity of the vibrating micro-probe, it is concluded that composite stylus 2b or composite stylus 2c should be manufactured for assembly. These styli have an aspect ratio above 10 (20 and 30 respectively), exhibit low resonance frequencies with respect to the associated assembled triskelion and result in similar sensor output signals to all other tested styli. However, the ability to manufacture these styli is a major consideration and, therefore, after discussion with possible manufacturers, the design was refined to a 2.5 mm long stylus, tapering from 0.15 mm in diameter to 0.045 mm in diameter. This design is shown in figure 4.8.

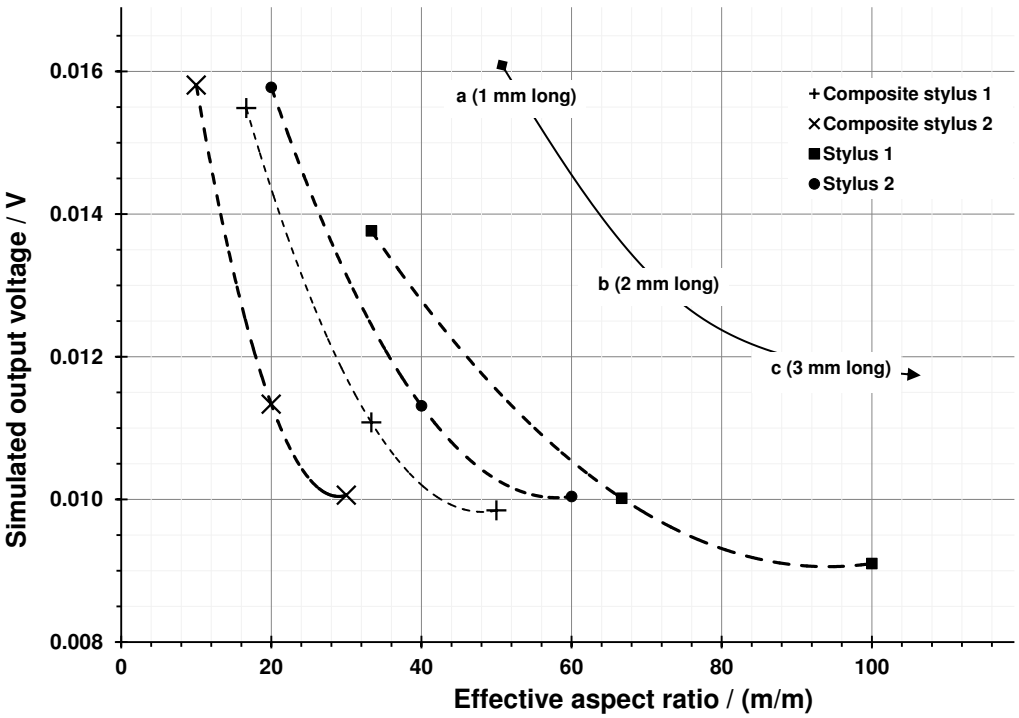

Figure 4.7: Graph of simulated output voltage versus effective aspect ratio for each of the twelve micro-styli tested [158]. The increase of aspect ratio in the case of each group is due to an increase in overall length (1 mm, 2 mm and 3 mm). The groups are joined using "curves of best fit", however these curves are for indication and clarity only and do not indicate any calculated trend.

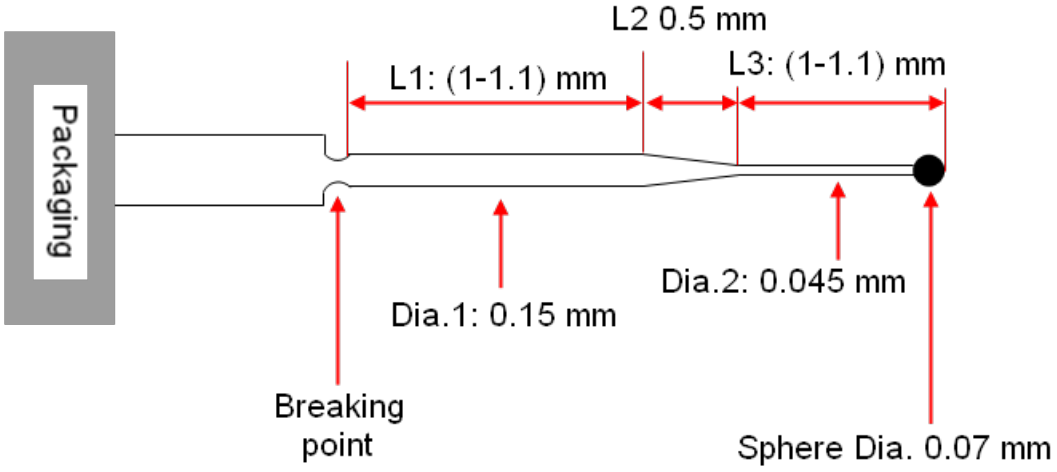

Figure 4.8: Final design of the sphere-tipped micro-stylus for manufacture.

Table 4.4: Calculated physical properties of the manufactured stylus. The results shown in [square brackets] are estimated only.

Feature	Value
Aspect ratio	16.67
Effective aspect ratio	22.22
Mass / µg	151
Triskelion resonance / Hz	890.63
Stylus resonance / kHz (analytical)	[58.17]
Stylus resonance / kHz (FE)	16.30

The tapered section was designed into the manufactured stylus to increase overall stiffness. This taper represents a common feature of ideal stylus design, but is noticeably absent from the modelled styli (as shown in figure 4.6).

The physical properties of this manufactured stylus can be calculated, according to the previously described methods. The results are shown in table 4.4.

It can be seen that the resulting stylus to be manufactured has an effective aspect ratio of above 20, and is expected to result in a probe resonance of about 0.9 kHz. Also, the resonance frequency of the stylus itself is in the range of 16 kHz, which is far above the expected operation frequency of the vibrating micro-probe. Therefore, it is unlikely that the stylus will couple to any of the operational frequencies of the vibrating micro-probe, and if it were to couple, then the resulting vibration amplitude at the stylus tip will be very small related to that of the programmed vibration vector amplitude.

Finally, it is concluded that it is possible to design and manufacture a stylus that is suitable for use with the NPL vibrating micro-probe, as required by **Research Question 1.1**.

4.3 Modelling the motion of the vibrating micro-probe

4.3.1 Introduction to motion modelling

Following the modelling of the triskelion-flexure MEMS and the micro-stylus, a more detailed appreciation of the assembled vibrating micro-probe can be determined. This work is aimed at determining the motion of the probe during operation and while probing, and to ensure it can act isotropically, as required by **Thesis Objective 2**. Specifically, a new concept of isotropy applicable to a vibrating micro-probe is required, as defined in **Research Question 2.1**. Though piezoelectric analysis, an indication as to the control algorithm of the vibrating micro-probe's actuators will also be developed.

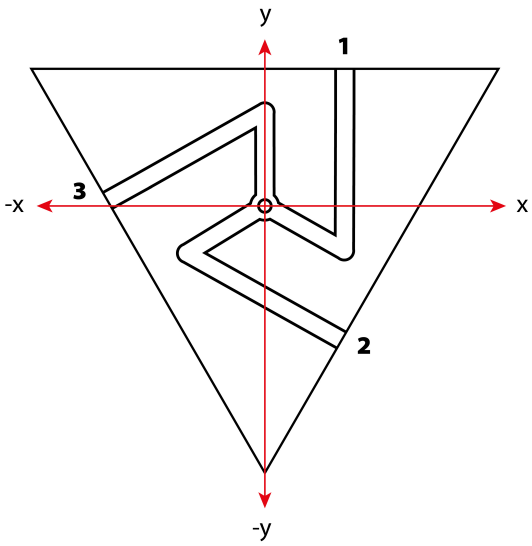

Figure 4.9: Geometrical design of the triskelion-flexure MEMS device, including a co-ordinate system for all subsequent analytical modelling.

Due to the complexity of the FE model, this work will continue using an analytical approach. It is known that the modelling of the surface interaction forces later in this chapter will be completed analytically, and the combination of the operational model and the surface interaction model will be easier to complete if both are analytical.

A mechanical analysis of the probe will be developed, through the use of the designed geometry of the probe and beam theory. Piezoelectric analysis will be used to determine the effect of the mechanical behaviour of the probe in operation on the actuators and sensors. From this, a new concept of isotropy for vibrating micro-probes can be developed, based on the ideal operation of the probe.

4.3.2 Mechanical analysis of the vibrating micro-probe

Using the known ideal geometry of the vibrating micro-probe, an analytical model can be developed to investigate its mechanical kinematics. The aim of this work is to calculate the motion of the point where the flexure meets the connecting arm, referred to as the elbow, with respect to stylus tip motion. Subsequently, the resulting shape of the flexures caused by that stylus tip motion can be calculated, which will be required for future piezoelectric analysis.

To begin, a geometrical appreciation of the triskelion body of the probe must be defined. This is shown in figure 4.9.

From the geometrical definitions shown in figure 4.9, including a co-ordinate system for all subsequent analytical modelling, it can be seen that the $+z$ direction is out of the page, and that the centre of the central island is the origin (0,0,0). The three flexures, 1, 2 and 3, are constrained in all six degrees-of-freedom at the end farthest from the centre. All the flexures are joined to the

central island by rigid connecting arms, which connect to the flexures at the elbows. A graphical overview of the model of the vibrating micro-probe can be seen in figure 3.1, where the stylus is pointing in the -z direction. Any motion referred to within this section is as a result of deflection of the stylus tip.

Several initial observations can also be made with regards to the final aim.

Firstly, it is essential to point out that, given that the size of the stylus and the triskelion body of the probe is several millimetres, and that the operational deflections of the stylus tip during operation is not expected to exceed 10 µm, then it is useful to note that the small angle approximation is always assumed to be valid. Due to this assumption, Cartesian translations of the stylus tip in x, y and z is expected to result in only z translations of the elbows.

Secondly, it is clear that any vertical, or z, translation of the stylus tip will be transferred directly to the central island and subsequently to the elbows. This transfer is, of course, dependent on the stiffness of the stylus in the axial direction, which although not infinite, is very large compared to the flexural stiffness of the flexures. Therefore, the direct transfer of z motion can be assumed.

From figure 4.9, it can be seen that the connecting arm from the central island to flexure 3 is co-linear with the y-axis. It is, therefore, logical that the first step of the analysis is completed using flexure 3 for ease of calculation. The ease of the calculation when focusing on leg 3 stems from the fact that only stylus tip movement in the y direction will result in motion of the elbow of leg 3. A more detailed diagram of leg 3 from above and from the side is shown in figure 4.10, which highlights the global co-ordinate system and labels certain important geometries.

From figure 4.10 it can be seen that: L_b is the length of the connecting arm between the central island and the flexure, l_{st} is the length of the stylus, and R is the length of the hypotenuse of an isosceles triangle with sides of length L_b and l_{st}.

By adhering to the small angle approximation, it can be seen that any motion of the stylus tip, at $(0, 0, l_{st})$, will result in z motion at the elbow of arm 3, at $(0, L_b, 0)$. This conclusion currently ignores rotations about any axis collinear with the connecting arms, and also ignores any bending of the stylus. This is shown in figure 4.11.

From figure 4.11, it can be seen that the y component, Y, of any motion of the stylus will result in z motion at the elbow of arm 3 equal to Q_3. This can also be expressed as

$$(L_b - Y)^2 + (l_{st} + Q_3)^2 = R^2. \tag{4.2}$$

If equation 4.2 is solved for Q_3, it can be calculated that for any movement of the stylus tip, $\begin{bmatrix} X \\ Y \\ Z \end{bmatrix}$, the motion of the elbow of arm 3 will be

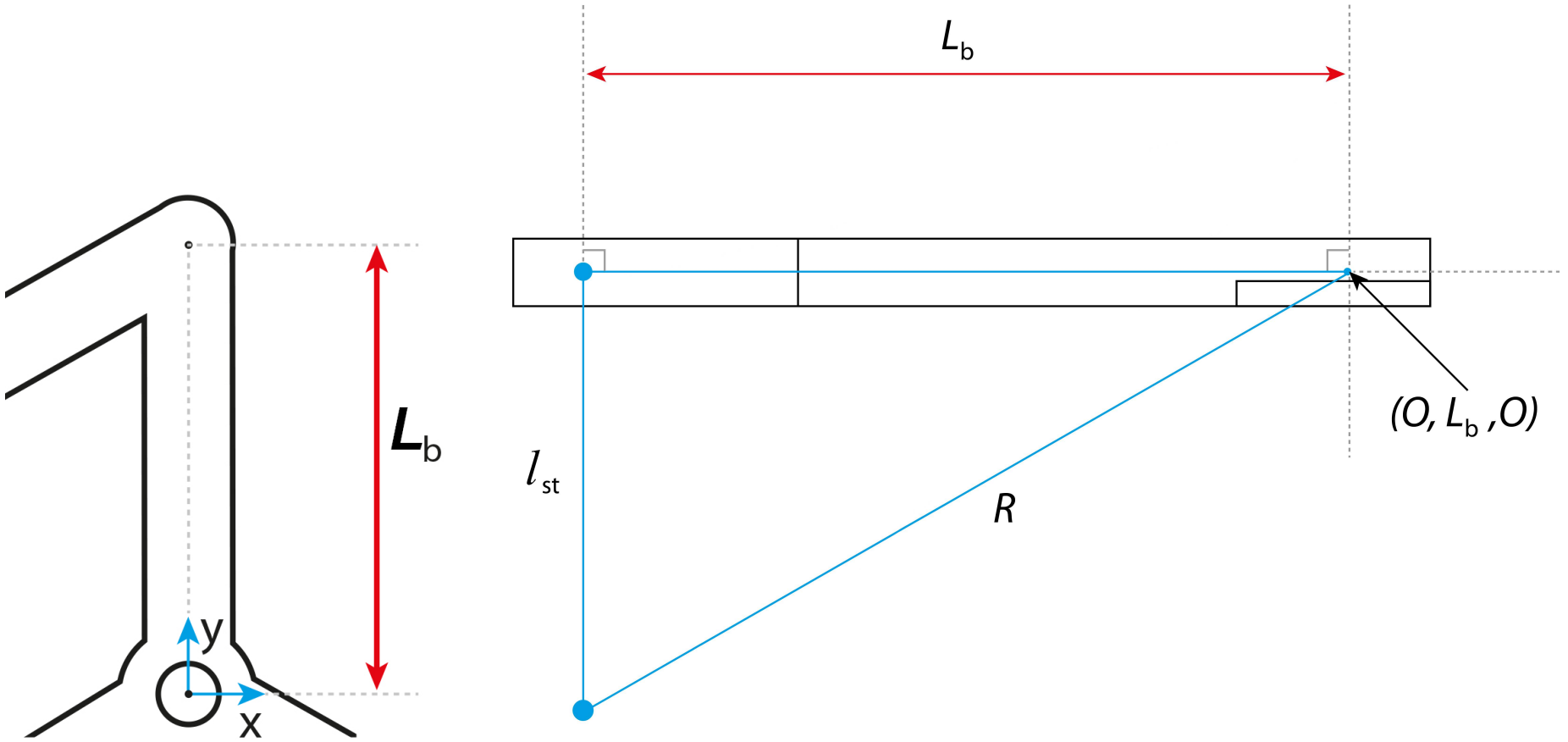

Figure 4.10: Schematic of Leg 3 from above, looking in the $-z$ direction (left) and from the side, looking in the $-x$ direction (right).

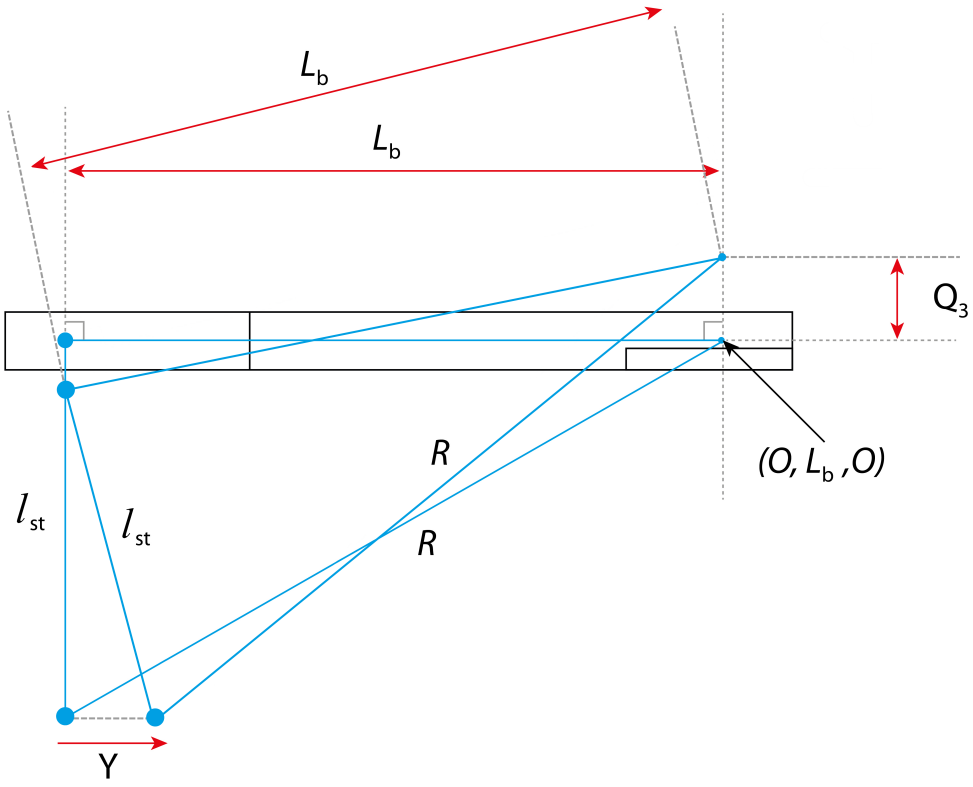

Figure 4.11: Leg 3 from the side, looking in the $-x$ direction, experiencing a displacement, Y, in the y direction.

$$Q_3 = \begin{bmatrix} 0 \\ 0 \\ \left(\frac{-2l_{st}+\sqrt{4l_{st}^2+8L_bY-4Y^2}}{2}\right)+Z \end{bmatrix}. \tag{4.3}$$

A similar analysis can be completed for leg 1. A schematic diagram of leg 1, showing additional derived geometric lengths, is shown in figure 4.12.

Due to the geometry of the triskelion body, and the chosen global co-ordinate system, it can be seen that the motion of the stylus tip in both x- and y-directions will result in z motion at the elbow of leg 1. Therefore, if each component of the motion is considered separately, the following motion can be calculated for elbows 1 and 2,

$$Q_1 = \begin{bmatrix} 0 \\ 0 \\ \left(\frac{-2l_{st}+\sqrt{4l_{st}^2+8x_sX-4X^2}}{2}\right)-\left(\frac{-2l_{st}+\sqrt{4l_{st}^2+8y_sY-4Y^2}}{2}\right)+Z \end{bmatrix}, \tag{4.4}$$

$$Q_2 = \begin{bmatrix} 0 \\ 0 \\ -\left(\frac{-2l_{st}+\sqrt{4l_{st}^2+8x_sX-4X^2}}{2}\right)-\left(\frac{-2l_{st}+\sqrt{4l_{st}^2+8y_sY-4Y^2}}{2}\right)+Z \end{bmatrix}. \tag{4.5}$$

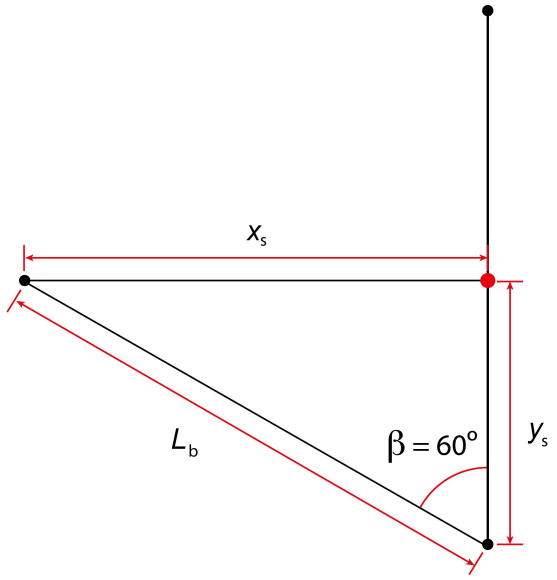

Figure 4.12: Schematic of Leg 1 from above (looking in the $-z$ direction). x_s and y_s are the effective lengths of L_b projected onto the x- and y-axes.

A similar set of calculations can be completed using the method of similar triangles, as described in [136], which results in the following z displacements for the elbows of leg 1, leg 2 and leg 3

$$Q_1 = \begin{bmatrix} 0 \\ 0 \\ Z - \frac{y_s}{l_{st}}Y + \frac{x_s}{l_{st}}X \end{bmatrix}, \tag{4.6}$$

$$Q_2 = \begin{bmatrix} 0 \\ 0 \\ Z - \frac{x_s}{l_{st}}Y + \frac{y_s}{l_{st}}X \end{bmatrix}, \tag{4.7}$$

$$Q_3 = \begin{bmatrix} 0 \\ 0 \\ Z - \frac{L_b}{l_{st}}Y \end{bmatrix}. \tag{4.8}$$

It has been confirmed numerically that both of these solutions result in the same z motion for each leg when any stylus tip motion (X, Y, Z) is input, as long as the small angle approximation is adhered to.

Following this analytical solution on the geometry of the vibrating micro-probe, it is now possible to predict the motion of the central island, the connecting arms, and the elbows resulting from any small motion of the stylus tip. To translate the z motion of the elbows to the shape of the associated flexure, and hence a mechanical understanding of the vibrating micro-probe, several equations derived from simple beam theory must be considered.

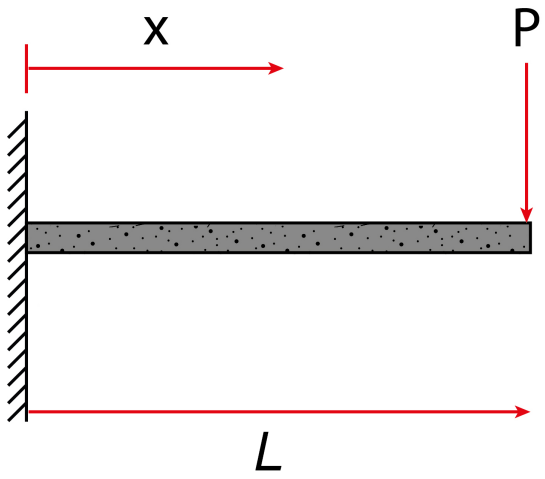

Figure 4.13: Schematic of a flexure, length L m, bending subject to a point load, P N.

When the motion of the probe body is considered to be reactive to motion of the stylus tip, the equations governing the bending of a flexure subject to a point load are sufficient. This situation is described in figure 4.13 [156].

It has been previously assumed [136] that the inverse of this situation is a good description of the operation of the vibrating micro-probe. However, this is not the case, as will now be demonstrated.

In figure 4.13, the deflection of the flexure at any distance, x, can be calculated as

$$W_{PL(x)} = \frac{Px^2\,(3L - x)}{6EI}, \tag{4.9}$$

where L is the length of the flexure, P is the point force imparted on the end of the flexure, E is the Young's modulus of the material and I is the second moment of area. The second moment of area is a function of the geometry of the flexure. For this rectangular cross section, I is calculated as

$$I = \frac{bh^3}{12}, \tag{4.10}$$

where b is the width of the flexure and h is the thickness [156].

The maximum deflection at a distance L can be used to determine the deflection of any point along the flexure. The maximum deflection value is equal to Q_1, Q_2 or Q_3, as calculated from either equation 4.3, 4.4 or 4.5, which determine the deflection of the elbows as a function of stylus tip motion. The maximum deflection, $W_{PL(L)}$, can be expressed as

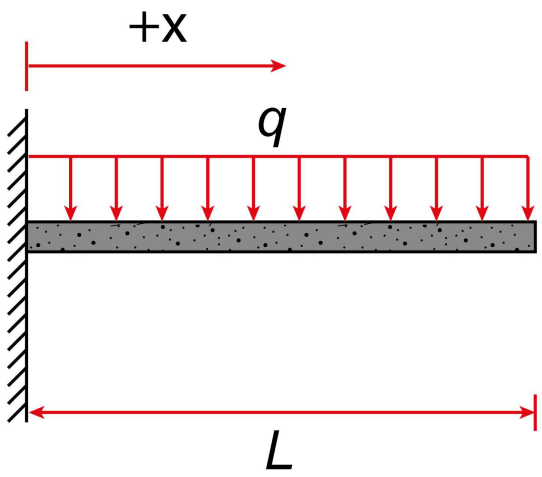

Figure 4.14: Schematic of a flexure, length L m, bending subject to a uniformly distributed load, q N m^{-1}.

$$W_{PL(L)} = \frac{PL^3}{3EI}, \tag{4.11}$$

which when substituted into equation 4.9, results in the following expression for the value of the deflection of the flexure at any point, x, along that flexure, as a function of maximum deflection

$$W_{PL(x)} = \frac{W_{PL(L)}x^2\,(3L - x)}{2L^3}. \tag{4.12}$$

The deflection and, therefore, curvature and strain, of each point along each flexure can be calculated as a result of movement of the stylus tip, by using equation 4.12. It is possible, therefore, to calculate the resulting voltage produced by any piezoelectric material deposited on the flexure, through knowledge of the material's piezoelectric properties.

However, careful consideration will lead to the conclusion that the situation of a point load deflecting the device does not fully describe the situation present when modelling the vibrating micro-probe. When the probe is reacting to a displacement at the stylus tip, it can be considered that the flexures are experiencing a deflection at the elbows. This interpretation is used in a previously developed model by Sun *et. al.* [136]. However, because of the nature of piezoelectric materials when operating as actuators, it is more appropriate to consider a different flexure-bending model.

When the motion of the stylus tip is considered to be reactive to motion of the flexures, the equations governing the bending of a beam subject to a uniformly distributed load may be more applicable. This situation is described in figure 4.14, where q is an uniformly distributed load, in Newtons per metre [156].

In figure 4.14, the deflection of the flexure at any point at a distance x, can be calculated as

$$W_{UDL(x)} = \frac{qx^2\left(6L^2 - 4Lx + x^2\right)}{24EI}, \tag{4.13}$$

where, as before, E is the Young's modulus and I is the second moment of area. As the second moment of area is a function of the geometry of the flexure, which is irrespective of the bending regime, I is still calculated as shown in equation 4.10.

As before, Q_1, Q_2 or Q_3 can be used to determine the deflection of any point along the flexure. For this bending regime, the maximum deflection, $W_{UDL(L)}$, is expressed as

$$W_{UDL(L)} = \frac{qL^4}{8EI}, \tag{4.14}$$

which, when substituted into equation 4.13, results in an expression for the value of the deflection of the flexure at any point, x, along that flexure, as a function of maximum deflection, when being subject to a uniformly distributed load,

$$W_{UDL(x)} = \frac{W_{UDL(L)}x^2\left(6L^2 - 4Lx + x^2\right)}{3L^4}. \tag{4.15}$$

The deflection and, therefore, curvature and strain, of each point along each flexure can be calculated as the result of this uniformly distributed load. This deflection is then responsible for the movement of the stylus tip. It is possible, therefore, to calculate the required voltage input to any piezoelectric material deposited on the flexure, through knowledge of the material's piezoelectric and dielectric responses, which will result in this deflection. Hence, a set of control signals can be calculated that will operate the probe to output a predefined set of stylus tip trajectories. The uniformly distributed load, q, in this model is used to approximate the effect of the two separate piezoelectric actuators.

The difference between the two flexure-bending situations described is subtle, but important. Even though the bending calculations for each situation rely on a maximum deflection that is irrespective of the load (either point or evenly distributed), bending due to the different regimes will result in different curvatures at each point along the flexure. Different curvatures will subsequently result in different strain calculations and, therefore, different piezoelectric voltages. The strain profile along the beams will also be different in the two flexure-bending situations. The main distinction between the situations is that, with the flexure subject to a point load, the resulting model describes the probe operating as a passive contact sensor (relying on the piezoelectric effect), whereas when the flexure is subject to a uniformly distributed load, the resulting model describes the probe operating as an active device (relying on the converse piezoelectric effect).

Following on from the determination of the deflections of the flexures, an understanding of the resulting strain is required. This is the next step in transforming tip deflection values into input voltage for the piezoelectric actuators.

A common equation used in the modelling of MEMS devices is Stoney's formula, which describes the stress of thin films on cantilevers [159, 160]. By modelling a plate system consisting of a stress bearing thin film of uniform thickness, h_f, deposited on a thick substrate, h_s, a relationship between the curvature of the system, κ, and the stress of the film, σ_f, can be derived as

$$\sigma_f = \frac{E_s h_s^2 \kappa}{6h_f \left(1 - \nu_s\right)}, \tag{4.16}$$

where E_s is the Young's modulus of the substrate and ν_s is the Poisson's ratio of the substrate. It should also be noted that the thickness of the substrate should be large relative to that of the film, usually below a factor of 10 [160].

In order that Stoney's formula can be applied to the vibrating micro-probe, an appreciation of the curvature, κ, of the flexures is needed. Beam theory defines the curvature of a beam as the second derivative of the deflection of that beam

$$\kappa = \frac{\mathrm{d}^2 W_{UDL(x)}}{\mathrm{d}x^2}, \tag{4.17}$$

which, for a uniformly distributed load, results in an expression for curvature,

$$\kappa_{UDL(x)} = \frac{q\left(L - x\right)^2}{2EI}. \tag{4.18}$$

Following this derivation of the curvature of the flexure, the stress at any point along the flexure can be calculated using Stoney's formula.

4.3.3 Electrical analysis of the vibrating micro-probe

The calculated strain can be converted into voltage through the use of the constitutive mechanical and the constitutive electrical equations.

The most common constitutive equation is Hooke's Law, which relates the stress and strain of a material to its compliance. Hooke's law, for the purposes of this investigation, can be written as

$$S = sT, \tag{4.19}$$

where S is the strain, s is the compliance of the strained material and T is the stress. Although the compliance of the flexures has not been derived, for this simple case of unconstrained uniaxial deformation, the inverse of the Young's modulus can be used.

There is also a constitutive electrical equation for materials where the relationship between the movement of charge carriers is related to the applied voltage and the permittivity. This equation, which can be used to describe the electric behaviour of a dielectric material, is

$$D = \varepsilon E, \tag{4.20}$$

where D is the electric charge density, ε is the electric permittivity of the material and E is the electric field strength.

Using the constitutive equations 4.19 and 4.20, concerning mechanical behaviour and electrical behaviour of a material, the coupled piezoelectric equation can be derived as

$$\{S\} = \left[S^E\right]\{T\} + \left[d^t\right]\{E\}, \tag{4.21}$$

and

$$\{D\} = [d]\{T\} + \left[\varepsilon^T\right]\{E\}, \tag{4.22}$$

where the coupling term, $[d]$or $[d^t]$, is the piezoelectric matrix (direct and converse respectively) [161, 162]. From equations 4.21 and 4.22, the electric behaviour of a piezoelectric material can be calculated as a function of applied strain, and conversely, the strain of a piezoelectric material can be calculated as a function of applied electric potential. To apply the coupled equation, knowledge of the electrical behaviour of the dielectric material, and its electrical permittivity must be obtained. Once known, the pertinent coupled piezoelectric equation can be applied in a simpler form [163]

$$\frac{V_z}{t_{pzt}} = g_{31}S_x + g_{32}S_y + g_{33}S_z, \tag{4.23}$$

where V_z is the voltage potential due to movement in the z direction, and the g coefficients are related to the piezoelectric coefficients in the piezoelectric matrix through the permittivity of the piezoelectric material and the permittivity of free space, ε_0. An appreciation of the voltage potential due to z movement, V_z, can therefore be calculated as

$$V_z = g_{33}S_z t_{pzt}\,. \tag{4.24}$$

Table 4.5: Geometrical and physical parameters of the vibrating micro-probe

Symbol	Value	Description
L_b	2.0 mm	The length of the connecting beam
l_{st}	2.5 mm	The length of the stylus
b	200 µm	The width of the nickel flexures
h	10 µm	The thickness of the nickel flexures
t_{pzt}	2 µm	The thickness of the piezoelectric film
E_s	200 GPa	The Young's modulus of the nickel substrate
ν_s	0.309	The Poisson's ratio of the nickel substrate
E_f	11 GPa to 20 GPa	The Young's modulus of the piezoelectric film
e_{33}	593×10^{-12} C m^{-1}	The [3,3] coefficient from the manufactures piezoelectric matrix
ε_r	870	The relative electric permittivity of the piezoelectric material

In equation 4.24, strain in the z direction, S_z, can be expressed, as described in Hooke's Law, as stress multiplied by compliance. In this case, stress is as calculated through Stoney's formula and compliance is estimated as the inverse of the Young's modulus of the material. Likewise, the g coefficient can be expressed as the relevant piezoelectric coefficient divided by the electrical permittivity of the material. Therefore, the resulting equation for the voltage potential due to z movement, V_z, is

$$V_z = \frac{e_{33}}{\varepsilon_0 \varepsilon_r} \frac{q\,(L-x)^2}{bhE\,(1-\nu_s)}\,. \tag{4.25}$$

It can be seen from equation 4.25 that the voltage potential due to z movement is not related to the thickness of the piezoelectric material. This is because Stoney's formula assumes that the piezoelectric layer is significantly thinner than the substrate.

4.3.4 Results of the electrical model of the vibrating micro-probe

Following the previously derived definitions of flexure motion with respect to stylus tip movement, and the resulting flexure strains and, therefore, voltage potentials, an appreciation can be gained of the relationship between the desired motion of the stylus tip and a set of relative voltage signal inputs required to replicate that desired movement. If the situation of a uniformly distributed load is considered, the output of this model for each of the six actuators is expected to indicate the relative signal strengths required for operation. These indicated signals can be used, along with several initial conditions, to estimate the actual required input for operation of the vibrating micro-probe.

To realise the previous models, several initial parameters must be defined. These are shown in table 4.5, and are both geometrical and related to the properties of the materials used.

It can also be seen from table 4.5 that the nickel flexures are five times thicker than the piezoelectric film, and that nickel is ten times as stiff as the piezoelectric material. Therefore, it is a

reasonable assumption that the strain of the system is related mostly to the strain of the nickel, as is assumed by Stoney's formula.

All of the results described in section 4.3.2 and 4.3.3 were compiled into a single model of the vibrating micro-probe. The input parameters for the model, as described in table 4.5, must also be coupled with experimental data concerning the quality of the individual actuators on each leg, and an indication of the overall strength of the piezoelectric actuators and how they compare to each other across the vibrating micro-probe. The determination of these actuator strength coefficients is better described in Chapter 5, section 5.3.1.12. However, to continue with the reporting of the results of this model, it is assumed that all six actuators act similarly under any input signal, and that an input signal of 1 V at the natural frequency of the vibrating micro-probe results in a vibration amplitude in the z direction of 1 µm.

When considering the geometrical model of the vibrating micro-probe, an appreciation of the motion of the elbows can be derived from any stylus tip motion. Therefore, in order to replicate the ideal operation of the probe when interacting with a sidewise facing measurement surface, the stylus tip was programmed to vibrate laterally at an amplitude of 1 µm. A set of thirty-six vibration vectors were programmed in the xy plane, one every 10°, and the resulting values of Q_1, Q_2 and Q_3 were calculated. The results are shown in figure 4.15.

The motion of the elbows, as shown in figure 4.15, indicates the ideal operation of the vibrating micro-probe in the xy plane and, therefore, indicates true isotropic behaviour for the probe. It is therefore concluded that, as required for **Research Question 2.1**, a concept of isotropy for a vibrating micro-probe can be developed with respect to the vibration characteristics of that probe.

It should be noted that the data in figure 4.15 is an indication of the amplitude of the vibration of the elbows and contains no indication of phase. However, the output of the software does indicate the phase of the output signal, which alternates between 0°, in phase with the vibration of the stylus tip, and 180°, out of phase with the stylus tip.

Similar results can be obtained for the expected voltage input to the actuators to gain the required stylus tip motion. The input voltages for the outer and inner actuators are defined as the output voltage potential of the piezoelectric film at $\frac{L}{4}$ and $\frac{3L}{4}$ respectively, multiplied by the previously mentioned actuator strength coefficients. The resulting calculated input voltage amplitudes are shown in figure 4.16.

Again, the data in figure 4.16 contains no indication of phase. However, the output of the software does indicate the phase of the input signal for each desired vibration vector.

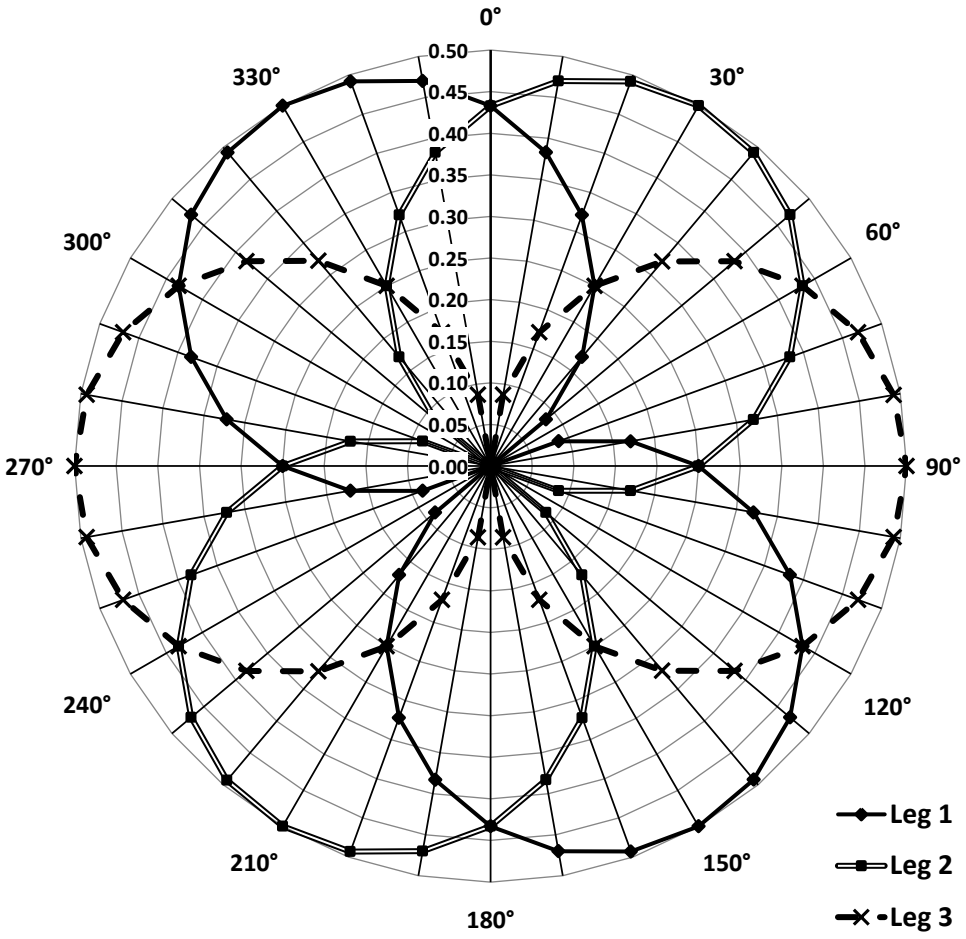

Figure 4.15: Graph showing the values of Q_1, Q_2 and Q_3 at the elbows of the triskelion, resulting from an input stylus tip vibration amplitude of 1 µm in thirty-six vectors (one every 10°) in the xy plane. The radial scale is in micrometres.

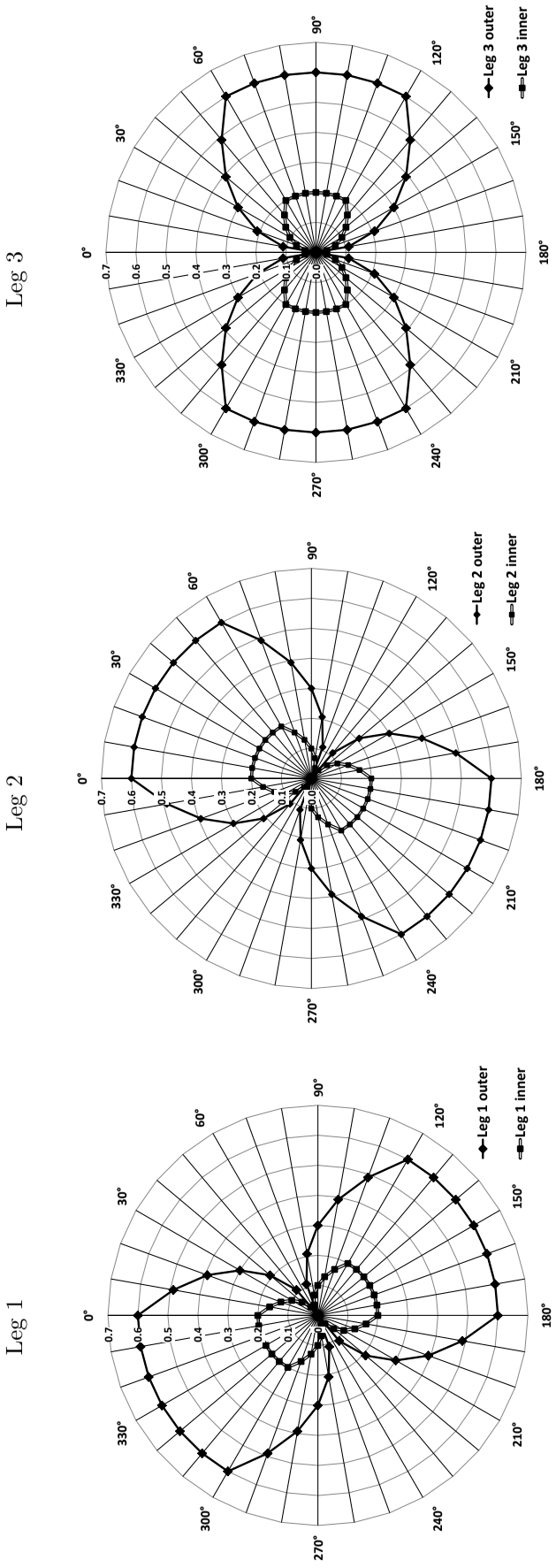

Figure 4.16: Graphs showing the calculated input voltage amplitudes that result in a desired vibration vector of the stylus tip. The radial scale is in volts.

4.3.5 Summary of modelling the motion of the vibrating micro-probe

Several analytical models have been developed to describe the operation of the assembled vibrating micro-probe. These models describe the vibrating micro-probe in three ways: geometrically, mechanically and electrically (with respect to the piezoelectric actuators).

By using the geometrical model, which defines the motion of the elbows, Q_1, Q_2 and Q_3, with respect to stylus tip motion, a definition of probe response during ideal and isotropic operation can be obtained as required in **Thesis Objective 2**, specifically **Research Question 2.1**. These results can be used as a comparison for the experimental test results on the isotropy of the vibrating micro-probe.

A combined mechanical and electrical model was developed to give an indication as to the expected input voltage signals required to operate the probe. A similar investigation can be completed with respect to the piezoelectric sensors, however it was expected that an experimental determination of their behaviour would be more useful.

4.4 Modelling the surface interaction forces

4.4.1 Introduction to the surface interaction model

Following the development of several new micro-CMM probes, as reviewed in Chapter 2, it has become continually apparent that surface interaction forces become problematic when probing at the micro-scale [69, 82]. It is, therefore, essential that any work done to advance the capability of micro-CMM probes take into account the need to counteract the effect of surface interaction forces. Therefore, a detailed analysis of the surface interaction forces prevalent in low force, high accuracy contact probing at the micrometre scale has been conducted [164]. The analysis is based on a set of analytical descriptions of the five main interaction forces thought to be most prominent at the micrometre scale: capillary, Van der Waals, electrostatic, squeeze film and Casimir [105].

Following the definition of these surface interaction forces, specifically towards their effect on the interaction of a sphere-tipped stylus with a test measurement surface, an appreciation of their effect on a vibrating sphere can be considered. This dynamic consideration will enable the operation of the probe to be modelled while it is interacting with a test measurement surface, in a similar fashion to its intended mode of use.

Finally, a set of conclusions can be drawn, pertaining to the expected success of the vibrating micro-probe's ability to counteract the surface interaction forces, as required in **Thesis Objective 1**. To achieve this, a set of initial conditions will be set out for the operation of the vibrating micro-probe. Then, the limitations of the surface forces model will be highlighted, allowing for

some understanding of the realistic results expected from the experimental work. The effect of the surface interaction forces on the operation of the probe can then be predicted, enabling a set of detection conditions to be considered.

4.4.2 Analytical model of the surface interaction forces

An analytical model will be developed to describe the effects that the surface forces will have on the vibration behaviour of the probe. The model shall be used to determine whether the amplitude of the probe is sufficient to counteract the surface interaction forces.

It is assumed that the device can be directly compared to a driven oscillator subject to a damping force. The second order differential equation that describes this situation is

$$m\frac{\mathrm{d}^2 z}{\mathrm{d}t^2} + D\frac{\mathrm{d}z}{\mathrm{d}t} + kz = F_0 \cos(\omega t), \tag{4.26}$$

where m is the mass of the oscillator, z is the position of the stylus tip, D is the damping coefficient, k is the spring constant of the oscillator, F_0 is the driving force and ω is the angular frequency of the oscillation. A good understanding of the vibration behaviour of the probe can be gained from equation 4.26. To solve for z, an appreciation of D, and hence the surface interaction forces, is required. Therefore, the individual surface interaction forces prevalent at the micrometre scale will now be investigated. A similar investigation has been conducted for the Virtual Probe [114].

4.4.2.1 The capillary force

Capillary forces play a dominant role in micro- and nano-scale interactions [165]. The basis of the capillary force is the thin liquid film layers that accumulate on surfaces from condensation and contamination. As two surfaces are brought together, the films join and surface tension causes an adhesion effect. At the micro- and nano-scale these forces can often be the dominant force governing interactions. Contact angle plays a large role in determining the magnitude of capillary forces and can be affected by the material surface chemistry as well as the surface form and texture. A schematic representation of contact between a sphere and a surface with a liquid layer is shown in figure 4.17 where z is the distance from surface, h_m is the height of meniscus and θ is the contact angle.

The equation used to describe the capillary force between a sphere and a plane surface is

$$F_{\text{capillary}} = \frac{4\pi R\gamma_L \cos\theta}{1 + \frac{z}{h_m - z}}, \tag{4.27}$$

where γ_L is the surface tension of the liquid [165].

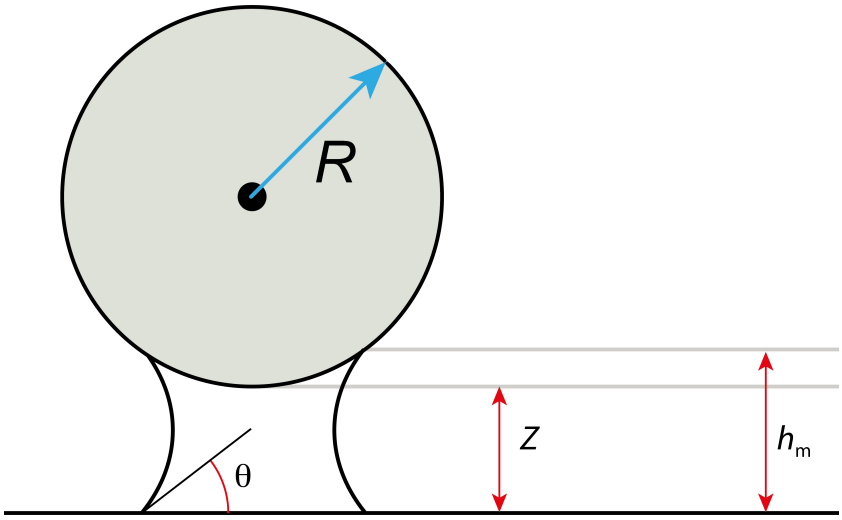

Figure 4.17: Schematic representation of a sphere, radius R, interacting with a liquid layer on a surface

4.4.2.2 The electrostatic force

Electrostatic forces result from generation of an electrical potential difference or charge transfer between two surfaces. Under most circumstances the amount of charge separated is small due to the breakdown strength of the surrounding air. However, as gap size decreases below the mean free path for air, the magnitude of the charge density can increase by orders of magnitude [105]. The strength of the electrostatic force also depends strongly on the material characteristics of the interacting bodies. The electrostatic force is determined by the electrical potential difference of the two interacting surfaces and is given by

$$F_{\text{electrostatic}} = \frac{\varepsilon_0 \varepsilon_r U^2 \pi R^2}{z^2}, \tag{4.28}$$

where ε_0 is the permittivity of free space, ε_r is the relative permittivity of the material layer between the sphere and the surface, and U is the potential difference between the two interacting surfaces [166].

4.4.2.3 The Van der Waals force

Van der Waals forces arise from the polarisation of atoms and molecules as they are drawn together. To determine the Van der Waals force, an appreciation of the Hamaker constant for the interacting surfaces must be gained [167]. There are multiple methods of calculating the Hamaker constant, all of which require empirical data. Additionally, Van der Waals forces can be significantly altered by surface roughness. A schematic representation of contact between a sphere and a surface is shown in figure 4.18.

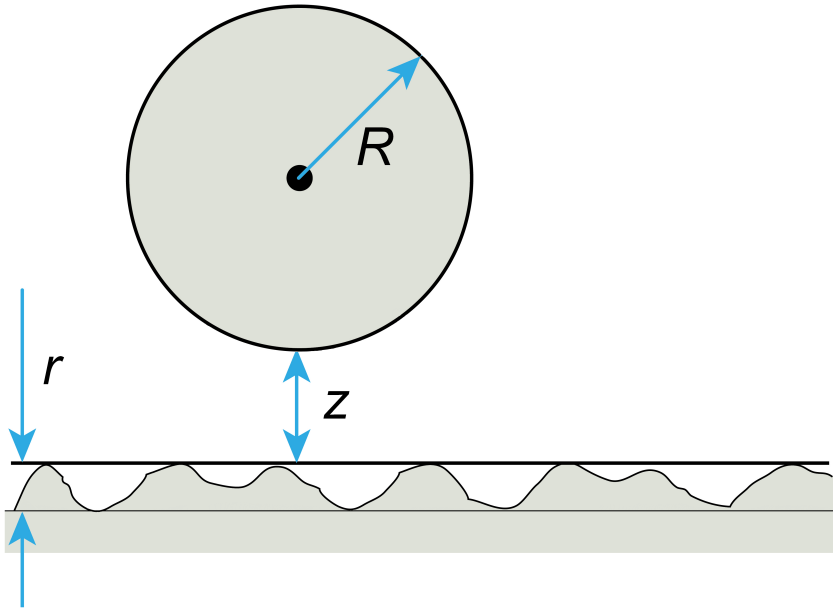

Figure 4.18: Schematic representation of a sphere, radius R, interacting with a rough surface. Reduced Van der Waals forces depends on a surface parameter, r.

An approximation of the Van der Waals force that includes the effects of surface roughness is given by

$$F_{Van\,der\,Waals} = \left(\frac{2z}{2z+r}\right)^2 \frac{HR}{6z^2}, \tag{4.29}$$

where r is a constant describing the average surface roughness of the two surfaces and H is the Hamaker constant for the materials involved [168].

4.4.2.4 The Casimir force

A prediction of quantum electrodynamics is that the exclusion of electromagnetic modes will cause two closely spaced conducting plates to be mutually attracted at the micro-scale [169]. Even though this attraction is extremely weak, especially between a sphere and a plate (as opposed to two parallel plates), when the separation distance is below several hundred nanometres, the Casimir force tends to be stronger than the Van der Waals force and the electrostatic force. The equation to describe the Casimir force between a sphere and a plane is

$$F_{\text{Casimir}} = \frac{R\pi^3\hbar c}{360z^3}, \tag{4.30}$$

where $\hbar$ is Planck's constant divided by 2π and c is the speed of light in a vacuum [169].

When operating at the boundary between micro- and nano-scale mechanical interactions, the inter-molecular forces (Van der Waals) and the Casimir force can both interfere with the meas-

urements. Although these two effects are manifestations of the same phenomena [170], they are considered separate for the purposes of this model. This is so as to differentiate between essentially large-scale interactions (dependent on the material properties and the surface textures of the spherical stylus tip and the measurement surface) and small scale interactions (dependent on predictions of quantum electrodynamics).

4.4.2.5 The squeeze-film effect

Any micro-device not enclosed within a vacuum will experience damping due to the finite viscosity of air [171]. The squeeze film effect due to a device operating in air is described in several papers and reports [172, 173]. An analytical solution has been derived [174, 175, 176] for the situation of a micro-sphere interaction with a plane surface, where the damping co-efficient due to the squeeze film effect, D_{squeeze}, on a sphere is

$$D_{\text{squeeze}} = \frac{6\pi R^2 \eta \Psi}{z}, \tag{4.31}$$

where η is the viscosity of the film, and Ψ is a derived parameter,

$$\Psi = 2\frac{z}{2d}\left[\left(1 - \frac{z}{6d}\right)\ln\left(1 + \frac{6d}{z}\right) - 1\right], \tag{4.32}$$

where d is the slip length. Subsequently, the slip length is a derived constant

$$d = \lambda\left(\frac{2.01}{\tau} - 0.73 - 0.16\tau\right) \tag{4.33}$$

where λ is the mean free path of the film and τ is the accommodation coefficient of the film material and the surface materials.

Following this definition, these equations can be applied to both the air layer above the measurement surface, and the liquid layer encountered close to the surface, to calculate the respective damping co-efficients. To calculate the associated surface interaction force due to the squeeze-film effect, the velocity of vibrating micro-probe tip is required.

4.4.2.6 Combined probe-surface interaction forces model

The vibrating micro-probe was designed such that its vibration actively counteracts the influence of any surface interaction forces it is subject to while interacting with a measurement surface. These surface interaction forces, as described in the previous sections, are dependent on certain physical attributes of the system. These attributes include (but are not limited to) the densities of the two interacting materials (the probe material and the measurement surface material), the

Table 4.6: Table of the physical attributes of the probe system used in the combined probe-surface interaction forces model.

Physical Attribute	**Symbol**	**Value**
Density of tungsten		$19\,254\,\mathrm{kg\,m^{-3}}$
Density of tungsten carbide		$15\,000\,\mathrm{kg\,m^{-3}}$
Radius of stylus tip	R	$70\,\mu\mathrm{m}$
Permittivity of free space	ε_0	$8.854 \times 10^{-12}\,\mathrm{C\,V^{-1}\,m^{-1}}$ [155]
Relative permittivity of air at 20 °C	$\varepsilon_{\mathrm{Air}}$	1.000 [155]
Relative permittivity of water at 20 °C	$\varepsilon_{\mathrm{Water}}$	80.1 [155]
Combined depth of surface imperfections	r	100 nm
Contact angle of water with tungsten carbide	θ	85°
Surface tension of water	γ	$0.072\,75\,\mathrm{J\,m^{-2}}$ [155]
Height of liquid contamination layer		20 nm [177]
Hamaker constant for tungsten(VI) oxide through water	H	21×10^{-21} J [167]
Viscosity of air at 20 °C at 1 atm	η	$1.837 \times 10^{-5}\,\mathrm{N\,s\,m^{-2}}$ [155]
Mean free path of air at 20 °C	λ	65 nm [178]
Accommodation coefficient of air and tungsten	τ	Estimated at 1 [179]

Hamaker constant for the two interacting materials and air, the depth of the combined surface imperfections of the two interacting materials, and the contact angle of any liquid contamination between the two interacting surfaces.

To simplify the model it was assumed that the materials used for interaction experiments would be similar – tungsten in the case of the sphere tip, and tungsten carbide in the case of the measurement surface. Table 4.6 shows the assumed values of the physical constants used to populate the surface force and vibration model.

Previous research has suggested that van der Waals interactions between tungsten surfaces are solely determined by the oxide layer, even though this is relatively thin [180]. Hence, to simplify the model it was assumed that the materials used for interaction experiments would be similar – tungsten (VI) oxide in this case – even though the two bulk materials were tungsten (stylus tip) and tungsten carbide (measurement surface).

The contact angle of water with tungsten carbide was measured using a Krüss DSA100M picolitre dosing system. The reported angle is an average value over several tungsten carbide gauge block surface samples. The depth of the surface imperfections is estimated as a worst-case value for a grade K tungsten carbide gauge block surface.

The analytical model has been constructed accounting for the five main surface interaction forces. To approximate the total force that a probe would experience, the arithmetic sum of the individual surface forces was calculated. This force approximates the worst-case scenario in which all of the forces are acting against the probe and it is vibrating in the vertical direction. The strength of the individual forces and the total surface interaction force, F_s, are shown in figure 4.19.

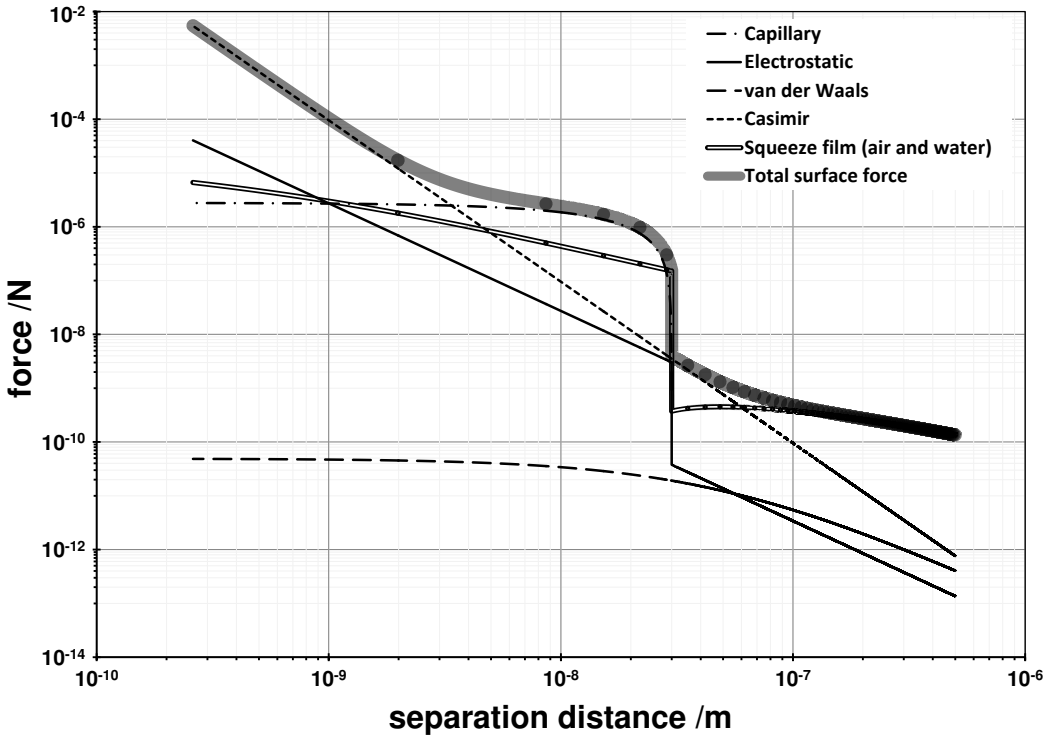

Figure 4.19: Graph of the theoretical surface force strength with respect to separation distance, z.

It can be seen that the squeeze film damping force dominates over a large range of separation distances. Upon interaction with the capillary layer, within 20 nm of the surface, the capillary force and the squeeze film damping force, due to the liquid contamination layer, dominate. It is only within several nanometres of the surface that the Casimir force begins to dominate. From the conditions described in table 4.6, the Van der Waals and the electrostatic forces are considered negligible.

4.4.3 Dynamic consideration within the probe-surface interaction model

Through this understanding of the theoretical surface force magnitude with respect to distance, an estimation of the minimum vibration amplitude required to counteract these surface forces can also be calculated. The minimum required amplitude (peak-to-peak) of vibration for the probe, based on surface conditions, probe mass and vibration frequency, is

$$A_{\min} = \frac{2F_s}{k}, \tag{4.34}$$

where F_s is the sum of all the constituent surface forces and k is the spring constant of the triskelion-flexure MEMS, as calculated in section 4.2.2. This relationship is analogous to the extension of a simple spring. Using the results of the sum of the individual forces shown in

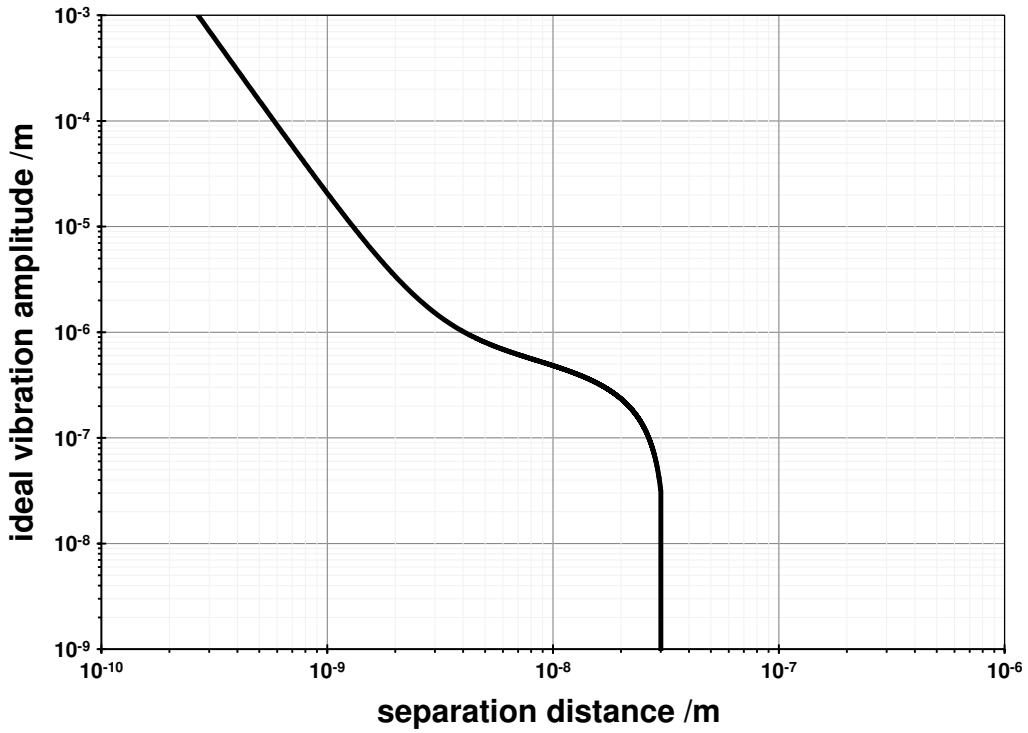

Figure 4.20: Graph showing an estimation of the minimum vibration amplitude required to counteract the surface forces present with respect to distance from the measurement surface.

figure 4.19, the minimum vibration amplitude required for intended operation of the micro-probe is shown in figure 4.20.

It can be seen from figure 4.20 that to approach within 10 nm of the measurement surface, any vibration amplitude of over 500 nm is sufficient to allow the vibrating micro-probe to retract from the test measurement surface without sticking. Through a simple set of experimental tests, it was confirmed that the micro-CMM probe can attain this vibration amplitude [164]. These results are described in Appendix B.

This understanding of the surface forces and the vibration requirements can subsequently be used to develop a basic operational model that will indicate their effect on the vibration interaction of the probe and the measurement surface.

In order to predict the operation of the micro-probe when interacting with a measurement surface, a model was devised that related the rate of change of vibration amplitude to distance from the measurement surface. The model was based on the solution of equation 4.26, the data from table 4.6, a vibration frequency of 1.6 kHz, being close to the first natural frequency, and a vibration amplitude of 1 µm. The ratios between the changes in vibration amplitude and the approach distances of the reference surface were calculated. When there is no interaction between the probe and the surface, this ratio is nominally zero, and when the probe is making contact with the surface, this ratio is nominally one. Any intermediate ratios are the result of a non-contact interaction between the probe and the measurement surface.

An example of suitable Matlab® code that would describe this developed model is shown in Appendix A, using the following pseudo-code:

Probe-surface interaction model

1. Set up initial conditions for the mechanical system (spring constant, vibration amplitude, vibration frequency, probe tip radius).
2. Calculate the ideal (undamped) motion of the probe as it approaches the measurement surface, and its associated amplitude.
3. Set up initial conditions for the surface interaction forces:
   (a) Capillary - surface tension, contact angle, *etc.*
   (b) Electrostatic - permittivity of free space, potential difference, *etc.*
   (c) Van der Waals - Hamaker constant for the two interacting materials, combined surface roughness, *etc.*
   (d) Casimir - Plank's constant, speed of light in a vacuum, *etc.*
   (e) Squeeze film - viscosity, mean free path, accommodation coefficients, *etc.*
4. Calculate the individual strengths of the surface interaction forces, and combine to determine the total force.
5. Through the knowledge of the velocity of the vibrating micro-probe (from point 2), calculate associated damping co-efficient due to the surface interaction forces.
6. Calculate the resultant (damped) motion of the probe as it approaches the measurement surface, and its associated amplitude.
7. Calculate the ratio between the undamped and the damped amplitudes of the vibration as a function of displacement from the measurement surface.

The results of the implementation of this model, using the physical attributes described in table 4.6, are shown in figure 4.21.

The model indicates interactions occurring within 100 nm of the surface. These interactions increase until contact with the surface is made, at 0 nm, where the change in amplitude is dominated by physical contact. Additional vibration amplitude reduction is caused by the continuing interaction with the surface; hence the ratio of vibration change to surface approach exceeds unity. Once the vibration amplitude is completely minimised by the approaching surface, the calculated ratio returns to zero.

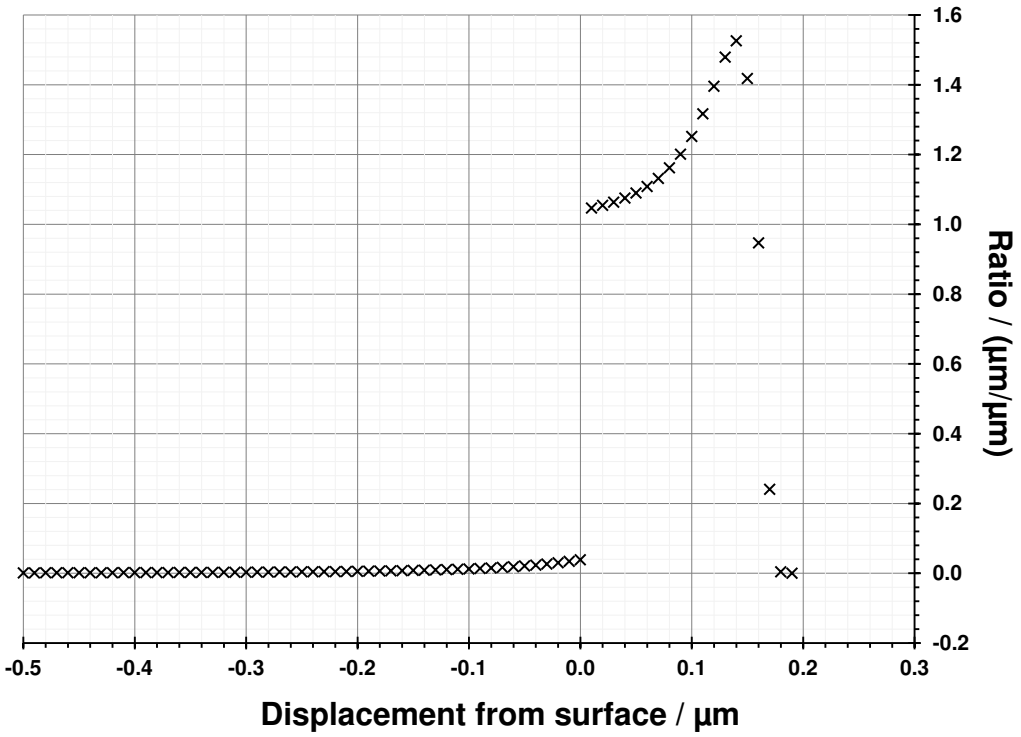

Figure 4.21: Graph of the results of the operational model of the vibrating micro-probe when interacting with a surface.

4.4.4 Limitations of the probe-surface interaction model

It is known that several limitations exist with the derived surface forces model. These limitations are separated into four main areas.

Firstly, the relationship between the Casimir force and the Van der Waals force is not well described. This could result in an incorrect description of the damping due to these forces. However, because the Van der Waals force is expected to act so weakly in the regime where the squeeze film effect is dominant, and also because the Casimir force is only dominant within several nanometres of the surface, any miscalculation is expected to have little effect on the result.

Secondly, the model is only concerned with the approach of the stylus tip to the measurement surface. The experimental work will focus on the approach of the probe to the measurement surface, and that the retract behaviour will only be studied for its lack of 'snap-back' or adhesion to the surface. Therefore, no further effort was dedicated to modelling retraction of the stylus tip from the measurement surface. It is, therefore, suggested that the retract behaviour will be similar to the approach behaviour.

Also, the model does not include a rigorous determination of the squeeze film effect. The work completed by Honig *et. al.* in this area [174], focused on a flow regime that is characterised by large characteristic lengths. It is, therefore, suggested that the characteristic length scale of the

air squeeze film interaction between the sphere tip and the measurement plane is in the region of 65 µm, implying that the damping is relevant in the final 65 µm of approach.

It can be quoted from Honig:

> *"as the Vinogradova solution invokes a first order boundary condition* [175]*, it is only valid when the mean free path is small relative to the separation...* [however] *although the assumptions limit the validity to about twice the mean free path [z ∼ 200 nm], the plot of the theory fits our* [174] *data to about 100 nm."*

Therefore, even though this description is an indication of the effect of the air squeeze film during the interaction of the spherical stylus tip with a measurement surface, the limits of using a continuum description and a first order approximation is that the solution is only valid from about 65 µm to 100 nm separation.

Following the completion of the air squeeze film model, a further consideration can be made for the squeeze film effect of the liquid layer. The mean free path of liquid water is about 0.3 nm, which suggests that this model is valid to 1 nm separation.

Finally, the derived model is dependent on many input variables whose values, although found in literature, should be considered as estimates. Small changes to their values have large effects on the outcome of the model, indicating its fragility when attempting to describe reality. Some of the variables of concern, that have a significant effect on the outcome of the model are: the thickness of the liquid layer, the contact angle of water with tungsten and the potential difference between the two surfaces. For this reason it is not expected that the surface forces model be a realistic indication of the expected force field strength, or that it results in a realistic ratio prediction. However, the model does serve to indicate initial starting conditions for the future experimental work, and it also indicates which variables are of importance when operating the vibrating micro-probe.

4.4.5 Summary of the probe-surface interaction model

The work completed in this section with regards to the surface interaction forces and the effect they have on the operation of the vibrating micro-probe, serves to furnish the future experimental work with certain predictions. It also addresses the developmental requirements of **Thesis Objective 1**.

These predictions are:

- the minimum vibration amplitude required for the vibrating micro-probe to operate as intended,
- the expected results of a physical interaction experiment when calculating the interaction ratio value,

- the expected position from the surface where the surface interaction forces will affect the operation of the vibrating micro-probe, and
- an indication of the maximum over-travel that the probe can experience while still operating as intended.

There are also limitations placed on the predictions of the model, specifically with respect to the combined strength of the surface interaction forces and their expected effect on the vibration of the stylus tip. The main limitation stems from the lack of information on the effect of the squeeze film effect on the motion of the stylus tip. It is, therefore, concluded that the results presented in figure 4.21 indicate an underestimation as to the effect of the surface interaction forces on the motion of the vibrating probe.

However, taking all this into account, the model of the surface interaction forces and their effect on contact probing, including the dynamic considerations associated with a vibrating probe, does provide some useful predictions. Taking all the starting conditions described in the model into account, the surface forces interaction model predicts that the vibrating micro-probe can detect the test measurement surface up to 100 nm prior to physical contact. Also, depending on the amplitude of the vibration, the maximum over-travel of the probe can be defined so that it still maintains suitable vibration amplitude to counteract the surface interaction forces while retracting from the test measurement surface.

4.5 Conclusion of all models of the vibrating micro-probe

This chapter has described the theoretical work conducted with regards to the development of models used to describe the behaviour of the vibrating micro-probe. Several models are described, including analytical models of the expected surface interaction forces and finite element (FE) models of the physical properties of the vibrating micro-probe and its constituent parts.

The mechanical aspects of the constituent parts of the vibrating micro-probe were modelled. The design of a suitable micro-stylus was considered, based on several initial conditions such as suitable aspect ratio, resonance frequency, the effect of the mass of the micro-stylus on the frequency response of the triskelion device and the sensitivity of the resulting assembled vibrating micro-probe. A further consideration for the design of the micro-stylus was the limitation of the manufacturing technique. The resulting design for the micro-stylus consists of a 2.5 mm long shaft, tapering from 0.15 mm in diameter to 0.045 mm in diameter. The stylus is terminated with a 70 µm diameter spherical tip. This stylus design fulfils the requirements of **Research Question 1.1**.

An analytical model was developed to describe the operation of the probe, geometrically, mechanically and electrically (with respect to the piezoelectric actuators). The geometrical model

was aimed at defining the motion of the probe, and acted as a definition of probe response during ideal and isotropic operation. This geometrical model can subsequently be used to test the isotropy of a real micro-probe, as required in **Thesis Objective 2**, and specifically, **Research Question 2.1**. The mechanical and electrical models were used to design an algorithm that indicates the estimated input voltage signals required to control the vibration of the probe.

Finally, an analysis of the surface interaction forces was conducted. This work resulted in the prediction that the surface interaction forces interfere with the operation of the probe 100 nm prior to physical contact with the measurement surface. This prediction enables the calculation of a suitable vibration amplitude to counteract the surface interaction forces while interacting with the test measurement surface, as required in **Thesis Objective 1**. The effect of this interference is estimated as a measurable effect on the vibration amplitude of the probe.

At all stages in the modelling process, the limitations of the developed models are considered and discussed.

Chapter 5

Experimental validation of the vibrating micro-probe

5.1 Introduction to the experimental validation

In this chapter the experimental validation of the vibrating micro-probe will be described. This experimental validation links directly to **Thesis Objective 1** and **Thesis Objective 2**, which are concerned with the validation of the operation of the vibrating micro-probe with respect to the ability to counteract the surface interaction forces and to act isotropically.

Initially, a list of experiments will be presented. These experiments will be designed to answer the research questions related to the experimental validation of the vibrating micro-probe. Following the design of experiment section, a thorough description of the experimental setup design, and technical specifications of all the constituent parts of the apparatus will be completed. A small section will also be dedicated to describing some elements of good practice for experiments that involve the development of high precision metrology systems.

The main procedures used in the experimental validation will then be presented. The procedures will include a step-by-step description of the preparation, setup and completion of each experiment. The experimental results will then be presented and discussed. A list of known error sources will also be presented and an estimated uncertainty calculation will be made, so that the results are comparable with results from similar investigations on other probes.

5.2 Design of Experiments

To complete the experimental validation of the vibrating micro-probe, several experiments must be designed and run.

- Test the ability of the vibrating micro-probe to counteract the surface interaction forces.
  - This is required by **Thesis Objective 1**. Initially, a set of experiments will be conducted to compare the true operation of the vibrating micro-probe with the theoretical operation, as determined in Chapter 4, section 4.4.3.
- Investigate the sensitivity of the probe to changes in the operating amplitude and to changes in operating frequency.
  - These two sensitivity experiments will assist in the further determination of the ability of the vibrating micro-probe to counteract the surface interaction forces. Several different operating conditions will be tested, and their effect on the ability of the vibrating micro-probe to counteract the surface interaction forces will be determined.
- Determine the probe point repeatability of the vibrating micro-probe.
  - This is required by **Research Question 1.2**. It is also assumed that, should the probe point repeatability of the vibrating micro-probe be below 10 nm, then this is a good indication of the ability of the probe to counteract the surface interaction forces.
- Determine the length measuring capability of the vibrating micro-probe, also called linearity error.
  - This is required by **Research Question 1.3**. Although this result is not formally required to determine if the vibrating micro-probe can successfully counteract the surface interaction forces, it is a prerequisite of the operation of any micro-CMM probe, and should therefore be determined.
- Investigate the capability of the probe to operate in a lateral direction.
  - Initially, the previously described tests will be completed with the vibrating micro-probe operating in the vertical direction. However, to determine the ability of the vibrating micro-probe to operate in 3D, as required in **Thesis Objective 1**, its operation should also be considered in the lateral direction.
- Investigate the capability of the vibration algorithm to realise isotropic operation.
  - Finally, the requirements of **Thesis Objective 2** will be addressed. The ability of the vibrating micro-probe to operate isotropically will be determined by applying the newly developed concept of isotropy determination for vibrating micro-CMM probes.

Specifically, these experiments will address the requirements of **Research Question 2.1**.

Following the design of experiments suitable to validate the operation of the vibrating micro-probe according to **Thesis Objective 1** and **Thesis Objective 2**, the design of a suitable experimental setup can be considered.

5.3 Experimental setups used for validation

Accurate validation of the vibrating micro-probe relies on the design, manufacture and use of a suitable experimental test setup that is capable of performing better than, or at least similar to, required from the probe itself. For simplicity, a single experimental setup was designed. This simple 'base setup' could be easily added to or augmented such that the range of different required experiments could easily be performed.

The design of the base setup will be presented, and the constituent parts will be described in detail. A description of the three distinct experimental setups will then be presented, highlighting the required changes from the base setup. An appreciation of any good practice rules that were applied during the design and build of the base setup will also be highlighted.

5.3.1 Design of the base setup

The basic design of the experimental setup is, that the vibrating micro-probe should be securely held in space, such that any external measurement surface can interact with it in a controlled way. Any control systems designed for the operation of the vibrating micro-probe should be easily interfaced with the base setup. Also, any external measurement or validation systems should have easy access to the vibrating micro-probe. A schematic diagram of the design of the base setup is shown in figure 5.1.

The labels in figure 5.1 refer to the constituent parts of the base setup. These constituent parts will now be described, including design rules followed (for custom-made parts) and selection criteria (for commercial systems). The manipulation column has various configurations, depending on which validation experiments are being performed. The constituent parts of the manipulation column will be described now, however, the various configurations will be highlighted in a section 5.3.2.

5.3.1.1 Kinematic stand

The vibrating micro-probe should be held stationary in space during testing. Any mount that is used to hold the vibrating micro-probe should be statically determined by physical contact

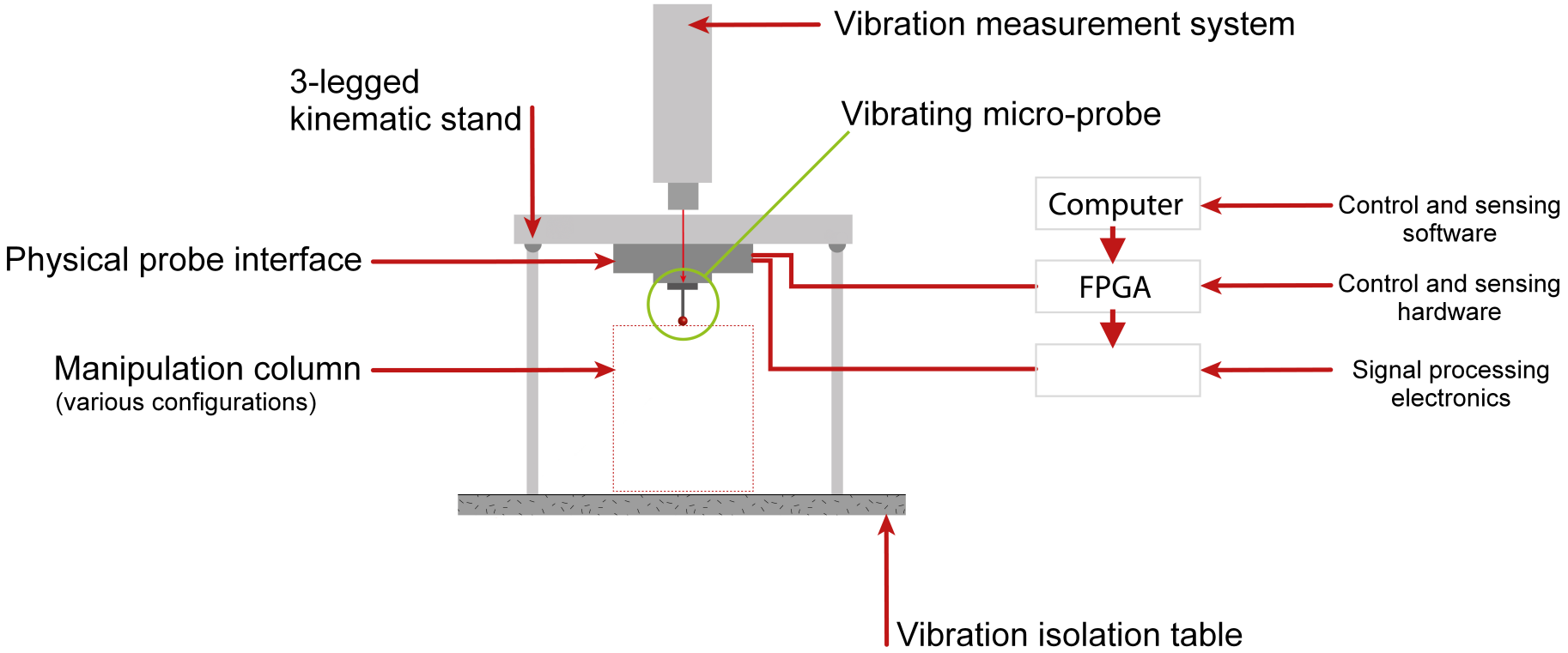

Figure 5.1: Schematic diagram of the base setup. The constituent parts are described in the sections that follow.

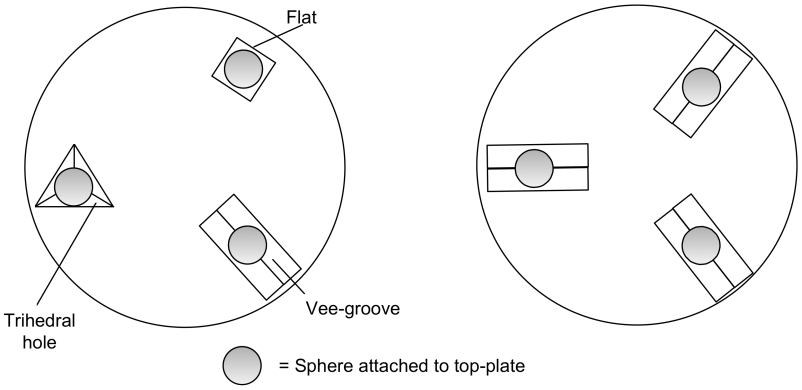

Figure 5.2: Graphic showing a Type I (left) and a Type II Kelvin clamp (right) [182].

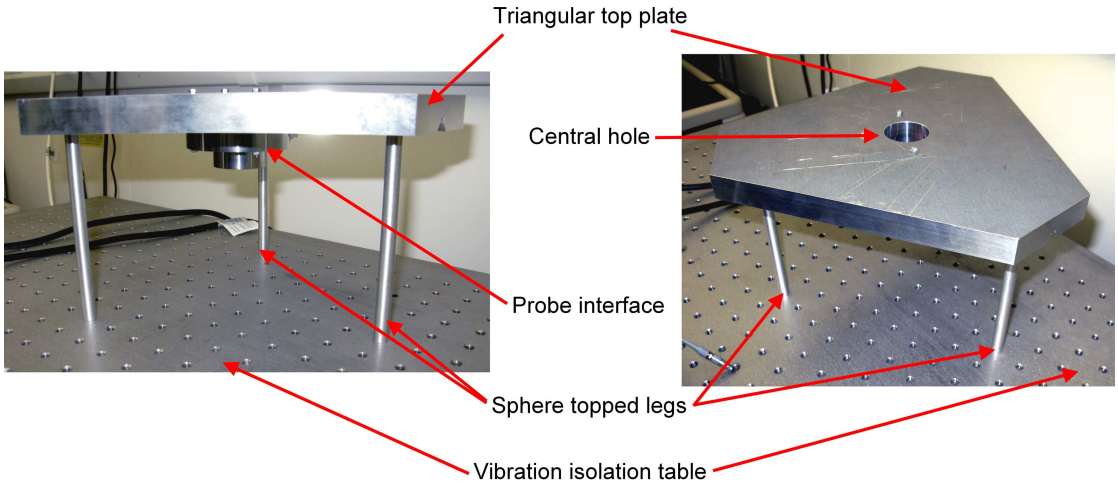

Figure 5.3: Image of the kinematic stand for the probe testing setup. Side view (left) and isometric view (right)

between solid legs and a dismountable top plate [181]. This determination can be attained by using kinematic coupling. Therefore, a kinematic stand was designed with a triangular top plate and three solid legs.

To ensure the stand acts kinematically when assembled and disassembled, a Type II Kelvin clamp system was used to mount a connecting plate onto three static legs. A Type II Kelvin clamp was chosen over a Type I Kelvin clamp as it is easier to manufacture, is symmetrical, and is less influenced by thermal variations [182]. A diagram showing a Type II Kelvin clamp compared to a Type I Kelvin clamp is shown in figure 5.2.

Two images of the manufactured kinematic stand are shown in figure 5.3.

The top plate of the stand is manufactured from Dural grade aluminium [183], which has a co-efficient of thermal expansion of $22.5 \times 10^{-6}\,\mathrm{K}^{-1}$. Thermal expansion of the top plate will, however, only result in uniform lateral expansion. The position of the bottom of the plate, where the probe will be mounted, is determined by the length of the legs. The three sphere-tipped legs are manufactured from aluminium; a material with a co-efficient of thermal expansion

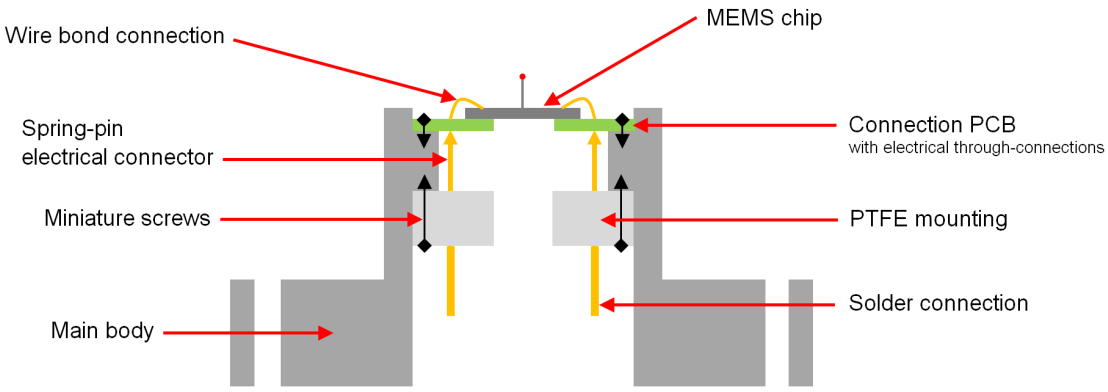

Figure 5.4: Schematic of the physical and electrical interface between the vibrating micro-probe and the kinematic stand (cross section).

similar to that of the manipulation column. Therefore any change in the length of the stand's legs due to temperature change, will be replicated in the manipulation column. This effect is also known as 'thermal matching'.

The top plate has a hole machined in the centre to allow visual access to the vibrating micro-probe. Hence any external optical measurements can be completed while the probe is secured in place.

5.3.1.2 Interface between vibrating micro-probe and kinematic stand

A physical interface is required to mount the vibrating micro-probe onto the kinematic stand. The interface should allow the probe stylus to stand proud of the kinematic stand, so that the test measurement surface is not obstructed during testing. The interface should also allow probes to be easily exchanged. The vibrating micro-probe requires an electrical interface to allow any control signals or detection electronics to be connected. The electronic interface should be combined with the physical interface into a dual interface that resembles the basic design of a CMM probing head.

A physical interface was designed that can be connected to the kinematic stand using three bolts. The probe is attached to the active end of the physical interface via three miniature screws onto spring-loaded connectors. To facilitate good electrical and mechanical connection to the interface, the triskelion-flexure MEMS chip of the vibrating micro-probe is first mounted onto a PCB. The PCB contains three holes for physical connection to the interface. Fifteen electrical through-connection pads allow for electrical connection between the pads on the triskelion-flexure MEMS chip (by wire bonding) and spring-loaded electrical connection pins. The spring-pins are secured in a custom-made PTFE mounting structure. The PTFE mount also serves to electrically isolate the spring-pins from each other, and from the surrounding interface structure. The spring-pins are subsequently wired to a 25 pin D-type male connector on the side of the interface. A schematic of the design of the interface (cross section) is shown in figure 5.4.

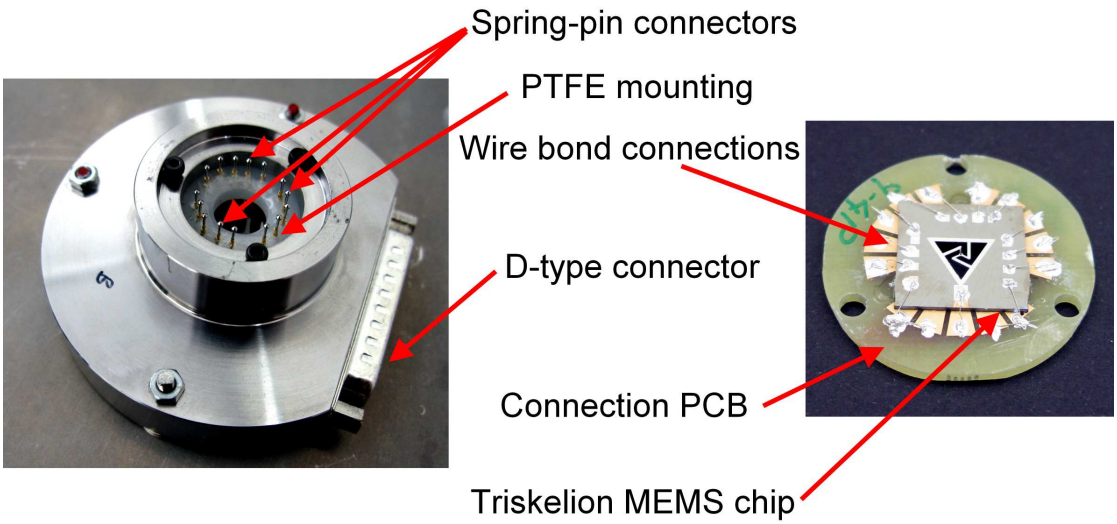

Figure 5.5: Image of the probe connection interface (left) and the connection PCB (right)

The final interface is manufactured from Dural grade aluminium. The probe connection PCB is manufactured externally by Integrated Electronics Ltd, Wraysbury, UK [184], according to a design developed specifically for this application. The spring-pin electrical connections are a commercial product from Harwin, supplied by RS Components Ltd [185]. An image of the physical interface (probe connection end) and of the probe connection PCB can be seen in figure 5.5.

5.3.1.3 Control and sensing hardware

The NPL vibrating micro-probe is operated through the activation of six piezoelectric actuators, two on each leg of the triskelion flexure array. The requirements of the control hardware is therefore to produce six actuation signals simultaneously, over a range of operational voltages and frequencies. The actuation signals should also be controllable through a programmable interface.

To realise the full operation of the vibrating micro-probe, each flexure is instrumented with two piezoelectric sensors. These sensors are used to realise the self-sensing capability of the probe during operation. Ideally, a similar hardware solution should be used for the collection of these sensor signals, capable of measuring multiple channels simultaneously over a wide range of voltages and frequencies.

A commercial product exists that will provide both of these functions; a National Instruments multifunction data acquisition system based on FPGA (field programmable gate array) technology. The system used is the R Series Multifunction RIO with Virtex-5 LX30 FPGA [186]. The system is capable of eight analogue inputs with independent sampling rates up to 200 kHz (16-bit resolution) and eight analogue outputs with independent update rates up to 1 MHz (16-bit

Table 5.1: The numerical designations of the output (left) and input (right) signals, with associated information on their intended use

Output	Info	Input	Info
1	Leg 1 – inner actuator	1	Leg 1 – inner sensor
2	Leg 1 – outer actuator	2	Leg 1 – outer sensor
3	Leg 2 – inner actuator	3	Leg 2 – inner sensor
4	Leg 2 – outer actuator	4	Leg 2 – outer sensor
5	Leg 3 – inner actuator	5	Leg 3 – inner sensor
6	Leg 3 – outer actuator	6	Leg 3 – outer sensor
7	Spare	7	Vibrometer
8	Spare	8	Spare

resolution). Both input and output signals are limited to $\pm 10\,\mathrm{V}$. The system can be programmed and controlled through National Instruments' LabView software.

A National Instrument's 'breakout box' is used to make electrical connections between the FPGA card and the signal processing electronics, and subsequently the probe. Connections between the FPGA card and the breakout box are made using a high-performance shielded cable supplied by National Instruments. Connections between the breakout box and the signal processing electronics are made using unshielded twisted pairs. The numerical designations of the output and input signals, including information on their connection to the experimental apparatus, is shown in table 5.1.

5.3.1.4 Control and sensing software

A software package will be required to program and control the FPGA hardware. This software will calculate the correct vibration signals to operate the vibrating micro-probe and then control the signal generation capabilities of the control hardware to deliver those signals. Likewise, a similar software solution will be required to receive, store and process the sensor signals. The sensing software will accept a large number of signals simultaneously over a range of voltages and frequencies. Subsequently, it will process those signals and store them in suitable formats such that post processing and detailed analysis can be completed.

With the chosen hardware solution being from National Instruments, it was advantageous that the software used for this project should be National Instrument's data acquisition and instrument control software, LabVIEW. The specific version used for this project was LabVIEW Version 10.0 [187]. Additionally, the FPGA Interface toolbox and the Express signal analysis toolbox were used. The FPGA card was programmed to output six sinusoidal signals and to accept seven input signals for processing. The numerical designations of the output and input

signals, including information on their connection to the experimental apparatus, is shown in table 5.1. Given the technical specifications of the FPGA system, the voltage range of the output is ±10 V, with a maximum frequency output of about 20 kHz, with similar viable ranges for sensing.

The signals from the vibrating micro-probe sensors, input to the FPGA card, are sampled at 50 kHz. The data is stored in packets of 5000 points, and these data packets are subsequently analysed. Through Fourier analysis (FFT) a frequency is calculated for the output of each sensor, along with a signal amplitude and a phase, calculated with respect to the input signal. Once these calculations have been completed, the data is written to a text file. The data output rate is approximately 10 Hz. This process runs continuously until either a pre-set condition is met, or the program is forcibly stopped. A basic pseudo-code implementation of this software, and an example set of raw data output, is shown in Appendix E.

5.3.1.5 Signal processing electronics

A set of signal processing electronics are an essential component of the experimental setup. The vibrating micro-probe will be activated through drive signals designed to control its vibration. The probe will also be producing sensor signals that will indicate the current dynamic behaviour of the probe, and will be used to detect changes indicative of surface interaction or contact. A set of electronic circuits are required condition the drive signals, and to properly filter and amplify the sensor signals.

Low-pass filters were installed between the control hardware and the piezoelectric actuators and sensors to ensure minimal high frequency noise interference with the probe operation and detection. These circuits were designed to be suitable for all probes regardless of their electrical properties. Therefore, the cut-off frequency was set at a maximum expected operational frequency of the probe of 2 kHz. The design of the simple low-pass filter is shown in figure 5.6.

The op-amp used for the low pass filter was powered using a simple ±12 V power supply. Several tantalum capacitors were also installed, in parallel with the power lines, to reduce the effect of external noise. To transfer all electrical signals to and from the probe via the 25-pin D-type connector, a set of shielded cables were produced, which contained shielded twisted pairs [188].

5.3.1.6 Precision manipulation stage

A high precision manipulation stage is required to move the test measurement surface during testing. This stage should be accurate and repeatable to an extent similar to, or ideally better than, the expected capability of the probe.

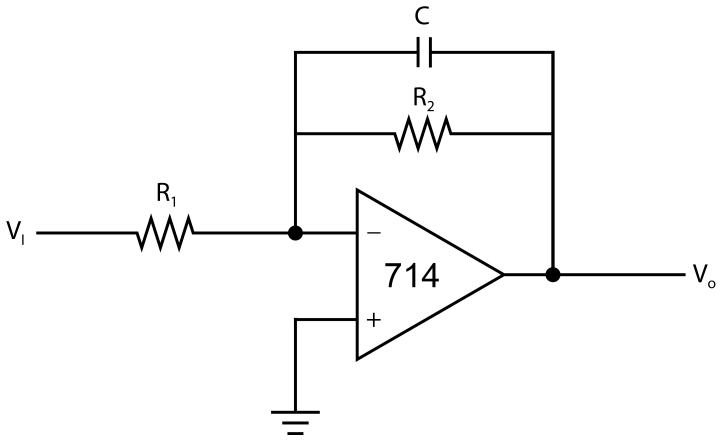

$R_1 = 1\,\mathrm{M\Omega}$

$R_2 = 10\,\mathrm{M\Omega}$

$C = 10\,\mathrm{pF}$

$f_0 = \frac{1}{2\pi R_2 C} = 1.6\,\mathrm{kHz}$

$Gain = \frac{-R_2}{R_1} = -10$

Figure 5.6: Circuit diagram of a simple low-pass filter, suitable for use with the vibrating micro-CMM probe

A commercially-available, piezoelectric stage was selected; a Physik Instrumente one-axis compact nanopositioner, P-611.ZS [189]. This stage is capable of closed-loop operation by virtue of an inbuilt linear sensor, and its motion can be controlled by LabView through a USB connection.

The stage has a 100 µm travel range while in closed-loop mode, and, according to the specification, should be capable of achieving a repeatability of better than 10 nm. Over the full 100 µm travel, it is specified to have a linearity error of no more than 0.1 % (this equates to 100 nm positional error over 100 µm). The capability of the stage was tested using a white-light interferometer, which measured various step positions within the central travel range of the precision manipulation stage. The step positions measured by the white-light interferometer were compared to the positions reported by the internal sensors on the precision manipulation stage. These results are shown in figure 5.7.

It can be seen from figure 5.7 that over 80 % of the measured data points fit within the ±0.1 % error bars, which are guaranteed by the manufacturer. It is assumed that the stray points, which are all clustered at the start position of the test, are due to noise in the experimental setup. Therefore it is assumed that the precision manipulation stage can operate as specified.

5.3.1.7 Test measurement surface

A suitable test measurement surface should be mounted on the precision motion stage to act as a test measurement surface during the contact experiments. This surface should be well characterised in terms of topography and material properties. An ideal surface, that is readily available, is the gauging surface of a gauge block. A grade K gauge block, 2.5 mm nominal length,

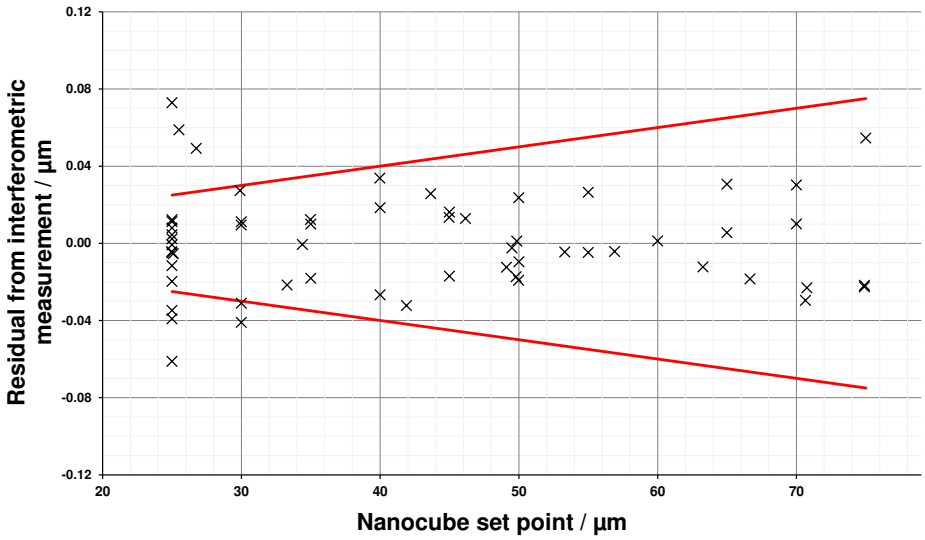

Figure 5.7: Verification of the precision manipulation stage. The measured points indicate the residuals of the measurements taken on the white-light interferometer from the positions reported on the internal sensors of the precision manipulation stage. The red lines indicate an error of $\pm 0.1\,\%$.

made of tungsten carbide, is used as the test measurement surface. A grade K gauge block has a flatness specification of 50 nm over the entire surface of the gauging face (local deviations will, therefore, be smaller than this) [190]. The interaction model for the vibrating micro-probe, developed in Chapter 4, section 4.4.2.6, included the physical and material properties of a tungsten carbide gauging surface, however other gauge block materials including stainless steel and ceramic would also be possible.

5.3.1.8 Vibration measurement system

A reliable, external vibration measurement system should be used to validate the ability of the probe to both vibrate and self-sense. This external vibration detection system should be non-contact, so that it does not interfere with the operation of the probe. The system can be positioned above the probe, with access afforded it through the hole in the top plate of the kinematic stand.

The system chosen to act as an external vibration measurement system is a commercial laser Doppler vibrometer (LDV) model CLV 2534-2 from PolyTec [191]. This LDV is a single point system, which operates according to the principles of laser Doppler vibrometry [192, 193, 194]. Laser Doppler vibrometry is a technique for the measurement of the velocity of a physical vibration from the determination of the Doppler shift of a reflected laser beam. The control system includes a digital integration card that enables the conversion of the velocity signals, which are the usual measurand detected by an LDV, to displacement signals. The output of the integrator card is scaled to $\pm\,10$ V, and is therefore suitable for input to the control and sensing hardware.

When operating with the displacement encoder, the system is specified with a $\pm 2.5\,\%$ linearity error.

This system also contains an analogue colour TV output, which allows visual appreciation of the surface being measured. This is particularly useful when using the LDV equipped with a microscope objective, when determining the position of best focus is very difficult to do by eye. The system includes the Vib-A-510 in-line illumination tool [191] and a $10\times$ microscope objective.

It should be noted that the CLV 2534-2 is equipped with a Class 2 laser, 633 nm (HeNe), with a power less than 1 mW. Although this laser is not eye safe (due to the focussing optics included in the experimental setup), the focal length of the $10\times$ magnification microscope objective is approximately 37 mm, and when focused on the probe, the objective fits fully into the hole in the top plate of the kinematic stand. Therefore, the free space travel of the laser beam is fully enclosed, and it is deemed safe for use without safety goggles.

5.3.1.9 Various coarse manipulation stages

The experimental setup was designed to ensure that the constituent parts could be positioned correctly. However, various aspects of the setup need to be adjusted or moved during testing. This was achieved by using a range of coarse manual manipulation stages (both linear and rotational).

There are several parts of the experimental setup that require coarse manipulation. Vertical (z-axis) manipulation of the LDV head is required to bring the laser spot into sharp focus on the vibrating micro-probe. Lateral (xy-axis) manipulation of the LDV head is also required, so that the laser spot can be manipulated about the top of the vibrating micro-probe. This will allow manufacturing and assembly errors to be compensated for (as the vibrating micro-probe may not always sit exactly central within the experimental setup), and will also allow the vibration of each individual leg to be measured (at the elbow position).

Coarse manipulation of the test measurement surface is required in at least four degrees of freedom in a Cartesian frame of reference. These are z, x, y and rotation about the z-axis. This will be realised as three degrees of freedom in a cylindrical frame of reference, z, rotation about the z-axis and a radial linear axis.

Along with the various course manipulation stages needed to complete the experimental setup, a wide range of fixtures and fittings are required to construct the setup. Several optical breadboards are used to serve as a structural base onto which all of the constituent parts are fixed.

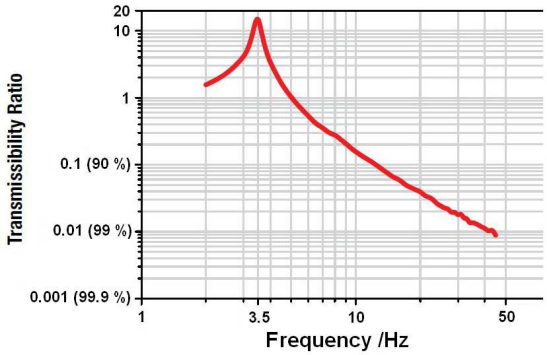

Figure 5.8: Graph showing the vertical transmissibility of the PFP51507 passive vibration isolation table

5.3.1.10 Environmental isolation

Any external vibration that could act on the experimental setup may interfere with the operation, or external measurement, of the vibrating micro-probe. It is, therefore, important that the setup is isolated from any external environmental vibration that may interfere with the completion of the experiment. Any isolation system should be large enough to incorporate the entire experimental setup.

A suitable vibration isolation system was identified. This system was an air-sprung passive isolation table, commercially available from Thorlabs (product reference PFP51507). This optical table was chosen for several reasons, including its vibration damping capability, its size and its cost. A graphical description of its damping capabilities, as provided by the manufacturer, is shown in figure 5.8.

It can be seen that transmissibility of vibration in the vertical direction is less than 1 % for frequencies above 50 Hz. Therefore, given that the optimal vibration frequency for the testing and operation of the vibrating micro-probe is over 1 kHz, the transmission of frequencies likely to interfere with its operation will be very low. However, the transmission of frequencies below 10 Hz, especially at the resonant frequency of the table itself at 3.5 Hz, is high. Therefore, steps should be taken, other than mechanical isolation, to ensure these effects do not affect the data processing. These steps include electrical filtering and software-based band-pass filters to remove any stray, or unwanted, signals. The LDV control system is also fitted with a software based band-pass filter to remove unwanted vibration frequencies during measurement.

The experiments should also be isolated from any external acoustic effects, air turbulence and air disturbances. This was achieved by placing the experimental setup in a physical enclosure.

5.3.1.11 Environmental control system

Isolation from external vibration and external acoustic effects is a realistic requirement of operation of a probe for micro-CMMs. Likewise, control of the external environment, specifically

Table 5.2: List of all vibrating micro-probes which are available for validation.

Probe	Approximate date of:		Notes
	Manufacture	Assembly	
MP-Ni-4-X	Before Oct 2008	April 2011	Tested - Surface interaction forces
MP-Ni-6-B	Oct 2010	April 2011	Tested - Surface interaction forces
MP-Ni-6-D		April 2011	Tested - Surface interaction forces
MP-Ni-6-F		April 2011	Used during temperature testing
MP-Ni-6-I		Feb 2013	Tested - Linearity and repeatability
MP-Ni-9-9P	Oct 2012	Feb 2013	Tested - Linearity and repeatability

temperature and humidity, is also a realistic requirement for high precision dimensional metrology.

The experimental setup was therefore operated in a controlled laboratory. The laboratory at NPL where the experiments were completed is specified to a temperature of $20\,^{\circ}\mathrm{C} \pm 0.1\,^{\circ}\mathrm{C}$, with a temperature gradient of better than $0.1\,^{\circ}\mathrm{C}$ per hour, and a humidity of between 40 %RH and 65 %RH. These specifications have been tested many times as part of NPL's UKAS accreditation and have been found to be realistic. However, a logging system was put in place for the duration of the tests to confirm these specifications.

It is expected that a single validation test will run over less than thirty minutes and, therefore, the thermal mass of the setup is likely to shield the experiment from major temperature excursions (for at least the duration of one test).

5.3.1.12 Vibrating micro-probes available for testing

Extensive background research has been completed with respect to the NPL vibrating micro-probe. This included the manufacture of the triskelion-flexure MEMS [131] and of the sphere-tipped micro-stylus [137], and the assembly of these constituent parts into a complete device [145]. This background work has resulted in various vibrating micro-probes being manufactured, which are available for validation.

A full list of the vibrating micro-probes available for validation is shown in table 5.2. This table includes the name of the probe, the approximate date it was manufactured and assembled, and any other notes that are of use. A full table of all manufactured probes is shown in Appendix C.

As part of the initial characterisation of these probes, a set of "Fact Sheets" were produced, allowing easy access to the pertinent data required to operate the probe during testing. The Fact Sheet for MP-Ni-9-4P is shown in figure 5.9. Several other Fact Sheets are shown in Appendix D.

The manufacturing process and activation of the piezoelectric material is variable, even across a single triskelion-flexure MEMS device. In an attempt to address this variation, a "strength coefficient" is determined for each actuator. These coefficients compare the capability of each actuator on the probe to produce a vibration at a given input voltage to the actuator which

produces the largest vibration at the voltage. If linearity of actuator strength is assumed, the strength coefficients allow input signals to be correctly scaled. The actuator strength coefficients are determined using only the base experimental setup. The actuator strength coefficients are calculated using the reported actuator data.

5.3.2 Details of the distinct experimental setups

A schematic diagram of the base experimental setup is shown in figure 5.1. The various constituent parts of the experimental setup have been described, along with explanations of any design choices made and any pertinent technical specifications. However, the base setup alone is not sufficient to complete the experiments described in section 5.2. Therefore, the required three distinct experimental setups will be described, which use the base setup and different arrangements of the various constituent parts.

5.3.2.1 Experimental setup for the testing in the vertical direction (z-axis)

To test in the vertical direction, the manipulation column must allow for vertical movement of the test measurement surface. Therefore, the test measurement surface, the precision manipulation stage, and a coarse vertical manipulation stage (a precision manual lab-jack) are secured below the vibrating micro-probe, such that the surface normal of the test measurement surface is parallel to the stylus. This will result in an ideal interaction between the probe and the test measurement surface when the probe vibrates vertically.

A schematic diagram of the manipulation column used with the base setup for testing in the vertical direction is shown in figure 5.10. An image of the experimental setup is shown in figure 5.11.

5.3.2.2 Experimental setup for the testing in the lateral direction (xy-axis)

To test in the lateral direction, the manipulation column must allow for lateral movement of the test measurement surface. Therefore, the test measurement surface and the precision manipulation stage are mounted onto the coarse vertical manipulation stage using an angle plate. Once secured below the vibrating micro-probe, the test measurement surface will be able to move laterally with respect to the direction of the stylus. This will result in an ideal interaction between the probe and the test measurement surface when the probe vibrates horizontally. By mounting the linear motion stages on top of the rotation stage, the system is converted into a cylindrical frame of reference, enabling all interaction experiments to be defined as a height, a rotation angle and a radial motion.

A schematic diagram of the manipulation column used with the base setup for testing in the lateral direction is shown in figure 5.12. An image of the experimental setup is shown in figure 5.13.

MP-Ni-9-9P

Images:

Front **Back**

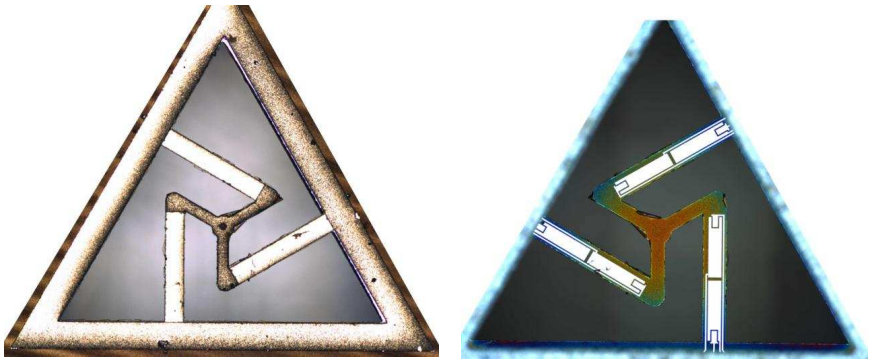

First natural frequency:

2.200 kHz (2nd natural frequency - ≈ 3.880 kHz)

Actuators:

Actuator designation	Working	Test freq / kHz	Amplitude at 1 V / µm	Voltage for 1 µm / V	Amplitude at 5 V	Amplitude at 10 V
Leg 1 – AI	Y	2.201	0.05	X	0.09	0.16
Leg 1 – AO	Y	2.202	2.00	0.490	X	X
Leg 2 – AI	Y	2.202	0.04	X	0.10	0.20
Leg 2 – AO	Y	2.201	7.25	0.130	X	X
Leg 3 – AI	Y	2.201	0.04	X	0.09	0.17
Leg 3 - AO	Y	2.201	7.00	0.134	X	X

Frequency response of 1AO – 1 V p2p:

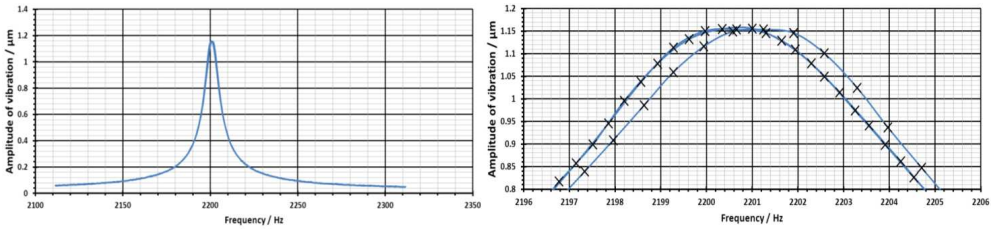

Sensors:

Sensor designation	Working	Amplitude jump / V	Phase peak / degrees
Leg 1 – SI	Y	< 0.05	0.2
Leg 1 – SO	Y	0.1	2.5
Leg 2 – SI	N	X	X
Leg 2 – SO	Y	< 0.05	0.2
Leg 3 – SI	Y	< 0.05	0.2
Leg 3 - SO	Y	< 0.05	0.2

Figure 5.9: The Fact Sheet for vibrating micro-probe MP-Ni-9-9P.

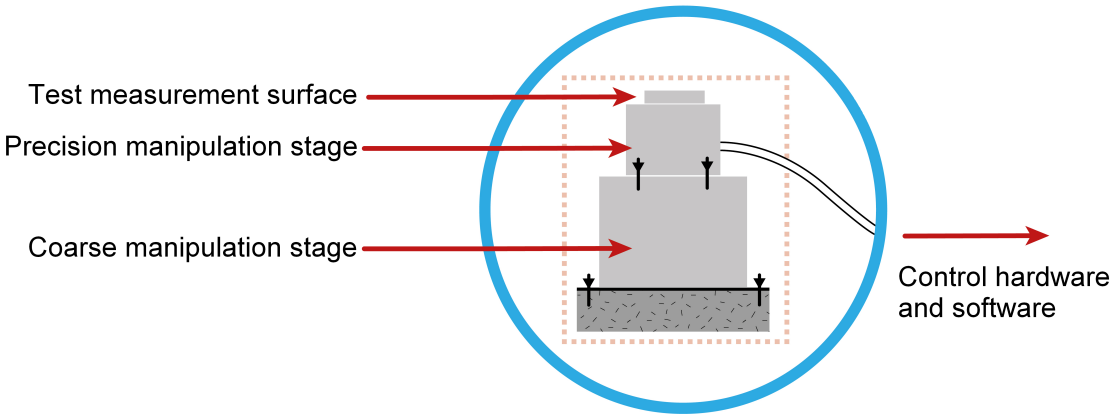

Figure 5.10: A schematic diagram of the manipulation column used with the base setup for testing in the vertical direction

During these tests, the LDV should be able to move lateral over the vibrating micro-probe to allow for measurement of the vibration of each of the legs of the triskelion-flexure MEMS device. This movement will be achieved through a lateral coarse manipulation stage on the base of the LDV stand. This lateral coarse manipulation stage can be seen in figure 5.11.

5.3.2.3 Experimental setup for the testing of isotropy

A new concept of isotropy has been developed for 3D vibrating micro-CMM probes, as described in Chapter 4, section 4.3.4. The isotropy of the vibrating micro-probe will therefore be defined according to the vibration characteristic, as controlled by the previously described vibration algorithm. To validate these vibration characteristics, the vibration of each leg should be measured.

The experimental setup suited for testing the vibration isotropy of a vibrating probe is simply the base setup. Similar to the vibration measurement requirements of the lateral experiments, the lateral coarse manipulation of the LDV head will be essential, as the individual vibration characteristics of each leg will have to be measured to fully define the isotropy of the probe.

5.3.3 Good practice for dimensional measurement

There are several design choices that have been made during the development of the experimental setup that were made on the basis of maintaining good practice for dimensional measurement. One important aspect of validating the capability of the experimental setup is to ensure that good practice is adhered to. It will then likely follow that the individual capabilities of the constituent parts are a good estimate of the total capability of the setup.

Several aspects of the assembly and operation of the experimental setup have been decided by considering good practice, in particular considering the desired accuracy of the results for

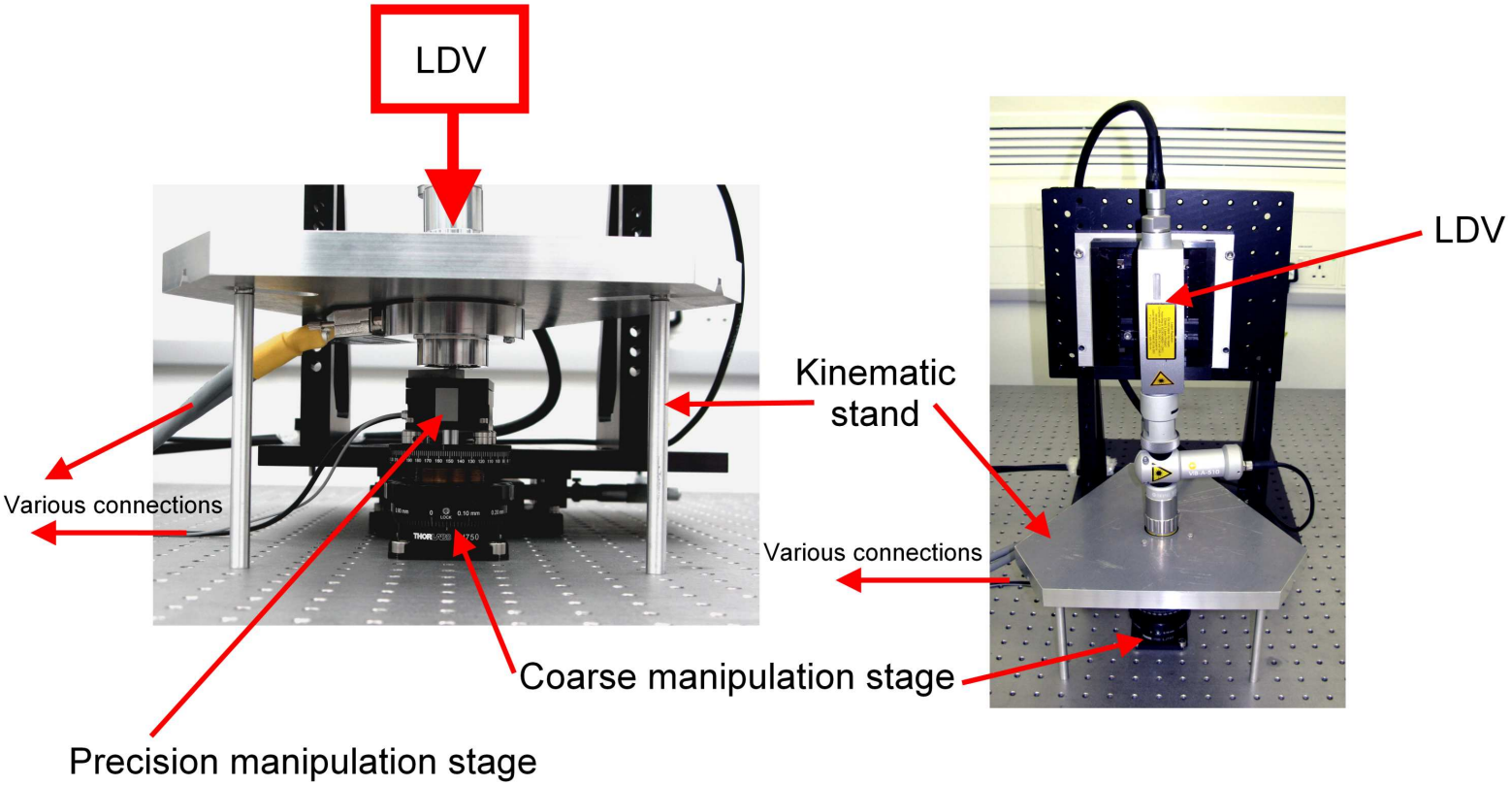

Figure 5.11: Photograph of the experimental setup used for testing the micro-probe in the z-direction.

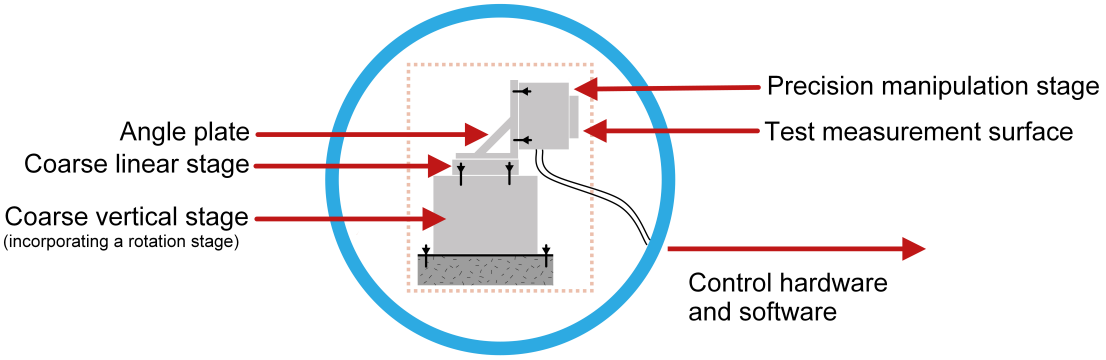

Figure 5.12: A schematic diagram of the manipulation column used with the base setup for testing in the vertical direction

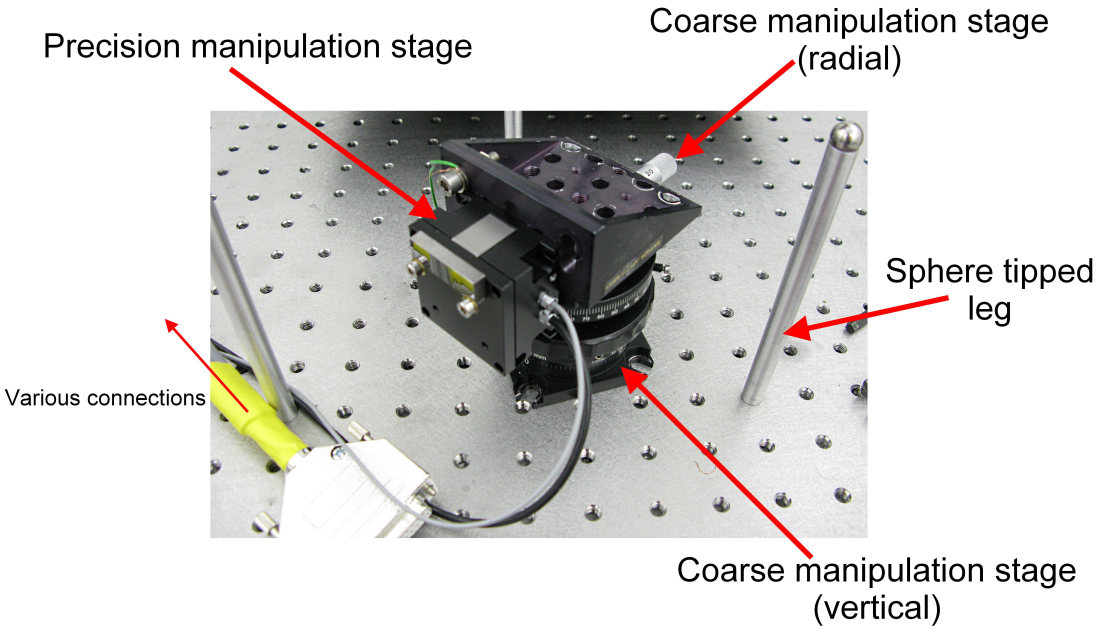

Figure 5.13: Photograph of the experimental setup used for testing the microprobe in the lateral direction – the kinematic stand has been removed for clarity

addressing **Research Question 1.2** and **Research Question 1.3**. Several good practice rules will now be considered, including strategies for their mitigation. These points will also be considered towards the end of the chapter when the uncertainty of the measurements performed will be addressed.

5.3.3.1 Abbé considerations

Abbé error, similar to other angular errors, describes a situation relating to the magnification of angular error over distance. A more detailed explanation can be found elsewhere [29, 30, 182], but for simplicity, it should be noted that Abbé error is minimised if the measurand and the measurement axis are co-axial.

There are several distances that are measured as part of the experimental setup. During assembly of the system, these distances, and the scales that were intended to measure them, were all considered with respect to the Abbé principle. These scales included: the measurement beam of the LDV, which was focused onto the centre of the vibrating micro-probe so as to be in-line with the probe stylus during vertical testing, and the internal measurement scale of the precision manipulation stage, whose position is unknown, and was therefore assumed to be in the centre of the device.

5.3.3.2 Metrology loop

A metrology loop can be defined as the path, through all constituent parts of the experimental setup, which defines the positioning reference [3]. During design of an experimental setup, the metrology loop should be clearly identified, allowing constraints on materials, dimensions and fixings used to ensure the maximum mechanical and thermal stability.

During the design of the experimental setup, especially the initial base setup, the mechanical stability and material makeup of the metrology loop was considered. To address the mechanical considerations, the kinematic stand was left unconstrained, and the legs were secured to a rigid optical table. A Type II Kelvin clamp was also used to allow for thermal expansion effects. To address another thermal consideration, the legs of the kinematic stand were made from aluminium, which was a best estimate as to the material make-up of the manipulation column. As no absolute measurements are taken using the LDV, the design of the LDV stand was not given much consideration, apart from mechanical stability and ease of manipulation.

5.3.3.3 Stability considerations

Following the setup of an experiment for any probe testing, it is essential to ensure that the system is stable prior to data collection. To achieve this, the experiment it prepared and left for at least one hour to settle mechanically and thermally. The experiment is then initiated

remotely, so that there is little further external influence. After the period of mechanical and thermal stabilisation, but prior to testing, the microprobe is activated and its behaviour recorded, to ensure stable vibration. Validation experiments are only completed if the vibration is stable.

5.4 Experimental procedures

The experiments required to validate the operation of the vibrating micro-probe have been defined in section 5.2. The experimental apparatus, including several specific setups which can be used to complete the validation experiments, have also been described.

The detailed procedures used to complete the validation experiments will now be defined. These procedures will relate specifically to the two validation objectives; **Thesis Objective 1,** pertaining to the validation of the ability of the vibrating micro-probe to counteract the surface interaction forces, and **Thesis Objective 2**, pertaining to the testing of the isotropy of the vibrating micro-probe.

5.4.1 Procedure for experiments to validate ability to counteract the surface interaction forces

A set of experiments will be conducted to determine whether the probe is capable of counteracting the surface interaction forces that are prevalent when operating at the micro-scale. The vibrating micro-probe will therefore be tested while approaching, interacting with and retracting from a test measurement surface. As these experiments will result in direct contact between the probe tip and the test measurement surface, they will also be referred to as 'contact experiments'.

The real operation of the vibrating micro-probe during these contact experiments will be compared to the theoretical operation. Several sensitivity experiments will also be completed with respect to vibration amplitude and frequency. Finally, the repeatability and linearity error of the vibrating micro-probe will be determined. Initially, these experiments will be completed in the vertical direction. However the experiments will also be repeated in the lateral direction to determine the ability of the vibrating micro-probe to counteract the surface interaction forces in 3D.

The procedures for these contact experiments will be split into three main sections: setup, pre-test, and test procedure.

5.4.1.1 Testing of the probe in the vertical (z) direction

Setup It is a prerequisite of these initial steps that the correct experimental setup has been selected and assembled. In this case, the vertical testing experimental setup should be built, as described in section 5.3.2.1.

- A vibrating micro-probe should be selected and mounted into the physical and electrical interface ready for testing.
  - Considering the safety of the vibrating micro-probe, the interface step is completed while the top plate of the kinematic stand is disassembled from its legs. While the kinematic stand is disassembled, the vibrating micro-probe can be unboxed, manually manipulated and attached to the interface in a safe environment, free from the obstruction of surrounding experimental apparatus, and in good working light.
  - After interfacing is complete, the kinematic stand can be reassembled. It is essential that, before reassembly takes place, the manipulation column is fully retracted so that there is no chance of the probe hitting the test measurement surface and breaking.
  - Reassembly results in the probe being held directly below the LDV, and directly above the fully retracted manipulation column.
- The LDV is focused on the centre of the back of the central island of the probe.
  - The design of the probe ensures that the central island and connecting arms are stiff enough, compared to the flexures, that they all move as one monolithic structure. Therefore, the LDV should detect a similar vibration amplitude anywhere in the central area of the probe.
  - However, the centre of the central island is positioned collinear with the direction of interaction. Measurements of vibration amplitude change at this position are, therefore, adherent to the Abbé principle.
- The test measurement surface is brought into position ready for testing.
  - The precision manipulation stage is first set to the mid-point of its full stroke.
  - The entire manipulation column is then coarsely moved up to a position whereby the test measurement surface is in direct contact with the sphere tip of the probe. This contact point is determined qualitatively through observation of the focus of the optical video system of the LDV on the back of the probe. Any change in focus is determined to be the result of physical interaction of the probe tip with the test measurement surface.
  - This contact point is minimised (by eye) though coarse manipulation, after which the precision manipulation stage is set to its zero position.
  - After this mix of manual and precision manipulations of the test measurement surface, it is determined that the surface should be within 100 µm of the probe tip and, therefore, within the range of full stroke travel of the precision manipulation stage.
- At this point, the setup steps for the experiment are complete.

Pre-test The entire system should be left to stabilise mechanically and thermally for at least one hour. It is suggested that all work is now conducted remotely to minimise any disturbing effects caused by movement in the lab.

- The experimental co-ordinate system is defined.
  - Currently, the manipulation stages are at their starting points for any subsequent tests.
  - The experimental co-ordinate system is defined as a linear (one dimensional) system, with the lowest position of the precision manipulation stage as the origin.
- An estimate of the position of the probe tip is obtained.
  - This step ensures that the over-travel of the probe during testing is minimum, and also that the tests do not run over unnecessarily long time frames.
  - The probe should be activated at a frequency and amplitude suitable for operation and testing.
  - The precision manipulation stage should then be programmed to move the test measurement surface towards the probe in steps of size at least one fifth the amplitude of the vibration of the probe.
  - This pre-test step should be run until the probe vibration, as measured by the LDV, has reduced in amplitude by a value of one or two steps of the precision manipulation stage. At this point, a reasonable estimate of the origin can be determined, to within one step size of the precision manipulation stage.

Test Following the determination of the origin point of the test co-ordinate system, an experiment can be run to test the capability of the probe to counteract the surface interaction forces while operating in the vertical direction.

- The test measurement surface is manipulated such that it approaches the probe normal to the direction of vibration.
  - The movement of the test measurement surface is controlled to approach the probe in the smallest repeatable steps that can be produced by the precision manipulation stage.
  - The movement of the test measurement surface is also controlled so that the over-travel after passing the origin is less than the amplitude of vibration of the test probe [195].
- The experiment should be repeated several times so that an accurate calculation of the repeatability and linearity can be made.

Following the completion of the experiment, the saved data is collected and analysed. The data processing steps are detailed later in this chapter.

5.4.1.2 Testing of the probe in the lateral (xy) directions

The lateral capability of the vibrating micro-probe is dependent on the ability of the vibration algorithm to control the probe's vibration. To have the probe interact with a lateral-facing surface, whose surface normal is perpendicular to the stylus of the probe, the probe must vibrate laterally, or parallel to that surface normal.

The experimental procedure for the testing of the vibrating micro-probe in the lateral direction will now be presented. Any details from the previously described vertical tests, especially regarding safety and good practice, should still be observed.

Setup It is a prerequisite of these initial steps that the correct experimental setup has been selected and assembled. In this case, the vertical testing experimental setup should be built, as described in section 5.3.2.2.

- A vibrating micro-probe should be selected for testing.
  - The selected vibrating micro-probe should have been previously characterised to be suitable for non-resonant vibration (*i.e.* lateral vibration under the control of the vibration algorithm), and also should have all the actuator strength coefficients determined.
- The selected vibrating micro-probe is mounted into the physical and electrical interface.
  - Particular care should be taken when reassembling the kinematic stand so that the side-facing test measurement surface, and the associated manipulation column, do not contact or damage the probe
- The LDV is focused on the back of the vibrating micro-probe.
  - The LDV should be focussed on the back of the probe at a position that exhibits the maximum vibration amplitude during activation.
  - Unlike in the vertical tests, the centre of the central island is no longer a suitable position for vibration measurement, because lateral vibration of the probe will result in little or no movement of the centre of the central island.
  - The measurement position should be selected by consulting the vibration algorithm. As a rule-of-thumb, the optimal position for measurement by the LDV is the point that is furthest from the centre of the central island in the direction of the surface normal with which the probe is interacting.

  - Due to both the off centre measurement of the vibration of the probe, and to the off vertical direction of the surface normal during testing, the measurements taken by the LDV are not adherent to the Abbé principle.

- The test measurement surface is brought into position ready for testing.
  - The precision manipulation stage is set to the mid-point of its full stroke.
  - The rotational stage is manually rotated to the correct angle for testing.
  - The test measurement surface is moved vertically (coarse) ensuring first that the radial manipulation stage is retracted so that the test measurement surface is far removed from the centre of the experimental setup.
  - The radial manipulation stage is moved to a position whereby the test measurement surface is in direct contact with the sphere tip of the probe. Contact between the sphere tip and the test measurement surface is observed directly to confirm contact. If this contact position is determined as before, using focus change of the LDV measurement point, there is little scope for determining the quality of the contact, especially whether contact is between the sphere tip and the gauging surface, rather than the sphere tip and the chamfer on the edge of the gauge block. The possibility of contact with the chamfer is high due to the geometrical design of a gauge block, in which the chamfer that is about 1 mm deep.
  - To directly observe contact, the optical video system of the LDV is focused on the stylus tip, around the central island. Direct viewing of the sphere is possible by virtue of the numerical aperture of the 10× magnification objective.
  - This contact point is minimised though coarse manipulation, after which the precision manipulation stage is set to its start position.
  - After this mix of manual and precision manipulations of the test measurement surface, it is determined that the surface should be within 100 µm of the probe tip and, therefore, within the range of full stroke travel of the precision manipulation stage.
  - The LDV should be returned to its original position, on the central section of the probe, at the position of maximum vibration amplitude.

- At this point, the setup steps for the experiment are complete.

Pre-test The entire system should be left to stabilise mechanically and thermally for at least one hour. It is suggested that all work is now conducted remotely to minimise any disturbing effects caused by movement in the lab.

- The experimental co-ordinate system is defined.
- An estimate of the position of the probe tip is obtained.

- This step is completed as previously described.
- However, the calculation of the precision manipulation stage step size and, therefore, the expected reduced amplitude of the vibration measured by the LDV should be altered to include the off axis measurement of the amplitude of the vibration. This is expected to be close to a one-to-one relationship, as the length of the connecting arm, L_b, and the length of the stylus, l_{st}, are similar.

Test Following the determination of the origin point of the test co-ordinate system, an experiment can be run to test the capability of the probe to counteract the surface interaction forces while operating in a lateral direction. This is completed as previously described.

5.4.2 Experiments to test the ability of the probe to act isotropically

A set of experiments will be conducted to determine the isotropy of the vibrating micro-probe. The definition of isotropy used for the probe can be summarised as follows: the vibrating micro-probe shall be considered to act isotropically if it is able to vibrate at the same amplitude and frequency in any chosen vibration vector.

Any tests of the isotropy of the vibrating micro-probe will directly validate the capability of the vibration algorithm to control the probe. Therefore the results of these tests will serve to assist in the further development of the vibration algorithm.

Setup It is a prerequisite of these initial steps that the correct experimental setup has been selected and assembled. In this case, the isotropy testing experimental setup should be built, as described in section 5.3.2.3.

- A vibrating micro-probe is selected and mounted for testing. This probe should have similar requirements to those for the lateral contact experiments.
- The LDV is focused on the back of the vibrating micro-probe.
  - Unlike the previous interaction tests, there is no single position on the central section of the probe that will provide full information on the vibration of the probe. Instead, each junction between the connecting arms of the central section and the three flexures should be investigated.
  - These measurements will be directly comparable to the interim results contained within the vibration algorithm calculations that refer to the positions of the end of each flexure, which are described in figure 4.15.
  - Therefore, each complete experiment will be a combination of three sub-experiments which contain measurements from three different positions about the top of the central section of the probe.

- As this experimental setup does not include the manipulation column, the setup steps for the experiment are complete.

Pre-test The entire system should be left to stabilise mechanically and thermally for at least one hour. It is suggested that all work is now conducted remotely to minimise any disturbing effects caused by movement in the lab.

- The isotropy experiments will be completed within no formal co-ordinate system.
  - The measurements taken will be comparable through the amplitude and phase of the vibration in comparison to a reference signal that is input to the probe.
  - The measured amplitudes and phases will be compared directly to the expected results calculated by the vibration algorithm, and through this comparison, isotropy will be characterised.
  - Due to the nature of the measurement, that the vibration of the junctions between the central body and the flexures are measured, and that these vibrations are calculated at one stage within the vibration algorithm, it is surmised that these measurements taken by the LDV are adherent to the Abbé principle.

Test The isotropy of the vibrating micro-probe is determined through the combination of measurements taken over several vibration vectors. Each measurement taken at a single vibration vector is the combination of three sub-experiments.

- Sub-experiment 1 is run, to measure the vibration of position 1 (nominally, the elbow of Leg 1) while the vibrating micro-probe is activated in one vibration vector.
  - The probe is activated by a set of actuation signals that are controlled by the vibration algorithm.
  - The LDV measures the motion of the vibrating micro-probe at the first position.
  - The motion is recorded for several minutes, after which the experiment is stopped and the vibrating micro-probe is deactivated.
- The LDV is moved such that it is focussed on position 2 on the vibrating micro-probe (nominally, the elbow of Leg 2).
  - To assist with maintaining this stability, the movement of the LDV between junctions it made quickly and carefully, to ensure as little disturbance as possible is made to the system.
  - The experimental setup is also left to rest for several minutes to ensure mechanical and thermal stability is maintained.

- This procedure is repeated for all three measurement positions, at the elbows of the three legs of the triskelion MEMS device.
  - The individual sub-experiments should be repeated several times so that an accurate comparison between the real capability of the probe and the calculated behaviour can be made.
- Following the completion of the sub-experiments, the saved data is collected and compiled to make up one set of results for one vibration direction of the vibrating micro-probe.
- The entire test, comprised of the three constituent sub-experiments, is repeated for all vibration vectors that are to be tested.
  - Particular attention should be taken when positioning the LDV at the junctions between the flexures and the central body, to ensure that the same positions are interrogated across all experiments.

Following compilation of data from several vibration vectors, analysis is completed that will describe the capability of the probe to act as expected and, therefore, conclude on the current isotropy of the probe.

5.5 Presentation and discussion of the experimental results

The individual experiments, designed to address the requirements of **Thesis Objective 1** and **Thesis Objective 2**, have been described in detail. During any of the described experiment, a great deal of data is automatically saved by the control software. Once processed, the experimental data can be discussed, compared and contrasted, and concluded upon.

The state of the raw data as it is collected from the experiments will be presented. Following this presentation, a set of calculations will be discussed that will process the results in a meaningful and useful fashion, such that it is comparable between experiments and to the model of the interaction. With reference to these calculations, a set of workflows will be presented that describe the steps taken to process data from the three experiments. Subsequently, the experimental results will be presented and discussed.

5.5.1 Raw data analysis

To demonstrate the state of the data as it is collected from the control software, a set of raw data will be presented in full. The data is saved automatically in comma-separated .txt format.

The data file is transferred to a separate PC and is processed using Matlab and Microsoft Excel. The data is separated into the following groups:

- three detected LDV signals (amplitude in micrometres, frequency in hertz and phase in degrees),
- eighteen detected signals from the sensors (amplitude, frequency and phase from each of the inner and outer sensors for each of the three legs),
- position of the precision manipulation stage,
- time from the PC clock in hours, minutes and seconds, and
- an error indicator.

Following the completion of each experiment, the raw data can be analysed and interpreted. These initial interpretations will be described in the following two sections, with respect to the contact experiments and the isotropy tests.

5.5.1.1 Interpretation of raw data from contact experiments

A trial experiment was run using vibrating micro-probe MP-Ni-6-D, vibrating at a frequency of 1.509 kHz and an amplitude of 1.0 µm. The experiment ran for approximately thirteen minutes, during which time the precision manipulation stage travelled from 50 µm to 52.7 µm in 40 nm steps (approach and recede), six times. This resulted in six interactions between the vibrating micro-probe and the test measurement surface. Approximately 17 000 lines of data were collected, and an appreciation of several lines of raw data is shown in Appendix E.

The three LDV signals indicate the detected physical reaction of the probe over the extent of the experiment, and can be plotted either in the time domain or, in the case of a contact experiment, the absolute distance domain (with respect to the origin of the precision motion stage, which is also the experimental co-ordinate system). The LDV signals for the demonstration experiment are shown in both the time domain and the distance domain in figures 5.14, 5.15 and 5.16.

The contact point between the probe and the test measurement surface can be seen as a feature on all six graphs shown in figures 5.14, 5.15 and 5.16. In figure 5.14 the interaction between the probe and the test measurement surface is visible as a reduction in amplitude at the contact point. In figure 5.15 the interaction between the probe and the test measurement surface is visible as a gradual change in phase on approach to the surface and a large change in phase at the contact point. In figure 5.16 the interaction between the probe and the test measurement surface is visible as an irregular set of measurements at the contact point.

A more detailed appreciation of the interaction of the probe and the test measurement surface, when in close proximity to the contact point, can be gained from a focused view of the data

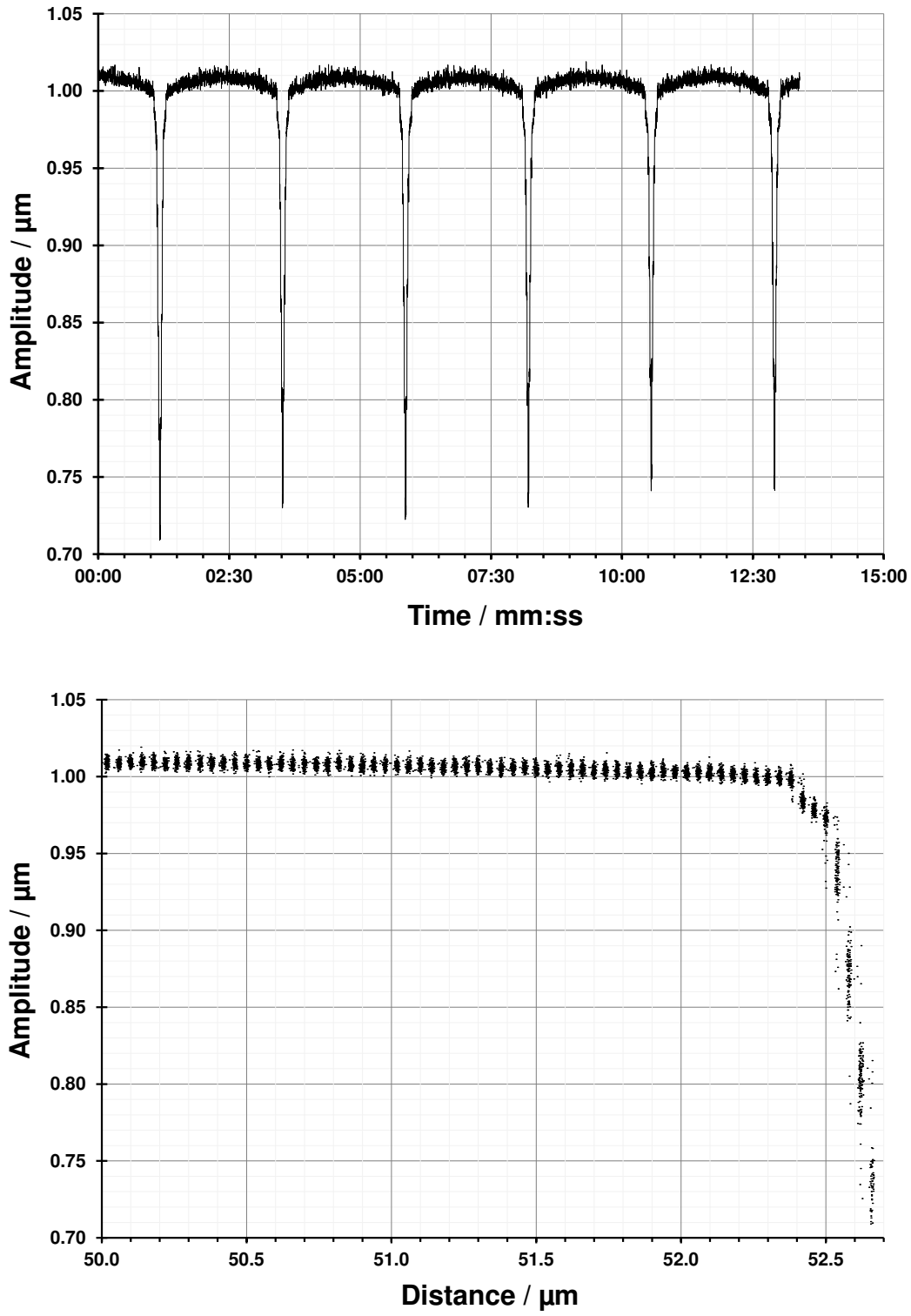

Figure 5.14: Raw data from the LDV taken during a trial contact experiment. Amplitude data is displayed in the time (top) and the absolute distance domain (bottom).

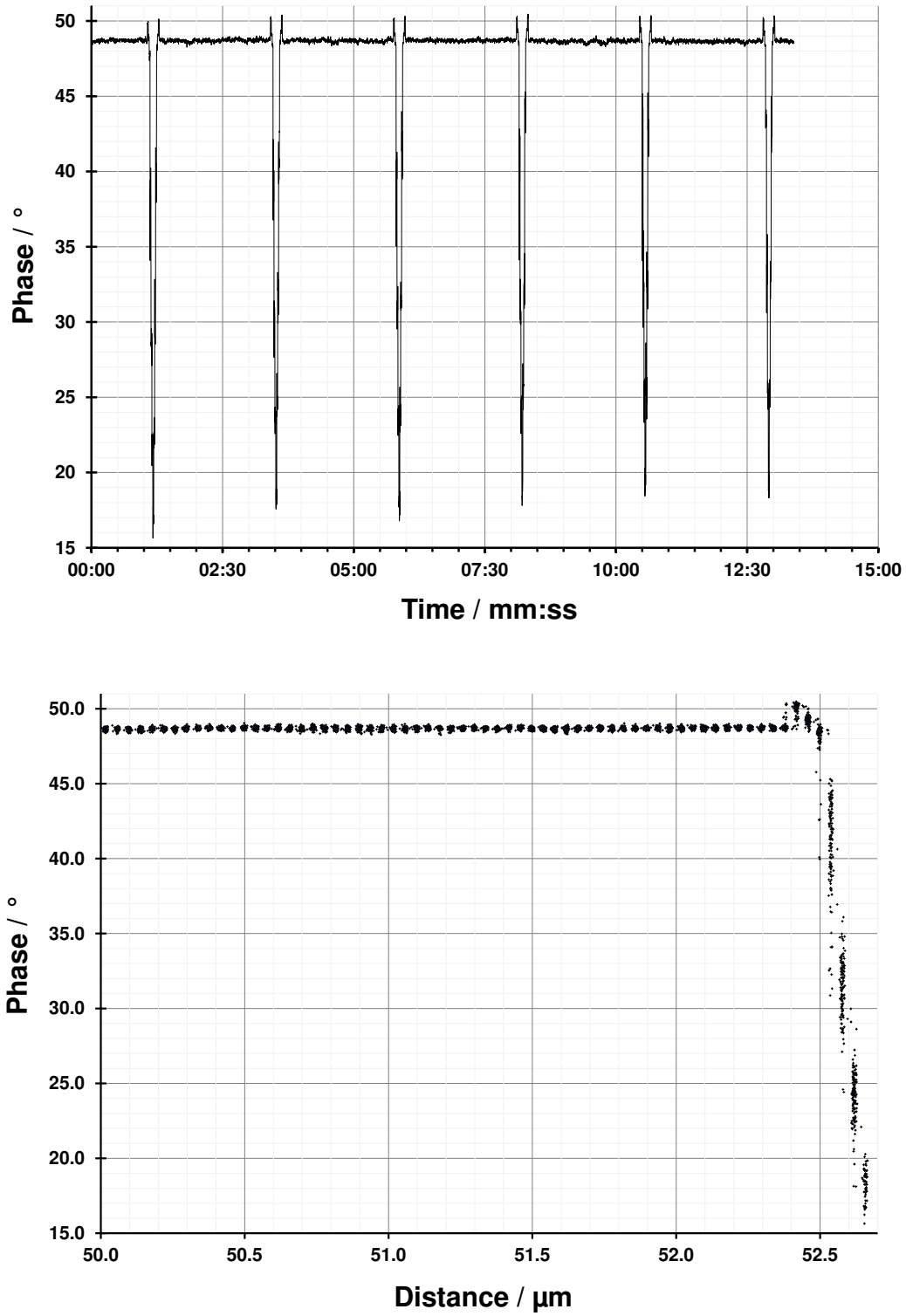

Figure 5.15: Raw data from the LDV taken during a trial contact experiment. Phase data is displayed in the time (top) and the absolute distance domain (bottom).

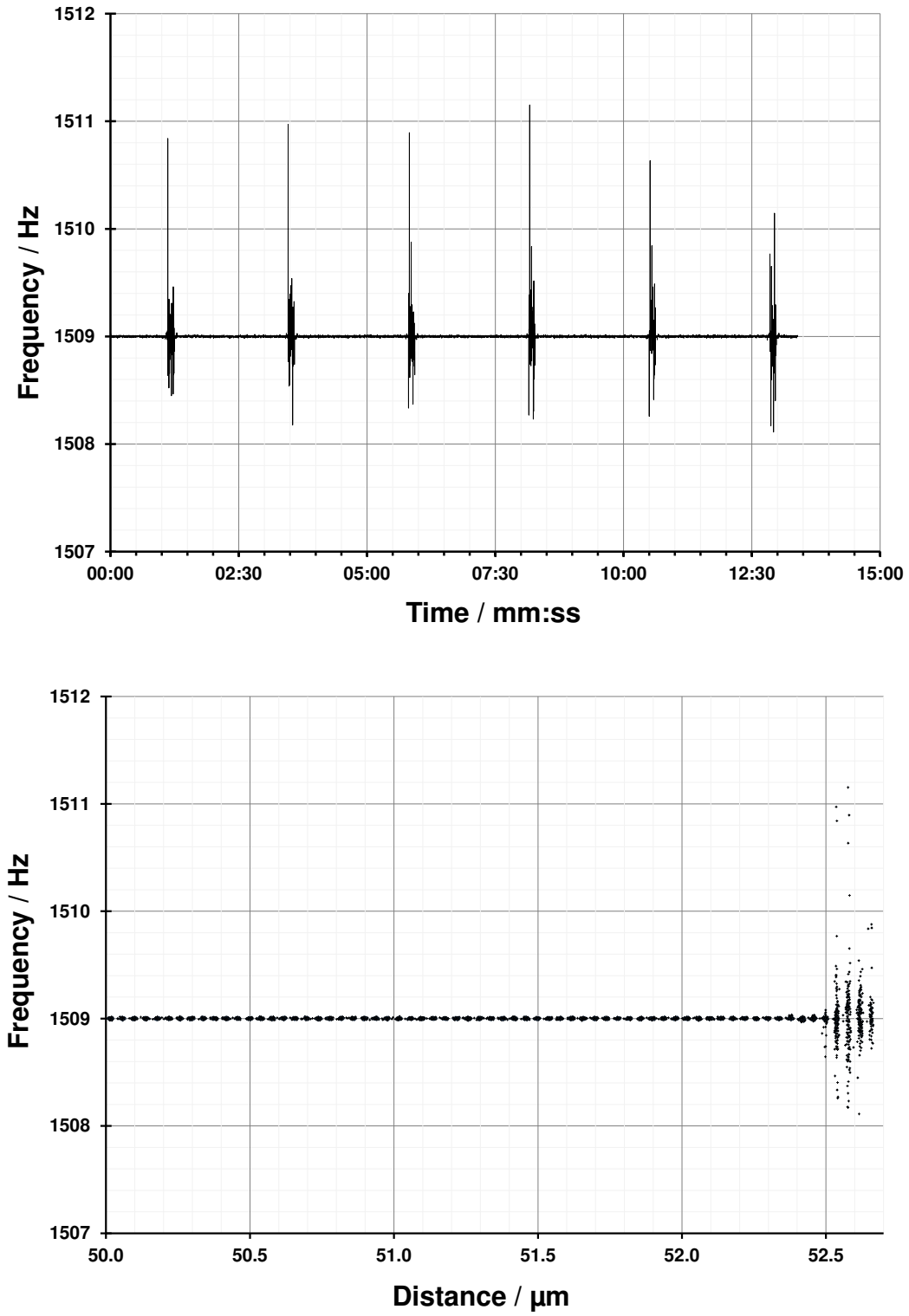

Figure 5.16: Raw data from the LDV taken during a trial contact experiment. Frequency data is displayed in the time (top) and the absolute distance domain (bottom).

between 51.7 µm and 52.7 µm in the distance domain. Although the data considered in the time domain is a good indication of the progression of the experiment, it is of little interest with respect to the processing of the data, which requires correlation to a physical property, such as displacement. The time domain data will, therefore, no longer be considered. A set of three graphs of the experimental data, plotted in the distance domain, are shown in figure 5.17 and are zoomed to between 51.7 µm and 52.7 µm in the distance domain.

When considering the amplitude data presented in figure 5.17, the interaction between the probe and the test measurement surface is again visible as a reduction in amplitude at the contact point. However, through the more focused view, it is clearer that these reductions in amplitude occur in ever more increasing steps, which tend to a value similar to that of the nominal step size of the precision manipulation stage. It was previously suggested in Chapter 4, section 4.4.3, that the ideal indicator of the progress of the experiment shall be a representation of the ratio of the change in measured amplitude with respect to the nominally constant approach steps of the test measurement surface.

The details of the effect of the interaction on the phase response of the probe and the detected frequency are more qualitative and require little further processing. Several processes used to clarify the data, reduce the number of data points, and to smooth the data will be described in section 5.5.2.

The data presented in figure 5.17 also shows some experimental drift, as the data approaching, at, and after contact seems to be unrepeatable. This experimental drift will be considered in section 5.5.3.6.

5.5.1.2 Interpretation of raw data from isotropy experiments

Data collected from the isotropy experiments consists of the amplitude and phase of the probe as measured by the LDV at the three investigated sites on the probe. Even though only one result is needed per experiment to represent the average motion of the investigated point at a given input signal, several seconds of data is collected resulting in several hundred data points. Even though the data from the isotropy experiments requires little, or no, processing prior to interpretation, several processes are used to simplify the data to reduce the number of data points to one average result. These are described in section 5.5.2, along with the ratio calculation procedure.

5.5.2 Data processing workflows

Several workflows can be developed that describe how the raw experimental data, as previously shown in figures 5.14, 5.15, 5.16 and 5.17, can be processed into reportable experimental results, such as the ratio value of surface approach to vibration reduction.

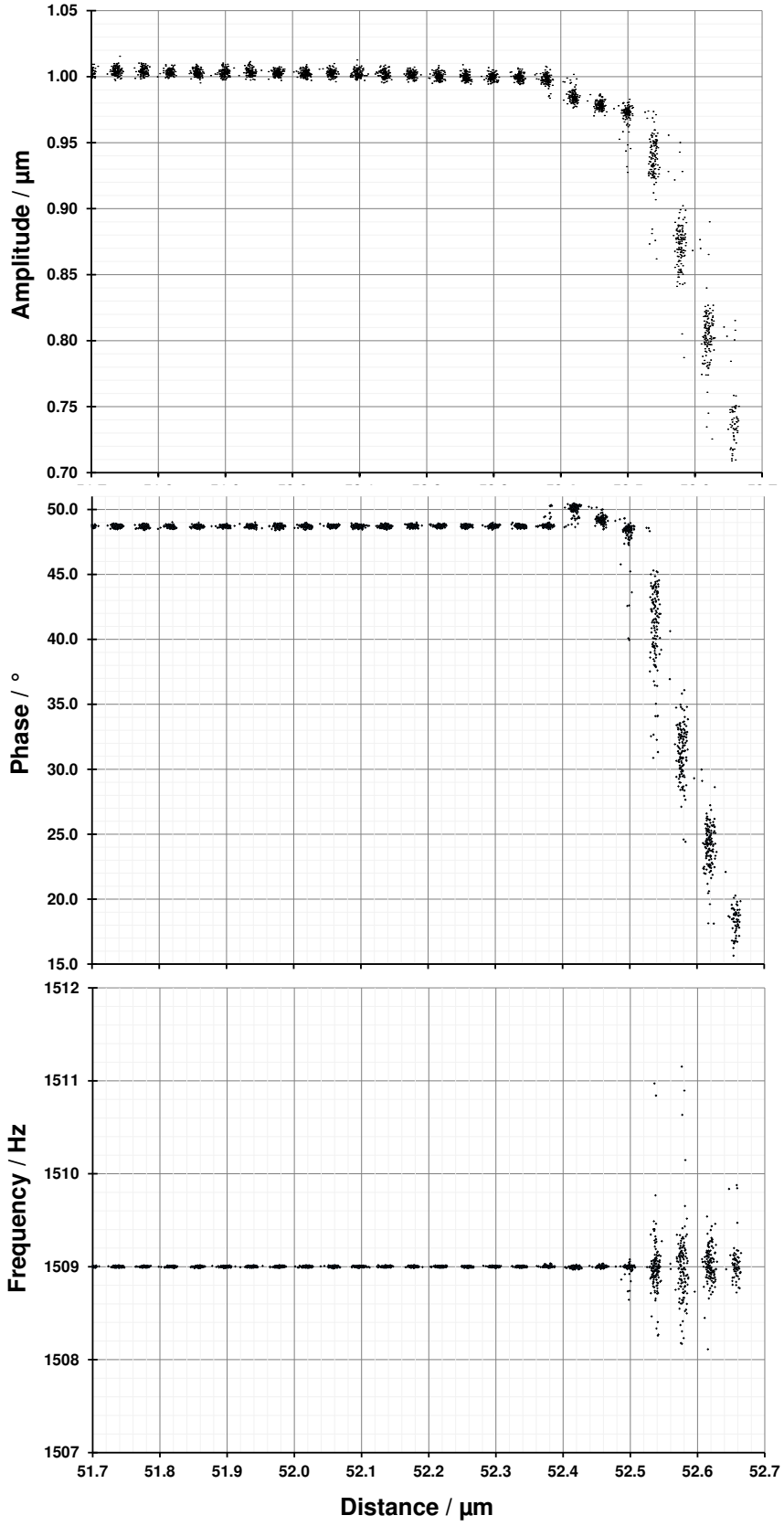

Figure 5.17: Raw data from the LDV taken during the trial contact experiment, displayed in the absolute distance domain, zoomed to the last 1 µm.

Workflow 1 describes how data is reduced from several hundred thousand raw data points to several thousand average points, from which the required ratio can be calculated.

Workflow 1 - Ratio determination

1. Tabulate all data – LDV signals, vibrating micro-probe signals, and precision manipulation stage position.
2. Calculate the change (Δ) in manipulation stage position for each data point.
3. At every step of the precision manipulation stage (where $\Delta(position)$ is approximately equal to the programmed step of the precision manipulation stage), calculate the average position ($\overline{\text{position}}$) and average vibration amplitude ($\overline{\text{vibration}}$) at that position, either from the LDV or direct from the sensors.
4. Subsequently, at every step of the precision manipulation stage, calculate the ratio $\Delta\left(\overline{\text{vibration}}\right)/\Delta\left(\overline{\text{position}}\right)$.
5. When the ratio exceeds unity set calculated surface position to 0 nm.
   (a) If the ratio does not reach unity, the calculated surface position is set to 0 nm at the maximal ratio value.

This workflow can be applied to any raw data for a contact experiment, where data is recorded from the LDV or the vibrating micro-probe. If phase data is used instead of amplitude data, steps 4 and 5 can be omitted.

Following the completion of the initial data processing, several further steps can be taken to complete a more detailed analysis. Workflow 2 shows a simple procedure that can be used to calculate the average ratio from an experiment that includes several interactions.

Workflow 2 - Combination of data

1. Using the previously mentioned 'calculated surface position', select data from -1 µm to the maximum position (usually ∼0.1 µm) for each data point of the probe while approaching the surface.
2. Align each point according to the distance from the surface
3. Calculate average position and ratio for each aligned data group, including the experimental error.
4. Present in graphical form.
5. Repeat for the retract data.

Again, this workflow can be applied to any raw data for a contact experiment, where data is recorded from the LDV or the vibrating micro-probe.

5.5.3 Results of tests of the contact experiments in the vertical direction

A set of tests were completed that describe the capability of the probe to act in the vertical, or z, direction. After the experiments were run, the data was collected and processed. The experiments are run according to the previously defined Design of Experiments, as described in section 5.2.

5.5.3.1 Counteraction of the surface interaction forces

A set of tests were run to characterise the probe in its ideal operating conditions. These optimal conditions relate to amplitude and sensitivity and are apparent at the first resonance frequency when the probe is acting vertically. The demonstration of the ability of the probe to counteract the surface interaction forces was completed using vibrating micro-probe MP-Ni-6-D, vibrating at a frequency of 1.509 kHz and an amplitude of 1.0 µm, as presented in section 5.5.1.

A contact experiment was completed where contact was repeated three times over fifteen minutes, with the surface retracting to 10 µm from the approximate contact position after each interaction. The surface was controlled to approach the probe in 30 nm steps, making one step approximately every two seconds. The data is recorded at a frequency of 10 Hz. The resulting raw amplitude data was processed to calculate an average for each step. This raw amplitude data from the LDV, which is averaged for each step, is shown in figure 5.18. The position of the surface is initially estimated due to a lack of detailed information that the raw data provides.

The results shown in figure 5.18 indicate the measurements taken by the LDV, which are a direct measurement of the mechanical vibration of the probe. The true operation of the probe is dependent on the ability of the sensors to detect signals that are indicative of interaction with a measurement surface. It is essential that the signals from the sensors during probing are comparable to the mechanical behaviour detected by the LDV.

As several of the probe sensors are affected by over-etching, resulting in incomplete or damaged connections, several of the tested device's sensors are not suitable for electrical sensing. However, measurements have been taken to validate the capability of the system to operate as intended, without direct optical measurement. The signals from the operational piezoelectric sensors were passed through a low-pass filter and were then analysed and directly compared to the output of the LDV. These results are shown in figure 5.19.

The raw data shown in figure 5.19 shows the advantages of the ratio calculation, which gives a better appreciation of the progress of the interaction and gives a quantitative indication of the position of the measurement surface. The ratios between the changes in vibration amplitude and the approach distances of the reference surface were, therefore, calculated. When there is no interaction between the probe and the surface, this ratio is nominally zero, and when the probe

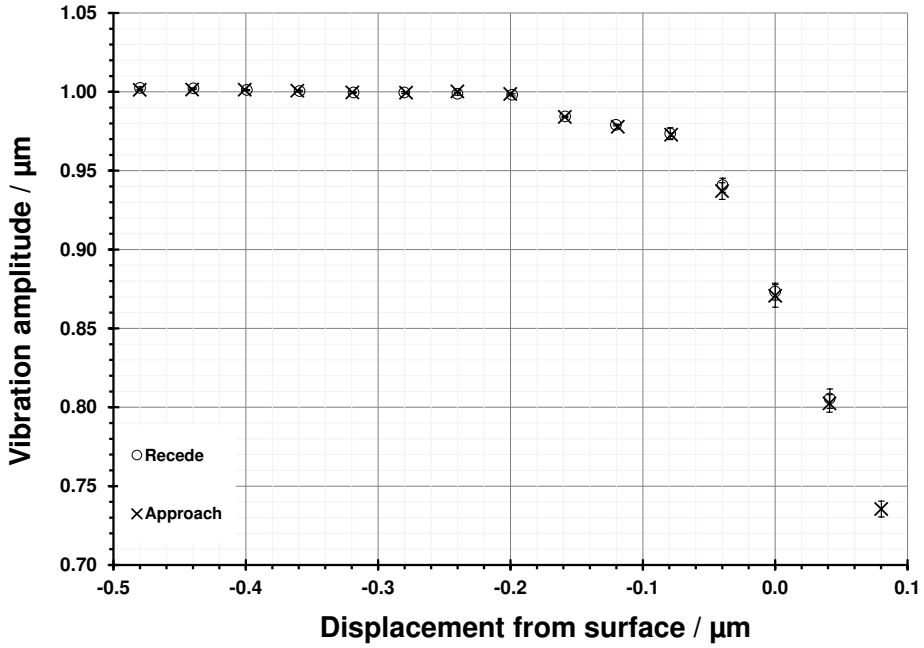

Figure 5.18: Graph of the raw vibration amplitude on approach and receding from the test surface. The error bars indicate the experimental standard deviation of the mean.

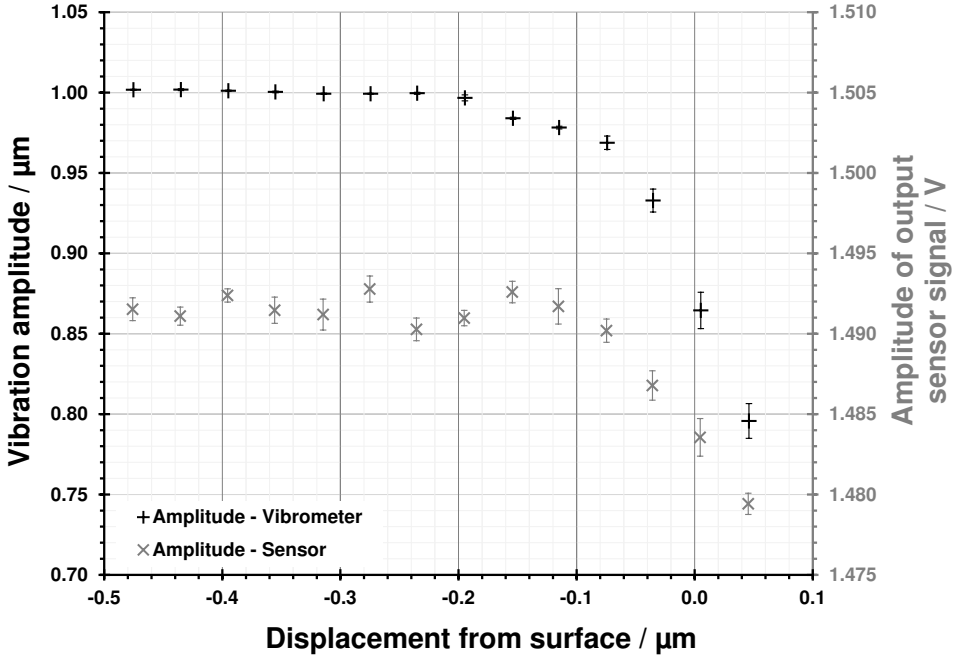

Figure 5.19: A comparison of the output of the LDV and the sensor amplitude during a probing interaction (approach only). The error bars indicate the experimental standard deviation of the mean.

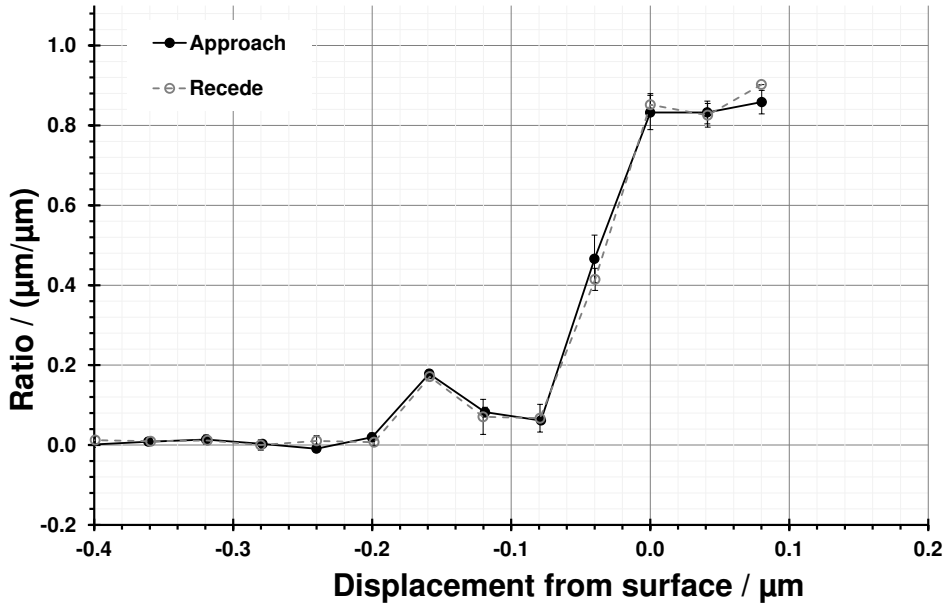

Figure 5.20: Graph of the calculated ratio values for the micro-CMM probe while interacting with a test surface. The error bars indicate the experimental standard deviation of the mean from six repeated measurement surface interactions.

is making contact with the surface this ratio is nominally one. Any intermediate ratios are the result of a non-contact interaction between the probe and the reference surface. The results of an interaction between the probe and a measurement surface are shown in figure 5.20. The ratios are calculated by using the measurement taken by the LDV, as the signals output by the sensors are not yet calibrated with respect to amplitude.

The results in figure 5.20 show a surface interaction experiment occurring in the z direction, with the precision manipulation stage moving in 30 nm steps. The position of the reference surface was defined as the position whereby the ratio first passed unity. In reality, as can be seen that errors in the experimental data result in ratios being below unity, even during direct contact with the surface. To mitigate these experimental errors, the position of the surface is aligned with the first maximal point of the approach data. Experimental data is averaged over nine data points, with data collected over three or more sets. Therefore, all data points are the mean of over twenty-seven data points.

The feature in figure 5.20 at approximately 150 nm from the surface is an indication of some interaction with the test measurement surface that is not included in the interaction model, which is shown in figure 4.21. It should be noted that this feature is not an indication of snap-in, but is instead assumed to be either some contamination on the test measurement surface, or an electrostatic interaction causing a premature reduction in the amplitude of the vibrating micro-probe. The repeatability of the feature when retracting from the test measurement surface indicates that contamination is more likely. Therefore, the experimental setup was dismantled, all parts, especially the test measurement surface, were cleaned and reassembled, and the interaction

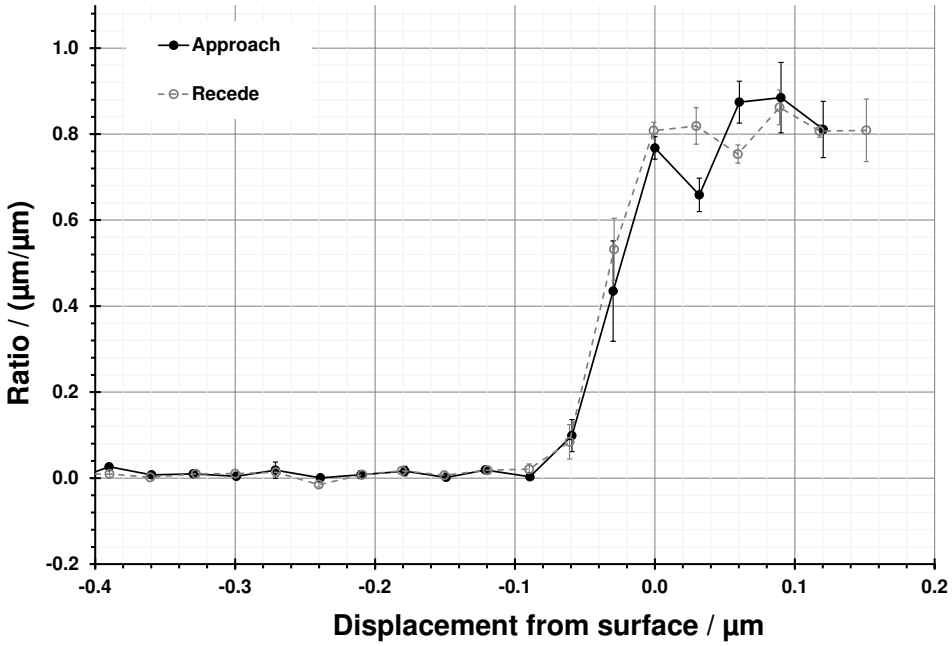

Figure 5.21: Graph of the calculated ratio values for the micro-CMM probe while interacting with a test surface during a second contacting experiment. The error bars indicate the experimental standard deviation of the mean from five repeated measurement surface interactions.

experiment was re-run. The results of this second interaction experiment between the probe and a measurement surface are shown in figure 5.21.

It can be seen from the results shown in figure 5.21 that the approach and retract behaviour of this probe, over several measurement runs, are similar. This is an early indication of the ability of the vibrating micro-probe to successfully counteract the surface interaction forces.

A direct comparison can be made with the previously described operational model. For ease of comparison only measured interaction data on approach are presented. The experimental data has been scaled so that the contact point is set to unity. This comparison is shown in figure 5.22.

The comparison of the theoretical and experimental data indicates some limitations of the model, but also indicates some explanations of the physical relationship. One similarity between the two data sets is the location of the onset of the non-contact interaction. The model and the experimental data both indicate that a non-contact interaction will occur within 100 nm of the surface. This number is highly dependent on the initial starting conditions of the model, which estimated the nature of the surface materials, the surface texture and other *a priori* knowledge. Both sets of data also indicate that, post contact, the interaction forces continue to act on the probe, causing ratios above unity to be observed. One major discrepancy between the two data sets is the relative magnitudes of the interactions. The experimental data indicate a far stronger surface interaction than was initially modelled. This discrepancy could be due to several factors, as discussed in Chapter 4, section 4.4.4.

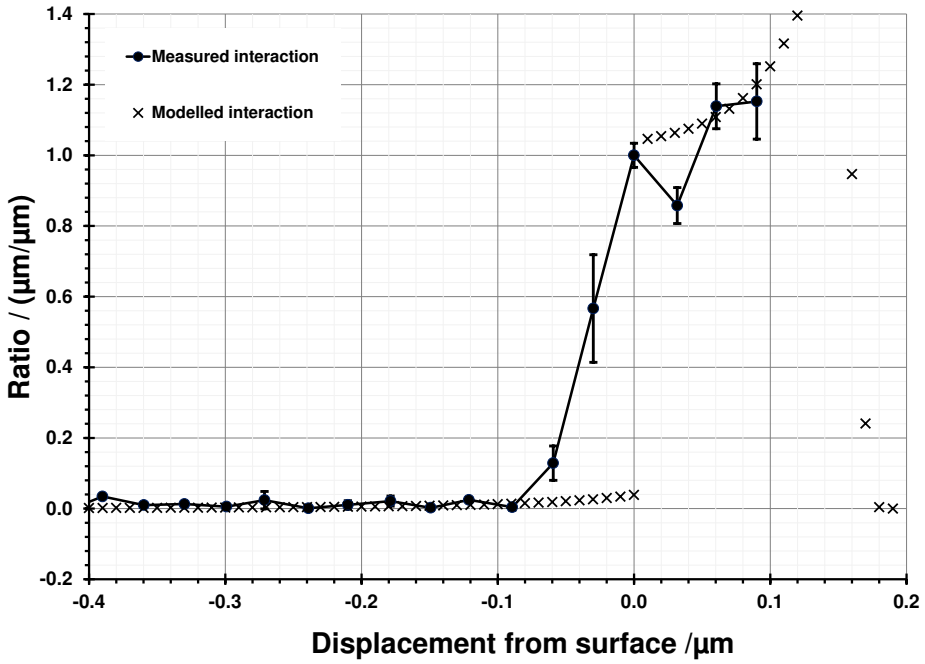

Figure 5.22: Comparison of theoretical data, as shown in figure 4.21 and the experimental data, as shown in figure 5.21.

The capabilities of several other vibrating micro-probes with respect to the ratio determination of surface interaction are shown in figure 5.23. For ease of comparison, the interaction is only shown on approach. This comparison indicates that the feature seen in figure 5.20 is not a true indication of the reaction of the vibrating micro-probe with the test measurement surface.

It can be seen from figure 5.19 that the amplitude of the signals recorded from the sensors of the vibrating micro-probe during interaction with a test measurement surface show some correlation with the physical changes recorded by the LDV. However, these sensor signals are relatively small and suffer from some amount of noise. Therefore, the data was re-processed to investigate the phase of the measured data (both from the LDV and the from the sensors) with respect to input drive signals. The result of this comparison is shown in figure 5.24, and also demonstrates the different scale on which these phase signals are detected. The sensor phase data from the contact experiment shown in figure 5.21 can also be calculated (on approach and retract) and is shown in figure 5.25.

These measurements show clearly that phase detection is also a suitable way to detect the surface interaction forces. The scale of figure 5.25 does not fully illustrate that the sensitivity of the phase measurements is superior to that of the amplitude measurements; the phase signal begins indicating surface interaction forces 100 nm before the amplitude data. Also, the phase data clearly confirms the assumption made to define full surface contact. A small difference can be seen between the approach and retract phase characteristics. This does indicate that, even

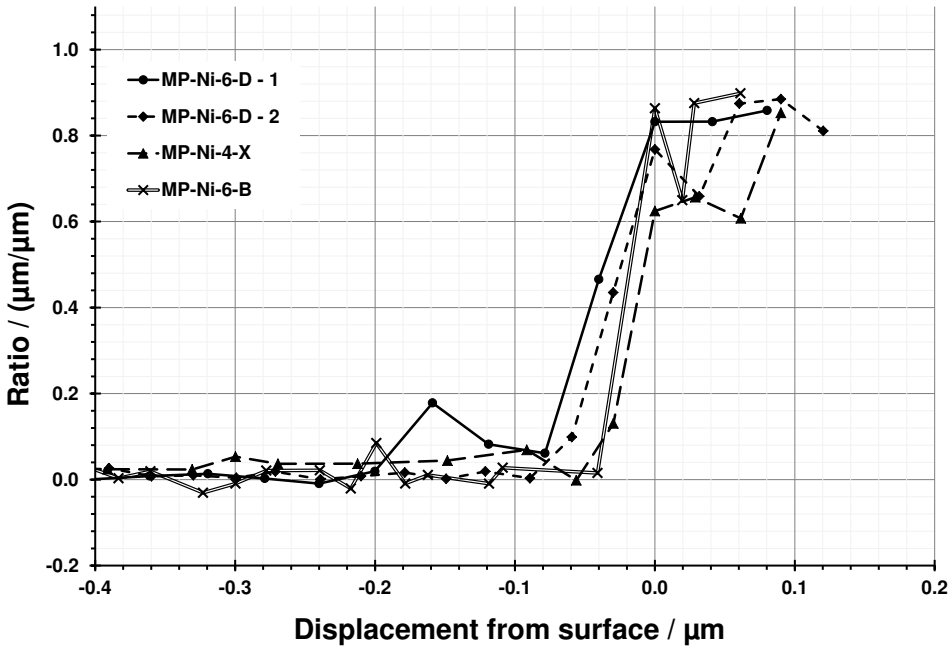

Figure 5.23: Graph of the calculated ratio values for several vibrating micro-probes while interacting with a test surface during a contacting experiment. For ease of comparison, only the approach reaction is shown and the error bars have been omitted.

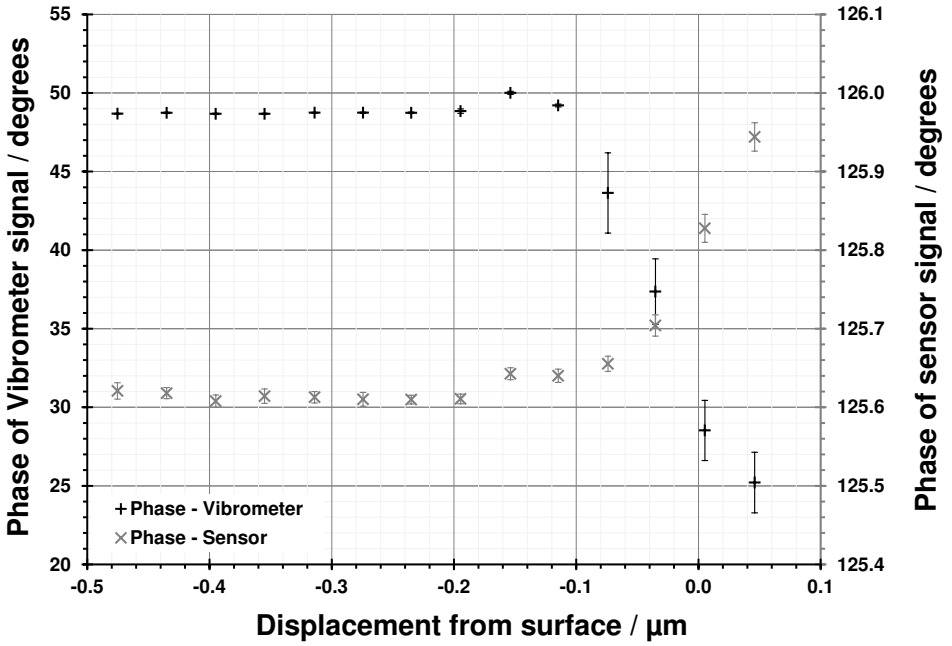

Figure 5.24: Comparison of the phase signals of the laser Doppler LDV and the piezoelectric sensors. The error bars indicate the experimental standard deviation of the mean. It should be noted that these two signals are plotted on radically different scales.

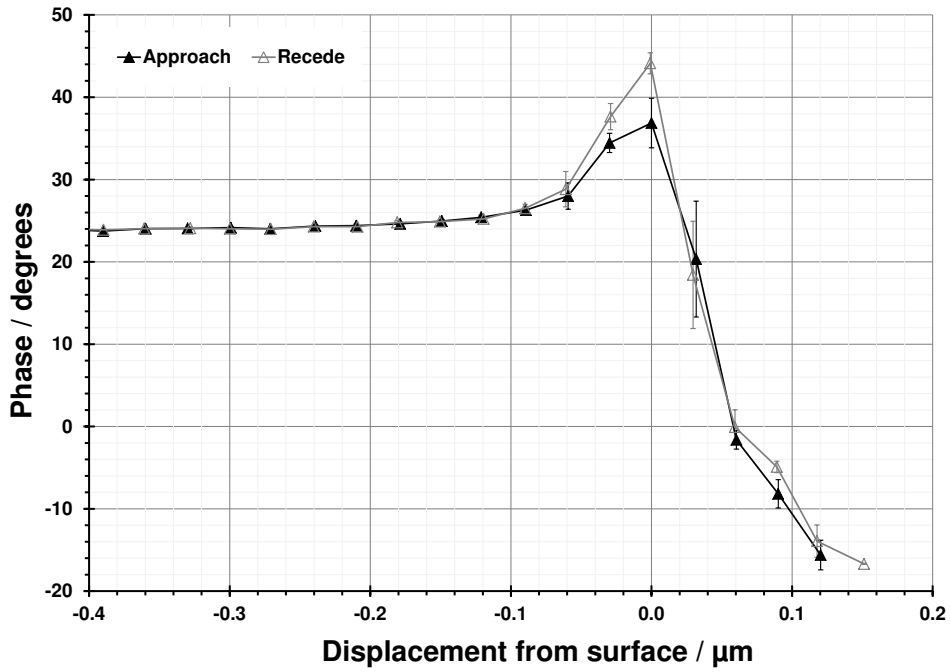

Figure 5.25: Phase of the output signal relative to the drive signal plotted against displacement from surface. The error bars indicate the experimental standard deviation of the mean.

though the probe may negate the effect of snap-in and snap-back, there are some differences in the behaviour of the probe on retract from approach.

It is also important to note that the use of phase data during the data processing negates the need to rely on the length measuring capability of the LDV.

To definitively conclude on the ability of the vibrating micro-probe to counteract the surface interaction forces, the effect of non-ideal operation must be demonstrated. The sensitivity of the operation of the vibrating micro-probe with respect to the vibration amplitude and frequency will be investigated. Following this investigation, the ability of the vibrating micro-probe to counteract the surface interaction forces can be concluded

5.5.3.2 Probe sensitivity tests with respect to amplitude

The operation of the probe was investigated using different vibration amplitudes. This entailed completing the previously-described interaction test three times while operating the probe at three different amplitudes. Vibrating micro-probe MP-Ni-6-D was used, which has a resonant frequency of approximately 1.5 kHz. The vibration amplitudes used to investigate the sensitivity of the vibrating micro-probe were 0.42 µm, 0.83 µm and 1.68 µm. The raw vibration amplitude data (normalised to remove slight variations in amplitude) is shown in figure 5.26 and the data resulting from a ratio calculation (of the associated amplitude data from the LDV) is shown in figure 5.27.

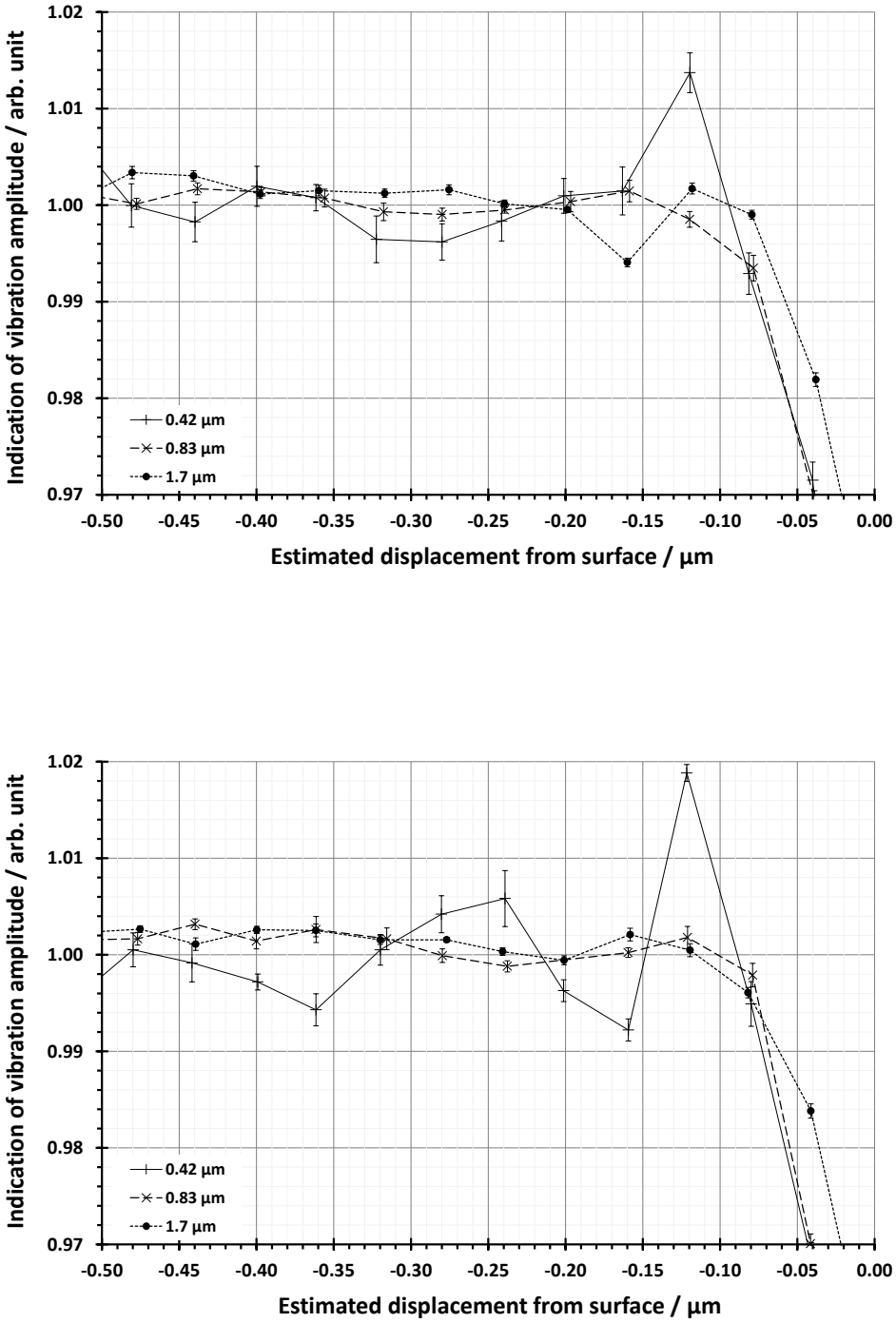

Figure 5.26: Amplitude results of a sensitivity analysis of probe operation (indicated in arbitrary units, "arb. unit") with respect to vibration amplitude, on approach (top) and while retracting (bottom)

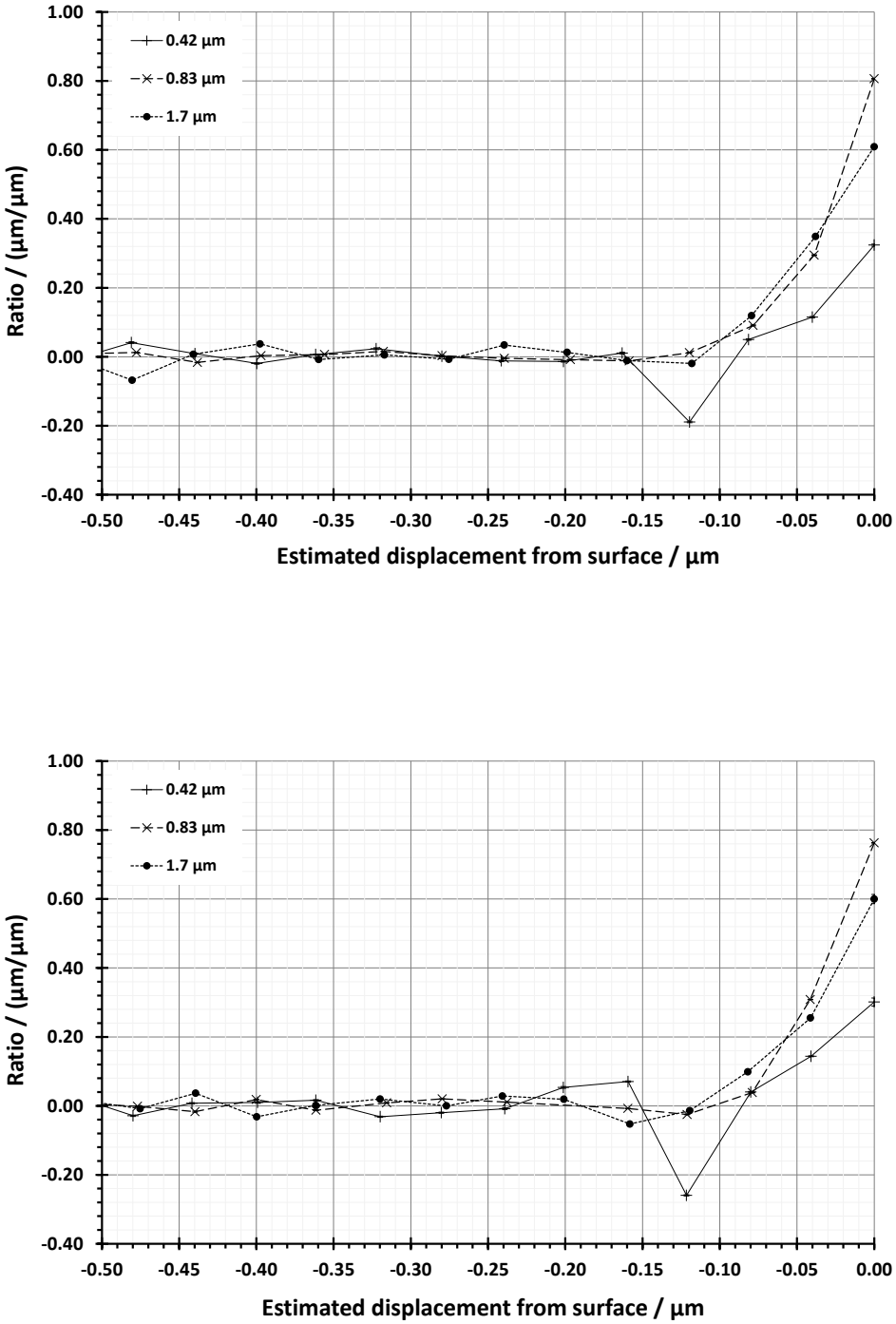

Figure 5.27: Ratio results of a sensitivity analysis of probe operation with respect to vibration amplitude, on approach (top) and while retracting (bottom)

It can be seen from figure 5.26 and figure 5.27 that a change in vibration amplitude results in the capability of the probe to counteract the surface interaction forces to be reduced. When vibrating with an amplitude of 0.42 µm, the micro-probe is unable to counteract the surface interaction forces, neither on approach, or retracting from the surface. Therefore, the previously suggested condition for a minimum vibration amplitude, A_{min}, of 0.5 µm, is seen to be valid.

5.5.3.3 Probe sensitivity tests with respect to frequency

The operation of the probe was investigated using different vibration frequencies. This entailed completing the previously-described interaction test three times while operating the probe at three different frequencies. Vibrating micro-probe MP-Ni-6-D was used, which has a resonant frequency of approximately 1.5 kHz. The test frequencies used to investigate the frequency response of the micro-probe were 1.42 kHz, 1.34 kHz and 1.25 kHz. These frequencies represent steps of approximately 80 Hz, 160 Hz and 250 Hz removed from resonance respectively.

The input drive signals were augmented so that the amplitude of vibration was similar in each test (approximately 0.7 µm). The raw vibration amplitude data (normalised to remove slight variations in amplitude) is shown in figure 5.28 and the data resulting from a ratio calculation (of the associated amplitude data from the LDV) is shown in figure 5.29.

It can be seen from figure 5.28 and figure 5.29 that a change in frequency results in the capability of the probe to counteract the surface interaction forces to be reduced. However, it is suggested that any frequency within 80 Hz of resonance, if operating with suitable amplitude, is sufficient to operate correctly.

5.5.3.4 Determination of the length measuring error

During contact with a measurement surface, the vibrating micro-probe must be able to determine tip deflection accurately, as is required by **Research Question 1.3**. To validate this capability, a set of contact experiments were run to investigate the behaviour of the probe after contacting the test measurement surface (while over-travelling).

It can be seen from previous data, *e.g.* the data presented in figure 5.17, that the vibrating micro-probe is considerably more sensitive to surface interaction than the minimum possible step of the precision manipulation stage, *i.e.* 30 nm. Therefore, a new method of control of the precision manipulation stage should be developed.

A set of surface contact experiments were run; however, each repeated contact run was preceded by a relatively large change (over 100 nm) in the set point of the precision manipulation stage. This change was aimed at achieving a more continuous set of data, which, over several repeated contact runs results in different data intervals.

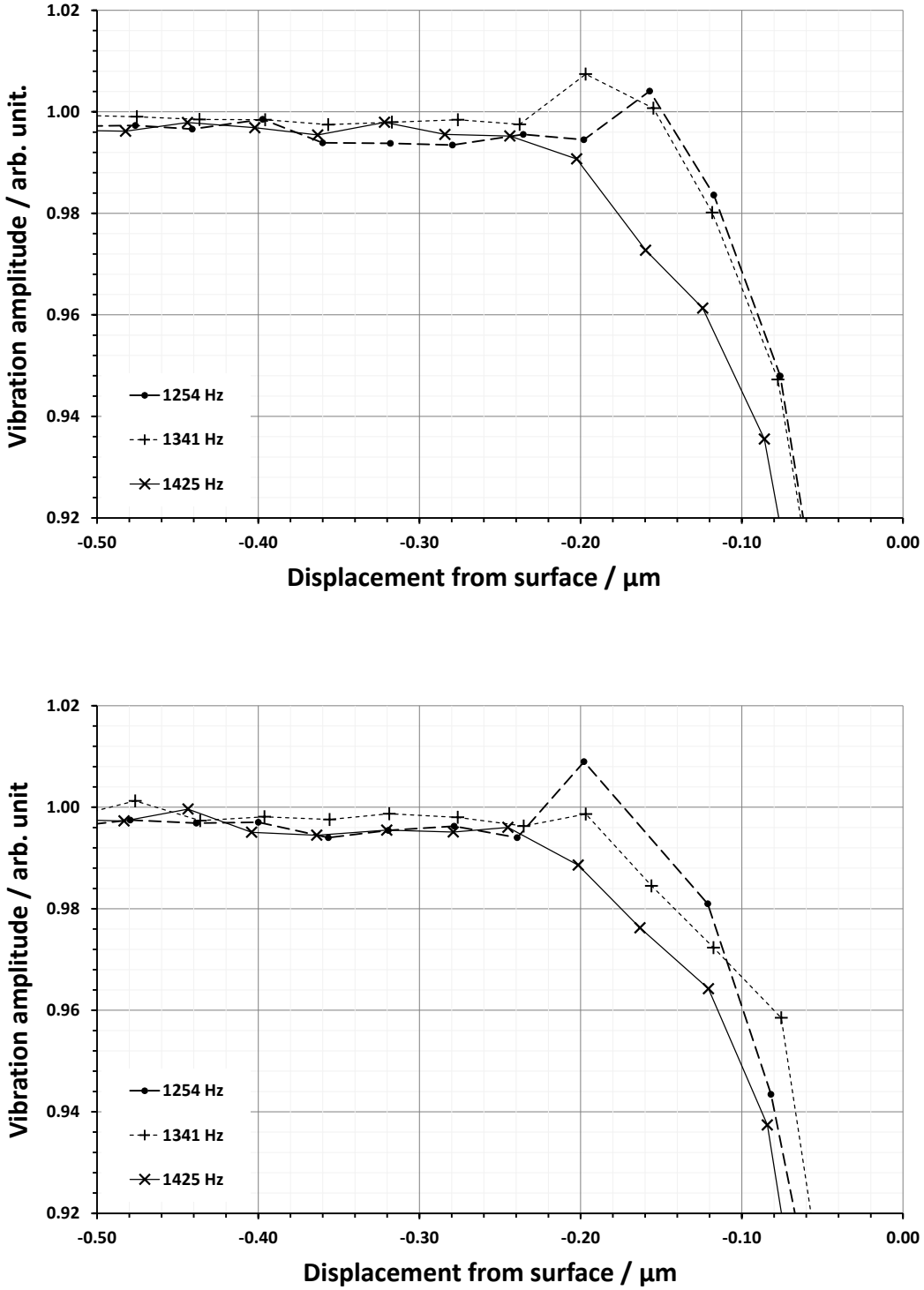

Figure 5.28: Amplitude results of a sensitivity analysis of probe operation with respect to vibration frequency, on approach (top) and while retracting (bottom)

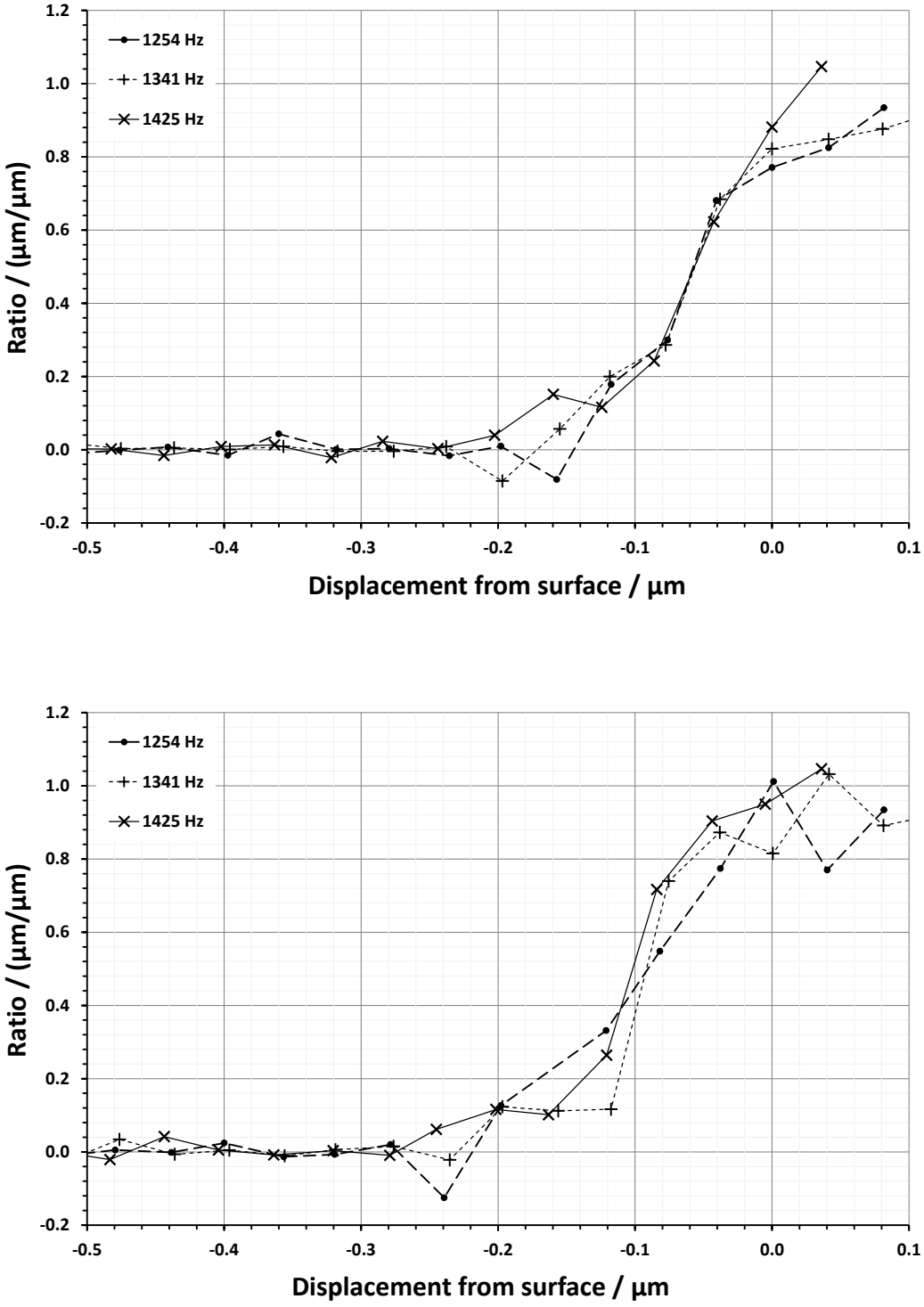

Figure 5.29: Ratio results of a sensitivity analysis of probe operation with respect to vibration frequency, on approach (top) and while retracting (bottom)

Table 5.3: Results from the determination of the length measuring capability for probe MP-Ni-9-9P and MP-Ni-6-1

Probe	Repeats	Fitting coefficient / µm per degree	Linearity error / nm
MP-Ni-6-I	11	0.004 26	8
MP-Ni-9-9P	7	-0.010 25	25

The over-travel data from a contact experiment using probe MP-Ni-6-I is shown in figure 5.30. During the experiment, eleven contact interactions were completed, using the previously described method for collecting more continuous approach and retract data. To determine the relationship between the behaviour of the probe during over-travel, the measured phase of the output vibration was compared to the over-travel distance, as measured by the internal sensor in the precision manipulation stage.

It can be seen from figure 5.30 that there is a linear relationship between the over-travel distance and the output phase of the vibration of the micro-probe. The fitting coefficient was calculated to be 0.004 26 µm per degree. The estimated error resulting from this linear fit is 8 nm, which is calculated as the standard deviation of the individual deviations of the measured data to the linear fit.

A similar set of tests were run using the data collected during the repeatability testing of probe 9-9P, and the fitting coefficient was calculated to be -0.010 25 µm per degree. The estimated error resulting from this linear fit is 25 nm. This data is shown in figure 5.31.

It can be seen that there is not a linear relationship between the over-travel distance and the output phase of the vibration of micro-probe MP-Ni-9-9P. This is evident from the high fitting error of 25 nm. The linear fit will continue to be used to allow for easier comparison between results.

It can be concluded that this method can determine the linear fitting coefficient of the micro-probe during contact, but that some extra effort is required to ensure good data is collected. A summary of the data relating to the determination of the length measuring capability of the vibrating micro-probe is shown in table 5.3.

5.5.3.5 Determination of the repeatability of the micro-probe

Following the determination of the length measuring capability of the vibrating micro-probe, consideration must be taken in determining the probing point repeatability, as required by **Research Question 1.2**.

It is possible to determine the probing point repeatability of the vibrating micro-probe by using the previously presented linearity data, as shown in figure 5.30 and figure 5.31. The position of the probing point is defined as the calculated position of the test measurement surface during

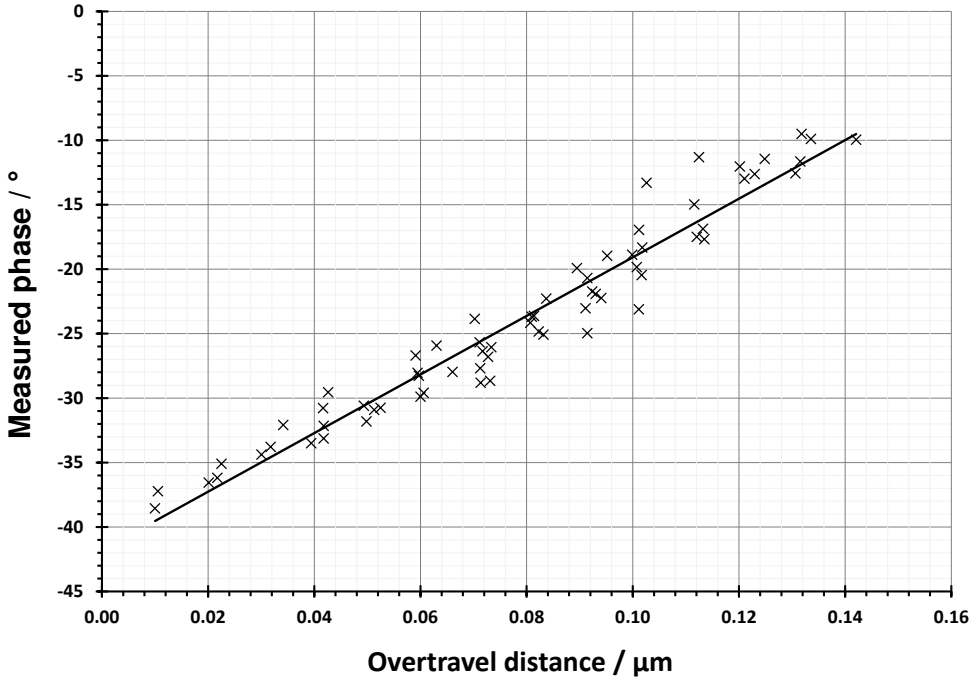

Figure 5.30: Post-contact data from probe MP-Ni-6-I over eleven repeated interactions. The trend-line represents a least-squares best fit linear relationship.

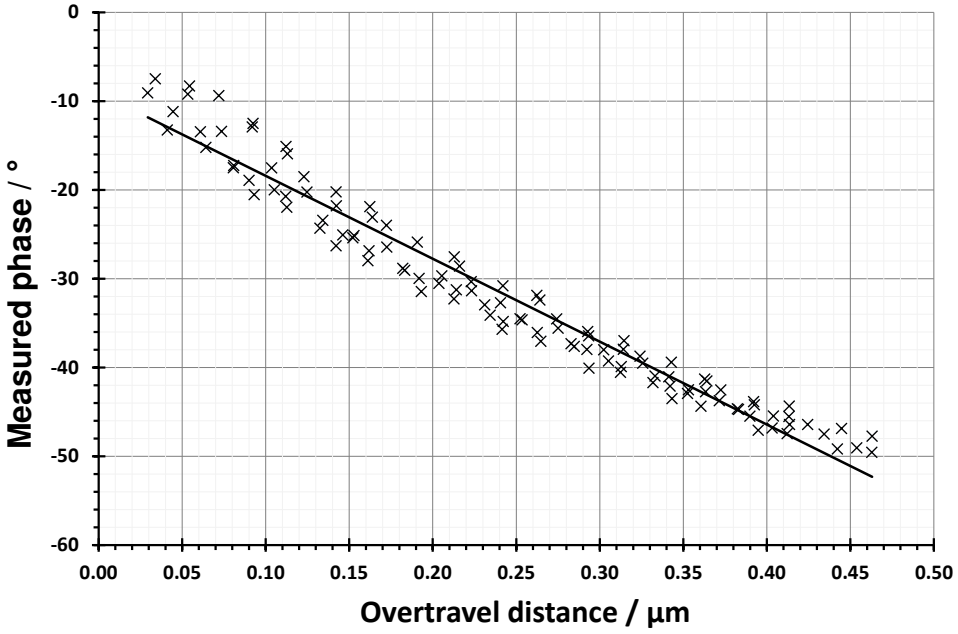

Figure 5.31: Post-contact data from probe MP-Ni-9-9P over seven repeated interactions. The trend-line represents a least-squares best fit linear relationship.

Table 5.4: Results from the determination of the repeatability error for probe MP-Ni-9-9P and MP-Ni-6-1

Probe	**Repeats**	**Repeatability error / nm**
MP-Ni-6-I	11	2
MP-Ni-9-9P	7	9

Table 5.5: Determination of the repeatability error for probe MP-Ni-9-9P across several distinct experiments

Repeats	**Repeatability error / nm**	**Fitting coefficient / µm per degree**	**Linearity error / nm**
5	23	-0.005 74	50
11	25	-0.008 72	35
7	9	-0.010 25	25

an interaction. Therefore, the individual interactions used for the determination of the linearity coefficients were re-processed to determine their individual probing point locations. The standard error of these individual probing points is calculated, and is reported as an indication of the probing point repeatability error. The results of the determination of the repeatability errors for probe MP-Ni-9-9P and MP-Ni-6-I are shown in table 5.4.

Although these indications are dependent on the arbitrary definition of the true surface position, which is defined according to the rules stated in Workflow 1, they are a true indication of the probing point repeatability of the vibrating micro-probe. The arbitrary definition of the true surface position will be mitigated once the probe is installed on a micro-CMM through the use of a calibrated test length, or material measure of size.

To investigate the influence of error due to experimental setup, a second and third set of interaction experiments were run using vibrating micro-probe MP-Ni-9-9P. These experiments were completed after disassembling and reassembling the experimental setup. The probing point positions were calculated using the original fitting co-efficient of -0.010 25 µm per degree. The results of these experiments are shown in table 5.5.

It can be seen from table 5.5 that there is some error associated with the determination of a fitting co-efficient that represents the true length measurement capability of the vibrating micro-probe. Although this error is below 30 nm for the experiments shown in table 5.5, it is suggested that there is some repeatability error associated with the mounting of the vibrating micro-probe in the experimental setup that causes small changes in its ability to measure length accurately.

5.5.3.6 Experimental drift

It can be seen from figure 5.18, and in many of the subsequent figures, that a change in the data trend occurs in both the LDV phase data and the sensor phase data at 150 nm from the surface.

It is suggested that this change indicates the beginning of the interaction between the surface interaction forces and the vibrating micro-probe. At 150 nm from the surface, it is most likely that this interaction is the squeeze film interaction.

Further investigation of the six individual vibration amplitude measurements that make up the average points shown in figure 5.19 over time are shown in figure 5.32. These six amplitude measurements relate to the six repeated measurement taken during the contact experiment.

It can be seen from the change in the amplitude of the probe measured at the expected interaction point with the capillary layer, at 40 nm from the surface that the strength of the capillary interaction changes over time. The increase of the measured vibration amplitude over time suggests that the effective strength of the capillary force is decreasing over time with repeated probing. A similar effect is also described in [82], but with a static probe, resulting in the opposite effect of increasing the effective strength of the capillary force. It is suggested that the use of a vibrating probe reduces the effective strength of the capillary force with repeated probing, either by reducing the thickness of the liquid layer through redistribution, repulsion or through increasing the action of evaporation from the surface.

An alternative conclusion that is possible from this data is that the experimental setup is moving by 30 nm, linearly and in one direction, over the fifteen minute duration of the experiment. This drift is unlikely because of the steps taken to ensure stability of the experimental setup. The conclusion regarding the change in effective strength of the capillary force is further supported by investigating the data collected at other positions during the test, which should all shift by 30 nm if within range of the surface interaction forces (*i.e.* within 100 nm to 200 nm). The data showing the individual points grouped by calculated position from the interaction experiment is shown in figure 5.33.

It can be seen that from 150 nm away from the surface, the interaction between the probe and the surface interaction forces is evident from the slowly reducing amplitude of the probe vibration. The effect of the reducing interaction force is not seen in the data relating to the amplitude of the probe measured at the interaction points at 150 nm, 120 nm and 80 nm from the surface, which are most likely due to the interaction of the probe with the effect of the air squeeze film near the surface. Therefore, as these data points are not affected by the 30 nm drift seen in the data collected closer to the measurement surface, it is concluded that this drift is from a change in the capillary action and not drift in the experimental setup.

5.5.3.7 Summary of contact results in the vertical direction

Several experiments have been completed to directly address the need to confirm that the vibrating micro-probe can counteract the surface interaction forces, can act repeatably and linearly. These results will be revisited in Chapter 7, with respect to the specific **Research Questions**.

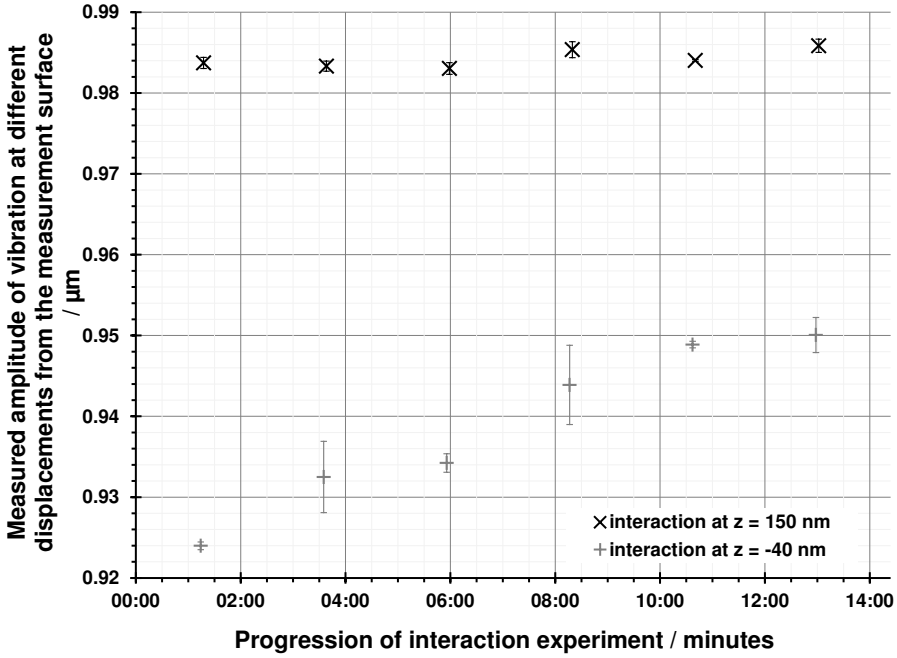

Figure 5.32: Plot of the change in vibration amplitude, as measured by the Doppler laser LDV, at the estimated interaction point with the capillary layer, over time. The error bars indicate the experimental standard deviation of the mean.

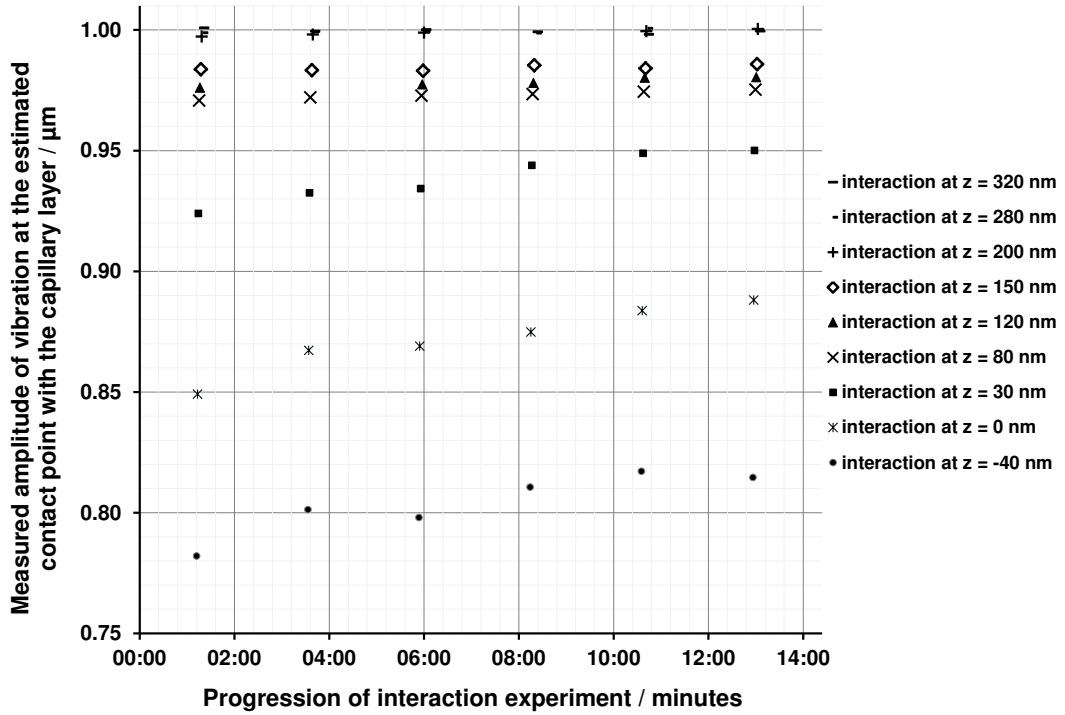

Figure 5.33: Graph of individual points grouped by calculated position from the interaction experiment against elapsed time.

However, one extra point should be highlighted. Referring to the extensive research completed in this section, it can also be concluded that there is a strong indication that the vibrating micro-probe could operate in a non-contact mode, through the repeatable detection of the surface interaction forces before direct contact with the test measurement surface is made.

5.5.4 Results of isotropy tests of the vibrating micro-probe

A set of experiments were conducted to determine if the newly developed concept of isotropy for 3D vibrating micro-CMM probes could be applied to the vibrating micro-probe. In doing so, the capability of the probe to act isotropically would also be tested, especially the ability of the vibration algorithm to control the vibration of the probe. This is a prerequisite for lateral operation of the vibrating micro-probe, and was therefore investigated prior to the lateral testing.

A graph of the ideal amplitude results, as calculated by the vibration algorithm, is shown in figure 4.15. Data was collected from the micro-probe, as has been previously described, to determine the extent of the isotropy of the system. It is expected that the system will need to operate away from the resonance peak, so that the primary mode of vibration (*i.e.* vertical vibration) is not dominant. A set of tests were conducted at the frequencies corresponding to the approaching half maximum amplitude and the approaching quarter maximum amplitude. For micro-probe MP-Ni-6-D, with a resonant frequency of 1.506 kHz, these frequencies are 1.500 kHz and 1.493 kHz respectively. These tests were completed with input signals corresponding to vibration vectors every 30° to reduce the length of the experiments. Graphs displaying the raw amplitude results of these tests are shown in figure 5.34. A direct comparison can be made to the ideal isotropic behaviour of the vibrating micro-probe, whereby the ratio between ideal operation and real operation is calculated for each leg. These comparison results are shown in figure 5.35.

It can be seen that the observed anisotropic behaviour of the system is currently inconsistent with the ideal situation derived from the operational model. This anisotropy is evident through the coupling of all of the legs to the vertical vibration mode. However, the test completed at the frequency corresponding to the approaching quarter maximum amplitude displays a slight decoupling of the vibration of leg 1 and leg 2 with respect to leg 3 at 0°, 180°, 210°, 300° and 330°. It should also be noted that the absolute amplitude of the resulting vibration of the vibrating micro-probe at this operational frequency is reduced by almost 50 % compared to operation closer to resonance.

These results demonstrate that tests should continue at lower frequencies to ensure further decoupling of the three legs from vertical vibration mode. It has been previously demonstrated that vibration frequencies within 80 Hz of resonance still result in ideal operation of the vibrating micro-probe. However, in order to maintain a suitable vibration amplitude, input signal amplitudes should be increased so that resulting vibration amplitudes remain large enough to counteract the surface interaction forces. This is not currently possible using the developed vi-

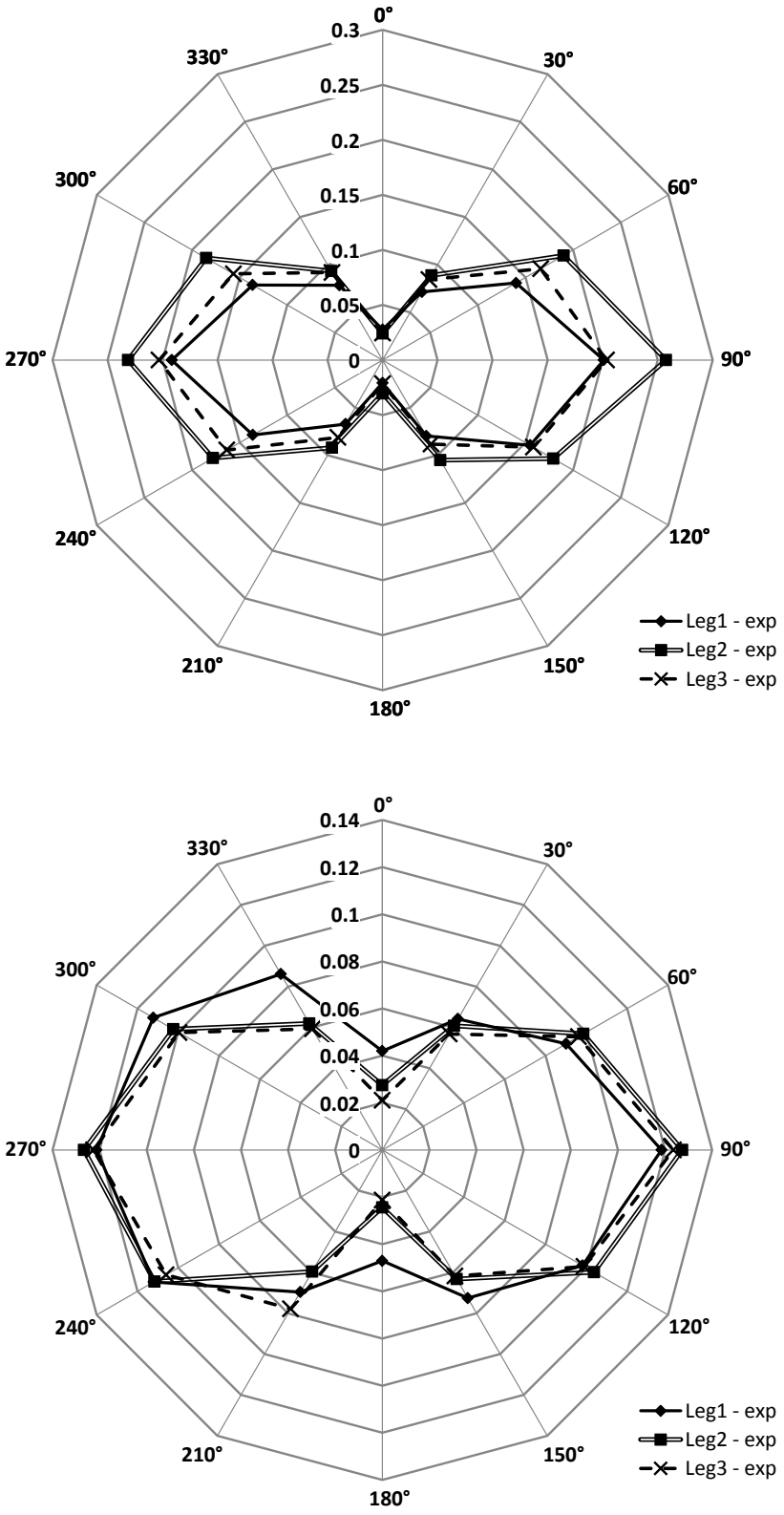

Figure 5.34: Results of the initial tests of the isotropy of the micro-probe. Vibration frequencies were 1.500 kHz (top) and 1.493 kHz (bottom) for a probe with a resonant frequency of 1.506 kHz. The radial axis is an indication of the vibration amplitude, and the circumferal axis is intended vibration vector.

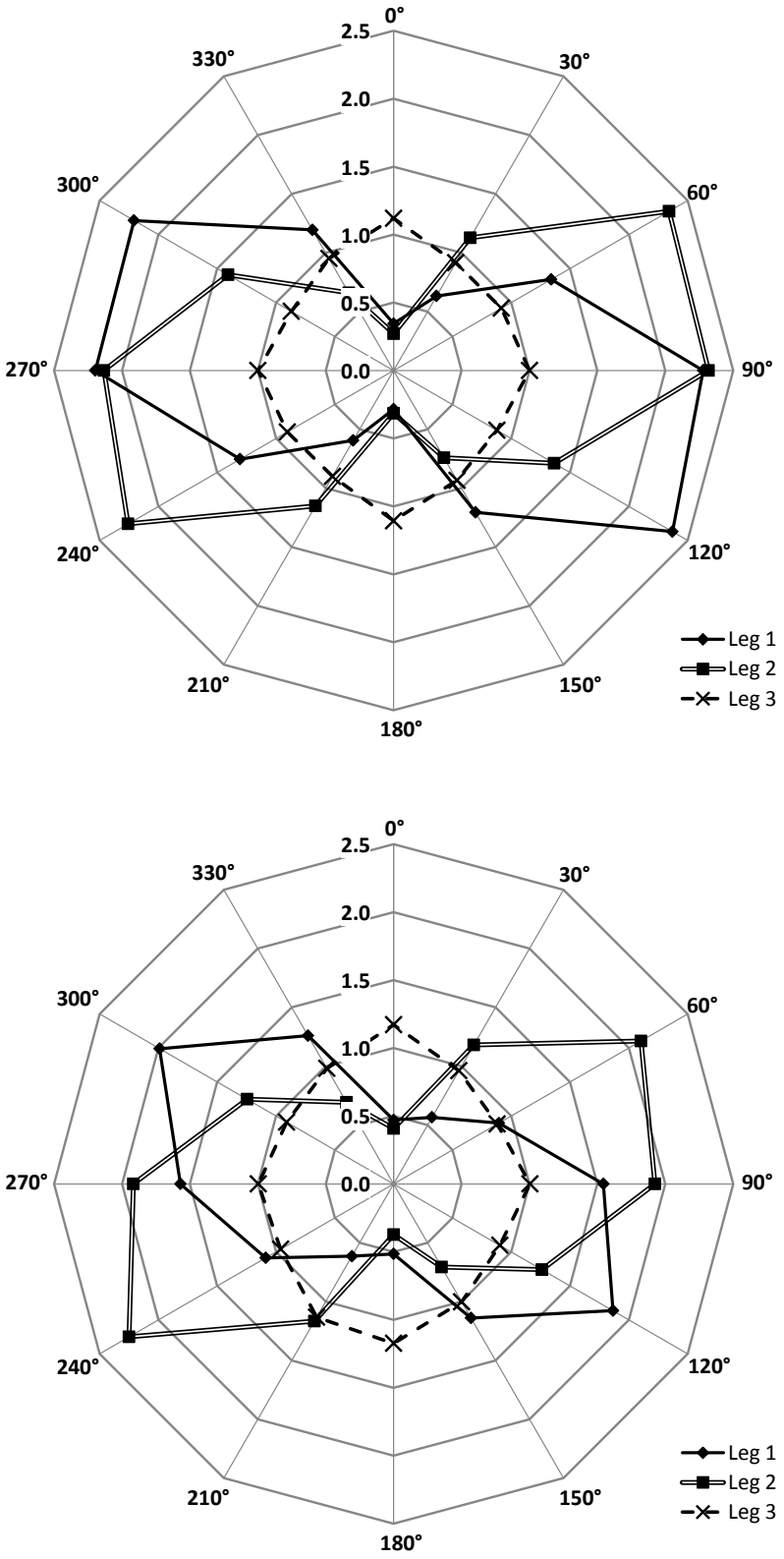

Figure 5.35: Results of the initial tests of the isotropy of the micro-probe. Vibration frequencies were 1.500 kHz (top) and 1.493 kHz (bottom) for a probe with a resonant frequency of 1.506 kHz. The radial axis is the relative amplitude with respect to the ideal isotropic response, and the circumferal axis is intended vibration vector.

bration algorithm, as the operational voltages used to demonstrate these isotropy results were close to exceeding the maximum 10 V.

Finally, it should be noted that the completion of one single isotropy experiment, at one operational frequency, takes several days. This is due to the limitation of the experimental setup, which is only automated in one dimension. Therefore, the continuation of this work into the investigation of the isotropy of the vibrating micro-probe relies on the further development of the experimental setup. This will be discussed further in Chapter 7.

5.5.5 Results of tests of the vibrating micro-probe operating in the lateral direction

Experiments testing the lateral interactions of the probe must be completed in order to continue the characterisation of the probe in 3D. Due to the current anisotropic operation of the probe, at least one other mode of operation was considered for lateral probing. This mode entails vibrating the micro-probe in the vertical direction, *i.e.* perpendicular to the test measurement surface normal. This operation mode is analogous to the UMAP probe from Mitutoyo, as described in Chapter 2, section 2.3.4.2. The operation of the probe in the lateral direction will also be tested, as intended for ideal use, and the previous isotropy results will used to identify the most appropriate vibration vector.

5.5.5.1 Lateral operation while vibrating vertically

An experiment was completed with the probe vibrating vertically while interacting with a laterally-facing surface. The precision manipulation stage and test measurement surface were mounted horizontally so that the test surface normal was perpendicular to the stylus and the direction of vibration. The precision manipulation stage was programmed to approached the probe in 50 nm steps. A comparison of the phase measurement (approach and retract) to the amplitude measurement (taken at the centre of the central island) is shown in figure 5.36.

It can be seen from figure 5.36 that the non-contact interaction is detected within 150 nm of the surface. However, the ratio calculation indicates that at contact, the vibration of the probe reduces by four times the test surface approach step. Not enough information is collected from the system to ascertain if this sudden decrease in amplitude is as a result of snap-in, or if the surface interaction forces are successfully detected and counteracted, and only complete surface contact results in complete amplitude damping. Also, the retraction of the probe indicates that the system is suffering from snap-back. Further investigation of this operating mode will not been completed, as this is not representative of the desired probe-surface interaction.

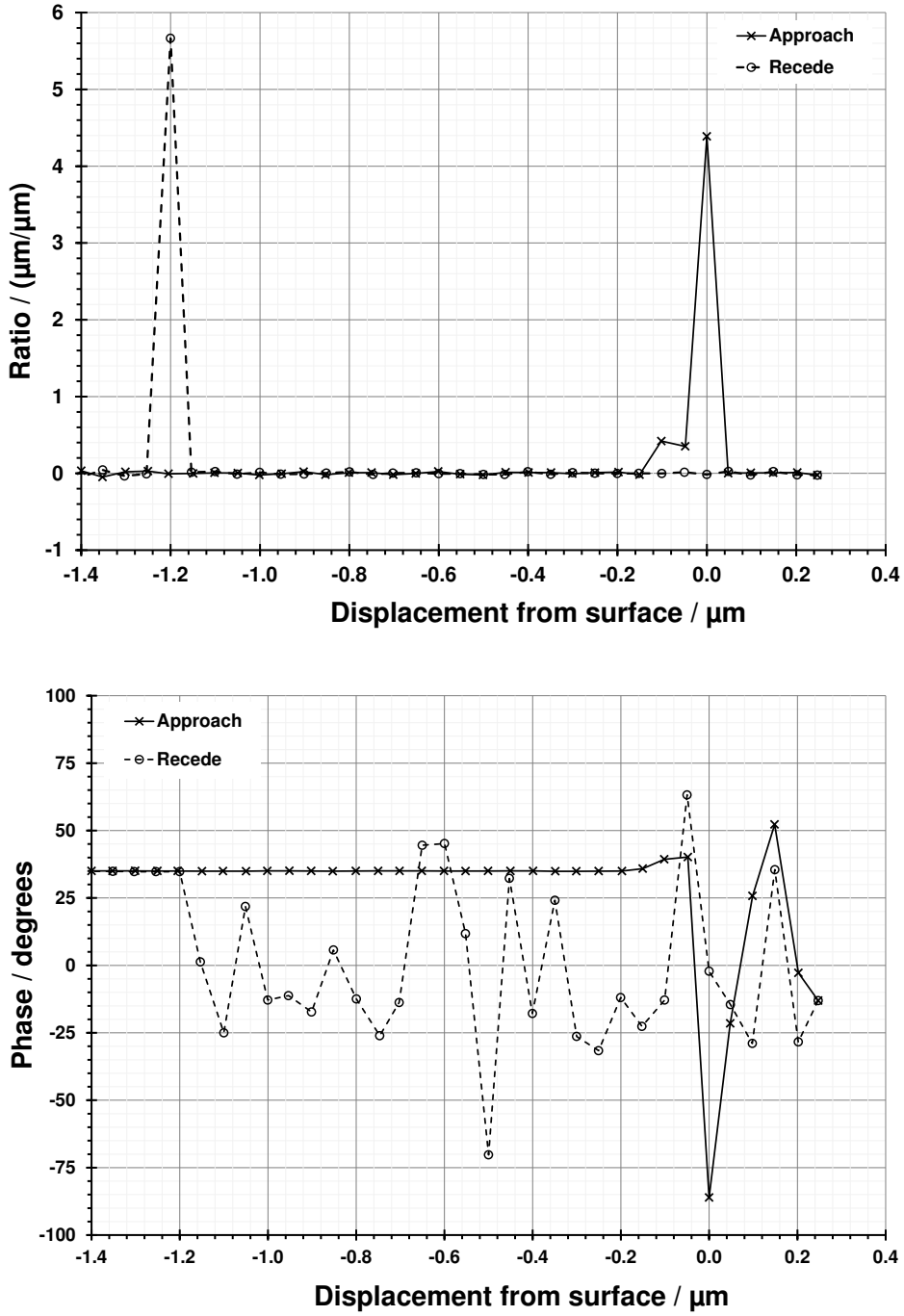

Figure 5.36: Probe vibration perpendicular to the surface normal; the comparison of the two measured signals: the ratio calculated from the amplitude measurement (top) and phase of the output signal relative to the drive signal (bottom), plotted against displacement from surface

5.5.5.2 Lateral operation of the vibrating micro-probe

Lateral probe-surface interaction experiments were completed with the probe vibrating parallel to the test surface normal. This is the desired probe-surface interaction mode and is representative of the expected operation of the probe.

Considering the previous determination of the isotropy of the probe, it was estimated that if micro-probe MP-Ni-6-D were used, at a vibration frequency of 1.493 kHz, and a vibration vector of 150°, then this would produce the most ideal lateral vibration available at this time. At this vibration vector, it is also estimated that positioning the LDV above leg 2 (aligned at 120°) then a good appreciation of the vibration amplitude of the stylus tip can be estimated. The test measurement surface is aligned such that it is interacting with the probe parallel to the estimated angle of vibration. The resulting contact interaction is shown in figure 5.37.

It can be seen from figure 5.37 that the non-contact interaction is detected within several hundred nanometres of the surface. It is suggested that due to the lateral interaction of the probe's micro-stylus with the test measurement surface, the interacting area has now considerably increased, which could also result in a considerable increase in the effect of the surface interaction forces. However, it is clear from the data that snap-back is recorded 1.8 µm from the surface while the probe is retracting. There are several situations that could suggest why the interaction exhibits a snap-back during the retract steps.

One possibility is that the probe is not vibrating parallel to the surface normal. This will result in a reduction in the effective amplitude of the vibration, and hence can be seen as a reduction in the effective force available to counteract the surface interaction forces.

A second possibility is an operational feature of using vibrating micro-CMM probes. The lateral experiment, as described by figure 5.37, is representative of the mode of operation of the probe such that the vibration vector is parallel to the measurement surface normal. However, due to the coarse approach of the probe to the surface, steps of almost 200 nm, the probe vibration is completely diminished through physical interaction with the surface after only two steps after contact with the measurement surface. Hence, while the probe is retracting, there is no scope for counteraction of the surface forces, due to there being no appreciable vibration. Therefore, these experiments are not a valid depiction of the operation of the vibrating micro-probe, and cannot be easily compared to similar vertical measurements taken with approach steps of only 30 nm.

Also, as with the previously described isotropy experiments, completion of a lateral contact experiment can take several hours, increasing the risk of experimental error. Therefore, as with the isotropy experiments, the continuation of this work relies on further development of the experimental setup. This will be discussed further in Chapter 7.

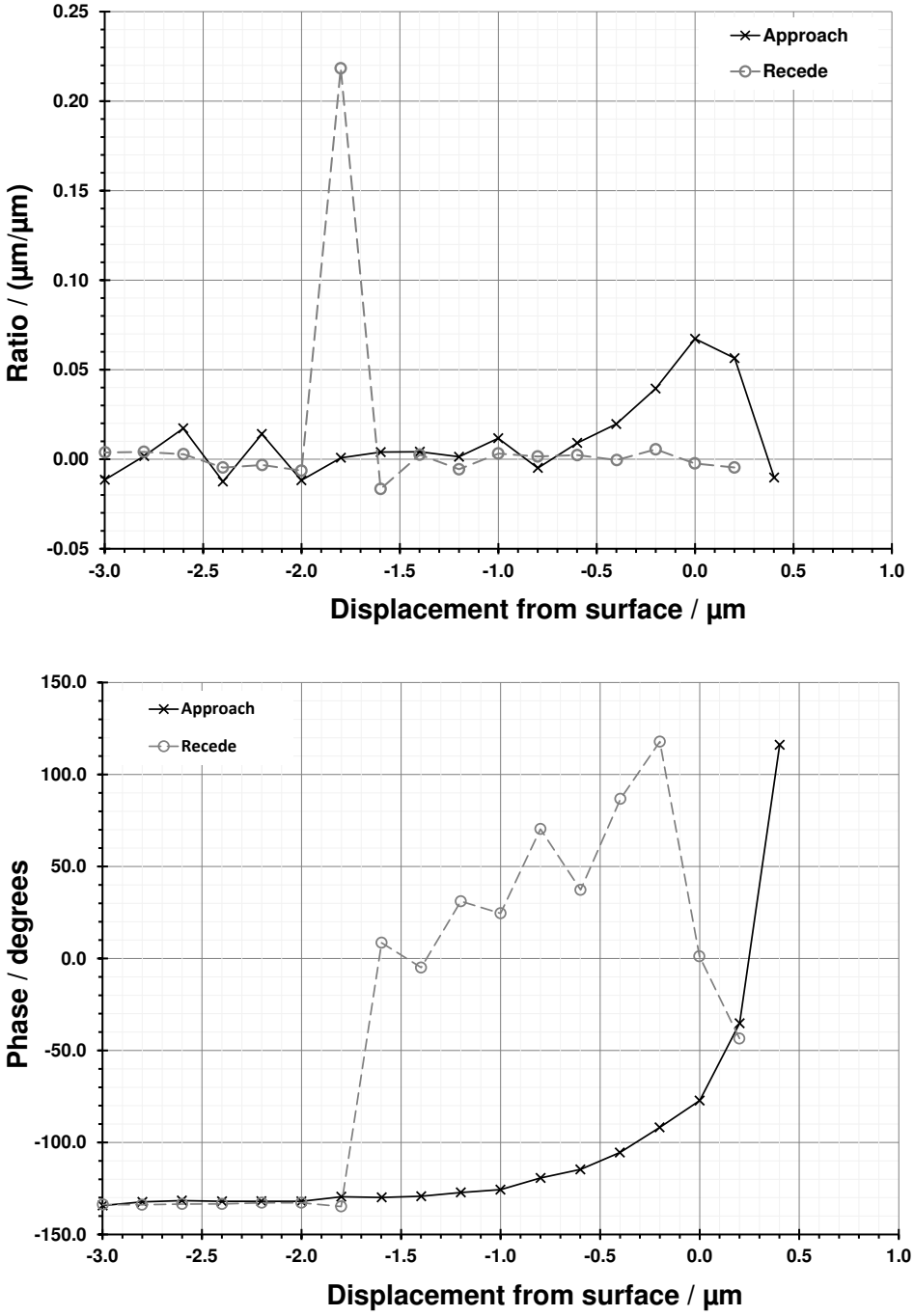

Figure 5.37: Probe vibration parallel to the surface normal; the comparison of the two measured signals: the ratio calculated from the amplitude measurement (top) and phase of the output signal relative to the drive signal (bottom), plotted against displacement from surface

5.6 Uncertainty analysis and final declaration of results

Several experiments have been completed, aimed at determining the repeatability and length measuring error of the vibrating micro-probe. Through the combination of these results, including an appreciation of the uncertainties involved in taking these measurements, it is possible to report a single probing error result for the tested probes. Therefore, an estimate the uncertainty associated with the experimental results should be calculated.

Initially, a description of known error sources will be given, along with estimates as to their error contribution. These estimates will then be combined with the experimentally determined errors to determine an estimate of the total error associated with the tested vibrating micro-probes.

5.6.1 Error sources due to local environment

During the design of the experimental setup, several known error sources were considered. Several design choices were made to counteract environmental effects, such as temperature changes and external vibration.

Any temperature effects associated with the experimental setup can be estimated. The setup was designed such that temperature changes in any common paths were compensated for by the use of similar materials. The effect of temperature changes on the experiment was addressed by using aluminium legs in the kinematic stand to compliment the aluminium construction of the manipulation column. Therefore, only the effect of the tungsten carbide in the stylus and the gauge block that defined the test measurement surface, and the stainless steel balls at the end of the legs of the kinematic stand, need be considered.

The effect of humidity on the operation of the vibrating micro-probe must also be considered. It has been determined experimentally that a slow change of 1 %RH will affect the amplitude of the vibrating micro-probe by -10 nm. If the humidity change is fast, the resulting change in vibration amplitude could be -20 nm. These results are presented in Chapter 6, section 6.5.1.2.

5.6.2 Error due to instability in the operation of the vibrating micro-probe

The underlying stability of the probe will play a role in the probing error. The error due to probe stability was determined by activating the probe in free space and observing any drift in the physical vibration output. Over a period of thirty minutes, the stability error was determined to be 9 nm.

5.6.3 Linearity errors of the measurement systems

Other error sources in the setup include the linearity error on the measurements taken by the precision manipulation stage and the LDV. These are specified by the manufacturers as 0.1 % and 2.5 % respectively. The linearity error of the precision manipulation stage affects the positional aspects of the experiment, and the linearity error of the LDV affects the probe signal. However, as only the phase signal from the LDV was used during the determination of the probing error of the vibrating micro-probe, its linearity errors can be neglected.

5.6.4 Other errors

There is at least one other error of note; the Abbé error associated with the alignment of the precision manipulation stage. The position of the internal measurement scale is unknown, but is assumed to be at the centre of the top plate. The perpendicularity of the probe stylus to the movement of the test measurement surface was optimised by using the video optical system on the LDV. It is estimated that this can be achieved to several arc seconds. It is known that there is a small misalignment of the system, which is evident when considering the raw ratio results, as presented in figure 5.21. It is estimated that the error due to the misalignment of the measurement scale in the precision manipulation stage is in the order of 10 nm.

5.6.5 Estimate of expanded probing error

From the determined systematic errors, a Type B standard uncertainty can be estimated. All contributions are assumed to have a rectangular distribution. These results are shown in table 5.6.

The total probing error associated with the tested vibrating micro-probes can be calculated by combining the experimentally determined errors, and the Type B errors. These results are shown in table 5.7. A coverage factor $k = 2.00$ is applied to the calculated standard errors, providing a confidence level of approximately 95 %.

It can be seen from table 5.7 that the repeatability errors of the two tested vibrating micro-probes in the vertical direction are below 10 nm, as required by **Research Question 1.2**. It can also be seen that, in certain cases, the linearity errors are quite far removed from 20 nm required by **Research Question 1.3**; although some individual results suggest that this objective is not inconceivable.

Several contributing factors could lead to these large linearity errors, and suggestions for future work in this area will be discussed in Chapter 7.

Table 5.6: The individual errors (systematic) from the experimental setup

Error source	**Notes**	**Value / nm**	**(u) / nm**
Thermal expansion	8 mm of WC against Dural, over 0.05 K	6	4
Thermal expansion	5 mm of SS against Dural, over 0.05 K	2	2
Humidity	An estimated humidity change of 0.5 %RH	5	3
Stability	Stability of the probe over 30 minutes	9	6
Linearity error (manipulation)	Estimated over a measured distance of 2 µm	2	2
Abbé error	Misalignment of measurement scales	10	6
	Type B standard uncertainty, u_B		**11 nm**

Table 5.7: Combined standard error associated with the repeatability and linearity measurements in the vertical direction

	MP-Ni-6-I	**MP-Ni-9-9P**
Linearity error / nm	8	25
Repeatability error / nm	2	9
Systematic error (Type B) / nm	11	11
Combined standard error	14	29
Expanded error (k = 2.00)	**28 nm**	**58 nm**

5.7 Conclusions of the validation of the vibrating micro-probe

The experimental validation of the vibrating micro-probe has been presented.

Prior to the presentation of the results, the experimental setup design was described, along with the technical specifications of all the constituent parts of the apparatus. Step-by-step experimental procedures were also presented.

The ability of the vibrating micro-probe to counteract the surface interaction forces was tested. A set of experiments were conducted to compare the true operation of the vibrating micro-probe with the theoretical operation. Results from several contact experiments initially suggested that the vibrating micro-probe was capable of counteracting the surface interaction forces. The initial results also suggested that the vibrating micro-probe could conceivably operate in non-contact mode, triggering a surface contact signal immediately prior to physical surface contact. To definitively conclude on the ability of the vibrating micro-probe to counteract the surface interaction forces, the effect of non-ideal operation was investigated in the form of several sensitivity tests.

The sensitivity of the probe to changes in the operating amplitude and to changes in operating frequency was tested. It was concluded from these tests that the previously determined minimum operational amplitude, A_{min}, of 0.5 µm, was a realistic requirement. Also, it was concluded that the vibrating micro-probe could operate as intended while vibrating at a frequency within 80 Hz below the resonant frequency. Following these sensitivity tests, several of which demonstrated unsuccessful counteraction of the surface interaction forces, it was concluded that the vibrating micro-probe could operate as intended, as required by **Thesis Objective 1**.

As required by **Research Question 1.2** and **Research Question 1.3**, the probe point repeatability and length measuring capability of the vibrating micro-probe were tested. The error associated with the linear fitting of the relationship between detected phase of the probe sensors and over-travel distance was determined. The resulting linearity errors were recorded as being below 25 nm for two tested probes. Following this linearity determination, the associated probing point repeatability values were determined. The resulting probing point repeatability errors for two tested probes were below 10 nm. Further tests suggested that unrepeatability in the mounting of the vibrating micro-probes could result in up to 25 nm repeatability error, and up to 50 nm linearity error.

Some consideration was also afforded to the apparent experimental drift recorded during validation. Though careful investigation of the changing effects of the surface interaction forces, it was determined that the capillary layer is constantly changing over time, especially when being contacted by a vibrating micro-CMM probe. These experiments also served confirm the mechanical stability of the experimental setup, which was observed to be considerably lower than 30 nm over a 15 minute experiment.

To address the requirements of **Thesis Objective 2**, specifically **Research Question 2.1**, a set of experiments were run to investigate the capability of the vibration algorithm to realise isotropic operation of the vibrating micro-probe. Anisotropic behaviour of the system was observed, which is inconsistent with the ideal situation derived from the vibration control algorithm. Slight decoupling of the vibration of the individual legs from resonance behaviour was observed at vibration frequencies more than 10 Hz below the resonance frequency. Several other mitigating factors combine to result in the conclusion that isotropic operation of the vibrating micro-probe is not yet possible using the current vibration control algorithm or the current experimental setup. This conclusion will be addressed further in Chapter 7. Regardless of the anisotropic behaviour of the probe, several lateral experiments were conducted. Although the results indicated successful detection, and therefore counteraction of the surface interaction forces, the limited capability of the vibration control algorithm and the experimental setup resulted in few further conclusions.

A description of the known error sources within the experimental setup was presented. These systematic errors were combined with the experimentally determined linearity and repeatability errors to estimate the combined standard errors of the two tested probes.

Chapter 6

Strategies for use

6.1 Introduction to strategies for the use of the vibrating micro-probe

The use of micro-CMMs is of great interest to the precision manufacturing industry because of their capability to perform length measurements in three dimensions to high accuracy with low uncertainties [3]. The verification of the performance of classical CMMs is well understood, with specification standards and calibrated artefacts available for users and manufacturers to ensure conformity. These specification standards include the ISO 10360 Geometric Product Specification (GPS) standards for the acceptance and reverification of CMMs [11, 138, 196, 197], and also the ASME B89.4 suite of standards, defining methods for performance evaluation of CMMs [198].

Thesis Objective 3 aims at determining if the NPL vibrating micro-probe can adhere to existing specification standards regarding the use of micro-CMM probes. To achieve this aim, a detailed description of the vibrating micro-probe's adherence to existing specification standards will be completed. Several concept operational strategies for the vibrating micro-probe will also be introduced, with specific focus on environmental and logistical issues.

6.2 Introduction to ISO 10360-5:2010

A common metric used to describe classical CMMs is the maximum permissible error, or $E_{\mathrm{L,MPE}}$, which is calculated according to ISO 10360-2:2009 - *Geometrical product specifications (GPS) — Acceptance and reverification tests for coordinate measuring machines (CMM) - Part 2: CMMs used for measuring linear dimensions* [199]. Also there are a set of metrological characteristics of the probing system which are defined according to ISO 10360-5:2010 - *Geometrical product*

specifications (GPS) — Acceptance and reverification tests for coordinate measuring machines (CMM) - Part 5: CMMs using single and multiple stylus contacting probing systems [138]. However, significant parts of these standards are not applicable to micro-CMMs due to their size and design. The details of this problem are clearly defined elsewhere [200]. The lack of specification standards does not mean, however, that the performance of micro-CMMs is not understood or tested. It is essential that the accuracy of micro-CMMs can be estimated and their traceability confirmed before they are widely accepted and used by precision manufacturing engineers. Therefore, the manufacturers of these micro-CMMs, and various NMIs, advanced users and interested parties, must confirm the capabilities of micro-CMMs using the available specification standards as a guide.

This chapter will highlight how the specification standard ISO 10360-5 can be applied to the NPL vibrating micro-CMM probe. ISO 10360-5 is of immediate interest to anyone wishing to develop a new probing system, as it defines the verification and acceptance tests for CMMs using single (and multiple) contact probing systems.

It should be noted that the applicability of ISO 10360-2 falls out of the scope of this project, as it only defines the acceptance and reverification tests for CMMs used for measuring linear dimensions once their probes have been fully tested. However, the contents of ISO 10360-2 are essential to ensure the full verification of a contacting micro-CMM and, therefore, work is being completed separately to this probe development project to help define how the standard acceptance tests for measuring linear dimensions can be completed on a micro-CMM [200].

A final important aspect of probe use is the application of accepted metrological good practice. Although the contents of the specification standards should allow a user to complete the reverification tests to a suitable degree of accuracy, knowledge of metrological good practice is key to ensure efficient testing, and to gaining the most accurate results. Some of the aspects of good practice use of CMMs is reported in NPL Good Practice Guides 41, 42 and 43 (CMM Measurement Strategies, CMM Verification and CMM probing respectively) [201, 9, 83].

Specification standard ISO10360-5 has extensive information pertaining to the acceptance testing and reverification of contacting CMM probes. For clarity, ISO 10360-1:2001 - *Geometric Product Specification (GPS) – Acceptance and reverification tests for coordinate measuring machines (CMMs) – Part 1: Vocabulary* [11], defines acceptance tests and reverification tests as follows:

- **Acceptance test** – a set of operations agreed upon by the CMM manufacturer and the user to verify that the performance of a CMM is as stated by the manufacturer. This test is performed when the CMM is installed or after any major modification.
- **Reverification test** – a test to verify that the performance of a CMM is as stated by the user and executed according to the same procedures as those of the acceptance test. This test is performed periodically as required by the user (usually every year), or as a

check when the circumstances of the CMM change (*i.e.* environmental excursions, electrical faults or any significant down time).

Also, it is important to note that a third test, the interim check, is also available for the user of a CMM.

- **Interim check** – a test specified by the user and executed between reverifications to maintain the level of confidence is the measurements taken on the CMM. This test can be performed by the user at any time.

A short analysis of the contents of ISO 10360-5 will define which areas are of immediate interest for the development of the vibrating micro-probe, and hence where conformity must be confirmed.

Firstly, the scope of ISO 10360-5 is clearly defined as specifying the acceptance and periodic reverification tests of CMM performance with contacting probing systems. Also, ISO 10360-5 is only applicable to CMMs using contacting probing systems, in a discrete point probing mode, using spherical (or hemispherical) stylus tips. Therefore it is apparent that the vibrating micro-probe, when installed onto a micro-CMM, should conform to ISO 10360-5.

ISO 10360-5 then defines several normative references to other GPS specification standards and also to the BIPM document, *JCGM 200:2012(E/F) - International vocabulary of metrology—Basic and general concepts and associated terms (VIM)* [8]. Following these references, two sections are dedicated to definitions and symbols respectively. Of the fourteen definitions in ISO10360-5 section 3, there are four that will be immediately applicable to the vibrating micro-probe, and will be described in detail later. The remaining terms and definitions relate to multi-stylus parameters, or parameters relating to single styli incorporated onto indexing probe heads and will, therefore, not be considered. For reference, and including the section designation from the specification standard, the four immediately applicable definitions are:

- 3.4 – effective stylus diameter,
- 3.9 – single-stylus form error, P_{FTU},
- 3.10 – single-stylus size error, P_{STU}, and
- 3.14 – maximum permissible single-stylus form error, $P_{\mathrm{FTU,MPE}}$.

The main (technical) sections of ISO 10360-5 are entitled “Section 5 – Requirements for metrological characteristics”, “Section 6 – Acceptance and reverification tests” and “Section 7 – Compliance”. Section 5 clearly describes the main requirements that must be considered for probe verification, and section 6 describes the probe verification tests in detail, including for all single and multi-stylus configurations and angles. Section 7 defines the rules by which the test results should be judged, defining what results can be concluded to be compliant to the specification standard.

The final sections summarise and conclude, suggesting when the various tests should be applied, how the results should be documented and also several notes on how to check the probing system prior to completing a test according to ISO10360-2.

In this chapter, the sections of ISO 10360-5 that are specifically associated with single stylus probes will be described and analysed with respect to the vibrating micro-probe. The assumption that that the novel operation of the vibrating micro-probe is not compliant to ISO 10360-5 will be considered and suitable strategies will be suggested that will allow the probe to be acceptance tested and reverified to a similar degree, once installed on a suitable micro-CMM.

Following the completion of the verification tests, described in Chapter 5, it was concluded that the vibrating micro-probe could conceivably operate in one of two modes of operation: contact and non-contact. The compliance of the probe to ISO 10360-5 will be considered with respect to both of these modes of operation.

6.3 Terms, definitions, and requirements for metrological characteristics when using the probe in contact mode

6.3.1 Metrological characteristics for contact mode

Initial considerations will be taken with respect to the probe operating in contact mode, where the sphere tip is actually a virtual contacting sphere (VSC) tip. In this operating regime, the vibrating micro-probe is considered to be operating as a vibrating contact probe, where physical contact with the surface is made. The three main metrological characteristics of the probe, as described in section 3 of ISO 10360-5, will be addressed. These are: effective VCS tip diameter, form error and size error. The content of section 5 of ISO 10360-5 relating to the operation of the probe, will also be addressed.

6.3.2 Section 3.4 – effective stylus tip diameter

This is the first item in Section 3 of ISO 10360-5 – Terms and definitions - that is applicable to the vibrating micro-probe operating in contact mode. The effective stylus diameter is defined as the diameter used for the tip correction vector when compensating for measured feature sizes, *etc.* It is noted in ISO 10360-5 that this may be a parameter that is established by completing a probing system qualification test and that this test usually involves probing a reference sphere.

As with classical CMMs, most micro-CMMs using contact probes often use a calibrated reference sphere to determine the effective stylus tip diameter. The main exception is the optomechanical probes described in [86, 88] that tend to have their effective stylus tip diameter calibrated by the manufacturer, and recalibrated annually [87]. The more regular qualification test involves probing

the surface of a calibrated reference sphere over several evenly spaced points (usually pole, several points on the equator and several points at 45° inclination) and calculating a resulting Gaussian best fit sphere corresponding to the average diameter of the probe sphere tip.

When considering the VCS tip, the effective VCS tip diameter is directly related to both the physical diameter of the sphere tip and the vibration amplitude of the vector vibration being controlled at any given time. As the probe cannot operate in a static mode, the separate calibration of the effective physical stylus tip diameter is not possible, or useful. Therefore, measurement of the vibration amplitude, as described in Chapter 5, will not be useful either. Instead, a direct measurement on the effective VCS tip diameter should be completed using similar methods to those for classical CMM probes. It is therefore suggested that the effective VCS tip diameter be determined through the measurement of a reference sphere.

It is suggested that the effective stylus tip diameter of classical micro-CMM probes, currently considered by CMM manufacturers and users, and indeed by ISO, as a single number describing the best fit Gaussian diameter, is not suitable for micro-CMM stylus tip qualification because the form deviations of the stylus tips could be a large percentage of the overall uncertainty of the machine [140].

Some level of control can be exerted over the effective VCS tip diameter. This comes about from the definition of the effective VCS tip diameter as a combination of the physical diameter of the stylus tip and the vibration amplitude during operation. The physical stylus tip size and form error experienced by high precision classical, static, contacting sensors, however, may not affect the operation of the NPL vibrating micro-probe. An iterative qualification procedure could be devised that allows for local geometry deviations to be compensated for by the amplitude of the vibration. This would require a large number of points to be taken over the surface of a calibrated reference sphere. The reference sphere should be of a suitable size for the VCS tip used, and calibrated to a suitable uncertainty. It is estimated that a 0.3 mm diameter reference sphere, whose local diameter is calibrated to an uncertainty of 10 nm, should be considered. Following this iterative process, the control algorithm could allow the effective VCS tip diameter to be a constant.

It has been reported that high quality CMM stylus tips can have a full 3D roundness error of around 40 nm [140]. If the control algorithm of the vibrating micro-probe were able to control the vibration of the probe to a fraction of this, any roundness errors inherent to the sphere tip could be compensated for. This level of control is already available in the vertical direction, as is evident for the stability and repeatability results previously presented.

6.3.3 Section 3.9 – single-stylus form error, $P_{\mathbf{FTU}}$

This is defined as the error of indication within which the range of probe tip radii can be determined by a least squares fit of points on a test sphere. For the VCS tip, this could be seen

to be analogous to the repeatability to which the vibration can be established and maintained in any given vector. If the effective VCS tip diameter is a constant, because the vibration amplitude of the probe in any given vector is controlled, the repeatability of that controlled vibration amplitude is an indication of $P_{\mathrm{FTU,VCS}}$. For an isotropic probe, with nanometre level repeatability on vibration amplitude in all vectors, $P_{\mathrm{FTU,VCS}}$ could reach just a few nanometres. Any anisotropy in the vibration of the probe will impact directly on this value.

6.3.4 Section 3.10 – single stylus size error, $P_{\mathbf{STU}}$

This is defined as the error of indication of the difference between the diameter of a least squares fit of points measured on a test sphere and its calibrated diameter. For the VCS tip, this could be seen to be analogous to the accuracy to which the vibration can be controlled in any given vector. If the effective VCS tip diameter is a constant, because the vibration amplitude of the probe in any given vector is controlled, the repeatability of that controlled vibration amplitude is an indication of $P_{\mathrm{STU,VCS}}$. For an isotropic probe, with nanometre level repeatability on vibration amplitude in all vectors, $P_{\mathrm{STU,VCS}}$ could reach just a few nanometres. Again, any anisotropy in the vibration of the probe will impact directly on this value.

In combination, the parameters P_{FTU} and P_{STU} are an indication of the capability of the probe to act as an isotropic, perfect spherically-tipped probe. For the vibrating micro-probe, these two parameters, $P_{\mathrm{FTU,VCS}}$ and $P_{\mathrm{STU,VCS}}$, are an indication of the isotropy of the probe, i.e. how repeatable the vibration is in any given vector, and how accurately the vibration in any given vector can compensate for local geometrical errors in the physical sphere tip to result in a spherical VCS.

6.3.5 Section 3.14 – Maximum permissible stylus form error, $P_{\mathbf{FTU,MPE}}$

This is defined as the extreme value of P_{FTU} permitted by the manufacturer's specifications or by any regulations that are in place. It is noted that the $P_{\mathrm{FTU,MPE}}$ can be specified by a stylus system description. Also, $P_{\mathrm{FTU,MPE}}$ is comparable to $E_{\mathrm{P,MPE}}$ in ISO 10360-2, which is a common descriptor used when describing a CMM.

A maximum permissible stylus form error for the VCS tip, $P_{\mathrm{FTU,MPE,VCS}}$ can be estimated based on its contribution to a desired $E_{\mathrm{P,MPE}}$. Also, as it is closely related to the repeatability and isotropy of the vibrating micro-probe, it can be suggested that

$$P_{\mathrm{FTU,MPE,VCS}} < 20\,\mathrm{nm}.$$

6.3.6 Section 5.1 – single stylus probing error

There are many requirements within Section 5 of ISO 10360-5 – *requirements for metrological characteristics* – that apply to the vibrating micro-probe when operating in a contact mode, but most of them have no specific changes due to the VCS tip. Of the several that are important, there are some noteworthy sections.

The requirement of single stylus probing error states that the single stylus form error must be less than the maximum permissible single stylus form error, or

$$P_{\mathrm{FTU}} < P_{\mathrm{FTU,MPE}}\,.$$

It is noted that $P_{\mathrm{FTU,MPE}}$ can be defined by either the manufacturer (in the case of acceptance testing) or by the user (in the case of reverification testing).

However obvious the statement is when considering the definitions in the previous four sections, the definition of $P_{\mathrm{FTU,MPE}}$ is important because it defines the specification of repeatability of the vibration of the probe. Also, the definition clearly defines that $P_{\mathrm{FTU,MPE}}$ is not necessarily a constant, and can change according to the requirements of the user. In most situations, it is assumed that $P_{\mathrm{FTU,MPE}}$, when defined by the manufacturer, will be larger than when defined by the user.

6.3.7 Section 5.2 – single-stylus probing configuration

It is stated that $P_{\mathrm{FTU,MPE}}$ refers to one specific probe configuration, which is defined by the manufacturer (in the case of acceptance testing) or by the user (in the case of reverification testing), but within very specific limits.

With regards to the vibrating micro-probe, and, in fact, most micro-CMM probes, this section is almost entirely redundant. This is because the user has little, or no, control over the configuration of the probing system. The technology related to the precision probes employed by micro-CMMs is so restrictive due to the complexity of the technology and delicacy of the parts that the user is limited to the materials, lengths, diameters and directions decided by the manufacturer.

This limitation of stylus choice also has implications for the measurement of workpieces after successful qualification and verification. It is suggested in ISO 10360-5 that a specific stylus configuration should be chosen for the measurement task at hand. This suggestion can rarely be realised by micro-CMMs.

6.3.8 Section 5.5 – Styli

In a similar note to section 5.2, this section states that the styli used in the acceptance tests (to be described later) shall be those approved by the manufacturer. The manufacturer will state approved materials, shaft diameters, lengths and stylus tip quality. This is not applicable to the vibrating micro-probe, or indeed most micro-CMM probes, because the styli are not interchangeable. A further requirement of this section is that the stylus lengths used during probe acceptance testing be within 6 mm, or 10 %, whichever is larger, of those defined by ISO. These lengths are 20 mm, 30 mm, 50 mm and 100 mm. Therefore, this requirement is impossible for all but the longest of micro-CMM probes.

6.3.9 Other requirements

There are two further requirements described within section 5 of ISO 10360-5 that are applicable to the verification of the vibrating micro-probe while operating in contact mode. These sections relate to the environmental conditions within which the operation of the CMM is acceptable (section 5.6), and also to the operating conditions and procedures to be followed when completing the probe acceptance or probe reverification tests (section 5.7). These sections are of vital importance to the use of the vibrating micro-probe and will, therefore, be afforded their own section in this chapter.

6.3.10 Summary of the metrological characteristics for contact mode

Several sections of ISO 10360-5 have been considered for their applicability to the vibrating micro-probe. The requirement of **Thesis Objective 3** and specifically **Research Question 3.2** is to ensure that the probe is compliant with these specification standards, several interpretations have been suggested. The main sections considered were the effective VCS tip diameter, and the size, form and probing errors of the probe. Wherever possible and practicable, parameter values have been suggested.

It should be noted that there is a published set of guidelines available for micro-CMMs, VDI/VDE 2617 Part12.1 (2011) *Accuracy of coordinate measuring machines Characteristics and their testing: Acceptance and reverification test for tactile CMM measuring micro-geometries* [24], which is published by the Association of German Engineers. This guideline completes a similar analysis to that contained within this chapter, with respect to the applicability of the ISO 10360 series of specification standards to classical micro-CMM probes and micro-CMMs. The guideline includes a brief description of some pertinent technologies, and includes suggestions for completing acceptance tests on micro-CMMs (both probing acceptance tests and machine acceptance tests). In contrast, this chapter focusses directly on the applicability of existing international specification standards to the operation of the new concept of 3D vibrating micro-CMM probes.

6.4 Terms, definitions, and requirements for metrological characteristics when using the probe in non-contact mode

6.4.1 Metrological characteristics for non-contact mode

At the end of Chapter 5 it was concluded that the vibrating micro-probe was capable of operating in a non-contact mode, where the probe would operate using a virtual non-contact sphere (VNCS) tip. It is important, therefore, to complete some analysis on the possible test procedures for the vibrating micro-probe using a VNCS tip. This analysis will not be exhaustive, because the operation of the probe in contact mode has not yet been fully realised. However, simply extending the tests to the probe working in non-contact mode may not be sufficient, although the analogies are important and should be highlighted. The three main metrological characteristics that will be addressed are; effective VNCS tip diameter, form error and size error. The requirements from section 5 will not be considered.

6.4.2 Section 3.4 – effective stylus tip diameter

The effective VNCS tip diameter is related to the physical diameter of the sphere tip, the vibration amplitude of the vector vibration and the size of the surface interaction force field during any probing operation.

Following on from the concluding remarks on the determination of the effective VCS tip diameter, an additional step can be included to determine the size of the surface interaction force field. It has been confirmed that the surface interaction forces rely heavily on the operational parameters of the probe, and the material parameters of the combined probe and measurement surface system. Therefore, if the determination of the size of the surface interaction force field is completed using the same reference sphere as for the effective VCS tip qualification, the probe will only be qualified to measure features manufactured from the same material to the same surface finish. For any other measurement tasks, the determination of the size of the surface interaction force field should be completed with a reference artefact of similar material and surface properties to the desired measurement surface.

It should be noted that this reference artefact may not need to be a calibrated reference sphere or even a sphere at all. This is because the effect of the surface interaction forces is irrespective of direction, *i.e.* by their nature they are isotropic. This is a useful note, because the main reasons behind wanting to extend the capability of the vibrating micro-probe to non-contact probing is because the use of novel materials in precision engineering applications, although not commonplace, is becoming more apparent. Therefore, the fabrication and subsequent calibration

of a reference sphere manufactured from a novel material, such as HIPE or aerogel [117], polymer or a coated precision optic, is likely to be difficult.

As the effective VNCS tip diameter is analogous to the effective VCS tip diameter plus the size of the surface interaction force field, a determination of the size of the surface interaction force field can be made on a flat surface, and the resulting distance added to the previously determined effective VCS tip diameter. This definition will also have an effect on the determination of the probe point repeatability error that was previously determined for contact probing. The probing point repeatability error requires a reliable determination of the contact point with the surface, which will not be available when using the probe in non-contact mode. Therefore, it is not unlikely that the probe point repeatability error could be as much as doubled if using the probe in a non-contact mode.

6.4.3 Section 3.9 – single-stylus form error, $P_{\mathbf{FTU}}$

For the VNCS tip, this parameter is an indication of the repeatability of a combination of the vibration stability and the detection of the surface interaction forces.

This parameter can be determined during the acceptance or reverification test, using the existing test sphere. However, because the contents of ISO 10360-5 assume that the probes will react similarly to all materials, there is little indication of whether $P_{\mathrm{FTU,VNCS}}$ should be calculated for all relevant materials. A comparison can be drawn to optical sensors, which do react differently when faced with different material surface properties or colours [202]. The problem of material properties is also raised in ISO/CD 10360-8.2 - *Geometrical Product Specifications (GPS) — Acceptance and reverification tests for coordinate measuring machines (CMM) — Part 8: CMMs with optical distance sensors* [203], which states that the materials used in any calibrated test lengths should be suitable for the chosen optical sensor as

> *"different materials have different optical characteristics such as reflectivity, optical penetration depth (volume scattering), colour, scattering characteristics, etc., which means that the values of the probing errors and the value may differ".*

As the vibrating micro-probe's reaction to the surface interaction forces will be similar in repeatability and accuracy regardless of strength due to different materials, it is suggested that it is not necessary to determine $P_{\mathrm{FTU,VNCS}}$ using reference spheres of various materials.

6.4.4 Section 3.10 – single stylus size error, $P_{\mathbf{STU}}$

For the VNCS tip, this is an indication of the accuracy of the vibration coupled with the accuracy of the detection of the surface interaction forces. Similar to $P_{\mathrm{STU,VCS}}$, the determination of $P_{\mathrm{STU,VNCS}}$ can be completed using a standard test sphere.

6.4.5 Summary of the metrological characteristics for non-contact mode

Several sections of ISO 10360-5 have been considered for their applicability to the NPL vibrating microprobe operating in non-contact mode. This work is purposely lacking in detail as little can be surmised without suitable comparisons being made to the probe operating in contact mode. It is expected that operating the probe in non-contact mode will decrease the measurement accuracy of the associated micro-CMM when compared to using the probe in contact mode. However, the virtue of using the VNCS tip is that the lack of surface contact enables delicate and novel materials to be probed without fear of causing any surface damage, and in these situations, increased measurement uncertainty may be acceptable [117].

6.5 Environmental conditions and operating conditions

The specifications of the environmental conditions and operating conditions for CMMs are contained within Section 5 of ISO 10360-5. These two conditions will be discussed separately from the other requirements due to the marked effect they could have on the operation of the vibrating micro-probe, regardless of operation mode.

6.5.1 Section 5.6 - Environmental conditions

Section 5.6 of ISO 10360-5 states that the environmental requirements for completing the acceptance and reverification tests, and indeed for normal operation of the CMM, should be as required by the manufacturer. Section 5.6 also states that it is the responsibility of the user to ensure the environmental conditions are met, and that if the environmental conditions are outside the specified limits, then none of the maximum permissible errors or limits can be required to be verified. These limited requirements are actually well conceived for the purpose of this specification standard in that they do not interfere with the manufacturer's specifications. However, they do ensure that the manufacturer is required to report these specifications. When the operation of micro-CMMs and their probing systems is concerned, the environmental specifications are very stringent.

The national specification from the American Society of Mechanical Engineers, ASME B89.4.1-1997 - *Performance evaluation of CMMs* [198] is more detailed in its description of the environmental conditions than ISO 10360-5. ASME B89.4.1-1997 also includes several tests to determine whether the environmental conditions are suitable. These environmental tests are especially important to micro-CMMs, which are able to take measurements to an uncertainty often comparable to the resolution of classical CMMs, and hence environmental factors could have a significant effect on their operation. ASME B89.4.1 highlights thermal testing, vibration

testing, electrical testing and utility air testing, but other environmental effects that may affect the operation of micro-CMMs could be relative humidity and local air turbulence.

The environmental conditions in which the NPL vibrating micro-probe operates, both in contact and non-contact mode, are critical for its accuracy and repeatability. There are four main environmental considerations which must be highlighted: temperature stability, relative humidity, local mechanical vibration and air turbulence. The following sections will describe these environmental conditions, focusing on the effect they have of the ideal operation of the probe. Several suggestions will be made to define the ideal environmental conditions for operation of the probe. There is also a secondary consideration of MEMS photosensitivity, which will be addressed.

6.5.1.1 Temperature stability

Temperature stability is an important consideration for all dimensional measurement, so much so that specification standard ISO 1:2002 - *Geometrical Product Specifications (GPS) — Standard reference temperature for geometrical product specification and verification* defines the standard reference temperature for geometrical product specification and verification as being fixed at 20 °C [204]. Therefore, any length measurement not taken at 20 °C should be corrected through the use of the co-efficient of thermal expansion of the materials involved.

Temperature stability becomes even more important when considering the operation of micro-CMMs, whose error statements put their maximum permissible error on length measurement in the order of 250 nm. For example, on an aluminium test length, 10 mm long (co-efficient of thermal expansion for aluminium is $20 \times 10^{-6}\,\mathrm{K}^{-1}$ [155]), a temperature rise of 0.5 K would result in a 100 nm increase in the length of that sample, which would be a significant contribution to the error of the measurement result. A change in temperature will not only affect the measurement sample, but also the entire measurement system of CMM and probe. This has a significant effect on measurements taken using micro-CMMs, hence several strategies have been devised to counteract, or quantify the resulting errors.

The effect of temperature change on the vibrating micro-probe can be demonstrated through a set of simple experiments. These involved activating the probe in a stable environment and then altering the temperature while the probe is active. The results of this test, using vibrating micro-probe MP-Ni-6-F, can be seen in figure 6.1.

It can be seen from figure 6.1 that there is a linear relationship between temperature and the vibration amplitude of the probe. The results in figure 6.1 show a temperature rise of 0.6 K resulting in an increase in vibration amplitude of 0.9 µm. Therefore, it can be estimated that a temperature rise of 0.1 K results in a change in amplitude of 150 nm. After the temperature has risen, over the course of one hour, the temperature returns to normal and the probe requires over 1.5 hours to stabilise.

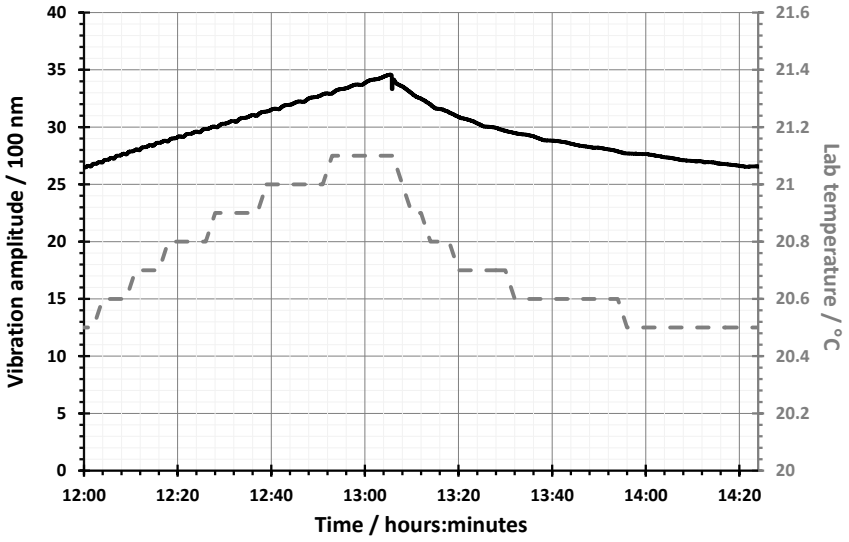

Figure 6.1: Plot of the laboratory temperature (grey dashed line) against measured vibration amplitude (solid black line) over two and a half hours and a temperature excursion of 0.6 °C

A similar trend is seen in the phase data, where the same temperature rise results in a 9° phase change over one hour. It can be estimated, from the linearity coefficients previously calculated in Chapter 5, that a temperature change of 0.1 K could result in a further 15 nm error in the length measuring capability of the vibrating micro-probe. This is a good reason to use the phase information as a detection mechanism, rather than direct amplitude measurements, or inferred amplitude measurements from absolute sensor voltage outputs.

It is essential to ensure the system has reached thermal equilibrium before measurement takes place. This is especially important if the user has been in the same environment as the CMM and, therefore, acted as a heat source, or if the user has been in thermal contact with the CMM or the measurement sample. This effect is counteracted by allowing the measurement system to thermally stabilise. Stabilisation could take several hours depending on the size (and, therefore, thermal mass) of the CMM, the surrounding environment and the material properties of the measurement sample.

Another solution to remove residual thermal drift is to measure all the features on the artefact twice, with the second sequence being measured in reverse order. Then, any effect of any thermal changes can be quantified [205]. Otherwise, it is essential to ensure that the measurement procedure is efficient such that the elapsed time is short and, therefore, any thermal effects can be ignored.

It is concluded that the vibrating micro-probe should operate in a thermally stable environment. The following specifications are suggested: $20\,^{\circ}\mathrm{C} \pm 0.1\,^{\circ}\mathrm{C}$, with no thermal gradients larger than $0.05\,^{\circ}\mathrm{C}$ per hour.

6.5.1.2 Relative humidity

Humidity levels are not usually specified for CMM operation outside of obvious extreme limits. It is usual for the humidity ranges to be wide, for example, 40 %RH ± 20 %RH, and that the operational humidity is usually related to the safe running of the CMM, rather than its detrimental effect on the measurements.

However, the operation of the vibrating micro-probe is greatly affected by humidity changes. There are two main routes by which changes in humidity affect the probe and its operation: changes in humidity which result in changes to the material properties of the piezoelectric actuators and sensors of the probe, and changes in humidity may also result in changes in the strength of the capillary forces which act on the probe during operation.

The effect of humidity on piezoelectric material is well documented [206] and can be observed by completing a similar experiment to that described for the determination of the effect of temperature. The probe is activated and then the relative humidity of the environment is altered. The results of this experiment, using vibrating micro-probe MP-Ni-4-X, are shown in figure 6.2.

It can be seen from figure 6.2 that the surrounding humidity in the laboratory effects the operation of the vibrating micro-probe. Using the previously calculated fitting coefficients, it can be concluded that a slow change of 1 %RH will affect the length measuring capability of the vibrating micro-probe by -10 nm. If the humidity change is fast, the resulting length measuring error could be -20 nm.

It is, therefore, concluded that the vibrating micro-probe should operate in an environment with the following suggested humidity specifications: 50 %RH ± 5 %RH, with no relative humidity gradients larger than 3 %RH per hour.

Also, it is suggested that a polymer encapsulation barrier, deposited onto the flexures, can be used to significantly reduce the effect of humidity changes on the piezoelectric actuators and sensors. As the deposited layer is only several nanometres thick, it is assumed that the mechanical effects of the operation of the vibrating micro-probe will be negligible. It should be noted that this step has already been implemented in several of the Version 9 probes (any probe designated 'P' has been encapsulated in PTFE).

6.5.1.3 Photosensitivity

It has been determined that the triskelion-flexure MEMS device is, as with many MEMS, photosensitive [207]. This effect has not been quantified, and as long as the ambient light intensity remains constant throughout testing, it is assumed that the effect is only systematic and is, therefore, compensated for in the data analysis steps.

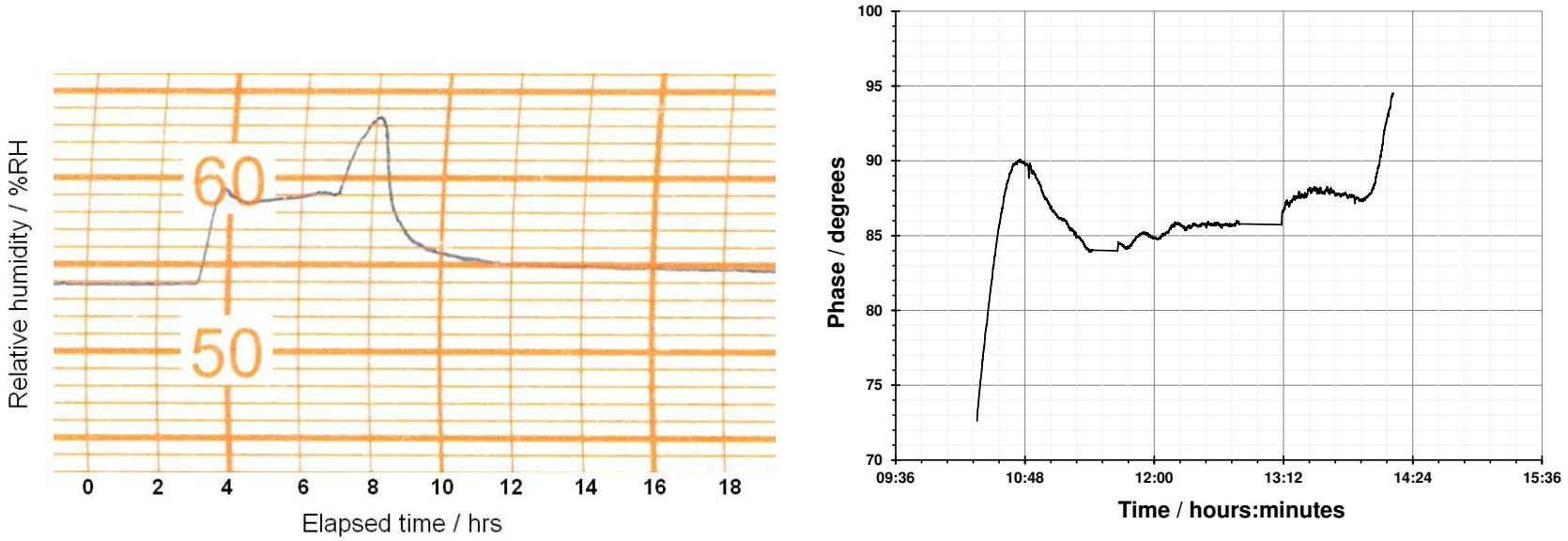

Figure 6.2: Change in humidity in the laboratory (left) and resulting change in measured sensor phase (right). On the left graph (scan of a physical plot) each graduation on the horizontal axis indicates 2 hours. Each graduation on the vertical axis indicates 1 %RH.

6.5.1.4 Local mechanical vibration

The isolation of a CMM from local mechanical vibration is very common, and often relies on the physical mass of the machine coupled with several damping devices. These vibration isolation systems could be either solid isolation pads, more usual for very large and heavy machines, or active air supply damping. The latter is more common in classical CMMs, and is essential for high-precision CMMs. Active continuous air supply systems, which are distinct from active vibration isolation systems, hold the whole CMM on a cushion of compressed air. They act to reduce the effect of external mechanical vibration on the operation of the CMM. These continuous air supply systems damp any low frequency mechanical vibration and act as a levelling system to compensate for the moving mass of the CMM. Typical continuous air supply systems have damping capabilities that filter high frequency mechanical noise.

External mechanical vibration could seriously affect the operation of the microprobe by coupling to the device at its resonance frequency. However, because normal mechanical vibration tend to be below 100 Hz, and most isolation technologies are efficient at damping vibration of about 10 Hz and above, it is unlikely that the operation of the probe will be directly affected by external vibration. Therefore, existing isolation techniques already implemented in micro-CMMs will be adequate.

6.5.2 Section 5.7 - Operating conditions

The conditions for operation during probing error testing are specified in section 5.7 of ISO 10360-5. The main highlighted conditions relate to start-up and warm-up cycles, and cleaning procedures for the stylus tip, tests sphere and reference sphere. These conditions are all pertinent to the operation of the vibrating micro-probe, and consideration should be taken to ensure that all of these points (except for the stylus system configuration and assembly) have been considered.

6.5.2.1 Start-up and warm-up procedures

In ISO 10360-5 part 5.7, the reference to start up and warm up cycles is in reference to those of the CMM itself, *i.e.* drive and motor start up, zeroing operations, stabilising time, *etc.* Similar procedures are, however, needed for the vibrating microprobe.

It is assumed that the start-up procedure is related to the physical start-up of the system, from 'not active' to 'ready for operation'. The warm-up procedure is then related to the stabilisation of the machine; mechanically, thermally and dynamically, before measurement can take place. It is expected that the start-up procedure could take only several minutes, whereas the warm-up cycle could take several hours.

As part of the start-up procedure for the vibrating micro-probe, the actuator strength coefficients will need to be input into the operation software, and some testing programmes can be run, confirming the current status of the probe (such as electrical connections).

Due to the dynamic nature of the vibrating micro-probe, it is essential to ensure thermal equilibrium before operation, which means the warm-up procedures of any CMM being used should be adhered to first. Once the vibrating micro-probe has been installed and initialised (following the start-up procedure), it should be left installed on the machine for at least one hour to ensure thermal equilibrium between the probe and the CMM. During the warm-up procedure, the stability of the probe should be confirmed by operating it in several vibration vector directions and recording the repeatability of the output signals. It is also suggested that the probe is activated for about one minute prior to starting measurement so that the stability of operation can be determined.

The probe should also not be left activated beyond the time required for measurement. Although a robust life-time analysis of the microprobe has not been completed, several test probes were found to be damaged following extensive use (most notably MP-Ni-6-D). This damage was apparent either as physical, usually due to fatigue of the stylus-triskelion device glue joint resulting in the loss of the stylus, or as electrical, resulting in damaged and not working actuators or sensors.

These procedures have been suggested based on experience from using the probe in a laboratory environment. Their content is expected to be a suitable first step in the development of full start-up and warm-up procedures for operation of the probe on a commercial micro-CMM.

6.5.2.2 Cleaning procedures for the stylus tip, tests sphere and reference sphere

It is a requirement of ISO 10360-5 that cleaning procedures are put in place by the manufacturer for the stylus tips of the probing system. This requirement is a serious issue, not only for the operation of the NPL vibrating micro-probe, but also for the operation of all micro-CMM probes. Currently, it is usually suggested that the measuring operation is maintained contaminant free so as to reduce the risk of probe tip contamination. Therefore, test sphere, reference sphere and measurement surface cleaning is of considerable importance.

Due to the delicacy and size of the stylus tips of micro-CMM probes, there are very few mature solutions available for direct cleaning. Several solutions may be useful to consider; delicate manual cleaning under a microscope, dipping the tip in a solvent, or several solvents, or immersing the tip in an ultrasonic bath, or a combination of all of these. All of these solutions are used currently by micro-CMM users, but their effectiveness is limited and completing the cleaning task using these methods is time consuming. Most of the development work being undertaken in the area of probe tip cleaning is being completed by the users of the machines rather than the instrument manufacturers. One recently successful attempt at addressing the cleaning of stylus

tips considers the application of CO_2 snow jet cleaning [208, 209]. The application of this to the vibrating micro-probe may be possible, if the cleaning force of the CO_2 snow jet is low enough to not damage either the probe tip or the flexures, but still be able to clean the surface of the probe tip.

6.5.3 Summary of environmental and operating conditions

Sections 5.6 and 5.7 of ISO 10360-5 have been reviewed with respect to the NPL vibrating micro-probe. These sections were discussed separately from the other requirements due to the marked effect they could have on the operation of the vibrating micro-probe, regardless of operation mode.

It can be concluded that the vibrating micro-probe should operate in a stable environment; $20\,^{\circ}\text{C} \pm 0.1\,^{\circ}\text{C}$, with no thermal gradients larger than $0.05\,^{\circ}\text{C}$ per hour and $50\,\%\text{RH} \pm 5\,\%\text{RH}$, with no relative humidity gradients larger than $3\,\%\text{RH}$ per hour. Also, the micro-probe should be isolated from external mechanical vibration through the use of common vibration isolation techniques.

Several start-up and warm-up procedures have also been suggested, based on the experience gained during the validation of the vibrating micro-probe.

Finally, the issue of micro-probe tip cleaning has been highlighted, although no specific research has been completed with regards to this issue within this project..

6.6 Logistical issues

As well as the previously discussed issues with regards to the application of relevant specification standards, and suitable environmental and operation conditions, there are also logistical issues that arise for the use of a vibrating micro-probe. These are issues associated with the storage, handling and transport. Several of these issues can be associated with any micro-CMM probe due to their delicate nature, however, several issues have specific relevance to the vibrating micro-probe.

6.6.1 Storage

Given previously discussed environmental conditions for the ideal use of the vibrating micro-probe that have been described, it is logical to ensure that any unused probes are stored in the same, or similar, conditions. This will ensure that the constituent materials, especially the glue used in assembly process and the piezoelectric materials, do not degrade. Of course, there is a limit to how long a vibrating micro-probe can remain unused and in storage before it will no

longer operate. As has been previously stated, a full lifetime analysis has yet to be completed on the vibrating micro-probes, but it is estimated that, if storage conditions are similar to the environmental conditions for operation, an unused probe could be stored safely for at least one year.

6.6.2 Handling and mounting

Manual handling operations are unavoidable when dealing with micro-CMMs. These are either related to mounting the workpieces, or changing probes. For classical CMMs, automated systems exist for probe mounting but this is not the case for probes used with micro-CMMs. Probe changes for micro-CMM probes often involve several delicate handling steps, and also mechanical fixing to the CMM.

When developing the vibrating micro-probe and considering the validation tests that had to be completed, careful consideration for the mounting on the experimental setup was taken. To this end, several test solutions were considered for probe mounting to the test setup, which concluded with the system described in figure 5.4. One of the first designs is shown in figure 6.3.

The probe mount shown in figure 6.3 is manufactured from aluminium. It has a recessed section where a triskelion-flexure MEMS chip can be placed, with the contact pads facing upwards. The chip can then be clamped in place using a flexible printed circuit board (PCB), which is screwed into the mount. The PCB has thirteen conductive pads, nominally aligned with the connection pads on the chip. Electrical contact is made with elastomeric connectors, which act as both electrical connectors between the probe and the control electronics, and, due to their elastic nature, help transfer the clamping force from the PCB to the chip.

This probe mount has many disadvantages compared to the actual probe head design used for the validation tests. Firstly, the process of fully mounting the vibrating micro-probe is very time consuming. Also, the manual handling operations are directly on the triskelion-flexure MEMS, usually with tweezers, meaning there is a risk of damage. The probe is also mounted upside down, meaning that assembled probes will be more difficult to test through mechanical contact with the stylus tip.

All of these issues, and several more, are addressed by the probe mounting system designed and manufactured for the validation experiments, as shown in figure 5.5. There is, however, one advantage of the original, over the final, interface; that the triskelion-flexure MEMS chip remains unconstrained before, during, and after testing in the original system. This is not possible in the final mount, as the triskelion-flexure MEMS is physically attached to the connection PCB. This is completed using three small amounts of cyanoacrylate at positions indicated in figure 6.4.

Once the triskelion-flexure MEMS device is mounted on the connecting PCB, it is possible to safely handle the probe, safely mount it to the test head (as long as the operation is completed

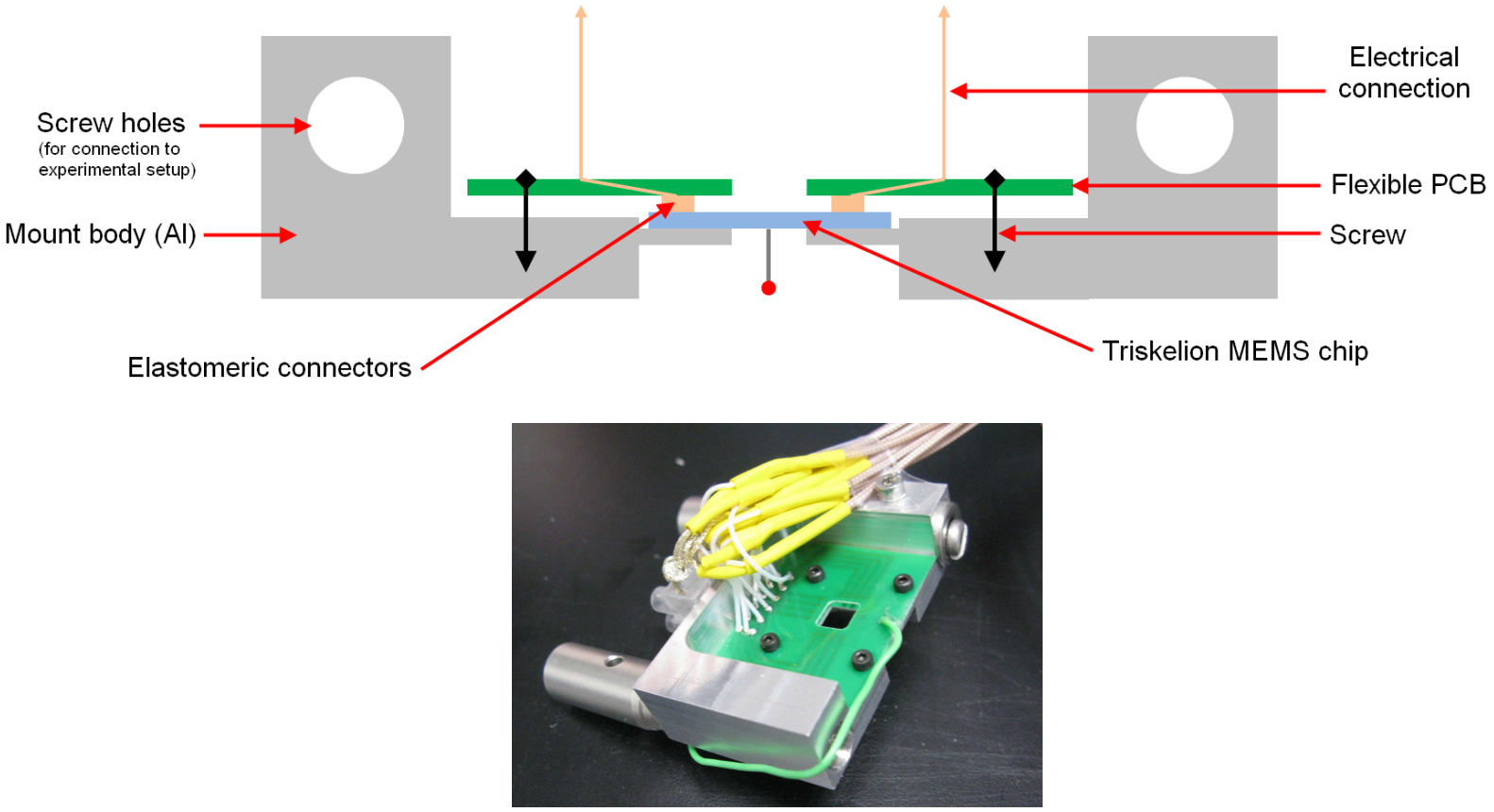

Figure 6.3: An early probe mounting apparatus, schematic diagram (top) and image (bottom)

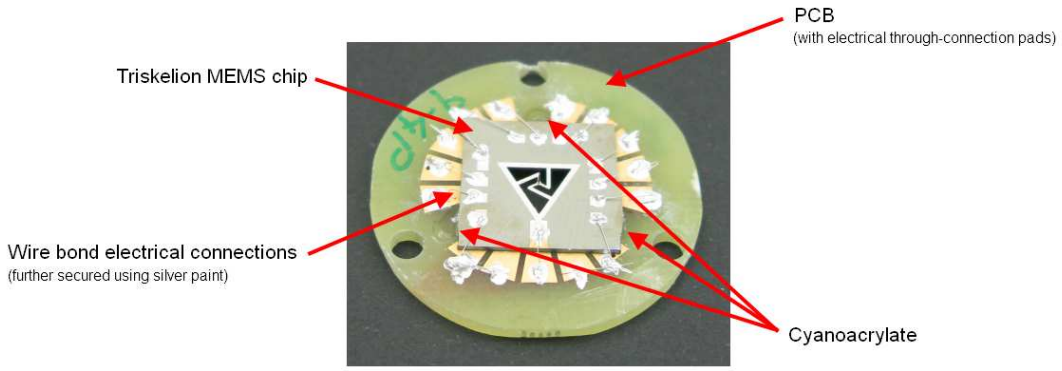

Figure 6.4: The probe mounted on a connection PCB using three small drops of cyanoacrylate glue

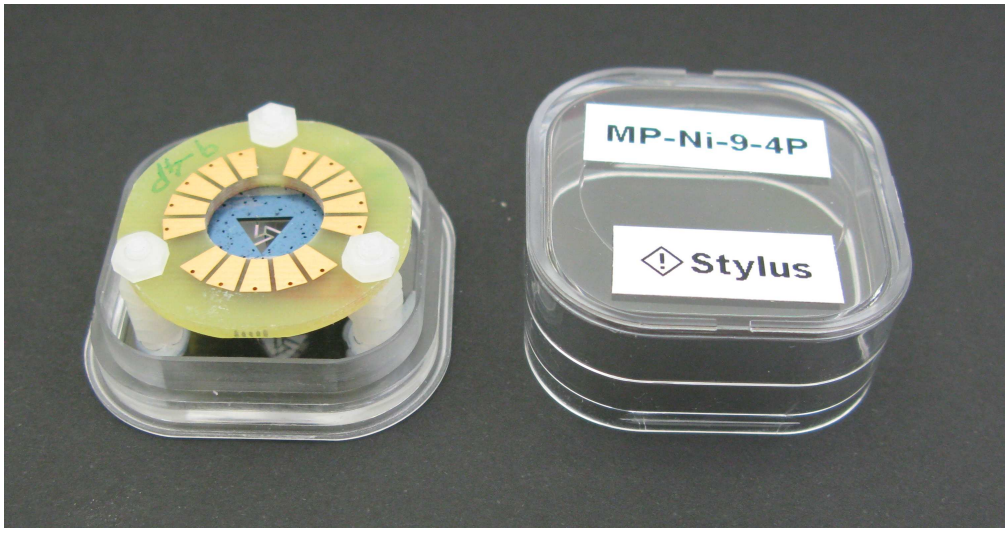

Figure 6.5: Storage boxes designed and manufactured for the vibrating micro-probe

with extreme care) and also safely store the probe. The probes are stored in plastic boxes, such as those shown in figure 6.5.

The vibrating micro-probe is more compliant in comparison to other existing micro-CMM probe systems. The probing system is able to accept displacements of up to two millimetres without over-straining the flexures. This is due to the dynamic nature of the probe, that it was designed to vibrate at amplitudes exceeding several micrometres, and that the resulting flexures have relatively low spring constants. This is a feature that is not exhibited in many classical micro-CMM probes, whose delicate flexures can easily break during mishandling or forceful probing. Common micro-CMM programming errors will not be so destructive to the vibrating micro-probe.

6.6.3 Transport

Similar to the previously mentioned handling considerations, certain precautions should be taken when transporting the vibrating microprobes. Through the use of the storage boxes shown in figure 6.5, the assembled probes have been successfully transported, undamaged, from Germany to the UK by courier. The storage boxes were enclosed within a second, larger, foam lined flight case, which was again packed in a cardboard box filled with polystyrene. The resulting package, measuring 1 m by 0.5 m by 0.4 m, carried five probes (and could conceivable carry up to twenty probes), undamaged via international courier for less than £100.

6.6.4 Summary of logistical issues surrounding the vibrating micro-probe

Several logistical issues relating to the vibrating micro-probe have been highlighted. Several viable solutions have been developed and tested for storage, handling, mounting and transport of the vibrating micro-probe. However, one major issue remains. The issue of probe-tip cleaning is very urgently in need of addressing, such that all micro-CMM probes, including the NPL vibrating micro-probe, can operate efficiently.

6.7 Operational strategies

It is a requirement of **Thesis Question 3.1** that several strategies should be developed for the operation of the vibrating micro-probe. While validating the operation of the probe, several strategies were developed to ensure efficient testing. These strategies will be reported here with respect to the intended operation of the vibrating micro-probe on a micro-CMM. Likewise, similar strategies should be developed for using the probe with a VNCS tip. The operation strategies used for the VNCS tip will be dependent on more experience being gained during more extensive validation of the ability of the probe to operate in a non-contact mode. However, an introduction to possible strategies will be given here.

6.7.1 Operational strategies - VCS

6.7.1.1 Travel speed - VCS

The travel speed of a CMM probe determines how fast the probe moves with respect to the measurement surface, or vice versa. This should not be confused with probing speed, which is the speed at which the probe approaches the measurement surface while taking a measurement.

During the validation tests, there was no distinction between the travel speed and the probing speed, because there was not enough travel length to warrant variable speeds. It is suggested

that the travel speed of the CMM when using the vibrating micro-probe is slower than that of a CMM using a classical micro-CMM probe. This is because any changes in air pressure due to acceleration of the probe could result in false triggering. This point considered, however, unlike classical CMMs, it has become more common for micro-CMM probes to remain stationary while the product table moves [18, 31, 35]. This has several advantages, including that it is possible for the probe to now remain at the Abbe point in the machine, and also, more useful for the operation of the vibrating micro-probe, the probe head is stationary and, therefore, not subject to acceleration forces or air pressure changes.

If the vibrating micro-probe is installed on a CMM whose probe head remains stationary while the measurement table moves, the travel speed need not be restricted. If installed on a CMM with a moving probe head, the vibrating micro-probe will require lower travel speeds than other micro-CMMs using more classical microprobes.

A major consideration of the operation of the probe while travelling is the provision for collision protection. Any micro-CMM probe should remain activated during operation of the micro-CMM, so that any unexpected collisions can be recorded, and any safety procedures (such as an emergency stop) can be activated. Therefore, is it suggested that the vibrating probe remain active at all times while the micro-CMM is in motion. Then, similar collision detection, and any existing safety procedures, can remain in place.

6.7.1.2 Probing speed - VCS

Conversely, the probing speed of a CMM using a vibrating micro-probe will have to be considered carefully. During the validation tests, the test measurement surface was controlled to approach the probe tip at approximately $50\,\mathrm{nm\,s^{-1}}$. This is significantly slower than the normal operating speed of micro-CMMs, which is usually closer to $100\,\mathrm{\mu m\,s^{-1}}$. The testing speeds were slower than intended for operation when installed on a CMM, so that extra data could be collected successfully to fully understand the operation of the probe (approximately ten data points per position, as controlled by the precision manipulation stage). This very slow speed will not be required when the vibrating micro-probe is installed on a micro-CMM. Therefore, a true probing speed of the vibrating micro-probe should be estimated.

Currently, the data output rate of the control software is limited to several tens of hertz. This limitation is due to extra calculations being completed by the software to allow the validation experiments to be completed. It is expected that this data output rate can be increased to, at most, 100 Hz. Given that the typical amplitude of vibration is 1 µm, and that a suitable desired over-travel length would be 500 nm, a suitable probing speed would be $10\,\mathrm{\mu m\,s^{-1}}$. This probing speed is an order of magnitude less than current existing micro-CMM probing systems.

6.7.1.3 VCS surface detection – pre contact

A useful feature of the vibrating micro-probe is its ability to detect the surface interaction forces before physical contact is made with the measurement surface. This feature should allow for the operation of the vibrating micro-probe in a non-contact mode, using the VNCS tip. With regards to contact probing, the ability of the probe to detect these surface interaction forces will allow the system to calculate a warning signal prior to contact. This capability could impact on the previously mentioned probing speed, resulting in possibly two probing speeds being implemented; the pre-probing speed, when the system is moving slow enough to accurately detect the surface interaction forces, but too fast to accurately detect surface contact, and the actual probing speed, where the system has detected the presence of the surface interaction forces and has, therefore, reduced speed ready for surface contact.

Following pre-contact surface detection, the system moves the probe towards the measurement surface at the probing speed, and surface contact is them made.

6.7.1.4 Sampling rate - VCS

The sensitivity of surface detection is dependent on the sampling rate of the probing system. The higher the sampling rate, the more measurements can be taken during probing, both pre-contact and post-contact, and more average measurements can be taken for the determination of the position of the surface. However, the sampling rate of the vibrating micro-probe is heavily dependent on computer power and efficiency of the operational software to calculate the output signals, which depend on averaging calculations over several thousand sampled points, and the completion of several FFT calculations. Currently, the output data rate is 10 Hz. Any increase in this data output rate will result in faster operation of the probe, faster travel speeds, and is ideal for commercial viability of the system.

6.7.1.5 VCS surface detection – post contact

The ability of the probe, coupled with a micro-CMM, to determine the true position of a measurement surface is the principle error source associated with the system. The determination of this error source is the main purpose of the probing error tests described in ISO 10360-5. It is, therefore, essential that any probing strategies used are replicated during the probing error tests and during measurement. An initial indication of the probing errors of the vibrating micro-probe are calculated in Chapter 5

The post contact surface detection operational strategy is identical to that used for the determination of the probing point repeatability error, as described in Chapter 5, section 5.5.3.5.

In the specifications of a CMM probe, the resulting force that the probe imparts on the surface at the measurement point is usually referred to as the probing force. There is a problem with

this definition, because the force imparted on the surface post-contact is often far greater than the probing force. The actual post-contact force, due to over-travel, causes significant damage to the measurement surface. The operational probing strategy for the vibrating micro-probe should be designed to combat this, resulting in little, or no, surface damage, and resulting in a probing force that is comparable to the actual total force imparted on the surface.

To achieve this, the over-travel of the probe will be limited to half of the amplitude of the operating vibration. Through necessity, the amplitude of this reduced vibration must not be below 500 nm if the probe is to successfully counteract the surface interaction forces.

Following this definition, it is now possible to calculate an appreciation of the probing force expected while operating the vibrating micro-probe. A simple description of the probing force can be gained by considering the impulse of the vibrating micro-probe when interacting with the measurement surface. The impulse of an interaction, **J**, can be described as a change in momentum, or

$$\mathbf{J} = \int F\, dt = \Delta \mathbf{p}\,. \tag{6.1}$$

The maximum probing force imparted by the vibrating micro-probe will result from all the kinetic energy of the system transferring to the measurement surface in a period of time considerably shorter than the vibration period. It is therefore estimated that

$$F_{probing} = \frac{m_{\text{eff}} v}{\Delta t}\,, \tag{6.2}$$

where $F_{probing}$ is the estimated probing force, m_{eff} is the effective mass of the vibrating micro-probe system, v is the velocity of the probe and Δt is the time period in which the interaction takes place.

A maximum probing force of approximately 0.02 mN is expected when the probe interacts with the measurement surface at maximum velocity, and the interaction occurs over one tenth of the total vibration period. It is more realistic to assume that the over-travel distance will be in the order of 100 nm, which results in an estimate of the real probing force during true operation of the vibrating micro-probe of 0.01 mN or 10 µN. A similar value has been previously calculated as the probing force for a vibrating surface profilometer probe [210, 211]. It is therefore concluded that this is a reasonable estimate of the contact probing force of the NPL vibrating micro-probe.

6.7.2 Operational strategies - VNCS

A similar set of operational strategies can be developed for the vibrating micro-probe working in a non-contact mode, with the obvious exception of post-contact surface detection. These operational strategies are a best guess, due to lack of experience with working with the VNCS

tip. More in-depth and complete operational strategies can only be developed when further validation experiments have been completed for the probe operating in non-contact mode.

6.7.2.1 Travel speed - VNCS

It is suggested that the travel speed of the vibrating micro-probe working in non-contact mode be similar to that of the probe working in contact mode. This is because in both regimes the pre-detection of the surface interaction forces is used to indicate pre-contact. Similar to the contact mode operation, the probe will remain active at all times, so that any safety systems and collision protection can be implemented. These systems are likely to operate exclusively in contact-mode, as any collisions will negate the operation of the probe in non-contact mode!

6.7.2.2 VNCS Probing speed and surface detection – pre-contact

Probing speed, however, is now significantly different from that of contact-mode operation. During non-contact operation, the VNCS tip will not contact the measurement surface, but will instead interact with the surface interaction forces. The effect of the surface interaction forces can be detected by the probe over a shorter distance to the post-contact detection range; about 100 nm rather than several hundred nanometres. It is, therefore, suggested that the non-contact probing speed should be at least several times slower than that of the probe when operating in contact mode. This is to ensure that the shorter detection distance is not overshot, resulting in unwanted surface contact. It is, therefore, estimated that the probing speed for the probe when operating in non-contact mode will be $1\,\mu m\,s^{-1}$ (if a data output rate of 100 Hz is used).

A further strategy to ensure satisfactory triggering from the surface interaction forces would be to determine each surface point from several approaches. Then the surface position, after compensating for the effective VNCS tip radius, can be determined by averaging the individually determined surface positions.

6.7.2.3 Sampling rate - VNCS

Due to the inevitable reduction in probing speed during operation in non-contact mode, a similar sampling rate to that used in contact mode will result in more data points for determination of the surface position. Also, this number will greatly increase as it has been suggested that pre-contact surface detection should be the result of repeated interactions between the VNCS tip and the measurement surface interaction forces.

6.7.3 Summary of operational strategies

Several operational strategies have been suggested with respect to the vibrating micro-probe operating in a contact mode, as required by **Research Question 3.1**. These strategies were based on knowledge and experience gained during the testing stages of the probe. Several initial parameters have been suggested, including probing speed and sampling rate for the sensing software. Also, a possible strategy for surface detection has been suggested, based on the procedure from the previously completed validation experiments.

When considering the operational strategy for completing measurements in contact mode, an appreciation of the resulting probing force was calculated to be approximately 10 µN. This estimation relies on several assumptions, and also on the mechanical models described in Chapter 4, section 4.4.3. This estimate of the probing force is required by **Research Question 2.2**.

The definition of the operational strategies is an essential pre-requisite for full testing of the vibrating micro-probe on a micro-CMM.

Several operational strategies were also suggested with respect to the probe operating in a non-contact mode. These strategies are not well developed, however, several initial parameters have been suggested, along with a suggested surface detection strategy. It is expected that the operation of the probe in non-contact mode will increase the probing point repeatability error by at least a factor of two.

6.8 Conclusions on strategies for use of the NPL vibrating micro-CMM probe

It is a requirement of **Thesis Objective 3** to ensure that the developed probe could be used in an industrial metrology environment and could adhere to existing specification standards. A review of the operation and the metrological characteristics of the vibration micro-probe was completed, and these were compared to all pertinent sections within ISO 10360-5:2010 [138]. This review directly addresses **Research Question 3.2**. It can be concluded that for every requirement of ISO 10360-5, which focuses on classical, macro-scale probing systems and CMMs, there is an equivalent characteristic of the vibrating micro-CMM probe. Many of the limitations put in place by the ISO 10360 series exclude the vibrating micro-CMM probe due to geometry or mechanical limitations, but this is a problem associated with all micro-CMM probes.

The definitions of the environmental conditions in which the vibrating micro-probe should operate were given particular care, as suggested by ASME B89.4.1-1997 [198]. Several operational requirements were suggested with respect to temperature and humidity for any environment in which the probe will operate. Several logistical issues were also highlighted, especially the problems associated with cleaning micro-CMM probe tips.

Finally, a set of strategies were developed for the probe when operating in a contacting-mode, such that it would perform in a similar manner to existing micro-CMM probes. These strategies defined several important parameters, such as probing speed, and suggested definitions for surface detection strategies. Following these definitions, it can be concluded that, once installed onto a micro-CMM, the probe will be able to operate in a similar manner to existing micro-CMM probes, and any measurements taken using this system will be immediately comparable to measurements taken with a classical micro-CMM probe. This conclusion directly addresses **Research Question 3.1**.

Several of these requirements and strategies were also defined for the probe when operating in a non-contact mode. However, it is expected that these non-contact strategies will require further development as validation tests into the further capability of the vibrating micro-probe are completed.

Chapter 7

Conclusions

The **Thesis Aim** was clearly defined in Chapter 1 as:

"to develop and operate a contacting probe such that it enables existing micro-CMMs to reliably measure sub-100 µm features in three dimensions to an uncertainty below 100 nm".

To address this **Thesis Aim**, which can be considered to be an overall **Aim** for the area of micro-CMM probe development, three **Thesis Objectives** were developed specifically for this work. These **Thesis Objectives** were developed through identification of specific knowledge gaps in this research area. The concluding remarks with regards to these **Thesis Objectives**, along with the seven **Research Questions**, identified as suitable metrics of success, will be reported here.

7.1 Conclusions on the Thesis objectives and research questions

Thesis Objective 1: To develop methods to operate the NPL vibrating micro-CMM probe such that it can counteract the surface interaction forces in 3D, and to test those methods.

- **Research Question 1.1: Can a stylus be designed that has a stylus tip diameter below 100 µm, an aspect ratio similar to existing micro-manufactured features, and is suitable for use with a vibrating micro-CMM probe?**

A stylus was designed with a spherical-tip diameter of 70 µm and an effective working aspect ratio of 16 (the full aspect ratio is 22). When the stylus was analysed for its dynamic properties, its resonance frequency was estimated at 16 kHz. When assembled with the FE model of the

triskelion-flexure MEMS device, it was estimated that the resulting resonance frequency of an assembled vibrating micro-probe would be around 0.9 kHz. It was concluded that it was unlikely that these frequencies would couple, and that if any vibration were to be excited in the stylus through probe actuation, the amplitude would be inconsequential.

This stylus was successfully manufactured through electro-discharge machining and was successfully assembled onto the triskelion-flexure MEMS device to form a working micro-CMM probe [137, 145, 146]. It is, therefore, concluded that it is possible to design and manufacture a stylus that is suitable for use with the NPL vibrating micro-probe. This work is described primarily in Chapter 4, section 4.3.2.

- **Research Question 1.2: Can a vibrating micro-probe be operated with a probe point repeatability of 10 nm?**

A set of models were developed to describe the operation of the vibrating micro-probe, including an analytical model of the expected surface interaction forces and a finite element (FE) model of the physical properties of the vibrating micro-probe and its constituent parts. From these models, the ideal operation of the probe could be modelled, allowing for the development of a vibration algorithm from which the assembled vibrating micro-probes could be controlled and tested experimentally.

Two probes were used to test a procedure for determining the probing point repeatability of the vibrating micro-probe. The results for the two tested probes, MP-Ni-9-9P and MP-Ni-6-I, were 9 nm and 2 nm respectively. When investigating the repeatability of device MP-Ni-9-9P over various experiments and timeframes, the probing point repeatability error ranged from 9 nm to 25 nm. This stemmed from changes in the fitting coefficients.

During the completion of the probing point repeatability tests, a new method of operating the precision manipulation stage was devised in order to achieve a more continuous interaction with the surface. This method aimed to increase the resolution of the experimental results above that of the precision manipulation stage.

It can be concluded that the micro-probe is able to perform to the required specification of a probing point repeatability of 10 nm, an often performs better. However, the experimental setup is not adequate to fully determine the true result. This work is described primarily in Chapter 5, section 5.5.3.5.

- **Research Question 1.3: Can a vibrating micro-probe be operated with a length measuring error over the maximum deflection length of 20 nm?**

Two probes were used to test a procedure for determining the ability of the probe to accurately determine probe tip deflection, also known as linearity. The linearity of the probes was determined using over-travel (or post-contact) data. The results for the two tested probes, MP-Ni-9-9P

and MP-Ni-6-I, were 25 nm and 8 nm respectively. When investigating the repeatability of device MP-Ni-9-9P over various experiments and timeframes, the linearity error ranged from 25 nm to 50 nm.

The results indicated that the post-contact behaviour may not be truly linear, and instead a polynomial approximation may be more realistic. Also, the variability of measurements from experiment to experiment, with fitting coefficients varying by up to 50 %, indicates that the operation and handling procedures for the vibrating micro-probe need to be stringently adhered to, and investigated further.

It is concluded that the vibrating micro-probe is able to operate with a length measurement error of the maximum deflection length of 8 nm to 50 nm. Further investigation into the post-contact behaviour of the probe is required. This work is described primarily in Chapter 5, section 5.5.3.4.

It should be noted that, by combining the repeatability and linearity errors of the tested vibrating micro-probes with the systematic errors of the experimental setup, an expanded probe error ($k = 2$) of MP-Ni-9-9P and MP-Ni-6-I can be estimated at 28 nm and 58 nm respectively. This work is described primarily in Chapter 5, section 5.6.5.

Thesis Objective 2: To develop the concept of isotropy when applied to a 3D vibrating micro-CMM probe

- **Research Question 2.1: Can a new concept of isotropy be developed that related to a vibrating micro-probe, and can this concept be used to test the NPL vibrating micro-CMM probe?**

It is suggested that the isotropy of a vibrating micro-CMM probe is related to the vibration characteristics. Therefore, isotropy for the NPL vibrating micro-probe was defined as its determined ability to vibrate with the same amplitude and frequency in all probing directions. The ability of the micro-probe to act isotropically is determined by the vibration algorithm, which was developed from a mechanical and geometrical model of the probe. Therefore, any test of the isotropy of the probe is also a test of the ability of the vibration algorithm to control the probe. This work is primarily described in Chapter 4, section 4.4.3.

A set of tests were run to determine whether the operation of the probe was similar to that determined by the modelled motion of the probe, as controlled by the vibration algorithm. The tests involved measuring the vibration amplitude of the individual legs of the device during operation. It is concluded that the current vibration algorithm may have the ability to operate the probe isotropically, as some result in the tests indicate the motion of the legs begins to be uncoupled from the first mode of vibration when the vibration frequency corresponds to the full width quarter maximum. However, it should be noted that more consideration must be taken

to ensure that the vibration amplitude does not fall below the required 500 nm. These results are described primarily in Chapter 5, section 5.5.4.

- **Research Question 2.2: Can any indication of the probing force of a vibrating micro-probe be determined?**

The probing force of any micro-CMM probe is of great interest given the current trend for precision manufacturing using novel materials. Therefore, a low probing force is expected from any newly developed micro-probe, especially as these probes aim to have sub-100 µm stylus tips. The theoretical probing force of the vibrating micro-probe, given the ideal vibration frequency and amplitude, was estimated at around 10 µN. This work is primarily described in Chapter 6, section 6.7.1.5.

However, it can be concluded, from all of the tests completed during the experimental stage of this work, that the probe's ability to counteract the surface interaction forces also enables it to operate in a non-contact mode. During the operation of this tactile, non-contact vibrating micro-probe the probing force would be near 0 N.

Thesis Objective 3: To ensure that the developed probe can be used in an industrial metrology environment and can adhere to existing specification standards

- **Research Question 3.1: Can a set of operational strategies be developed for a vibrating micro-probe that proves its ease of use?**

During the development and testing stages of this work, a great deal of experience was gained in the operation of a vibrating micro-CMM probe. This experience related to experimental setup, operating conditions and useful operating strategies. Several operating strategies were developed specifically towards travel speed during use, probing speed, surface detection algorithms (both pre- and post-contact) and sampling rates for operational software. It was concluded that the NPL vibrating micro-probe was able to operate in a similar manner to other micro-CMM probes currently available commercially.

- **Research Question 3.2: Can a vibrating micro-CMM probe be adherent to existing specification standards?**

As well as determining suitable operational strategies for the probe, its adherence to relevant specification standards in the area of co-ordinate metrology was also considered. The operation of the vibrating micro-probe was considered with respect to the relevant sections of ISO 10360, ASPE B89 and VDI/VDE 2617. It was concluded that all sections of these standards that related to the operation and testing of a CMM probe were transferable to a vibrating micro-CMM probe, as long as any size and geometry limitations were compensated for. Due to this conclusion, it

is expected that the use of this probe in an industrial metrology environment will be easier to justify through its adherence to existing specification standards, and through its ability to be directly comparable to existing CMM and micro-CMM probing systems.

7.2 Future work

Throughout the completion of this thesis, it has become apparent that several issues related to the operation and validation of the NPL vibrating micro-CMM probe require further study. These issues had little effect on the successful completion of the thesis, but are pertinent when considering the **Thesis Aim**, and the global **Aim** of developments in the micro-CMM area.

7.2.1 Real probing force

During the completion of this work, some indication of the theoretical probing force expected when using the probe was developed. This estimate was also revised when it became apparent that the micro-CMM probe was able to operate in a non-contact mode (theoretically near zero probing force). However, an indication of the actual probing force would be useful to confirm the theoretical number. This measurement of probing force could be completed in a similar way to classical low-force measurements [151, 152], but will require some careful consideration into the dynamic nature of the operation of the micro-probe.

7.2.2 Probe specific electronics

It became apparent, while completing the experimental validation of the test probes, that the electrical characteristics of each probe are unique. Although a simple low-pass filter was designed to consider the minimum requirements for operation of all the probes, it is expected that more complex band-pass filters, with a certain amount of amplification, specifically tailored to each probe, would result in a better operation of the probe. A possible design for a band-pass filter, with amplification, is shown in Appendix F, along with the operational specifications.

7.2.3 Continuous precision manipulation

One issue relating to the experimental setup, that was noted especially when determining the probing point repeatability and the linearity coefficients, was that the smallest repeatable step that could be realised by the precision manipulation stage was 30 nm. This was one of the limiting factors of the determination of these characteristics, and methods had to be developed to ensure more continuous data was collected. Therefore, it is suggested that a more suitable precision manipulation stage would be one capable of continuous motion at a set, low speed. Also, the use of an external measurement system to determine the position of the measurement surface

would be useful to reduce the uncertainty contribution of the measurement capability of the precision manipulation stage. Therefore, the implementation of a differential laser interferometer to determine test measurement surface motion is also suggested.

7.2.4 Physical isotropy tests

Currently, the isotropy, or anisotropy, of the probe is determined though the interrogation of the individual flexures in comparison to the model of the vibration control algorithm. The results presented indicate that, although the system is not yet performing as expected, that the vibration control algorithm is succeeding in de-coupling the motion of the individual legs and is beginning to promote isotropy. However, the completion of these tests is time consuming, resulting in many other possible implementations of the control algorithm not being fully tested. It is, therefore, suggested that further testing of the isotropy of the probe be completed on a dedicated 3D manipulation stage, such that isotropy can be confirmed through operational means, rather than physical measurements of the motion of the probe. It is therefore suggested that probe be installed on a micro-CMM

7.2.5 Installation of the probe on a micro-CMM

It is essential that any further testing of the NPL vibrating micro-CMM probe happen when installed on a micro-CMM. Through the use of the described operational strategies, the device could be installed and operated such that the true probing error can be determined. Also, further testing of the isotropy and vibration control algorithm will be easier once the probe is installed on a CMM, which can act as a 3D precision manipulation system. Work has begun to install the NPL vibrating micro-probe onto the Isara 400, in collaboration with IBS Precision Engineering, Eindhoven, NL.

7.2.6 Validation of the probe in non-contact mode

It became apparent during the testing and validation stages that the ability of the vibrating micro-probe to counteract the surface interaction forces also enabled it to detect, and possibly trigger from those same forces. Therefore, a set of tests should be completed to validate the probe when operating in non-contact mode. These tests will be similar to those completed to validate the probe in contact mode; however, some changes to the procedure and data processing will be required. These changes will form part of the detailed operational strategies for operation of the micro-probe in non-contact mode.

The ability of the vibrating micro-probe to operate in a non-contact mode will have far reaching implications, especially as the use of new materials become prevalent in precision manufacturing,

e.g. organic materials, aerogels, novel coatings on optics or medical implants, structured surfaces on 3D objects, *etc.*

7.2.7 Design changes to the micro-probe

Throughout the testing stages, several environmental factors proved to be detrimental to the operation of the probe. Two of these factors, humidity and photosensitivity, can be compensated through design changes to the probe. Initially, a barrier layer of PTFE was incorporated into the design of the probe to counteract humidity changes. The ability of this PTFE layer should be confirmed, and other methods for protecting the probe should be considered. One such method may be complete encapsulation of the device.

A similar issue arose during testing where the ambient light intensity affected the absolute set point of the probe. Any changes in light intensity on the surrounding environment caused a systematic error in the average phase reading of the probe when vibrating in free-space. To ensure this did not affect any of the measurements, it was ensured that the ambient light level remained similar during all tests, and the data processing steps negated any small changes that might have occurred. However, during full operation of the probe when installed on a micro-CMM, the ambient light intensity may change significantly as the probe moves around the measurement volume and interacts with a work-piece. Therefore, a method should be developed to ensure this does not adversely affect the operation of the probe. An opaque barrier layer, which could also act as a barrier to humidity changes, should be considered. Also, complete encapsulation of the device in an opaque material may be necessary. This capsule should also act as the commercial packaging for the probe, to also allow safe handling.

7.3 General conclusions

Following the completion of this work, and considering the current conclusions drawn with respect to the **Thesis Objectives** and specific **Research Questions** posed, a more general conclusion can be drawn directed at the **Thesis Aim**.

It is concluded, therefore, that there is scope to confirm that a contacting probe can be designed and operated such that it enables existing micro-CMMs to reliably probe sub-100 µm features in three dimensions to an uncertainty below 100 nm. The NPL vibrating micro-probe, while operating in contact mode, will be able to address this need well, and has the added capability of being able to operate in a non-contact mode.

Appendix A

Surface interaction code

An example of suitable Matlab® code that would describe the developed surface forces interaction model is shown below.

```
echo off;
clear all;
clc;

%% SET UP CONSTANTS FOR PROBE
k1=15;                  % Spring constant of the device in N/m
A0=  0.0000002;         % Initial amplitude of the vibration in m
%Aend=0.0000005;        % End amplitude of the vibration in m
%Ares=0.0000005;        % Resolution of amplitude investigations in m
F0=1500;                % Initial frequency of the vibration in Hz
R=0.000035;             % Probe radius in m
m=k1/(F0)^2;            % Apparent mass of the device in kg

%% SET UP CONSTANTS FOR SURFACE FORCES
        % Capillary
    r=0.00000002;       % Liquid layer 'radius' in m
    gamma=0.07275;      % Surface tension of liquid in N/m
    angle=(85*pi)/180; % Contact angle of the liquid with the probe in degrees
    zstar=4.32675e-10; % Rupture distance in m

        % Electrostatic
    E0=8.85e-10;        % Permitivity of free space in F/m
    U=0.001;            % Potential difference in V

        % Van der Waals
    H=2.1e-20;          % Hamaker constant in J
    sr=0.00000001;      % Combined surface roughness in m

        % Casimir
    hbar=1.05e-34;      % Plank's constant over 2*PI in (m^2*kg)/s
    c=299792458;        % Speed of light in a vacuum in m/s

        % Gravity
    g=9.81;             % Acceleration due to gravity in m/s^2

%% SET UP PARAMETERS FOR ITTERATIONS
res=0.00000001;         % Resolution of calculations in m
Z1=0.000003;            % Starting position for probe stepping

kmax=((Z1)/res);

%% SET UP VIBRATIONS
t=0.000001;             % Time interval in s
n=1000;                 % Number of steps in the vibration
s=[1:n];
T=s'*t;                 % Time array in s
W0=F0*pi*2;             % Frequency in degrees/s
```

```
  V0=A0*sin(T*W0);     % V0 = original vibration
%plot(V0);

    for k=1:kmax;
    V1=V0+(Z1-(k*res));       % V1 = original vibrations with step
    Vel1=A0*t*cos(W0*T);
        if min(V1)<0;
          V2=((V0/A0)*(Z1-(k*res)))+((Z1-(k*res)));
          Vel2=(Z1-(k*res))*t*cos(W0*T);
        else
            V2=V1;
            Vel2=Vel1;
        end;
    V2x(:,k)=V1;
        if min(V2)<0;
            V2=0;
        end;
    V3(:,k)=V2;         % V3 = matrix of all steps
    Vel(:,k)=Vel2;

    end;

    for k=2:kmax;
        D=(Z1-((k-1)*res))-A0;
        Dist(k-1,:)=D;       %:=i
    end;

disp('vibration setup');
plot(Dist);
%plot(Vel);
%plot(V3);

%% CAPILLARY
    for k=1:kmax;
        for j=1:n;
            if V3(j,k)>r
                Fc1(j,k)=0;
            else
                Fc1(j,k)=(4*pi*gamma*cos(angle))./(1+((V3(j,k))./(((3*r)/2)-(V3(j,k)))));
            end;
        end;
      Fc=Fc1;
    end;

disp('capilary force calculated');
%plot(Fc);

%% ELECTROSTATIC
    for k=1:kmax;
        Fe(:,k)=(E0*(U^2)*pi*(R^2))./((V3(:,k).*(V3(:,k))));
    end;

disp('electrostatic force calculated');
%plot(Fe);

%% VAN DER WAALS
for k=1:kmax;
    Fvdw(:,k)=(V3(:,k)./((V3(:,k)).*(sr/2))).*((H*R)./(6.*(V3(:,k)).*(V3(:,k))));
end;

disp('van der waals force calculated');
%plot(Fvdw);

%% CASIMIR
    for k=1:kmax;
        Fcas(:,k)=(hbar.*(pi^3).*R.*c)./(360.*(V3(:,k).*V3(:,k).*V3(:,k)));
    end;

disp('casimir force calculated');
%plot(Fcas);

%% GRAVITY
    for k=1:kmax;
       Fgrav(:,k)=m.*g;
    end;
```

```
disp('gravitational force calculated');
%plot(Fgrav);

%% TOTAL F
    for k=1:kmax;
       Ftotal(:,k)=Fc(:,k)+Fvdw(:,k)+Fcas(:,k)+Fe(:,k);
    end;

disp('total force calculated');
%plot(Ftotal);
%axis manual;
%axis([0 n 0 1]);

%% VELOCITY
    for k=1:kmax;
        %Vel1(:,k)=(V3(:,k)./V0).*T.*(cos(T*W0));
        for j=2:n
        Vel1(j,k)=(V3(j,k)-V3(j-1,k))./t;   %From k=2:n
        end
    end

disp('velocities calculated');
%plot(V3);
plot(Vel1);
%axis manual;
%axis([0 n -0.0010 0.0010]);

%% DAMPING
    for k=1:kmax;
         DCoeff(:,k)=Ftotal(:,k)./Vel1(:,k);
    end;

disp('damping coefficients calculated');
plot(DCoeff);
axis manual;
axis([0 n -1000 1000]);

%% RESULTING AMPLITUDE
   for k=1:kmax;
       if min(V2x(:,k))>0;
          A2(:,k)=(A0).*(exp(-(DCoeff(:,k).*t)./(2*m)));
       else
          A2(:,k)=(Z1-(k*res)).*(exp(-(DCoeff(:,k).*t)./(2*m)));
       end;
   A1=A2;
    end;

A1(isnan(A1))=0;
disp('resulting amplitudes calculated');
plot(A1);
axis manual;
axis([0 n 0 A0*2]);

%% DAMPED VIBRATION
    for k=1:kmax;
         V4(:,k)=(A1(2,k).*sin(W0*T))+(Z1-(k*res));
    end;

disp('damped vibrations calculated');
plot(V4);
axis manual;
axis([0 n 0 0.000005]);
V4(1,:)=zeros;

%% RATIO
    for k=2:kmax-1;
        Ratio(k,:)=((A1(5,k-1))-(A1(5,k)))./res;        %i=:
        %Ratio(k,:)=(((max(V4(k-1,:))-min(V4(k-1,:)))./2)-((max(V4(k,:))-min(V4(k,:)))./2))./res;
    end;

disp('ratio calculated');
scatter(Dist,Ratio,'x');      %k=i
axis manual;
axis ([min(Dist) max(Dist) -1.5 1.5]);
%hold on;
%end;
```

Appendix B

Initial vibration capability

Initial work on an assembled vibrating micro-CMM probe investigated the amplitude of the vibration with respect to varying actuation voltages and offsets [164]. These text were completed with the probe vibrating remote from any test measurement surface. The amplitudes were measured using a laser Doppler vibrometer. These results are shown in figure B.1.

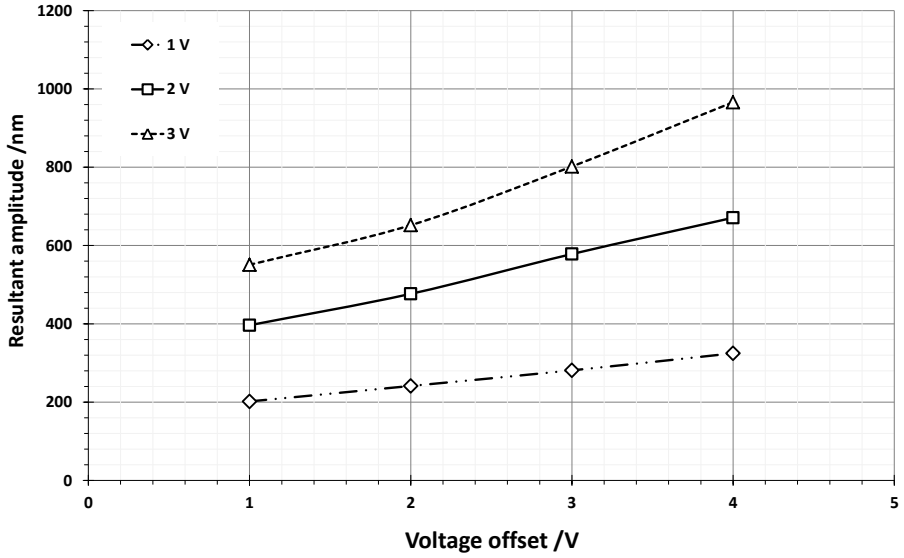

Figure B.1: Measured vibrating micro-CMM probe vibration amplitude with respect to voltage offset on the actuators for three different actuation voltage amplitudes

It can be seen from figure B.1 that a wide range of amplitudes ranging from 200 nm to 1 μm can be achieved with the vibrating micro-CMM probe. These experimental results, when compared to the theoretical minimum required amplitudes (as described in figure 4.20) suggest that the probe has suitable versatility to counteract any surface interaction forces during probing.

Appendix C

Vibrating micro-probes

A list of all vibrating micro-probes manufactured and assembled during this PhD are shown in table C.1.

Table C.1: List of all vibrating micro-probes manufactured and assembled during this PhD

Probe	Approximate date of: Manufacture	Assembly	Notes
MP-Ni-4-3	Before Oct 2008	-	Additional chrome layer added to assist measurement via LDV
MP-Ni-4-7		-	Fixed into 1st Generation holder
MP-Ni-4-8		July 2010	Broken during physical characterisation. Used for assembly trial at TUB
MP-Ni-4-9		August 2010	Successful trial assembly at NPL
MP-Ni-4-X		April 2011	Tested - Surface interaction forces
MP-Ni-6-B	Oct 2010	April 2011	Tested - Surface interaction forces
MP-Ni-6-C		April 2011	-
MP-Ni-6-D		April 2011	Tested - Surface interaction forces - After extensive testing - over 1 year - adhesive bond failed
MP-Ni-6-E		April 2011	-
MP-Ni-6-F		Feb 2013	Used during temperature testing [Subsequently calibrated]
MP-Ni-6-H		-	-
MP-Ni-6-I		Feb 2013	Tested - Linearity and repeatability
MP-Ni-8-1	Sept 2012	-	Error during polling operation - Mechanical model only
MP-Ni-8-2		-	Error during polling operation - Mechanical model only
MP-Ni-8-3		-	Error during polling operation - Mechanical model only
MP-Ni-9-5	Oct 2012	-	-
MP-Ni-9-2P		Feb 2013	[Tested - Linearity and repeatability]
MP-Ni-9-4P		Feb 2013	[Tested - Linearity and repeatability]
MP-Ni-9-6P		-	-
MP-Ni-9-9P		Feb 2013	Tested - Linearity and repeatability

Appendix D

Fact Sheets

As part of the initial characterisation of these probes, a set of "Fact Sheets" were produced, allowing easy access to the pertinent data required to operate the probe during testing. The Fact Sheet for MP-Ni-9-4P is shown in figure 5.9. Several other Fact Sheets are shown below. The Fact Sheet for MP-Ni-6-I is conspicuous in its absence, as it was not compiled before the probe was irreparably damaged.

MP-Ni-9-2P

Images:

Front **Back**

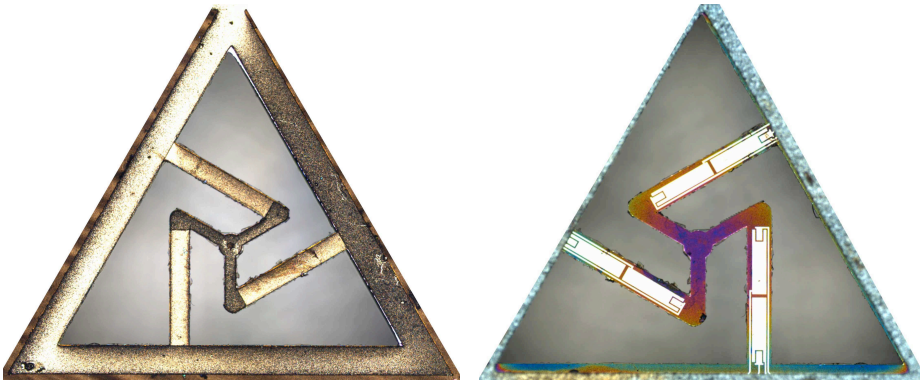

First natural frequency:

2.195 kHz

Actuators:

Actuator designation	Working	Test freq In kHz	Amplitude at 1 V / µm	Voltage for 1 µm / V	Amplitude at 5 V	Amplitude at 10 V
Leg 1 – AI	Y	2.159	0.07	X	0.26	1.35
Leg 1 – AO	Y	2.159	0.06	X	0.22	0.92
Leg 2 – AI	Y	2.159	0.05	X	0.16	0.36
Leg 2 – AO	Y	2.159	0.04	X	0.13	0.27
Leg 3 – AI	Y	2.159	0.04	X	0.16	0.37
Leg 3 - AO	Y	2.159	0.04	X	0.16	0.37

Frequency response of 1AO – 5 V p2p:

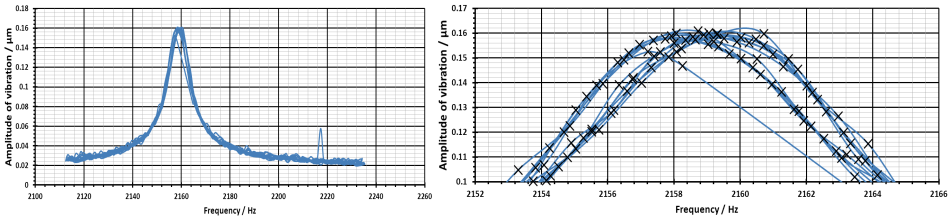

Sensors:

Sensor designation	Working	Amplitude jump / V	Phase peak / degrees
Leg 1 – SI	N	X	X
Leg 1 – SO	N	X	X
Leg 2 – SI	N	X	X
Leg 2 – SO	N	X	X
Leg 3 – SI	N	X	X
Leg 3 - SO	N	X	X

Figure D.1: The Fact Sheet for vibrating micro-probe MP-Ni-9-2P.

MP-Ni-9-4P

Images:

Front **Back**

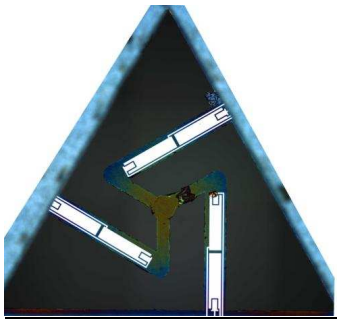

First natural frequency:

2.184 kHz (2nd natural frequency - ≈ 4.380 kHz)

Actuators:

Actuator designation	Working	Test freq In kHz	Amplitude at 1 V / µm	Voltage for 1 µm / V	Amplitude at 5 V	Amplitude at 10 V
Leg 1 – AI	Y	2.1835	0.63	1.620	X	X
Leg 1 – AO	Y	2.183	1.95	0.505	X	X
Leg 2 – AI	Y	2.183	4.75	0.273	X	X
Leg 2 – AO	Y	2.182	8.10	0.120	X	X
Leg 3 – AI	Y	2.1825	5.40	0.177	X	X
Leg 3 - AO	Y	2.182	8.00	0.120	X	X

Frequency response of 1AO – 1 V p2p:

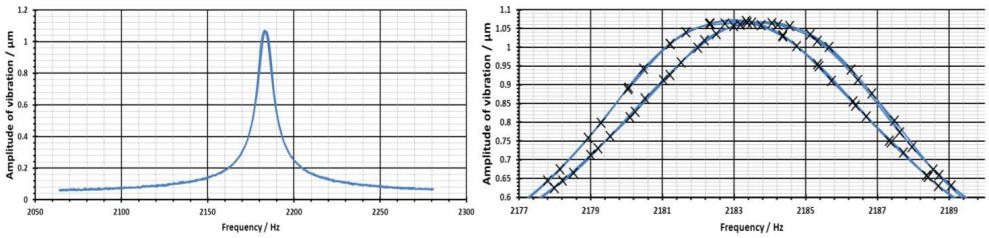

Sensors:

Sensor designation	Working	Amplitude jump / V	Phase peak / degrees
Leg 1 – SI	Y	0.15	5.5
Leg 1 – SO	Y	0.05	3.25
Leg 2 – SI	N	X	X
Leg 2 – SO	Y	0	0.2
Leg 3 – SI	Y	< 0.05	2.2
Leg 3 - SO	Y	< 0.05	0.75

Figure D.2: The Fact Sheet for vibrating micro-probe MP-Ni-9-4P.

MP-Ni-9-5

Images:

Front **Back**

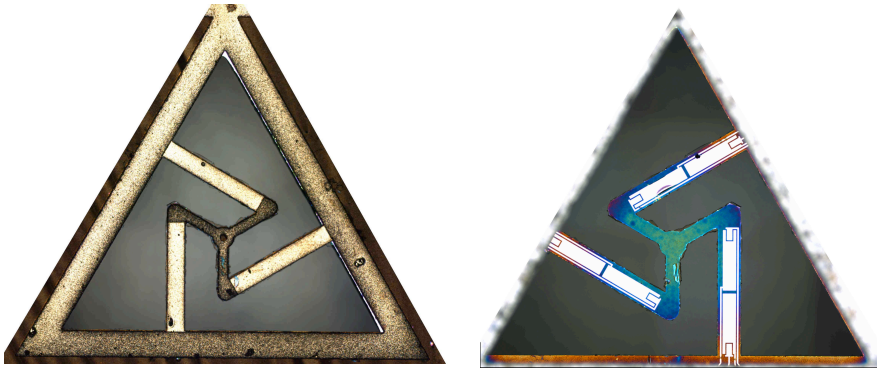

First natural frequency:

2.185 kHz

Actuators:

Actuator designation	Working	Test freq In kHz	Amplitude at 1 V / µm	Voltage for 1 µm / V	Amplitude at 5 V	Amplitude at 10 V
Leg 1 – AI	Y	2.186	0.04	X	0.07	0.1
Leg 1 – AO	Y	2.186	0.05	X	0.08	0.14
Leg 2 – AI	Y	2.186	0.03	X	0.05	0.09
Leg 2 – AO	Y	2.186	0.03	X	0.07	0.12
Leg 3 – AI	Y	2.186	0.02	X	0.05	0.09
Leg 3 - AO	Y	2.186	0.04	X	0.08	0.12

Frequency response of 2AI – 5 V p2p:

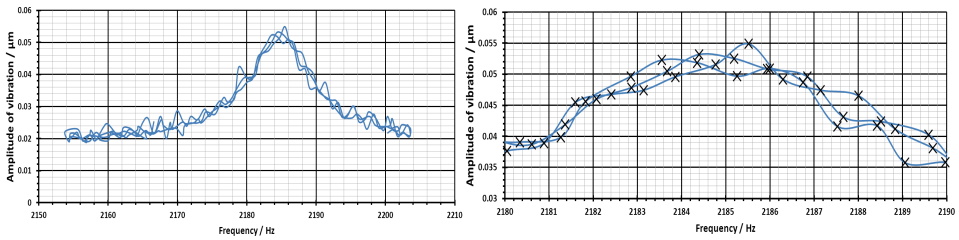

Sensors:

Sensor designation	Working	Amplitude jump / V	Phase peak / degrees
Leg 1 – SI	X	X	X
Leg 1 – SO	X	X	X
Leg 2 – SI	X	X	X
Leg 2 – SO	X	X	X
Leg 3 – SI	X	X	X
Leg 3 - SO	X	X	X

Figure D.3: The Fact Sheet for vibrating micro-probe MP-Ni-9-5.

MP-Ni-9-6P

Images:

Front **Back**

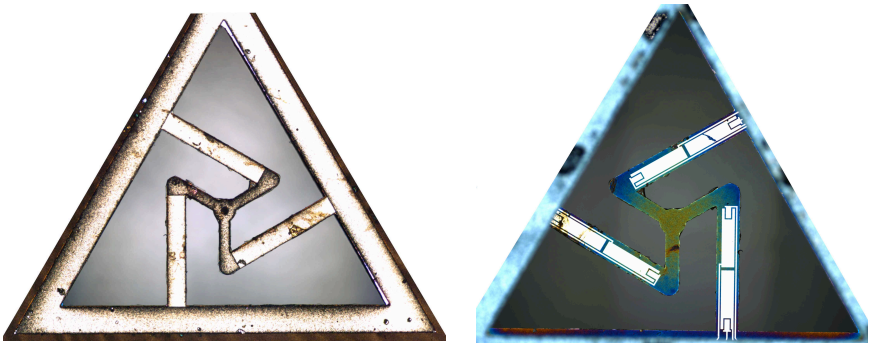

First natural frequency:

2.175 kHz

Actuators:

Actuator designation	Working	Test freq In kHz	Amplitude at 1 V / µm	Voltage for 1 µm / V	Amplitude at 5 V	Amplitude at 10 V
Leg 1 – AI	Y	2.174	0.04	X	0.06	0.10
Leg 1 – AO	Y	2.174	0.04	X	0.08	0.15
Leg 2 – AI	Y	2.174	0.04	X	0.08	0.13
Leg 2 – AO	Y	2.174	0.04	X	0.09	0.16
Leg 3 – AI	Y	2.174	0.04	X	0.07	0.12
Leg 3 - AO	Y	2.174	0.04	X	0.09	0.15

Frequency response of 1AI – 5 V p2p:

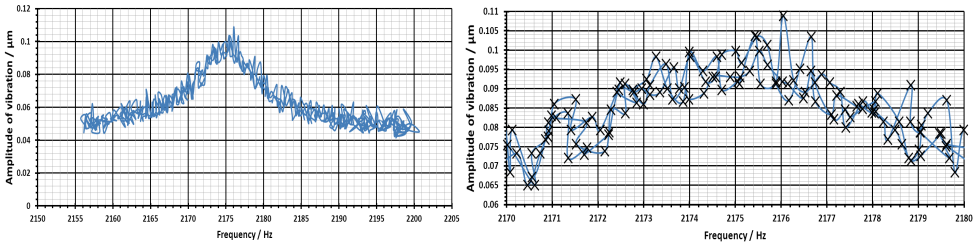

Sensors:

Sensor designation	Working	Amplitude jump / V	Phase peak / degrees
Leg 1 – SI	X	X	X
Leg 1 – SO	X	X	X
Leg 2 – SI	X	X	X
Leg 2 – SO	X	X	X
Leg 3 – SI	X	X	X
Leg 3 - SO	X	X	X

Figure D.4: The Fact Sheet for vibrating micro-probe MP-Ni-9-6P.

Appendix E

Control and sensing software and raw data example

An example of a pseudo-code implementation of the control and sensing software is shown overleaf.

Approximately 17 000 lines of data were collected in the trial experiment with MP-Ni-6-D, but an appreciation of several lines of raw data is shown in table E.1. Several columns of repeat data for all the sensors have been removed.

Control and sensing software

1. Input start parameters:
   (a) Precision manipulation stage - start position, end position, step height and set point variation (as described in section 5.5.3.4).
   (b) FPGA hardware - sample rate and packet size.
   (c) Control signals - output frequency, signal amplitude and phase offset of each of the six control signals.
2. Initialise and reset the precision manipulation stage and operate:
   (a) according to previously input start parameters,
   (b) on a separate processor to the FPGA hardware,
   (c) indefinitely until program finishes, or is terminated by the user.
3. Initialise the FPGA hardware according to previously input start parameters.
4. Output channels operate:
   (a) according to the previously input start parameters,
   (b) indefinitely until program finishes, or is terminated by the user.
5. Input channels sample:
   (a) according to the previously input start parameters,
   (b) indefinitely until program finishes, or is terminated by the user.
6. Data processing on each individual input channel occurs as follows:
   (a) collect data in packets according to the previously input start parameters,
   (b) calculate the frequency, amplitude and phase (with respect to a predefined input signal) for each packet.
7. Output results of data processing operation, including current time, current precision manipulation stage position and an error indicator. An example of this output is shown in table E.1.

Table E.1: Several lines of raw data from the trial experiment

Frequency LDV /Hz	Amplitude LDV /V	Phase shift LDV /deg	Frequency SL2I /Hz	Amplitude SL2I /V	Phase Shift SL2I /deg	[Various sensor signals]	Nanocube position /µm	Time	Remaining elements
1508.641	0.825	57.849	1509.021	1.664	126.333		49.979	11:25:17.53	88686
1509.031	0.971	50.696	1509.005	1.490	125.741		49.981	11:25:17.64	72900
1509.009	1.002	49.197	1509.005	1.483	125.687		49.981	11:25:17.74	58140
1509.012	1.006	48.721	1508.997	1.486	125.640		49.974	11:25:17.83	42345
1509.000	1.009	48.450	1508.999	1.494	125.614		49.978	11:25:17.94	64431
1509.006	1.012	48.521	1508.999	1.493	125.602		49.988	11:25:18.03	48703
1508.995	1.013	48.514	1509.006	1.494	125.624		49.978	11:25:18.13	35073
1509.009	1.014	48.588	1509.004	1.484	125.647		49.980	11:25:18.24	19395
1509.001	1.011	48.480	1509.003	1.482	125.657		50.008	11:25:18.33	5778
1508.998	1.012	48.411	1509.003	1.493	125.607		50.015	11:25:18.44	0
1508.994	1.012	48.435	1508.999	1.493	125.587		50.014	11:25:18.53	0
1508.992	1.008	48.601	1509.003	1.500	125.602		50.013	11:25:18.64	0
1509.010	1.007	48.643	1508.999	1.489	125.637		50.023	11:25:18.74	0
1509.002	1.010	48.614	1509.002	1.502	125.654		50.023	11:25:18.83	0
1508.999	1.013	48.554	1509.001	1.482	125.584		50.024	11:25:18.94	0
1509.008	1.011	48.452	1509.000	1.487	125.558		50.019	11:25:19.03	0
1508.993	1.008	48.541	1508.998	1.483	125.608		50.015	11:25:19.14	0
1508.999	1.007	48.708	1508.998	1.494	125.678		50.022	11:25:19.24	0
1509.004	1.013	48.586	1509.001	1.491	125.651		50.020	11:25:19.33	0
1509.005	1.007	48.629	1508.999	1.489	125.595		50.064	11:25:19.44	0
1509.001	1.007	48.635	1509.003	1.489	125.573		50.056	11:25:19.53	0
1509.003	1.011	48.691	1509.002	1.492	125.604		50.056	11:25:19.64	0
1508.994	1.010	48.655	1508.991	1.481	125.649		50.056	11:25:19.74	0
1508.995	1.008	48.618	1508.996	1.486	125.642		50.066	11:25:19.83	0
1509.004	1.010	48.630	1509.001	1.501	125.588		50.062	11:25:19.94	0
1509.001	1.011	48.714	1509.001	1.505	125.560		50.065	11:25:20.03	0
1508.996	1.009	48.607	1508.996	1.496	125.632		50.062	11:25:20.13	0
1509.008	1.008	48.703	1509.005	1.489	125.646		50.055	11:25:20.24	0
1508.994	1.011	48.643	1508.997	1.494	125.624		50.051	11:25:20.33	0

Appendix F

Band-pass filter

A possible design for a band-pass filter is shown in figure F.1. The desired characteristics for this filter for vibrating micro-probes MP-Ni-6-I and MP-Ni-9-9P are shown in table F.1. The resulting characteristics of these filters are also presented, when the component values are restricted to standard values in the E96 sequence (resistors) and E6 sequence (capacitors). The component selection was completed with the aid of MultiSim 12.0 from National Instruments [187].

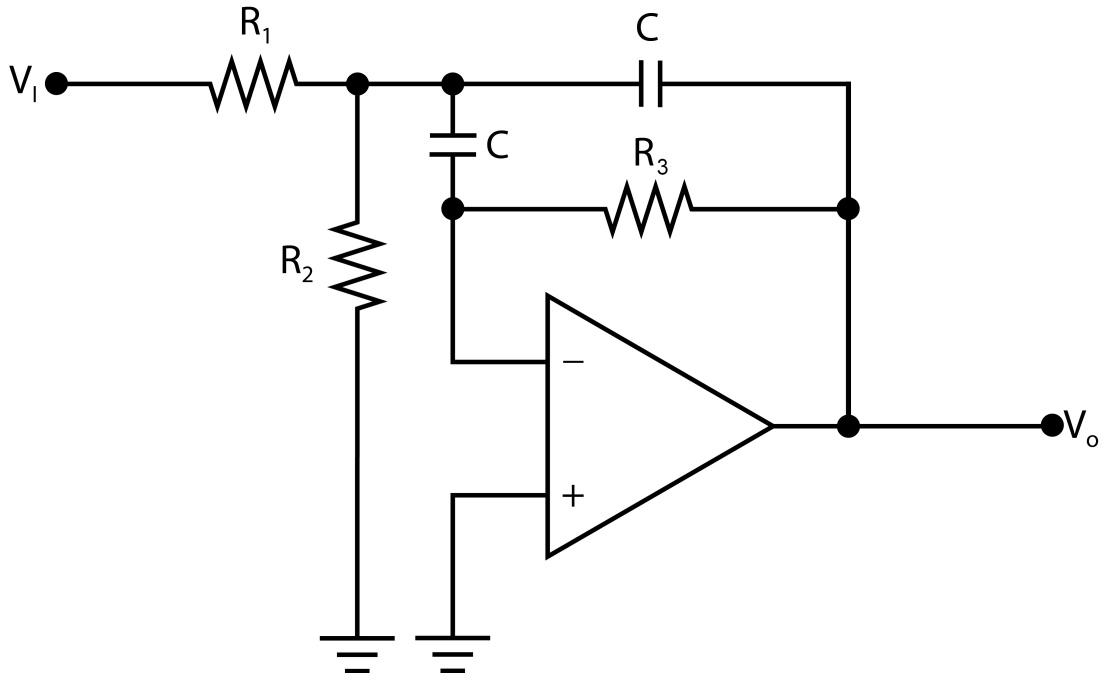

Figure F.1: Circuit diagram of a simple band-pass filter, suitable for use with the vibrating micro-probe

Table F.1: Desired characteristics, selected components and resulting characteristics of band-pass filters for use with specific vibrating micro-probes.

MP-Ni-6-I

Desired characteristics		**Component values**		**Output characteristics**	
f_0	1 320 Hz	R_1	3.65 kΩ	f_0	1 323 Hz
Q	10	R_2	191 Ω	Q	10.0
Gain	10	R_3	73.2 kΩ	Gain	10.0
		C	33 nF		

MP-Ni-9-9P

Desired characteristics		**Component values**		**Output characteristics**	
f_0	1 440 Hz	R_1	1.62 kΩ	f_0	1 450 Hz
Q	10	R_2	84.5 Ω	Q	10.0
Gain	10	R_3	32.4 kΩ	Gain	10.0
		C	68 nF		

Bibliography

[1] Brousseau, E., Dimov, S. & Pham, D. Some recent advances in multi-material micro-and nano-manufacturing. *The International Journal of Advanced Manufacturing Technology* **47**, 161–180 (2010).

[2] Hume, K. *Engineering metrology* (Macdonald, London, 1970), 3rd edn.

[3] Leach, R. K. *Fundamental Principles of Engineering Nanometrology* (Elsevier, Amsterdam, NL, 2010), 1 edn.

[4] Evans, C. *Precision Engineering: and evolutionary view* (Cranfield Press, Bedford, UK, 1989).

[5] Thomas, G. G. *Engineering Metrology* (Butterworths, 1974).

[6] Bosch, J. (ed.) *Coordinate measuring machines and systems* (Taylor & Francis, 1995), first edit edn.

[7] Bureau International des Poids et Mesures. 17th General Conference on Weights and Measures - Resolution 1 (Sevres, Paris, FR, 1983).

[8] Bureau International des Poids et Mesures. JCGM 200:2012(E/F) - International vocabulary of metrology - Basic and general concepts and associated terms (VIM), 3rd edn. (Sevres, Paris, FR, 2012).

[9] Flack, D. NPL Good Practice Guide 42: CMM Verification - Issue 2. Tech. Rep., National Physical Laboratory, Teddington, UK (2011).

[10] McKeown, P. The role of precision engineering in manufacturing of the future. *CIRP Annals-Manufacturing Technology* **36**, 495–501 (1987).

[11] ISO 10360-1:2001 - Geometrical Product Specifications (GPS) - Acceptance and reverification tests for coordinate measuring machines (CMM) - Part 1: Vocabulary (International Organisation for Standardisation, Geneva, CH, 2001).

[12] Hermann, G. Geometric error correction in coordinate measurement. *Acta Polytechnica Hungarica* **4**, 47–62 (2007).

[13] Durakbasa, M. Utilization of co-ordinate measurement technique in biomedicine to evaluate the shape of non-technical structures. *Measurement* **33**, 157–161 (2003).

[14] Peggs, G., Lewis, A. J. & Oldfield, S. Design for a Compact High-Accuracy CMM. *CIRP Annals - Manufacturing Technology* **48**, 417–420 (1999).

[15] Leach, R. K. *et al.* Advances in traceable nanometrology at the National Physical Laboratory. *Nanotechnology* **12**, R1 (2001).

[16] Lewis, A. J. Fully traceable miniature CMM with submicrometer uncertainty. *Proc. SPIE* **5190**, 265–276 (2003).

[17] Vermeulen, M., Rosielle, P. & Schellekens, P. Design of a high-precision 3D-coordinate measuring machine. *CIRP Annals - Manufacturing Technology* **47**, 447–450 (1998).

[18] Küng, A., Meli, F. & Thalmann, R. Ultraprecision micro-CMM using a low force 3D touch probe. *Meas. Sci. Technol.* **18**, 319–327 (2007).

[19] Brand, U. & Kirchhoff, J. A micro-CMM with metrology frame for low uncertainty measurements. *Measurement Science and Technology* **16**, 2489–2497 (2005).

[20] Seggelen, J. *et al.* An Elastically Guided Machine Axis with Nanometer Repeatability. *CIRP Annals - Manufacturing Technology* **54**, 487–490 (2005).

[21] Fan, K.-C., Fei, Y., Yu, X., Wang, W. & Chen, Y. Study of a noncontact type micro-CMM with arch-bridge and nanopositioning stages. *Robotics and Computer-Integrated Manufacturing* **23**, 276–284 (2007).

[22] Kramar, J. *et al.* Toward nanometer accuracy measurements. In *Microlithography 99*, vol. 3677, 1017–1028 (International Society for Optics and Photonics, SPIE, 1999).

[23] Takamasu, K., Fujiwara, M., Yamaguchi, A., Hiraki, M. & Ozono, S. Evaluation of Thermal Drift of Nano-CMM Basic concept of Nano-CMM Thermal drift of Nano-CMM. In *2nd International Conference of the European Society for Precision Engineering and Nanotechnology*, 1–4 (Turin, Italy, 2001).

[24] VDI/VDE 2617 Part12.1 (2011) Accuracy of coordinate measuring machines - Characteristics and their testing: Acceptance and reverification test for tactile CMM measuring microgeometries (Verein Deutcher Ingenieure, Berlin, DE, 2011).

[25] F25 - Measuring Nanometres (Carl Zeiss Industrial Metrology GmbH, 2006).

[26] Vermeulen, M. *High-precision 3D-coordinate measuring machine: design and prototype-development.* Phd thesis, Technische Universiteit Eindhoven, NL (1999). URL `http://www.narcis.info/publication/RecordID/oai:library.tue.nl:527295`.

[27] Wagener, M., Grow, C. & Haertig, F. F25 from Carl Zeiss - PTB Confirms Very High Accuracy. URL `http://www.zeiss.com/C1256A770030BCE0/WebViewAllE/4F5E112E153BE0D3C125756A003DEB44`. Accessed: 1st March 2013 (2009).

[28] IBS Precision Engineering. Isara 400 - Next generation ultra-precision coordinate measuring machine. URL `http://www.ibspe.com/public/uploads/content/files/Isara400\_Webversion.pdf`. Accessed: 8th August 2013.

[29] Zhang, G. A study on the Abbe principle and Abbe error. *CIRP Annals - Manufacturing Technology* **38**, 525–528 (1989).

[30] Bryan, J. The Abbé principle revisited: an updated interpretation. *Precision Engineering* **1**, 129–132 (1979).

[31] Widdershoven, I., Donker, R. & Spaan, H. Realization and calibration of the Isara 400 ultra-precision CMM. *J. Phys: Conf. Series* **311**, 1–5 (2011).

[32] Spaan, H., Donker, R. & Widdershoven, I. Isara 400: development of an ultraprecision CMM for 3D measurement of large parts. *Proc. ASPE Spring Meeting* (2009).

[33] SIOS Messtechnik GmbH. Nanopositioning and Nanomeasuring Machine - NMM-1. URL `http://www.sios.de/ENGLISCH/PRODUKTE/NMM-1\_e\_2013.pdf`. Accessed: 18th August 2013 (2013).

[34] Werth Messtechnik. Werth VideoCheck UA - Measurement in the Submicron Range - most accurate multi-sensor coordinate measuring machine worldwide. URL `http://www.werth.de/en/unser-angebot/products/multisensor-cmms/for-laboratory-and-inspection-room/werth-videocheck-ua.html`. Accessed: 12th December 2013.

[35] Xpress Precision Engineering. Trinano N100 nano CMM. URL `www.trinano.eu/n100.php` (2012).

[36] Bos, E. J. C., Delbressine, F. & Haitjema, H. High-accuracy CMM metrology for micro systems. *VDI BERICHTE* 511–522 (2004).

[37] McMurtry, D. R. Probes (U.S. Patent and Trademark Office., 1979).

[38] Hocken, R. J. & Pereira, P. (eds.) *Coordinate Measuring Machines And Systems* (Taylor & Francis, 2012), 2nd edn.

[39] Weckenmann, A., Estler, T., Peggs, G. & McMurtry, D. R. Probing systems in dimensional metrology. *CIRP Annals - Manufacturing Technology* **53**, 657–684 (2004).

[40] Peggs, G., Lewis, A. J. & Leach, R. K. Measuring the Metrology Gap-Three-Dimensional Metrology at the Mesoscopic Level. *Journal of Manufacturing Processes* **6**, 117–124 (2004).

[41] Thalmann, R. Novel design of a one-dimensional measurement probe. *Proceedings of SPIE* **4401**, 168–174 (2001).

[42] Meli, F. *et al.* High precision, low force 3D touch probe for measurements on small objects. In *4th International Conference of the European Society for Precision Engineering and Nanotechnology*, May, 411–414 (Aachen, DE, 2003).

[43] van Vliet, W. & Schellekens, P. Accuracy limitations of fast mechanical probing. *CIRP Annals - Manufacturing Technology* **45**, 483–487 (1996).

[44] Meli, F. & Küng, A. AFM investigation on surface damage caused by mechanical probing with small ruby spheres. *Measurement Science and Technology* **18**, 496–502 (2007).

[45] Puttock, M. & Thwaite, E. *Elastic compression of spheres and cylinders at point and line contact*. 25 (Commonwealth Scientific and Industrial Research Organization, Melbourne, Australia, 1969).

[46] Mecartex SA. 3D Nanotouch Probe - Ultraprecision Coordinate Measuring Machines for Small Parts. URL `http://www.mecartex.com/products/details.cfm?Prod=1`. Accessed: 12th December 2013.

[47] Hughes, B., Wilson, A. & Peggs, G. Design of a high-accuracy CMM based on multi-lateration techniques. *CIRP Annals - Manufacturing Technology* **49**, 391–394 (2000).

[48] Pril, W. *Development of High Precision Mechanical Probes for Coordinate Measuring Machines*. Ph.D. thesis, Technische Universiteit Eindhoven, NL (2002). URL `http://citeseerx.ist.psu.edu/viewdoc/download?doi=10.1.1.119.2122\&rep=rep1\&type=pdf`.

[49] Pril, W., Struik, K. & Schellekens, P. Development of a 2D probing system with nanometer resolution. *Proc. of 16th ASPE* 438–442 (1997).

[50] Haitjema, H., Pril, W. & Schellekens, P. Development of a silicon-based nanoprobe system for 3-D measurements. *CIRP Annals - Manufacturing Technology* **50**, 365–368 (2001).

[51] Yang, S., Li, S., Kaiser, M. J. & Eric, F. H. K. A probe for the measurement of diameters and form errors of small holes. *Measurement Science and Technology* **9**, 1365–1368 (1998).

[52] Hausotte, T., Percle, B. & Jäger, G. Advanced three-dimensional scan methods in the nanopositioning and nanomeasuring machine. *Measurement Science and Technology* **20**, 084004 (2009).

[53] Ruijl, T. & van Eijk, J. A Novel Ultra Precision CMM based on Fundamental Design Principles. In *Proceedings of the ASPE summer conference on ...*, 33–38 (Charlotte, North Carolina, USA, 2003).

[54] Ruijl, T. *Ultra Precision Coordinate Measuring Machine: Designing, Calibration and Error Compensation*. Ph.D. thesis, Delft University of Technology, NL (2001).

[55] Donker, R., Widdershoven, I. & Spaan, H. Realization of Isara 400: a large measurement volume ultra-precision CMM. *Asian Symposium for Precision Engineering and Nanotechnology* **4** (2009).

[56] IBS Precision Engineering. Ultra precision tactile probe system. URL `http://www.ibspe.com/category/isara-400-3d-cmm/triskelion-touch-probe.htm`. Accessed: 19th July 2013 (2012).

[57] Chu, C.-L. & Lin, C.-H. Development of an optical accelerometer with a DVD pick-up head. *Measurement Science and Technology* **16**, 2498–2502 (2005).

[58] Chu, C.-L. & Chiu, C.-Y. Development of a low-cost nanoscale touch trigger probe based on two commercial DVD pick-up heads. *Measurement Science and Technology* **18**, 1831–1842 (2007).

[59] Fan, K.-C., Cheng, F., Wang, W., Chen, Y. & Lin, J.-Y. A scanning contact probe for a micro-coordinate measuring machine (CMM). *Measurement Science and Technology* **21**, 054002 (2010).

[60] Cheng, F., Fei, Y., Fan, K.-C. & Lei, Y. Measurement of Pre-Travel Distance of a Touch Probe for Nano-CMM. *Nanotechnology and Precision Engineering* **8**, 107–112 (2010).

[61] Li, R., Fan, K.-C. & Tao, S. Design of an analogue contact probe for nano-coordinate measurement machines (CMM). In *Seventh Internation Symposium on Precision Engineering Measurements and Instrumentation*, vol. 8321, 832114 (International Society for Optics and Photonics, SPIE, 2011).

[62] Takamasu, K. & Chi-Che, K. Development of pneumatic ball probe for measuring small hole. In *Proc. Int. Conf. Prec. Eng.*, 767 (Taipei, TW, 1997).

[63] Zhang, G. & Yang, S. A 3D probe for measuring small blind holes. *CIRP Annals - Manufacturing Technology* **44**, 461–464 (1995).

[64] Klocke Nanotechnik GmbH. Nanorobotics - Forming the 3D-Nanofinger. URL `http://www.3d-nanofinger.com/`. Accessed: 7th August 2013 (2007).

[65] Kao, S.-M. & Sheu, D.-Y. Developing a novel tri-switch tactile probing structure and its measurement characteristics on micro-CMM. *Measurement* **46**, 3019–3025 (2013).

[66] Park, J.-J., Kwon, K. & Cho, N. Development of a coordinate measuring machine (CMM) touch probe using a multi-axis force sensor. *Measurement Science and Technology* **17**, 2380–2386 (2006).

[67] Marinello, F., Savio, E., Bariani, P. & Carmignato, S. Coordinate metrology using scanning probe microscopes. *Measurement Science and Technology* **20**, 084002 (2009).

[68] Xpress Precision Engineering. Gannen series - a new era in metrology. URL `http://www.xpresspe.com/download/Xpress-Gannen-series.pdf`. Accessed: 5th August 2013 (2013).

[69] Bos, E. J. C. *Tactile 3D probing system for measuring MEMS with nanometer uncertainty.* Ph.D. thesis, Technische Universiteit Eindhoven, NL (2008). URL `http://wfwweb.wfw.wtb.tue.nl/pdfs/BosEdwin.pdf`.

[70] Kleine-Besten, T., Loheide, S. & Brand, U. Development and characterization of new probes for dimensional metrology on microsystem components. In *1st International Conference of the European Society for Precision Engineering and Nanotechnology*, 287–390 (1999).

[71] Brand, U., Kleine-Besten, T. & Schwenke, H. Development of a special CMM for dimensional metrology on microsystem components. In *Proceedings of the 2000 Annual Meeting of ASPE*, October, 361–364 (2000).

[72] Bütefisch, S., Büttgenbach, S., Kleine-Besten, T. & Brand, U. Micromechanical three-axial tactile force sensor for micromaterial characterisation. *Microsystem Technologies* **7**, 171–174 (2001).

[73] Cao, S. *et al.* Recent developments in dimensional metrology for microsystem components. *Microsystem Technologies* **8**, 3–6 (2002).

[74] Dai, G., Bütefisch, S., Pohlenz, F. & Danzebrink, H.-U. A high precision micro/nano CMM using piezoresistive tactile probes. *Measurement Science and Technology* **20**, 084001 (2009).

[75] Nesterov, V. & Brand, U. Modelling and investigation of the silicon twin design 3D micro probe. *J. Micromech. Microeng.* **15**, 514–520 (2005).

[76] Bütefisch, S. New packaging concept for ultra high precision 3D tactile probes for CMM applications. In *Electronic System-Integration Technology Conference (ESTC), 2010 3rd. IEEE*, 1–4 (2010).

[77] Ruther, P. *et al.* Novel 3D Piezoresistive Silicon Force Sensor for Dimensional Metrology of Micro Components. In *Sensors, 2005 IEEE*, 1006–1009 (Ieee, 2005).

[78] Wagener, M., Bader, F. & Seitz, K. Ensuring the quality of micro-parts. *Mikroniek 50(4)* 23–25 (2010).

[79] Wilson, A. & Leach, R. K. NPL Report ENG 15 - Manufacture and testing of a micro-stylus suitable for tactile probing in dimensional metrology. Tech. Rep. June, National Physical Laboratory, Teddington, UK (2009).

[80] Dai, G., Bütefisch, S. & Pohlenz, F. True 3D measurement on micro- and nano-structures. In *56th International Scientific Colloquium*, 12–16 (Ilmenau, DE, 2011).

[81] Peiner, E., Balke, M., Doering, L. & Brand, U. Tactile probes for dimensional metrology with microcomponents at nanometre resolution. *Measurement Science and Technology* **19**, 064001 (2008).

[82] Bos, E. J. C. Aspects of tactile probing on the micro scale. *Precision Engineering* **35**, 228–240 (2011).

[83] Flack, D. NPL Good Practice Guide 43: CMM Probing. Tech. Rep., National Physical Laboratory, Teddington, UK (2001).

[84] Guijun, J., Schwenke, H. & Trapet, E. Opto-tactile sensor for 2D and 3D measurement of small structures on coordinate measuring machines. In *Proc 18th ASPE*, 25–28 (1998).

[85] Fan, K.-C., Hsu, H.-Y., Hung, P.-Y. & Wang, W. Experimental study of fabricating a microball tip on an optical fibre. *Journal of Optics A: Pure and Applied Optics* **8**, 782–787 (2006).

[86] Thelen, R., Schulz, J., Meyer, P. & Saile, V. Approaching a sub-micron capability index using a Werth Fibre Probe System. In *Proceedings of the Multi-Material Micro Manufacture Conference 2008* (Cardiff University, Cardiff, UK, 2008).

[87] Meyer, P., Mäder, O., Saile, V. & Schulz, J. Comparison of measurement methods for microsystem components: application to microstructures made by the deep x-ray lithography process (x-ray LIGA). *Measurement Science and Technology* **20**, 084024 (2009).

[88] Meyer, P., Claverley, J. D. & Leach, R. K. Quality control for deep x-ray lithography (LIGA): a preliminary metrology study. *Microsystem Technologies* **18**, 415–421 (2012).

[89] Werth Messtechnik. Werth Fiber Probe WFP - Micro probe for high precision applications. URL `http://www.werth.de/en/unser-angebot/products/sensors/werth-fiber-probe-wfp.html`. Accessed: 5th August 2013.

[90] Werth Messtechnik. Werth 3D Fiber Probe WFP - High precision three dimensional measurement. URL `http://www.werth.de/en/unser-angebot/products/sensors/werth-3d-fiber-probe-wfp.html`. Accessed: 5th August 2013.

[91] Cui, J., Li, L. & Tan, J. Opto-tactile probe based on spherical coupling for inner dimension measurement. *Measurement Science and Technology* **23**, 085105 (2012).

[92] Muralikrishnan, B. *et al.* Fiber deflection probe for small hole measurements. In *Proceedings of the 2004 ASPE Annual Meeting*, 7, 24–27 (Orlando, USA, 2004).

[93] Muralikrishnan, B., Stone, J. & Stoup, J. Diameter and form measurement of a micro-hole in a fuel injector nozzle with the NIST fiber probe. In *Proceedings of the 2009 Annual Meeting of the American Society for Precision Engineering*, 3–6 (Monterey, USA, 2009).

[94] Muralikrishnan, B., Stone, J. & Stoup, J. Fiber deflection probe for small hole metrology. *Precision Engineering* **30**, 154–164 (2006).

[95] Muralikrishnan, B., Stone, J. & Stoup, J. Roundness measurements using the NIST fibre probe. In *Proceedings of the 2007Annual Meeting of the ASPE* (Dallas, USA, 2007).

[96] Muralikrishnan, B., Stone, J. & Stoup, J. Area measurement of knife-edge and cylindrical apertures using ultra-low force contact fibre probe on a CMM. *Metrologia* **45**, 281–289 (2008).

[97] Muralikrishnan, B., Stone, J. & Stoup, J. Enhanced capabilities of the NIST fibre probe for microfeature metrology. In *Proceedings of the 2006 Annual Meeting of the ASPE*, 3–6 (Monterey, USA, 2006).

[98] Ji, H., Kong, L., Hsu, H., Wedding, B. & Lin, G. Concept design of a novel tactile probe tip for down scaled 3D CMMs. In *Microelectronics, MEMS and Nanotechnology*, 70370Q (International Society for Optics and Photonics, SPIE, 2005).

[99] Kao, C.-C. & Shih, A. J. Form measurements of micro-holes. *Measurement Science and Technology* **18**, 3603–3611 (2007).

[100] Stone, J. & Muralikrishnan, B. Geometric Effects When Measuring Small Holes With Micro Contact Probes. *J. Res. Natl. Inst. Stand. Technol.* **116**, 573–587 (2011).

[101] Meyer, P., Claverley, J. D., Kaiser, K., Mohr, J. & Leach, R. K. Round-robin test concerning the dimensional measurement of microparts made using deep x-ray lithography (LIGA): first results. In *Proceedings of the 11th euspen*, 96–99 (Como, Italy, 2011).

[102] Mäder, O., Meyer, P., Saile, V. & Schulz, J. Metrology study of high precision mm parts made by the deep x-ray lithography (LIGA) technique. *Measurement Science and Technology* **20**, 025107 (2009).

[103] Oiwa, T. & Tanaka, T. Miniaturized three-dimensional touch trigger probe using optical fibre bundle. *Measurement Science and Technology* **16**, 1574–1581 (2005).

[104] Enami, K., Hiraki, M. & Takamasu, K. Nano-probe using optical sensing. In *IMEKO-XVI World Congress*, vol. 345, 189–192 (2000).

[105] Van Brussel, H. *et al.* Assembly of Microsystems. *CIRP Annals - Manufacturing Technology* **49**, 451–472 (2000).

[106] Masuzawa, T., Hamasaki, Y. & Fujino, M. Vibroscanning method for nondestructive measurement of small holes. *CIRP Annals - Manufacturing Technology* **42**, 589–592 (1993).

[107] Kim, B., Masuzawa, T. & Bourouina, T. The vibroscanning method for the measurement of micro-hole profiles. *Measurement Science and Technology* **10**, 697–705 (1999).

[108] Masuzawa, T., Kim, B., Bergaud, C. & Fujino, M. Twin-Probe Vibroscanning Method for Dimensional Measurement of Microholes. *CIRP Annals - Manufacturing Technology* **46**, 437–440 (1997).

[109] Hidaka, K. & Schellekens, P. Study of a Small-sized Ultrasonic Probe. *CIRP Annals - Manufacturing Technology* **55**, 567–570 (2006).

[110] Hidaka, K., Saito, a. & Koga, S. Study of a micro-roughness probe with ultrasonic sensor. *CIRP Annals - Manufacturing Technology* **57**, 489–492 (2008).

[111] Mitutoyo. UMAP Vision System. URL `www.mitutoyo.com/pdf/1631.pdf`. Accessed: 5th August 2013 (2003).

[112] Koopmans, H. Innovation and service. *Mikroniek 50(4)* **50**, 26–30 (2010).

[113] Bauza, M. B., Hocken, R., Smith, S. T. & Woody, S. C. Development of a virtual probe tip with an application to high aspect ratio microscale features. *Rev. Sci. Instrum.* **76**, 95–112 (2005).

[114] Seugling, R. & Darnell, I. Investigating scaling limits of a fibre based resonant probe for metrology applications. In *Proc. 12th ICPE* (Lawrence Livermore National Laboratory (LLNL), Livermore, CA, Portland, Oregon, USA, 2008).

[115] Bauza, M. & Woody, S. Microscale metrology using standing wave probes. In *Proceedings of the 23rd ASPE* (2008).

[116] Seugling, R., Woody, S. C. & Bauza, M. B. Standing wave probes for dimensional metrology of low density foams - LLNL-TR-426347. Tech. Rep., Lawrence Livermore National Laboratory, Livermore, CA, USA (2010). URL `http://www.osti.gov/bridge/product.biblio.jsp?osti\_id=975224`.

[117] Bauza, M. B., Woody, S., Seugling, R. & Smith, S. Dimensional measurements of ultra delicate materials using micrometrology tactile sensing. In *Proc. ASPE Vol. 50*, vol. 50, 73–76 (2010).

[118] Takaya, Y., Takahashi, S., Miyoshi, T. & Saito, K. Development of the nano-CMM probe based on laser trapping technology. *CIRP Annals - Manufacturing Technology* **48**, 421–424 (1999).

[119] Takaya, Y., Imai, K., Ha, T., Miyoshi, T. & Kinoshita, N. Vibrational Probing Technique for the Nano-CMM based on Optical Radiation Pressure Control. *CIRP Annals - Manufacturing Technology* **53**, 421–424 (2004).

[120] Takaya, Y., Imai, K., Dejima, S., Miyoshi, T. & Ikawa, N. Nano-Position Sensing Using Optically Motion-controlled Microprobe with PSD Based on Laser Trapping Technique. *CIRP Annals - Manufacturing Technology* **54**, 467–470 (2005).

[121] Eom, S. I., Hayashi, T. & Takaya, Y. Fundamental study on the position detection signal analysis for the fibre optical trapping probe. *International Journal of Surface Science and Engineering* **3**, 208 (2009).

[122] Eom, S. I., Takaya, Y. & Hayashi, T. Novel contact probing method using single fiber optical trapping probe. *Precision Engineering* **33**, 235–242 (2009).

[123] Kobayashi, M., Michihata, M., Hayashi, T. & Takaya, Y. Coordinate measurement of micro groove on MEMS device by optically controlled microprobe. In *2010 International Symposium on Optomechatronic Technologies - IEEE*, 1–5 (Ieee, 2010).

[124] Takaya, Y., Michihata, M., Hayashi, T. & Washitani, T. Dimensional measurement of microform with high aspect ratio using an optically controlled particle with standing wave scale sensing. *CIRP Annals - Manufacturing Technology* **61**, 479–482 (2012).

[125] Michihata, M., Hayashi, T., Nakai, D. & Takaya, Y. Microdisplacement sensor using an optically trapped microprobe based on the interference scale. *The Review of scientific instruments* **81**, 015107 (2010).

[126] van Riel, M. & Bos, E. 3D vibrating probe for measuring microfeatures with nanometer uncertainty. In *56th International Scientific Colloquium* (Ilmenau, DE, 2011).

[127] Schwenke, H., Hartig, F., Wendt, K. & Waldele, F. Future challenges in co-ordinate metrology: addressing metrological problems for very small and very large parts. In *Proceedings of IDW conference*, 1–12 (Knoxville, USA, 2001).

[128] Claverley, J. D. & Leach, R. K. A novel three-axis vibrating micro-CMM probe with isotropic probing forces. In *Proceedings of the 11th euspen*, vol. 1, 59–62 (Delft, NL, 2010).

[129] Nicolet, A., Küng, A. & Meli, F. Study of sapphire probe tip wear when scanning on different materials. *Measurement Science and Technology* **23**, 094016 (2012).

[130] Hansen, H. N., Carneiro, K., Haitjema, H. & De Chiffre, L. Dimensional Micro and Nano Metrology. *CIRP Annals - Manufacturing Technology* **55**, 721–743 (2006).

[131] Stoyanov, S. *et al.* Modelling and prototyping the conceptual design of 3D CMM microprobe. In *2nd Electronics Systemintegration Technology Conference*, 193–198 (IEEE, Greenwich, UK, September, 2008).

[132] Leach, R. K., Murphy, J. & Wilson, A. Design of a co-ordinate measuring probing system for characterising three-dimensional micro-structures. Tech. Rep. February, National Physical Laboratory (2004).

[133] Leach, R. K. & Murphy, J. The design of a co-ordinate measuring probe for characterizing truly three-dimensional micro-structure. In *Proceedings of the 4th euspen*, 230–232 (Glasgow, UK, 2004).

[134] Stoyanov, S. *et al.* Reduced order modelling for risk mitigation in design of miniaturised/integrated products. In *33rd International Spring Seminar on Electronics Technology (ISSE)*, 402–407 (IEEE, 2010).

[135] Rajaguru, P. *et al.* Numerical modelling methodology for design of miniaturised integrated products - an application to 3D CMM micro-probe development. In *11th International Thermal, Mechanical & Multi-Physics Simulation, and Experiments in Microelectronics and Microsystems (EuroSimE)*, 1–8 (Ieee, 2010).

[136] Sun, Y., Fowkes, C. R., Gindy, N. & Leach, R. K. Variation risk analysis: MEMS fabrication tolerance for a micro CMM probe. *Int. J. Adv. Manufac. Technol.* **47**, 1113–1120 (2009).

[137] Sheu, D.-Y. Multi-spherical probe machining by EDM. *J. Mat. Process. Technol.* **149**, 597–603 (2004).

[138] ISO 10360-5:2010 Geometrical product specifications (GPS) - Acceptance and reverification tests for coordinate measuring machines (CMM) - Part 5: CMMs using single and multiple stylus contacting probing systems (International Organisation for Standardisation, Geneva, CH, 2010).

[139] Sheu, D.-Y. Study on an evaluation method of micro CMM spherical stylus tips by micro-EDM on-machine measurement. *Journal of Micromechanics and Microengineering* **20**, 075003 (2010).

[140] Küng, A. & Meli, F. Self calibration method for 3D roundness of spheres using an ultraprecision coordinate measuring machine. In *Proceedings of the 5th euspen*, vol. 1, 3–6 (Montpellier, FR, 2005).

[141] Neuschaefer-Rube, U. EMRP-JRP59 - Multi-sensor metrology for microparts in innovative industrial products. URL `http://www.euramet.org/fileadmin/docs/EMRP/JRP/JRP\_Summaries\_2012/Industry\_JRPs/IND59\_Publishable\_JRP\_Summary.pdf`. Accessed: 13th Jan 2014 (2013).

[142] Smale, D., Ratchev, S., Segal, J., Leach, R. K. & Claverley, J. D. Assembly of the stem and tip of an innovative micro-CMM probe. In *Euspen 9th International Laser Metrology and Machine Performance Conference*, 442–451 (Brunel, London, UK, 2009).

[143] Smale, D. *et al.* Utilisation of FIB/SEM Technology in the Assembly of an Innovative Micro-CMM Probe. *Precision Assembly Technologies and Systems* **IPAS 2010**, 105–112 (2010).

[144] Burisch, A., Soetebier, S. & Wrege, J. Design of a parallel hybrid micro-scara robot for high precision assembly. *Mechatronics and Robotics* **4**, 1374 (2004).

[145] Claverley, J. D., Sheu, D.-Y. & Burisch, A. Assembly of a novel MEMS-based 3D vibrating micro-scale co-ordinate measuring machine probe using desktop factory automation. In *IEEE International Symposium on Assembly and Manufacturing (ISAM)*, 1–5 (Tampere, FI, 2011).

[146] Claverley, J. D., Burisch, A., Leach, R. K. & Raatz, A. Semi-automated assembly of a MEMS-based micro-scale CMM probe and future optimization of the process chain with a view to desktop factory automation. *Precision Assembly Technologies and Systems* **IPAS 2012**, 9–16 (2012).

[147] Iwftubs. Parvus Assembly NPL Microprobe. URL `http://www.youtube.com/watch?v=vgCwIWQqHJ8`. Accessed: 10th July 2012 (2012).

[148] Leach, R. K., Hughes, B. & Wilson, A. Microprobe, measurement system and method - UK Patent GB2452805 (UK Intellectual Property Office, 2011).

[149] Leach, R. K., Hughes, B. & Wilson, A. Microprobe, measurement system and method - U.S. Patent No. 20,110,047,661 (U.S. Patent and Trademark Office., 2011).

[150] Leach, R. K., Hughes, B. & Wilson, A. Microprobe, measurement system and method - WIPO Patent 2009063217 (World Intellectual Property Organization, Geneva, CH, 2009).

[151] Jones, C. W. & Leach, R. K. NPL Report ENG5 - Review of Low Force Transfer Artefact Technologies. Tech. Rep. March, National Physical Laboratort, Teddington, UK (2008). URL `http://publications.npl.co.uk/npl\_web/pdf/eng5.pdf`.

[152] Jones, C. W. *Development and characterisation of traceable force measurement for nanotechnology.* Ph.D. thesis, University of Warwich, UK (2012).

[153] Jones, C. W., Chetwynd, D., Singh, J. & Leach, R. K. Concept and modelling of a novel active triskelion low force transfer artefact. In *Proceedings of the 11th euspen*, 191–194 (Como, Italy, 2011).

[154] Ansys. Documentation for ANSYS Release 11.0. URL `http://www.kxcad.net/ansys/ansys/ansyshelp/ansys.set.html`. Accessed: 8th August 2013 (2007).

[155] Kaye, G. W. & Laby, T. H. *Tables of physical and chemical constants* (Longman, London, 1995), 16 edn.

[156] Young, W. & Budynas, R. *Roark's Formulas for Stress and Strain* (The McGraw-Hill Companies, 2011), 7th edn.

[157] SolidWorks. SolidWorks 2008 Release Notes. URL `http://files.solidworks.com/Supportfiles/Release\_Notes/2008/English/relnotes.htm`. Accessed: 8th August 2013 (2009).

[158] Claverley, J. D. & Leach, R. K. A vibrating micro-scale CMM probe for measuring high aspect ratio structures. *Microsystem Technologies* **16**, 1507–1512 (2009).

[159] Stoney, G. G. The tension of metalic films deposited by electrolysis. *Proceedings of the Royal Society of London. Series A, Containing Papers of a Methematical and Physical Chatacter* **82**, 172–175 (1909).

[160] Janssen, G., Abdalla, M., van Keulen, F., Pujada, B. & van Venrooy, B. Celebrating the 100th anniversary of the Stoney equation for film stress: Developments from polycrystalline steel strips to single crystal silicon wafers. *Thin Solid Films* **517**, 1858–1867 (2009).

[161] Sosa, H. & Castro, M. Electroelastic analysis of piezoelectric laminated structures. *Applied Mechanics Reviews* **46**, 21 (1993).

[162] Haojiang, D. General solutions for coupled equations for piezoelectric media. *International Journal of Solids and Structures* **33**, 2283–2298 (1996).

[163] Neubert, H. *Instrument transducers: An introduction to their performance and design* (Clarendon Press, Oxford, UK, 1975).

[164] Claverley, J. D., Georgi, A. & Leach, R. K. Modelling the interaction forces between an ideal measurement surface and the stylus tip of a novel vibrating micro-scale CMM probe. *Precision Assembly Technologies and Systems* **IPAS 2010**, 131–138 (2010).

[165] Lambert, P. *Capillary forces in microassembly: modeling, simulation, experiments and case studies* (Springer, 2007).

[166] Sitti, M. & Hashimoto, H. Controlled pushing of nanoparticles: modeling and experiments. *IEEE/ASME Transactions on Mechatronics* **5**, 199–211 (2000).

[167] Andersson, K. *Aqueous processing of WC-Co powders.* Ph.D. thesis, Royal Institute of Technology, Sweden (2004).

[168] Arai, F., Andou, D. & Fukuda, T. Adhesion forces reduction for micro manipulation based on micro physics. In *Proceedings of Ninth International Workshop on Micro Electromechanical Systems*, 354–359 (IEEE, 1996).

[169] Lamoreaux, S. K. Demonstration of the Casimir Force in the 0.6 to 6 μm Range. *Physical Review Letters* **78**, 5–8 (1997).

[170] Jaffe, R. Casimir effect and the quantum vacuum. *Physical Review D* **72**, 021301 (2005). `0503158v1`.

[171] Mukhiya, R. & Bhattacharyya, T. K. Squeeze film air damping analysis of MEMS piezoresistive accelerometer. *2008 IEEE International Conference on Semiconductor Electronics* 198–202 (2008).

[172] op den Camp, O., Janssen, J. D., Oomens, C. W. J. & Lankveld, V. M. *Theoretical analysis of squeeze films*. Ph.D. thesis, Technische Universiteit Eindhoven, NL (1991).

[173] Allen, C. W. & Wilson, M. P. An analytical solution of the squeeze film between a non-deformable sphere and groove. Tech. Rep. November, National Aeronautics and Space Administration (NASA) (1972).

[174] Honig, C. & Ducker, W. Effect of Molecularly-Thin Films on Lubrication Forces and Accommodation Coefficients in Air. *The Journal of Physical Chemistry C* **1**, 20114–20119 (2010).

[175] Vinogradova, O. I. Slippage of water over hydrophobic surfaces. *International Journal of Mineral Processing* **56**, 31–60 (1999).

[176] Hocking, L. The effect of slip on the motion of a sphere close to a wall and of two adjacent spheres. *Journal of Engineering Mathematics* **7**, 207–221 (1973).

[177] Santos, S., Verdaguer, A., Souier, T., Thomson, N. H. & Chiesa, M. Measuring the true height of water films on surfaces. *Nanotechnology* **22**, 465705 (2011).

[178] Jennings, S. The mean free path in air. *Journal of Aerosol Science* **19**, 159–166 (1988).

[179] Lau, C. A. GAM/ME/66B-14 - Thermal accommodation coefficient for air on tungsten. Tech. Rep., US Airforce Institute of Technology - Write-Patterson AFB - Ohio School of Engineering (1966). URL `http://oai.dtic.mil/oai/oai?verb=getRecord\&metadataPrefix=html\&identifier=AD0635231http://www.dtic.mil/docs/citations/AD0635231`.

[180] Sounilhac, S., Barthel, E. & Creuzet, F. The electrostatic contribution to the long-range interactions between tungsten and oxide surfaces under ultrahigh vacuum. *Applied surface science* **140**, 411–414 (1999).

[181] Sherrington, I. & Smith, E. H. Design of a Kelvin clamp for use in relocation analysis of surface topography. *Prec. Eng.* **15**, 77–85 (1993).

[182] Flack, D. & Hannaford, J. NPL Good Practice Guide 80: Fundamental good practice in dimensional metrology. Tech. Rep., National Physical Laboratory, Teddington, UK (2005).

[183] Goodfellow. Dural - Aluminium/Copper/Magnesium (Al 95/Cu 4/Mg 1) Material Information. URL `http://www.goodfellow.com/A/Dural-Aluminum-Copper-Magnesium.html`. Accessed: 8th August 2013 (2013).

[184] Integrated Electronics Ltd. IEL - The electronics sub-contract manufacturer of choice. URL `http://www.ielco.com/`. Accessed: 8th August 2013 (2013).

[185] RS Components Ltd. Pointed 2-part spring probe,1.27mm pitch. URL `http://uk.rs-online.com/web/p/spring-test-probes/2615137/`. Accessed: 8th August 2013 (2013).

[186] National Instruments Corporation. R Series Multifunction RIO with Virtex-5 LX30 FPGA. URL `http://sine.ni.com/nips/cds/view/p/lang/en/nid/207368`. Accessed: 8th August 2013 (2012).

[187] National Instruments Corporation. NI LabVIEW 2010 Service Pack 1 Release Details. URL `http://www.ni.com/labview/release-archive/labview2010SP-1/`. Accessed: 8th August 2013.

[188] RS Components Ltd. 6 pair individually shielded cable,30m. URL `http://uk.rs-online.com/web/p/twisted-multipair-industrial-cable/1119240/`. Accessed: 8th August 2013.

[189] PI (Physik Instrumente) GmbH & Co. P-611.Z Piezo Z-Stage - Compact Nanopositioner. URL `http://www.physikinstrumente.com/en/products/prdetail.php?sortnr=201730`. Accessed: 8th August 2013 (2013).

[190] ISO 3650-1999 - Geometrical product specifications (GPS). Length standards. Gauge blocks (International Organisation for Standardisation, Geneva, CH, 1999).

[191] Polytec GmbH. CLV-2534 Compact Laser Vibrometer. URL `http://www.polytec.com/uk/products/vibration-sensors/single-point-vibrometers/complete-systems/clv-2534-compact-laser-vibrometer/`. Accessed: 8th August 2013 (2013).

[192] Castellini, P., Revel, G. & Tomasini, E. Laser Doppler vibrometry: a review of advances and applications. *The Shock and vibration digest* **30**, 443–456 (1998).

[193] Castellini, P., Martarelli, M. & Tomasini, E. Laser Doppler Vibrometry: Development of advanced solutions answering to technology's needs. *Mechanical Systems and Signal ...* **20**, 1265–1285 (2006).

[194] Castellini, P., Revel, G. & Tomasini, E. Laser Doppler Viborometry. In *An Introduction to Optoelectonic Sensors 7*, 216–229 (2009).

[195] Claverley, J. D. & Leach, R. K. Development of a three-dimensional vibrating tactile probe for miniature CMMs. *Precision Engineering* **37**, 491–499 (2013).

[196] ISO 10360-2:2009 - Geometrical product specifications (GPS) - Acceptance and reverification tests for coordinate measuring machines (CMM) - Part 2: CMMs used for measuring linear dimensions (International Organisation for Standardisation, Geneva, CH, 2009).

[197] ISO 10360-6:2001 - Geometrical Product Specifications (GPS) - Acceptance and reverification tests for coordinate measuring machines (CMM) - Part 6: Estimation of errors in computing Gaussian associated (International Organisation for Standardisation, Geneva, CH, 2007).

[198] ASME B89.4.1-1997 - Performance evaluation of CMMs (American Society of Mechanical Engineers, 1997).

[199] EN ISO 14253-2:2011 Geometrical product specifications (GPS) - Inspection by measurement of workpieces and measuring equipment Part 2 : Guidance for the estimation of uncertainty in GPS measurement in calibration of measuring equipment (International Organisation for Standardisation, Geneva, CH, 2011).

[200] Claverley, J. D. & Leach, R. K. A review of the existing performance verification infrastructure for micro-CMMs. *Submitted to Prec. Eng* (2013).

[201] Flack, D. NPL Good Practice Guide 41: CMM Measurement Strategies. Tech. Rep., National Physical Laboratory, Teddington, UK (2001).

[202] Ehrig, W. & Neuschaefer-Rube, U. Artefacts with rough surfaces for verification of optical microsensors. In *Optical Metrology*, 661626 (International Society for Optics and Photonics, SPIE, 2007).

[203] ISO 10360-8.2:DRAFT - Geometrical Product Specifications (GPS) - Acceptance and reverification tests for coordinate measuring machines (CMM) - Part 8: CMMs with optical distance sensors (International Organisation for Standardisation, Geneva, CH, 2012).

[204] ISO 1:2002 - Geometrical Product Specifications (GPS) - Standard reference temperature for geometrical product specification and verification (International Organisation for Standardisation, Geneva, CH, 2002).

[205] Küng, A. & Meli, F. Comparison of three independent calibration methods applied to an ultra-precision micro-CMM. In *Proceedings of the 7th euspen*, May (Bremen, DE, 2007).

[206] Lipscomb, I. & Weaver, P. The effect of relative humidity, temperature and electrical field on leakage currents in piezo-ceramic actuators under dc bias. *Sensors and Actuators A: Physical* **151**, 179–186 (2009).

[207] Bogomolov, A. & Sergeeva, O. Pyroelectric and photoelectric responses of capacitors based on thin PZT films. *Physics of the Solid State* **48**, 1194–1196 (2006).

[208] Habeb, R. R. & Kinnell, P. K. Evaluation Tip Cleaning for a Micro CMM Touch Trigger Stylus Sensor. *Procedia Engineering* **47**, 306–309 (2012).

[209] Kinnell, P. K. & Habeb, R. R. An evaluation of cleaning methods for micro-CMM probes. *Measurement Science and Technology* **24**, 085603 (2013).

[210] Kanda, T. A flat type touch probe sensor using PZT thin film vibrator. *Sensors and Actuators A: Physical* **83**, 67–75 (2000).

[211] Kanda, T. & Morita, T. Estimation of resolution and contact force of a longitudinally vibrating touch probe sensor using lead zirconate titanate (PZT) thin-film vibrator. *Japanese Journal of Applied Physics* **40**, 3646–3651 (2001).